Exploring beyond the Standard Model: the Heavy and the Dark

Thèse N° 9846

Présentée le 1er novembre 2019

à la Faculté des sciences de base
Laboratoire de physique théorique des particules
Programme doctoral en physique

pour l'obtention du grade de Docteur ès Sciences

par

Kin Shanho Eliaou MIMOUNI

Acceptée sur proposition du jury

Prof. F. Courbin, président du jury
Prof. R. Rattazzi, R. N. Mahbubani, directeurs de thèse
Prof. M. Redi, rapporteur
Prof. A. Pomarol, rapporteur
Prof. A. Bay, rapporteur

2019

ÉCOLE POLYTECHNIQUE
FÉDÉRALE DE LAUSANNE

Acknowledgements

I want to thank first and foremost my thesis director Riccardo Rattazzi for his supervision and guidance during the four years of the PhD presented here. His deep understanding of physics has helped me a lot for my work but also for my own picture of the field. Many times I came out of Riccardo's office more puzzled than when I entered, only to understand his comments after a few days (or weeks) of work. Thank you for always finding interesting projects for me, for all the schools, conferences and travels that were possible thanks to you, and for defending me against the administrative documents!

Also I have to thank my thesis co-director Rakhi Mahbubani with whom I have worked on the project presented in the first chapter of this thesis. Thank you for the numerous discussions, your patience and your availability when new problems came up!

Moreover, I wish to thank Roberto Contino, my first thesis supervisor. Thank you for allowing me to work in Lausanne during these four years, I wish we had more opportunities to discuss and work together.

The thesis would not have been possible if not for my co-authors with whom I had great pleasure working with. First Adam Falkowski who also introduced me to particle physics phenomenology during the master thesis in LPT Orsay, Martín González-Alonso for the project on the running of four-fermion operators, Davide Greco for my first project in Lausanne, Raffaele Tito d'Agnolo and Adrien Florio for the TOTTI project.

This PhD follows from a longer academic process during which I had a lot of pleasure studying mathematics and physics. Among the teachers that helped me and inspired me to continue in science, I want to thank Michel Colin, Dominique Nessi, Clément De Pazzis, Camille Vecchiato and Guillaume Bossard, as well as Fawzi Boudjema and Cédric Delaunay for my first internship in a laboratory.

The four years in Lausanne have been a happy time abroad and this is mainly due to the fantastic people I met there because, after all, life is made of the people around you. My closest companions have been the students and postdocs of the Cubotron, they have shared my daily life at the office and also some week-end activities, in no particular order Lorenzo, Davide, Alberto, Andrea, Jérôme, Misha, Andrei, Bernardo my deskmate and flatmate from Paris, Gabriel the savior of my thesis, Adrien, João, Marten my new flatmate and professional mover, Andrea, Grégoire, Riccardo, Alfredo (sorry for the kayak adventure), Aditya, Kamran, Siyu, Gil, Francisco, Samuel, Jeanne, Ivo, Marc, John, David, Sanders, Denis, João and many more! Outside of physics, Lausanne offers a great scenery and easy access to the mountains. I

want to thank people from the Club Montagne and from the CAS for the activities and outings we did together. For my Swiss friends outside of physics, I want to give my thanks to Noémie for the visit in Liechtenstein, Minh-Kha for the climbing sessions, Franziska for the summer vacations, Serge and Manu for the mountaneering outings.

I have to thank the members of the Ensemble Vide and in particular David-Tristan for taking me in the group for one week and helping me writing my thesis, but also for skiing week-ends, many beautiful concerts and a challenging main role in one of their main productions. Also, I owe a lot to Odile for her hospitality in Paris and all her support during the hard times of the tesis.

My thanks also go to my friends from university, especially those who visited me in Lausanne ; the members of the extended Team Poney, Thibaut, Odile, Thomas, Isabelle, Sébastien, Sybille, Guillaume, Olivier ; the extended Ellipse group, Maxence, Laure, Guillaume (×2), Mathilde, William, Benjamin, Anthony, Alizée, PE, Nicolas, Hombeline, Antoine for his very hard questions about physics, Jean-Christophe, Anne, Fabien, Béatrice, Etienne, Benoît, Cédric, Julien and many other friends! From Thusy, thank you Lamine for your help in commuting to Lausanne.

Last but not least, this PhD would not have been possible without the constant support from my family ; my parents who are always here to help me and guide me, my sister who is like a role model for me.

Lausanne, September 27, 2019 Kin Mimouni

Abstract

Physics beyond the Standard Model can appear as new particles too heavy to be produced in experiments (the energy frontier) or interacting too weakly to be seen in our measurements (the intensity frontier).
In the first part of this thesis, we study two dark matter models of electroweak WIMP coming from two limiting cases in the MSSM: the Higgsino and the Wino model. The dark matter candidate is a particle too heavy to be directly seen in colliders but it could be seen indirectly by astrophysical observations. Dark matter particles in the galaxy can annihilate to Standard Model particles and be detected by satellites. We consider the charged neutral mass splitting as a free parameter in the theory and investigate its effect on the Sommerfeld enhancement which gives an important boost to the annihilation cross-section, the main observable of indirect detection.
In the second part of this thesis, we present an idea of a fixed target experiment to search for dark sector models, a class of model with very weakly interacting particles. This experiment uses the experimental setup needed for a future muon collider but is independent from the muon collider program. We study the reach of our experiment for three benchmark models, the dark photon, the dark Higgs, the heavy neutral lepton and we compare its expected performances to current and future experiments.
In the third part of this thesis, we consider a more model-independent approach to the search for new physics. If new states are heavy, they can be integrated out and their leading effects are encoded in effective operators made of Standard Model fields. Assuming baryon and lepton number conservation, one can classify the effective operators of dimension-6 which give the leading contribution and constrain the coefficient of these operators by looking at precision observables. We compile results from LEP-I and LEP-II experiments as well as neutrino scattering and other low-energy observables. We allow all operators to be present with an arbitrary flavour structure. Our result can then be used to translate these constaints to specific models of new physics.

Keywords: Physics beyond the Standard Model, Dark Matter, Supersymmetry, Sommerfeld enhancement, Dark photon, Dark Higgs, heavy neutral lepton, effective field theory

Résumé

De nouvelles particules au-delà du modèle standard peuvent exister sans avoir été détectées soit parce qu'elles sont trop massives pour être produite dans les accélérateurs de particules, soit parce qu'elles interagissent trop faiblement pour être produites ou détectées. Dans le premier cas, nous avons besoin d'accélérateurs plus puissants (energy frontier) ; dans le second nous avons besoin d'expériences plus précises (intensity frontier).

Dans le premier chapitre de cette thèse, nous étudions deux modèles de matière noire électrofaible de type WIMP qui proviennent de deux cas limites du MSSM : le modèle pur Higgsino et pur Wino. Dans ces modèles, la particule composant la matière noire est trop lourde pour être observée dans les accélérateurs mais elle pourrait être observée indirectement dans des signaux astrophysiques. En effet, des particules de matière noire dans le halo galactique pourraient s'annihiler et produire des particules énergétiques du modèle standard qui sont ensuite détectées par des satellites. L'absence d'observation de tel signaux place une borne supérieure sur la section efficace d'annihilation des particules de matière noire. Nous considérons la différence de masse entre la composante chargée et la composante neutre d'un multiplet de matière noire comme un paramètre libre et nous étudions ses effets sur la section efficace d'annihilation en prenant en compte le Sommerfeld enhancement.

Dans le deuxième chapitre de cette thèse, nous présentons une suggestion d'expérience de type collision de faisceau de particules sur cible. Le but de cette machine est la recherche de particules appartenant à des secteurs sombres qui interagissent très faiblement avec la matière ordinaire. Cette expérience utilise un faisceau de positrons nécessaire pour un futur collisionneur de muons mais peut être conduite indépendamment du reste de l'accélérateur. Nous étudions le potentiel de découverte d'un tel détecteur pour trois modèles de référence, le dark photon, le dark Higgs et heavy neutral lepton. Les performances de ce système sont comparées avec celles d'expériences similaires.

Dans le troisième et dernier chapitre de cette thèse, nous considérons une approche plus modèle-indépendante de la physique au-delà du modèle standard. Si les nouvelles particules sont lourdes, leurs effets principaux sont décrits par des opérateurs effectifs construits à partir des champs du modèle standard. Partant du principe que le nombre baryonique et leptonique est conservé, il est possible d'écrire tous les opérateurs de dimension-6 qui donnent la plus grande contribution et de placer des bornes sur les coefficients de ces opérateurs en étudiant leur contribution à des mesures très précises. Nous compilons ici les mesures faites à LEP-I et LEP-II ainsi que celles faites à basse énergie sur les neutrinos et les atomes. Nous n'imposons pas de symétrie de saveur sur les opérateurs de dimension-6. Notre résultat peut ensuite être

utilisé pour étudier les limites expérimentales placées sur des modèles spécifiques au-delà du modèle standard.

Mots clés : Physique au-delà du modèle standard, matière noire, supersymétrie, Sommerfeld enhancement, Dark photon, Dark Higgs, heavy neutral lepton, théorie effective des champs

Contents

Introduction

The Standard Model of particle physics (SM) is the current theory describing interactions of elementary particles valid in a wide range of scales, from low-energy precision atomic measurements to high-energy collisions at the LHC. It is the result of decades of experimental and theoretical efforts throughout the last century.

Starting in the 1920s with Dirac's theory of the electron, the first step in the building of the SM was the development of quantum electrodynamics (QED), the field theory of a charged particle and electromagnetic interactions. The success of QED include the prediction of the positron, the famous calculation of the correction to the electron anomalous magnetic moment a_e by Schwinger in 1948 and the computation of the Lamb shift by Bethe around the same time.

The 1950s saw the discovery of a large number of particles, the mesons and the baryons and their classification lead to the idea of more fundamental constituents, the quarks. The quarks interact via the strong interaction, described by a non-abelian gauge theory with gauge group $SU(3)_C$ (C for colour). The interaction is strong, i.e. non-perturbative at low energies, leading to quark confinement. This is why quarks are not observed directly, but indirectly in composite states (mesons and baryons) or as jets in high-energy collisions.

The radioactive β decay of nuclei was first described by Fermi in the 1930s using a four-fermion operator. In the 1950s, the weak interaction was shown to violate parity maximally and in the 1960s the electroweak theory was developped by Glashow, Salam and Weinberg. The weak and electromagnetic forces were explained by the $SU(2)_L \times U(1)_Y$ gauge group, with the associated vector bosons $W^{\pm}, Z$ discovered at CERN in 1983. However, at low energies, the $SU(2)_L \times U(1)_Y$ invariance is not manifest: this is because the symmetry is spontaneously broken by the vacuum state.

The SM implements electroweak symmetry breaking with the Higgs mechanism: a scalar field, charged under the electroweak gauge group, gets a vacuum expectation value (VEV) that breaks $SU(2)_L \times U(1)_Y$ down to the QED $U(1)_{\text{em}}$ describing electromagnetism. The discovery of the Higgs boson at LHC in 2012 was a great success for the SM and marked the discovery of the last predicted particle of the model.

The Standard Model

In the modern Wilsonian point of view, the SM is an effective field theory (EFT) valid up to a cutoff scale $\Lambda_{\rm SM}$ at which new unknown physics appears. Then dimensional-analysis allows us to classify the operators made of SM fields according to their mass dimension:

$$\mathscr{L} = \mathscr{L}^{D\leq 4} + \sum_i \frac{c_i}{\Lambda_{\rm SM}} O_i^{D=5} + \sum_i \frac{c_i}{\Lambda_{\rm SM}^2} O_i^{D=6} + \cdots \tag{1}$$

where D is the mass dimension of the operator O_i and c_i is a coefficient encoding the interactions of the heavy fields at the cutoff scale with the SM.

For example, Fermi's description of the weak β decay can be written in modern notation $\mathscr{L}_{\rm F} = \frac{G_F}{\sqrt{2}} \left(\nu^\dagger \bar{\sigma}^\mu e\right) \left(d^\dagger \bar{\sigma}^\mu d\right) + c.c.$ with an operator of dimension-6. Today, we know that this decay is mediated by the heavy W boson with interaction strength g_L to the lepton and quark doublet. Integrating out the W boson gives precisely Fermi's operator with the relation $G_F = \frac{\sqrt{2}}{8} \frac{g_L^2}{m_W^2}$. Knowing the full theory, the cutoff of the Fermi theory is m_W, the scale at which treating the gauge boson as a new degree of freedom becomes necessary and the Wilson coefficient is: $c = \frac{g_L^2}{8}$.

If the SM is valid up to a high scale $\Lambda_{\rm SM}$, then from the power counting (1), the physical observables are well described by the leading renormalizable terms. Operators with dimension larger than 4 (irrelevant operators) have their coefficient suppressed by inverse powers of the cutoff and are subleading compared to the $D \leq 4$ operators.

In this philosophy, the building of the SM proceeds from the following recipe: from the particle content summarized in table 1 and its quantum numbers, we write all the possible operators compatible with SM symmetries with dimension lower or equal to 4. These are the leading interactions observable at the weak scale. At dimension-4 level, the SM Lagrangian is schematically:

$$\mathscr{L}_{\rm SM}^{(D=4)} = -\frac{1}{4} F^{\mu\nu} F_{\mu\nu} + i \Psi^\dagger \overline{\sigma}^\mu D_\mu \Psi - y_{ij} \Psi_i H \Psi_j + D^\mu H^\dagger D_\mu H + V(H) \tag{2}$$

The first two terms contain the gauge and fermions kinetic term as well as their gauge interactions. The following term is the Yukawa couplings between the fermions and the Higgs field:

$$\mathscr{L}_{\rm Yukawa} = -(y_e)_{ij} \ell_i H^\dagger \bar{e}_j - (y_u)_{ij} H \cdot q_i \bar{u}_j - (y_d)_{ij} q_i H^\dagger \bar{d}_j + c.c. \tag{3}$$

where the dot represents the contraction of $SU(2)_L$ indices with an epsilon tensor and y_e, y_u, y_d are 3×3 matrices in family space. This part is responsible for the mass of the fermions and the misalignment between gauge and mass eigenstates in the quark sector after the Higgs field gets a VEV. The last term in (2) is the Higgs potential:

$$V(H) = m_H^2 H^\dagger H + \lambda \left(H^\dagger H\right)^2 \tag{4}$$

Field	$SU(3)_C$	$SU(2)_L$	$U(1)_Y$
$\ell = \begin{pmatrix} \nu \\ e \end{pmatrix}$	1	2	$-\frac{1}{2}$
$\bar{e}$	1	1	$+1$
$q = \begin{pmatrix} u \\ d \end{pmatrix}$	3	2	$-\frac{1}{6}$
$\bar{u}$	3	1	$-\frac{2}{3}$
$\bar{d}$	3	1	$+\frac{1}{3}$
G^a_μ	8	1	0
W^a_μ	1	3	0
B_μ	1	1	0
H	1	2	$+\frac{1}{2}$

Table 1 – Particle content of the SM with their charges under the group $SU(3)_C \times SU(2)_L \times U(1)_Y$. We use two component spinors for the SM chiral fermions so the bar on $\bar{e}, \bar{u}, \bar{d}$ is only a label for the field names and does not denote any conjugation. The Dirac spinor is given by: $\Psi_e = (e\ \bar{e}^\dagger)^T$. The first five fermion fields carry a familly index $i = 1,2,3$.

The crucial feature of the Higgs potential is that the parameter m_H^2 is negative, leading to the famous "Mexican hat" potential with a minimum at a non-zero Higgs field value. The Higgs VEV is then $\langle H^\dagger H \rangle = v^2/2$ with the tree-level relation $v^2 = -m_H^2/\lambda$.

At renormalizable level, the SM has 19 parameters, which can be chosen as follows: 3 gauge couplings, 9 quark and lepton masses, 3 quark mixing angles and 1 phase, 2 coefficients in the Higgs potential and the QCD θ angle.

The dimension-4 SM is very successful for describing all observed phenomena in various collider experiments. Precision measurements of electroweak parameters at the Z-pole and the W pair production threshold performed at LEP are in very good agreement with the SM predictions at the per mille level. At LHC, the Higgs boson behaves very much like the SM Higgs and its coupling to the heavy particles (t, b, W, Z) are the ones predicted by the SM with an experimental precision of around 10%. The fact that the renormalizable Lagrangian is enough to explain all experimental observations is a strong hint that our naive power counting is correct and $\Lambda_{\rm SM}$ is indeed large.

Furthermore, the SM explains elegantly the absence of processes like proton decay or $\mu \to e\gamma$ transitions: at renormalizable level, there is no operator breaking baryon number and the individual lepton number (e, μ, τ number). This is associated to the existence of symmetries called *accidental symmetries*. These processes can only go through higher dimensional operators and are suppressed by inverse powers of $\Lambda_{\rm SM}$.

The SM only hypothesis

In order to estimate limit of validity of the SM, one can look at higher dimensional operators and see what corrections they give to the SM. From dimentional analysis, if $\Lambda_{\rm SM}$ is large, leading corrections to the SM come from dimension-5 operators. At dimension-5, there is only one class of operator one can build out of SM fields, the Weinberg operator [1]:

$$\mathscr{L}_{\rm SM}^{(D=5)} = \frac{c_{ij}}{\Lambda_{\rm SM}} (\ell_i \cdot H)\left(\ell_j \cdot H\right) + c.c. \tag{5}$$

where the dot denotes contraction of $SU(2)_L$ indices with an epsilon tensor. This operator breaks lepton number by two units and after EWSB gives a Majorana mass to the neutrinos of order $m_\nu \sim v^2/\Lambda_{\rm SM}$. Neutrino masses are very small but non-zero as shown from neutrino oscillation experiments. In the SM, the smallness of neutrino masses is explained by the fact that their mass term is generated at dimension-5 and is suppressed by a factor $v/\Lambda_{\rm SM}$. Today, bounds from particle physics and cosmological observations limit the neutrino masses to be below 1 eV or so. Assuming the coefficients c_{ij} to be of order one, this leads to an estimate $\Lambda_{\rm SM} \sim 10^{14}$ GeV.

At dimension-6, there are many more operators. Among them, one can construct operators violating baryon number (for example $O_1^{\Delta B} = \epsilon_{abc} u_a d_b \left(q_c^\dagger \cdot \ell^\dagger\right)$ where a, b, c are colour indices) with coefficients suppressed by $\Lambda_{\rm SM}^2$. The most stringent test of baryon number conservation comes from the non-observation of proton decay; with the proton lifetime measured to be larger than 10^{34} years [2]. A rough dimensional analysis estimate of the proton lifetime gives $\Gamma \sim m_p^5/\Lambda_{\rm SM}^4$ and comparing it to the experimental bound results in a cutoff scale larger than $\Lambda_{\rm SM} \sim 10^{16}$ GeV.

These two observations, based on accidental symmetries of the dimension-4 SM, support the scenario where the Lagrangian (2) remains a very good description of microcospic phenomena up to a very high energy scale $\Lambda_{\rm SM} \sim 10^{14} - 10^{16}$ GeV, at least 10 orders of magnitude beyond the reach of our most powerful colliders. The theory above the cutoff could be a grand unified theory, or a theory of quantum gravity (the effects of gravity become important at the Planck mass $M_P \sim 10^{19}$ GeV). This is called the "SM only" scenario or sometimes the "desert" because there is no new particle between the electroweak scale $v \sim 100$ GeV and the cutoff scale $\Lambda_{\rm SM}$.

Direct exploration at LHC has, up to now, revealed no signal of unknown particle up to around 1 TeV (the precise bound on new particles depend on the details of the model considered). Also, electroweak precision observables measured at LEP are consistent with SM predictions at the per mille level, showing no sign of new physics at the TeV scale.

Other experimental measurements at lower energies of processes that are suppressed in the SM also give credit to a high cutoff scenario. Flavour-changing neutral current (FCNC) are very small in the SM because of the CKM structure in the quark sector (GIM mechanism) but receive contribution at dimension-6 from four-fermion operators. Examples include meson rare decays such as $K \to \pi\nu\bar{\nu}$, $K^0 - \overline{K}^0$ oscillations and other neutral meson-antimeson oscillations.

Comparing the experimental measurements to the SM prediction and the contribution of dimension-6 operators with generic order 1 coefficients leads to an estimate of the cutoff scale larger than $10^7 - 10^8$ GeV for the most precise measurements (from Δm_K and ϵ_K, see for example [3]).

All these experimental results suggest that the SM cutoff is very large. Of course, these constraints on $\Lambda_{\rm SM}$ can be relaxed if we allow for the coefficients c_i to be small. But the main advantage of the SM only scenario with a large $\Lambda_{\rm SM} \sim 10^{14} - 10^{16}$ GeV is that all experimental results listed above, baryon and lepton number conservation, smallness of the neutrino masses and of FCNC, can be explained by dimensional analysis only and without invoking some UV structure that cause the c_i's to be small. However, having $\Lambda_{\rm SM} \gg m_H$ leads to a theoretical problem, the famous *Hierarchy problem*.

The Hierarchy problem

It is interesting to note that there is only one dimensionful parameter in the renormalizable SM Lagrangian, namely m_H^2. This parameter is directly linked to the Higgs VEV v and from there gives mass to all other particles in the theory. Experimentally, $m_H^2 \sim (100\text{ GeV})^2$, but we would rather expect from dimensional analysis $m_H^2 \sim \Lambda_{\rm SM}^2$. If new particles with mass M_* at the cutoff scale couple (even indirectly) to the Higgs boson, they generate a correction to its mass $\delta m_H^2 \propto M_*^2$ resulting in δm_H^2 being 30 orders of magnitude or so (for a mass of 10^{16} GeV) bigger than m_H^2. The Higgs mass is quadratically sentitive to the heaviest particle that it couples to and keeping m_H^2 small requires a delicate cancellation between very large contributions, also called *fine-tuning*.

In order to remove the sensitivity of the Higgs mass to the highest scale in the theory, one needs new physics at the electroweak scale (from 100 GeV up to 10 TeV depending on the models) and thus requires $\Lambda_{\rm SM}$ to be small. But now the accidental symmetries are not explained by dimensional analysis alone and one must impose some structure to the model in order to comply with experimental bounds. So there is a tension between naturalness, which requires $\Lambda_{\rm SM} \sim m_H$ and the simple dimensional analysis explanation of the SM accidental symmetries, which support $\Lambda_{\rm SM} \gg m_H$.

A first popular solution to the Hierarchy problem is Supersymmetry, the introduction of a new space-time symmetry that links bosons and fermions. The Higgs boson is associated with a fermionic partner, the Higgsino, and in the $m_H^2 \to 0$ limit, the theory gains a new symmetry namely the chiral symmetry of the Higgsino. Thus corrections to m_H^2 remain proportional to m_H^2 and the Higgs remains naturally light. However, Supersymmetry is not observed in nature so it must be broken at some scale above the electroweak weak with superpartners not too heavy to avoid fine-tuning in the Higgs mass. In these models, it is easy to write terms violating baryon and lepton number and one must impose a global symmetry to forbid these terms.

Another solution is given by the class of Composite Higgs models. A strongly interacting sector with a global symmetry G confines at a scale f above the electroweak scale, breaking G to a subgroup H, resulting in a number of Goldstone bosons. The SM gauge interactions also break the H symmetry, giving a mass to the Goldstone bosons, some of which are identified with the Higgs doublet. Here the Higgs mass is protected by the shift symmetry of the Goldstones. The generic prediction of Composite Higgs models is the presence of numerous resonances at a mass $m_* = g_* f$ where g_* is the coupling of the new gauge group, similarly to mesons and baryons in QCD.

Other possible solutions to the Hierarchy problem include a dynamical evolution to a small m_H^2 term (the relaxion model [4]) or the presence of a very large number of SM-like sectors (N-naturalness [5]).

Other problems of the SM

There are other problems that motivate the presence of physics beyond the Standard Model (BSM). Here we present a few of them.

Dark matter: another very important issue in the SM is the absence of a suitable dark matter (DM) candidate. The existence of DM is strongly supported by astrophysical and cosmological observations with a cosmic abundance about 5 times higher than ordinary baryonic matter. DM is non-luminous (hence its name), almost non-interacting with ordinary matter, stable and subject to gravitational interaction. There is a priori no reason for DM to be linked to the electroweak scale and a wide range of mass scales is possible. But a simple way to explain the observed DM density is through the "freeze-out" mechanism: the DM candidate is weakly interacting with the SM and in thermal equilibrium with the SM particles until the expansion of the universe makes the process DM DM $\rightarrow$ SM too faint. At this point, the DM density freezes and is affected only by the cosmological evolution. It turns out that a particle with SM weak coupling (from the $SU(2)_L$ gauge group) needs a mass around 1 TeV to reproduce the correct DM density. This scenario is called weakly interacting massive particle (WIMP) and points towards new physics at the TeV scale, suggesting a link between DM and the Hierarchy problem. The neutralino in the MSSM is an attractive DM candidate of this class and will be presented in more details in chapter 1.

This is not the only explanation for the DM density, other mechanism and other models have been proposed, with a wide possible mass range. Other models do not require new particles but rely on new phases of QCD, or astrophysical compact objects. In any case, DM remains an important motivation for BSM physics and has led to a wide variety of models and of experimental effort to measure its properties.

The strong CP-problem: the SM Lagrangian contains all renormalizable operators made of SM fields and compatible with the SM symmetries. However, one of these operators is not observed experimentally, namely the QCD theta term: $\frac{\theta}{16\pi^2} G^a_{\mu\nu} \tilde{G}^{a\mu\nu}$ where G is the gluon

field strength and $\tilde{G}^{a\mu\nu} = \epsilon^{\mu\nu\rho\sigma} G^a_{\rho\sigma}$. From the limits on the neutron electric dipole moment measurements, one can infer $\theta < 10^{-10}$. The question of why the theta term is so small is the strong CP-problem. The most popular solution to this problem is to promote this parameter to a field, the Peccei-Quinn axion, and explain its small value by a dynamical evolution. If the original solution of Peccei and Quinn has been ruled out, similar models are still being considered and axion-like particles could be DM candidates.

Baryogenesis: the SM augmented with cold dark matter and the cosmological constant explains well the observations from the cosmic microwave background. But why does our universe contains baryons and not anti-baryons? In principle the SM contains the three sufficient Sakharov conditions for baryogenesis but in practice the source of CP-violation is too small and the electroweak phase transition is not first-order. Thus baryogenesis requires new physics and could be linked to the electroweak symmetry breaking if the asymmetry was generated at the electroweak phase transition.

Experimental anomalies: on the experimental side, there are a few measurements in tension with the predictions of the SM. Belle, BaBar and LHCb have detected some deviations from lepton flavour universality predicted by the SM [6]. The ratios $R_{D^{(*)}} = \frac{\Gamma(B\to D^{(*)}\tau\nu)}{\Gamma(B\to D^{(*)}\ell\nu)}$ and $R_{K^{(*)}} = \frac{\Gamma(B\to K^{(*)}\mu^+\mu^-)}{\Gamma(B\to K^{(*)}e^+e^-)}$ deviate from the SM predictions by $2.5\sigma - 4\sigma$. The ratio cancels a good part of the hadronic uncertainties and the anomalies were observed by several experiments over several years. These results have also driven much theoretical and experimental work, suggesting new physics coupling primarily to the second and third generations. However, the significance of these deviations is still debated in the community.

Another long-standing anomaly is the measurement of the muon and electron anomalous magnetic moment a_μ and a_e. These are measured and predicted in QED with an impressive precision (of 10^{-10} for a_e). Combined with an independent measurement of the fine structure constant α from Rydberg constant, one finds a_e smaller than the SM prediction by 2σ and a_μ larger than the SM prediction by 3.5σ. This also points to new physics breaking lepton universality but it is difficult to build a realistic model addressing both anomalies at once. Also, the theoretical uncertainties associated to the calculations are still debated.

One can also mention the proton radius puzzle, two different measurements of the proton radius diagreeing by 5 to 7σ. The first one uses electrons (spectroscopy and scattering) and the second one uses muons (muonic hydrogren spectroscopy), hinting to lepton non universality.

The search for BSM physics

On the one hand, the problems presented above are compelling arguments for the existence of new physics, in particular above the weak scale at the TeV scale. This logic has lead to the building of the LHC and has motivated numerous BSM models. On the other hand, despite a few intriguing anomalies, experimental results and precision tests of the SM support a high SM cutoff. The challenge on BSM model building is to find solutions to the problems of

the SM without spoiling the successes of the model, namely the accidental symmetries, the suppressed flavour-changing neutral currents, the electroweak precision tests.

There are two main directions for the search of BSM physics. The first one, which until now led to the discovery of the heavy quarks, the W, Z and Higgs boson, is the *energy frontier*. New physics consists of new heavy particles of mass M_* and have not been detected yet because of insufficient collider energy. The method to search for new physics is to access higher energies E with larger, more energetic colliders. Either the new particle can be produced on-shell and detected directly, or one can look for deviations from the SM. Indirect effects of new heavy particles are described by higher dimensional operators and their effect grow like powers of $\frac{E}{M_*}$. The energy frontier approach is linked to the Hierarchy problem and also to DM in the case of WIMP-like models.

The second direction, called the *intensity frontier*, is to consider new physics not as heavy particles but as dark particles, meaning with a very feeble interaction ϵ to SM particles. In this case, new particles have not been detected because their effects are suppressed by powers of the coupling ϵ. Direct searches of new physics are done with experiments with very high luminosity (typically on-target collisions) and indirect searches are performed with very precise measurements where small deviations from the SM can be measured. Many models of DM fall into this class, as well as axion-like particles.

Plan of the thesis

In this thesis, we will explore some topics in the quest for BSM physics at the energy and the intensity frontier. In chapter 1 we consider two well known DM models of electroweak WIMP coming from Supersymmetry, the Higgsino and the Wino. We consider the charged neutral mass splitting as a free parameter of the model. We study the effect of Sommerfeld enhancement, a non perturbative effect coming from the long range interaction due to the exchange of electroweak gauge bosons, and its dependence to the value of the splitting. We derive a few generic features of Sommerfeld enhancement and work out its consequence on the DM phenomenology.

In chapter 2 we consider a class of models with new particles interacting very weakly with the SM. We study the discovery potential of a fixed target experiment using the experimental setup of a future muon collider. We first present the phenomenology of the three classes of renormalizable interactions between a dark sector carrying no SM charges and our sector. We then show the expected exclusion limits from this experiment for the three models, the dark photon, the dark Higgs and the heavy neutral lepton.

In chapter 3, we take a more model-independent approach to new physics. If new physics is heavy, its effects are encoded in higher dimensional operators made of SM fields. Then, one can study the effects of these operators and set limits on their coefficients. These limits can then be translated to concrete BSM models by matching to the SM effective field theory. In

our work, we allow all operators to be present at the same time and we do not impose any flavour structure, leading to a large number of free coefficients. We compile experimental data from low-energy experiments to LEP electroweak precision tests and obtain constraints on 61 Wilson coefficients.

1 Sommerfeld enhancement and WIMP phenomenology

The nature of dark matter has been one of the longstanding problems of modern physics. There are compelling arguments for the existence of DM, coming from astrophysics (galactic rotation curves and gravitational lensing) and from cosmology. The most precise measurement of the DM density in the universe comes from the Planck observation of the cosmic microwave background (CMB). The fit of CMB data to the ΛCDM model yields the result [7]:

$$\Omega_{\mathrm{DM}} h^2 = 0.120 \pm 0.001 \tag{1.1}$$

From the particle physics point of view, DM cannot be one of the SM particles and calls for some new physics explanation. One popular class of model is the weakly interacting massive particle (WIMP): a new neutral and stable particle is added to the SM and the DM relic density is produced by the freeze-out mechanism. In the early universe, the DM particle is in thermal equilibrium with the SM. The expansion of the universe dilutes its density until the annihilation probability becomes too small, at which point the two sectors decouple and the density of DM "freezes". The calculation of the DM density with the freeze-out mechanism is described in appendix A. At leading order, the DM density depends only on the annihilation cross-section to SM particles and in order to reproduce the result (1.1), one needs a cross-section of $\langle \sigma\beta \rangle \approx 3 \times 10^{-26}\ \mathrm{cm}^3\mathrm{s}^{-1}$. It turns out that for a particle with SM weak interactions, one needs a mass around $M \sim 1$ TeV to get the correct $\langle \sigma\beta \rangle$, suggesting that the DM candidate has a link with the solution to the Hierarchy problem.

In Supersymmetry, one has to enforce a global symmetry to forbid baryon and lepton number violating terms. One consequence is that the lightest supersymmetric particle (LSP) is stable, making it an interesting DM candidate. The neutralino of the minimal supersymmetric Standard Model (MSSM) is the prime example of a WIMP DM. Despite null results in the search for supersymmetric particles at LHC, the neutralino WIMP is still a valid DM model, its high mass of a few TeV making it hard to produce at colliders.

This large separation of scales between the DM mass M and the weak force carrier mass

m_W, m_Z leads to a non-perturbative enhancement of the annihilation cross-section in the non-relativistic limit. This well-known effect is called Sommerfeld enhancement and can be interpreted as the effect of the long range interaction between the DM pair by the exchange of light gauge bosons. Sommerfeld enhancement is very dependent of the DM velocity β which makes it very important so the present day annihilation cross-section (with galactic velocities $\beta \sim 10^{-3}$) to SM particles which can be detected by telescopes (indirect detection signals). Sommerfeld enhancement is also dependent of the mass splitting δm between the charged and the neutral component of the DM multiplet, this mass splitting controlling how easily a neutral DM pair can flip to a charged pair by $W^{\pm}$ exchange and feel the Coulomb attractive potential.

In this chapter, we consider two well studied benchmark models of electroweak WIMPs: the DM doublet (also called Higgsino) and the DM triplet (or Wino) that can be seen as two limits of the MSSM parameter space. In these models, the DM candidate is a massive fermion in the TeV mass range charged under the weak interaction. The charged neutral splitting δm gets a contribution from electroweak loop corrections as well as a model-dependent contribution from heavier particles in the theory. In the litterature, the latter contribution is usually neglected and δm is set to the loop value. In this work, we consider the mass splitting as a free parameter and study its effect on the DM phenomenology, the relic density calculation and the bounds from indirect detection.

In this chapter, we will start in section 1.1 with a description of Sommerfeld enhancement and give some analytic properties in simple cases. In section 1.2, we present the minimal supersymmetric standard model (MSSM) and the Higgsino and Wino limit. The DM candidate and its properties in the Higgsino case are presented in section 1.3 and in section 1.4 in the Wino case. To finish, we detail the effect of changing the mass splitting δm on the relic density and on indirect detection in section 1.5 before concluding. This chapter is largely taken from the publication [8].

1.1 Sommerfeld enhancement

1.1.1 Definition

This is the enhancement of the short-distance cross section for a process due to the distortion of the wave function for the incoming state by a long-range potential. This effect increases with decreasing velocity, and was first noticed by Sommerfeld [9] in the context of electromagnetism. It has a classical gravitational analogue in the low-velocity enhancement of the cross section for a point particle hitting a massive object of radius R [10]:

$$\sigma = \pi R^2 \left(1 + \frac{\beta_{esc}^2}{\beta^2}\right) \tag{1.2}$$

where β is the velocity of the point particle and $\beta_{esc} = 2G_N M/R$ is the escape velocity from the surface of the extended object.

In quantum field theory it can be seen as the enhancement due to ladder diagrams in which a light force-carrier is exchanged. For non-relativistic muon annihilation for example, the amplitude for the n^{th}-order ladder diagram (due to n photon exchanges between the muon pair) is proportional to $(\alpha/\beta)^n$ in the non-relativistic limit, which means the perturbative expansion in α breaks down for small enough velocity, and the ladder diagrams must be systematically resummed. As shown in [11] the Sommerfeld factor can be determined by factorizing the short-distance and long-distance behaviour. The distorting effect of the long-range potential $V(r)$ on the two-particle wavefunction is computed by solving the Schrödinger equation in the presence of only this potential, and the total enhancement then computed by perturbing around the resulting inhomogeneous solution at leading order in the absorptive part, which encodes the short-distance behaviour. The same procedure was proved in [12] to be equivalent to explicit resummation of the ladder diagrams.

Two particles subject to a long-range potential $V(|\vec{r}|)$, satisfy the following Schrödinger equation in the centre-of-mass frame, where $\psi(\vec{r})$ is the two-particle wavefunction:

$$\frac{-1}{2\mu}\nabla^2\psi(\vec{r}) + V(|\vec{r}|)\psi(\vec{r}) = \frac{1}{2}\mu\dot{\vec{r}}^2\psi(\vec{r}) \tag{1.3}$$

with μ is the reduced mass of the system.

Separating variables to isolate the radial and angular parts as usual, we obtain, for two particles of equal mass $m_1 = m_2 = M$, with velocity β in the centre-of-mass frame[1], the following radial equation:

$$-\frac{1}{M}\frac{1}{r^2}\frac{d}{dr}\left(r^2\frac{dR}{dr}\right) + \left(\frac{l(l+1)}{Mr^2} + V(r) - M\beta^2\right)R = 0 \tag{1.4}$$

To isolate the dominant (s-wave) contribution, we take $l = 0$; substituting $R(r) = \chi(r)/r$ we obtain

$$\chi''(r) + \left(M^2\beta^2 - M\,V(r)\right)\chi(r) = 0\,. \tag{1.5}$$

This equation cannot be solved analytically for general potentials $V(r)$, but we can solve numerically for the irregular solution, which satisfies the boundary conditions:

$$\chi(0) = 1,\ \chi'(\infty) = -iM\beta\chi(\infty) \tag{1.6}$$

and then compute the Sommerfeld-enhanced cross section as

$$\sigma \equiv S\sigma_0 = \frac{|\chi(\infty)|^2}{|\chi(0)|^2}\sigma_0 \tag{1.7}$$

where σ_0 is the perturbative cross-section and S denotes the Sommerfeld enhancement

[1] We use the velocity β such that in the non-relativistic limit we have the Mandelstam variable $s = 4M^2 + 4M^2\beta^2 + O(\beta^4)$

factor.[2]

This method can be generalized to the case where there is an interaction that mixes distinct two-particle states. For N two-particle states $\chi_i(r)$, with $i = 1, \cdots, N$, the Sommerfeld enhancement can be computed by numerically solving the following set of N coupled radial Schrödinger equations:

$$\chi_i''(r) + M^2\beta^2\chi_i(r) - M\sum_j V_{ik}^{\rm tot}(r)\chi_k(r) = 0 \tag{1.9}$$

N times, with a different boundary condition at $r = 0$ each time, representing each distinct two-particle state participating in the short-distance interaction: $\chi_i(0)|_j = \delta_{ij}$ for the $j^{\rm th}$ solution. The boundary condition at infinity corresponds to a pure outgoing (decaying) wave for $(M\beta^2 - V(r\to\infty))$ positive (negative). Here all energies/potentials are defined with respect to the lightest two-particle state, consisting of two identical particles of mass M. Any mass differences with respect to the lightest state show up as additional radius-independent contributions to the total potential. [3]

The cross-section in the $i^{\rm th}$ channel is then given by:

$$\sigma_i = c_i(A.\Gamma.A^\dagger)_{ii} \tag{1.10}$$

where Γ_{jk} is the absorptive part of the two-to-two cross section $\chi_j \to \chi_k$, with j,k running over all possible two-particle states in each channel. c_i is a numerical factor that accounts for the different normalization of the two-body wavefunctions for identical and non-identical particles: $c_i = 2$ ($c_i = 1$) when the two particles are identical (distinct). The matrix A is computed as:

$$A_{ij} = \lim_{r\to\infty} \frac{\chi_i(r)|_j}{e^{i\sqrt{M(M\beta^2 - V_{ii}(\infty))}\,r}}\,. \tag{1.11}$$

We can also define a Sommerfeld factor in each channel i, in analogy with the unmixed case:

$$S_i = c_i\frac{(A.\Gamma.A^\dagger)_{ii}}{\Gamma_{ii}}. \tag{1.12}$$

Note that unlike in the unmixed case the mixed Sommerfeld factor is not only dependent on the potential, but also on the Γ matrix for the hard process of interest.

In practice, for mixed channels we must solve for the Sommerfeld factor numerically. The

[2] This procedure was shown in [10] to be equivalent to finding the regular solution and computing the enhancement using

$$S = \left|\frac{\frac{d\chi}{dr}(0)}{k}\right|^2 \tag{1.8}$$

[3] Note that for states χ_i with mass $M+\delta m_i$, β is *not* the physical initial velocity of the particle, but is defined such that the total energy of the heavy-particle pair with respect to the dark-matter pair is $E = M\beta^2$. The Sommerfeld enhancement calculation takes into account that the state χ_i cannot exist as an asymptotic state for $M\beta^2 < \delta m_i$.

numerical stability of the solution is an issue in the multi-state scenario, since the presence of an exponentially decaying part in the charged-charged wavefunction (due to the charged-neutral mass difference) makes the solution particularly unstable to rounding errors. Special care must be taken in the numerical recipe in order to favour convergence. We use the variable phase method, as detailed in [13].

1.1.2 Some analytical considerations

The electroweak potentials that we will consider have three individual constituents that combine in a complex way: the Coulomb interaction, the Yukawa interaction due to weak gauge boson exchange, and a mass splitting between different sets of asymptotic states. The effect on the Sommerfeld factor of each of these components individually can be understood analytically. Following [14], we will review these arguments below in order to build some intuition before we move on to tackle the full electroweak case in Section 1.3 and after.

Pure Coulomb potential

We first consider the scattering of a pair of particles of mass M and velocity β in their centre-of-mass frame interacting via a Coulomb potential $V(r) = \pm\alpha/r$, where the Sommerfeld factor can be computed analytically [10, 15]:

$$S = \left| \frac{\mp\frac{\pi\alpha}{\beta}}{1 - e^{\pm\frac{\pi\alpha}{\beta}}} \right|. \tag{1.13}$$

The enhancement is determined by the relative significance of the Coulomb binding energy $\alpha^2 M$ of the incoming particles and their kinetic energy $M\beta^2$, and is large when the binding energy dominates. Hence the Sommerfeld factor is independent of the particle mass M (as expected from dimensional analysis), and grows for small β with α/β for an attractive potential (in practice the arbitrary growth at small β will be cut off by finite temperature effects, when the photon acquires a thermal mass). On the other hand, for large velocities, S approaches unity as expected. For a repulsive potential it gives rise to an exponential suppression, due to the presence of a Coulomb barrier:

$$\lim_{\beta\to 0} S \sim \begin{cases} \frac{\pi\alpha}{\beta} & \text{attractive } V \\ \frac{\pi\alpha}{\beta} e^{-\frac{\pi\alpha}{\beta}} & \text{repulsive } V \end{cases} \tag{1.14}$$

Pure Yukawa potential

The enhancement due to a Yukawa potential $V(r) = \pm\frac{\alpha}{r} e^{-M_V r}$, arising from the exchange of a massive gauge boson of mass M_V, can only be treated analytically by approximating the

Yukawa potential as a Hulthén potential:

$$V(r) = \pm\alpha \frac{kM_V e^{-kM_V r}}{1 - e^{-kM_V r}} \tag{1.15}$$

where k is a fudge factor chosen phenomenologically to match the short- and long-range behaviour of the Yukawa potential ($k = \frac{\pi^2}{6}$ for s-wave enhancement [16]). The Sommerfeld factor can be expressed in closed form [14, 16, 17]:

$$S = \mp\frac{\pi\alpha}{\beta} \frac{\sinh\left(\frac{2\pi M}{kM_V}\beta\right)}{\cosh\left(\frac{2\pi M}{kM_V}\beta\right) - \cos\left(\frac{2\pi M}{kM_V}\beta\sqrt{\mp\frac{kM_V}{M}\frac{\alpha}{\beta^2} - 1}\right)} \tag{1.16}$$

The Yukawa form of the potential brings into play another relevant quantity: the size of the Bohr radius, $(\alpha M)^{-1}$ relative to the range of the potential M_V^{-1}; thus the Sommerfeld enhancement depends on two parameters: α/β and $\alpha M/M_V$. S displays different behaviour as β goes to zero:

$$\lim_{\beta\to 0} S \sim \begin{cases} k\left(\frac{\alpha}{\beta}\right)^2 \frac{M_V}{\alpha M} & \text{attractive } V,\ M = n^2\frac{kM_V}{\alpha} \quad \text{for integer } n \\ \frac{2\pi^2}{k}\frac{\alpha M}{M_V}\left(1 - \cos\left(2\pi\sqrt{\frac{\alpha M}{kM_V}}\right)\right)^{-1} & \text{attractive } V, \text{ non-resonant M} \\ \frac{2\pi^2}{k}\frac{\alpha M}{M_V}\left(\cosh\left(2\pi\sqrt{\frac{\alpha M}{kM_V}}\right) - 1\right)^{-1} & \text{repulsive } V \end{cases} \tag{1.17}$$

Unlike that for the Coulomb potential, the Sommerfeld factor for an attractive Yukawa potential tends to a constant as β approaches zero, except for specific values of M where the denominator of (1.17) vanishes, and the Sommerfeld factor undergoes even faster growth, as $1/\beta^2$. These values of M correspond to instances where the Hulthén potential admits zero-energy bound states. For a repulsive Yukawa potential, the Sommerfeld factor tends to a constant smaller than one, and there is no resonant structure. The resonances are also observed in numerical computation of the Sommerfeld factor in the Yukawa potential and are not specific to the Hulthén potential. Their position can be estimated using equation (1.17).

For larger values of β, the hyperbolic functions simplify and $S \sim \pi\alpha/\beta$ as in the electromagnetic case. The transition between the two regimes happens around $\beta \sim M_V/M$ [10], where the de Broglie wavelength of the particle becomes of order the range of the Yukawa interaction, and the particle begins to probe the short-range nature of the potential. See Figure 1.1 for a graphical display of the behaviour of Sommerfeld factor for an attractive Yukawa potential as a function of β/α, for $M_V(\alpha M)^{-1} = 0.2$ (solid green curve), as compared with the growth for an on-resonance mass, $M = M^* = kn^2 M_V/\alpha$ (solid yellow curve).

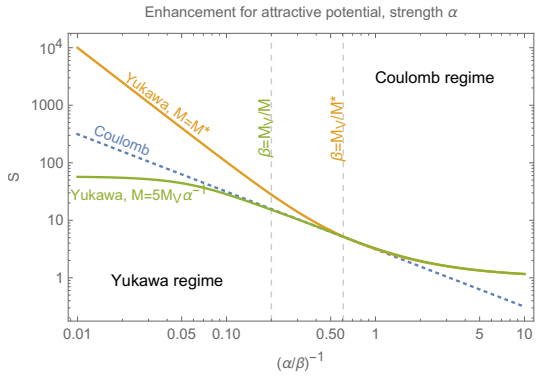

Figure 1.1 – Sommerfeld enhancement for an attractive Yukawa potential, showing both off-resonance saturation for $M_V(\alpha M)^{-1} = 1/5$ (solid green curve), and on-resonance growth for $M = M^* = kn^2 M_V/\alpha$ (solid yellow curve). The enhancement for a pure Coulomb potential is shown for comparison (dashed blue line). For further explanation of symbols, see text.

1.1.3 Mass splitting

The introduction of a mass splitting δm between the incoming state and a nearby state with which it mixes has two important consequences. Above some threshold velocity

$$\beta_{\rm th} = \sqrt{2\frac{\delta m}{M}}\,, \tag{1.18}$$

a pair of incoming states can scatter inelastically to a pair of heavy partners on-shell, giving the light states access to a new, perhaps stronger, annihilation channel. More crucial to our narrative, however, are the large enhancements that can occur at particular velocities below the heavy-particle threshold, due to threshold production of loosely-bound resonances of the heavy partner pair, lying between the light and heavy states in the mass spectrum. For a resonance with binding energy E_B, the corresponding resonant velocity can be written as:

$$\beta^* = \sqrt{\frac{2\delta m - E_B}{M}} \tag{1.19}$$

In the electroweak case, approximating the binding energy E_n of the nth bound state as being purely due to the Coulomb interaction to leading order, we expect to see corresponding peaks in the Sommerfeld factor in the neutral channel at velocities:

$$\beta_n^* = \sqrt{\frac{2\delta m}{M} - \frac{\alpha^2}{4n^2}} \tag{1.20}$$

The physically-relevant parameter encoding the splitting is then $\delta m/E_B$. The enhancement due to these below-threshold resonances was observed in [14, 18, 19], but their possible effects on the phenomenology of dark matter were not explored.

1.1.4 Mixed electroweak potential

We will be concerned with a two-component non-relativistic potential, due to mixing between the charged (DM^+DM^-) and neutral (DM^0DM^0) components of the dark matter multiplet, that takes the following schematic form:

$$V = \begin{pmatrix} \delta m + V_C + V_Y & V_Y \\ V_Y & V_Y \end{pmatrix} \tag{1.21}$$

where V_C, V_Y denote the Coulomb and Yukawa potentials, with coupling strength scaling like α and α_L, respectively. The combined effect on the Sommerfeld factor will result in different behaviour in different velocity regimes, as follows:

- High β, $\beta \gg \frac{m_W}{M}, \beta_{th}$: in this regime we can neglect the mass splitting and trust the analytical expressions for the Sommerfeld factor. The Yukawa contribution is of order $S_L \sim \pi\alpha_L/\beta$ and the electromagnetic contribution is of order $S_{\text{em}} \sim \pi\alpha/\beta$ and since $\alpha_L > \alpha$ we expect the Yukawa potential to dominate.

- Intermediate β, $\frac{m_W}{M} > \beta > \beta_{\text{th}}$: in this regime we can also neglect the mass splitting. Off resonance, the Yukawa contribution goes to a constant of order $S_L \sim \alpha_L M/m_W$ while the electromagnetic contribution continues to grow like $S_{\text{em}} \sim \pi\alpha/\beta$, so we expect the electromagnetic attraction to dominate. On resonance however, the Yukawa contribution behaves like $1/\beta^2$ and is the dominant one.

- Low β, $\beta < \beta_{\text{th}}$: the δm term in the potential dominates. In charged channels, the Sommerfeld factor is zero by construction because an initial on-shell charged pair cannot have an energy below $2(M + \delta m)$ (see footnote 3). Just below threshold the neutral channels exhibit resonant enhancement due to Coulomb bound states of DM^+DM^-. As β decreases still further, the weak Yukawa potential dominates. The Sommerfeld factor is growing like $1/\beta^2$ at masses where there is a zero-energy resonance and saturating to a constant away from the resonance as in equation (1.17), with the size of the enhancement set by the distance from the resonance.

We illustrate this behaviour in figure 1.2, left panel where we plot the Sommerfeld factors (S_1 and S_2, respectively, as defined in equation (1.12) and computed for the total annihilation matrix) for the 2×2 Wino potential (given below in equation (1.50)) for different Wino masses, on and off resonance. By construction, the charged-charged Sommerfeld factor S_1 is zero below the pair-production threshold for the charged state, β_{th} given by (1.18). We expect the enhancement in this channel to grow with decreasing $\chi^\pm$ velocity due to the Coulomb potential; this growth will be cut off by the non-Coulomb components of the interaction.

We see clearly the low β behaviour of the neutral-neutral Sommerfeld factor S_2: on resonance $M^* = 2.37$ TeV, S_2 grows with decreasing β to very high values. Away from resonance, the Sommerfeld factor goes to a constant as predicted by equation (1.17).

Also visible in this figure is the enhancement at specific velocities just below to the charged particle threshold, due to production at threshold of Coulomb 'bound states' of a charged DM pair. The true location of the peaks will depend on the energy levels of the bound states in the full electroweak potential. For Winos and Higgsinos with nominal mass splitting, the Coulomb resonances are squeezed in a narrow range of velocity just below the charged particles threshold, where the Sommerfeld factors display a complicated pattern of peaks and dips. The peaks can be large but are rather narrow in velocity [4]. Thus we expect the physical annihilation cross-section in the neutral channel to be enhanced at velocities just below the charged-particle threshold. We will come back to this point in our discussion of the Higgsino Sommerfeld factors below.

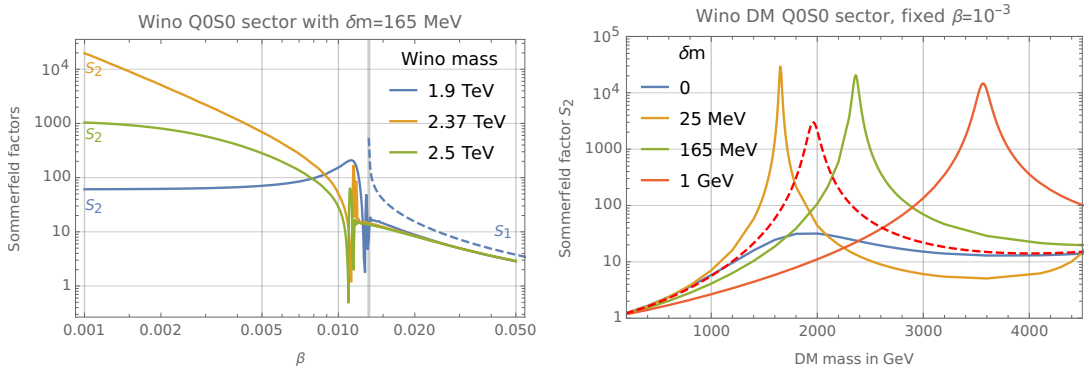

Figure 1.2 – Sommerfeld factors for a pure Wino state. Left panel: Sommerfeld factors in the neutral (solid) and charged (dashed) channels as a function of DM velocity for various masses around to $M^* = 2.37$ TeV, the position of the first zero-energy bound state. The charged-neutral splitting δm is fixed at the nominal electroweak-loop value, setting the position of the Coulomb resonances around $\beta \sim 0.01$. Right panel: Sommerfeld factor in the neutral channel computed at fixed velocity ($\beta = 10^{-3}$) as a function of Wino mass for varying splitting charged-neutral δm. We see that the resonant mass M^* at which there is a zero-energy bound state varies with δm. We also show the analytical result for $\sin\theta_W \to 0$ and zero splitting for comparison (dashed line).

These Coulomb peaks are even more clear in figure 1.3, left panel where we plot the Sommerfeld factors S_1, S_2 against velocity β for a 1.1 TeV Higgsino with small splitting $\delta m = 9.5$ MeV (the potential is given below in equation (1.44)) and we zoom in on the region around the charged-pair threshold (depicted as a solid black line). This allows us to clearly resolve the first three Coulomb resonances. The naive predictions for the velocities at which they are excited (using the pure Coulomb binding energies as in Equation (1.20)) are marked with vertical dashed lines, and are remarkably accurate. For the Wino this is not the case, the simple Coulomb approximation being off by approximately 20%. This is understandable in light of the larger weak Casimir factors that the Wino is subject to, being a triplet of $SU(2)_L$. A better approximation for the Coulomb resonances could be obtained by numerically solving the

[4] Here the tiny width of the resonance is due to decays of the Coulomb resonance to $\chi_0\chi_0$ only, and doesn't include decays to SM final states

mixed Sommerfeld equation for the bound states.

Another consequence of the mass splitting δm and the electromagnetic interaction is to shift the position of the Yukawa resonance naively predicted by equation (1.17). In figure 1.2, right panel we plot the analytical approximation to the Wino Sommerfeld enhancement at fixed, small velocity $\beta = 10^{-3}$ as a function of Wino mass. For comparison we also show the numerical results for the full electroweak potential for various choices of charged-neutral splitting, δm. The zero-energy bound states appear clearly as peaks in the Sommerfeld factor S_2. We see that varying the mass splitting shifts the position of these peaks to different values of the DM mass, away from the resonance position estimated using equation (1.17). The dependence of the resonant mass on the splitting can be understood using perturbation theory [20].

The Sommerfeld factors for the pure Higgsino display similar features, see figure 1.3. The right panel shows a similar plot of the Sommerfeld factor in the neutral-neutral channel with varying Higgsino mass, at a fixed $\beta = 10^{-3}$ and for different splittings, with the analytical result in the zero-hypercharge limit shown as a dashed red line. We observe the same phenomenon of shifting the position of the resonance as δm varies.

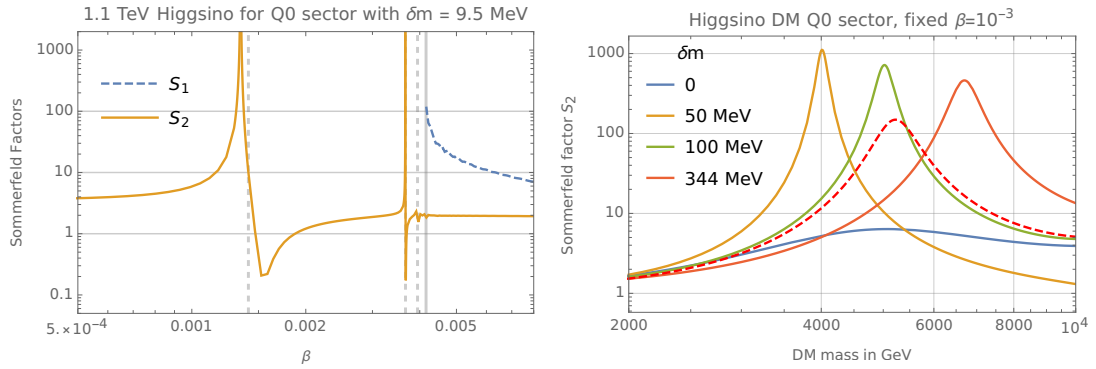

Figure 1.3 – Sommerfeld factors for a pure Higgsino. Left panel: zoom around the threshold region for a 1.1 TeV thermal relic Higgsino with splitting $\delta m = 9.5$ MeV. The solid grey line indicates the charged particle pair-production threshold β_{th} and the grey dashed lines show the predicted positions of the first three Coulomb resonances using (1.20). Right panel: Sommerfeld factor in the neutral channel computed at fixed velocity ($\beta = 10^{-3}$) as a function of Higgsino mass for varying charged-neutral splitting δm. The analytical result for $\sin\theta_W \to 0$ and zero splitting is shown for comparison (dashed line).

1.2 MSSM and MDM

Supersymmetry postulates the existence of a new symmetry relating bosons and fermions. Schematically, one adds to the Poincaré algebra the operators Q and $Q^\dagger$ which turn a bosonic state into a fermionic state and vice versa. Particles in a supersymmetric theory fall into irreducible representations of the supersymmetric algebra called supermultiplets, containing

an equal number of fermionic and bosonic degrees of freedom called superpartners of each other. For a more detailed introduction to supersymmetry, we refer to the reviews [21, 22].

Given the SM particle content, in order to build the minimal supersymmetric standard model (MSSM), one must add superpartners to each SM particle, doubling the spectrum. A chiral fermion and a superpartner complex scalar fied (called sfermion) form a chiral supermultiplet. For example in the lepton sector of the SM, the chiral fermions ν_L, e_L, e_R are associated to the three complex scalars (the sleptons) $\tilde{\nu}_L, \tilde{e}_L, \tilde{e}_R$ (here L, R are just part of the field name and do not denote any kind of projection) to form the supermultiplets L containing $(\tilde{\nu}_L, \tilde{e}_L)$ and (ν_L, e_L) with $SU(2)_L \times U(1)_Y$ charge $(2, -\frac{1}{2})$ and $\bar{e}$ containing $\tilde{e}_R^*$ and $e_R^\dagger$ with charge $(1, +1)$. The gauge bosons form with spin $\frac{1}{2}$ Majorana fermions called gaugino a gauge supermultiplet. Finally, the Higgs field is also embedded into a chiral supermultiplet with a fermionic Higgsino. However, in order to reproduce the SM Yukawa terms and to preserve anomaly cancellation, one needs two Higgs supermultiplets H_u and H_d with respective charges $(2, \frac{1}{2})$ and $(2, -\frac{1}{2})$.

Supersymmetry solves the hierarchy problem because now when m_H goes to zero the theory gains a new symmetry, chiral symmetry for the massless Higgsino. The chiral symmetry protecting the Higgsino mass is transfered to the Higgs mass by supersymmetry. In a diagrammatic language, the loop corrections to the Higgs mass quadratically sensitive to the UV scale are exactly cancelled by equal and opposite loop corrections from superpartners (at least when supersymmetry is unbroken).

The non gauge interactions in the MSSM are encoded in the superpotential:

$$W_{\text{MSSM}} = \bar{u} y_u q \cdot H_u - \bar{d} y_d q \cdot H_d - \bar{e} y_e \ell \cdot H_d + \mu H_u \cdot H_d \tag{1.22}$$

where y_u, y_d, y_e are 3×3 matrices in family space and the dot denotes contraction of $SU(2)_L$ indices with the epsilon tensor. The first three terms reproduce the SM Yukawa interactions and the last term gives a mass to the Higgs and Higgsinos. However, there are other terms that one can write down in the superpotential which are gauge-invariant and analytic in the superfields. These are:

$$\ell_i \cdot \ell_j \bar{e}_k, \quad \ell_i \cdot q_j \bar{d}_k, \quad \ell \cdot H_u, \quad \bar{u}_i \bar{d}_j \bar{d}_k \tag{1.23}$$

and they all break either lepton number or baryon number by one unit. These terms are constrained experimentally to be extremely small (for example from proton decay experiments). This is a clear disadvantage of the MSSM over the SM where baryon and lepton number conservation arise from an accidental symmetry of the dimension-4 Lagrangian. In order to forbid these terms, one enforces a new global symmetry called "matter parity" with the associated multiplicative quantum number defined as $P_M = (-1)^{3(B-L)}$. Quark and leptons have $P_M = -1$ while all other superfields have $P_M = 1$ so that the superpotential (1.22) conserves matter parity while the terms (1.23) all break matter parity. Matter parity is often written in terms of the equivalent "R-parity" defined as $P_R = (-1)^{3(B-L)+2s}$ where s is the spin of the particle. Then one can see that all SM particles have $P_R = 1$ and all superpartners have $P_R = -1$.

Imposing matter parity or R-parity has an important phenomenological consequence: the lightest particle with $P_R = -1$, or lightest supersymmetric particle (LSP) is stable. If the LSP is neutral, it makes a natural DM candidate. In the MSSM, adding R-parity to conserve baryon and lepton number seems artificial from the theory point of view, but has the advantage of providing a viable DM candidate. In this chapter, we will study a scenario where the LSP is the neutralino, a mixed state between the Higgsino and the Gaugino.

The last ingredient for a realistic theory is the breaking of supersymmetry: we do not observe sfermions with the same mass as SM fermions so supersymmetry must be broken at some scale Λ. There are several proposed mechanism for supersymmetry breaking, however one can be ignorant about the precise mechanism and parametrize its effects in soft terms, non supersymmetric operators built of MSSM fields with dimension less than 4. We do not list all the possible soft terms here, but they include sfermion masses, gaugino masses, trilinear terms. In all generality, there are 105 physical parameters in the MSSM, most of them coming from the soft terms. Not specifying the supersymmetry breaking mechanism introduces a lot of arbitrariness in the theory.

In conclusion, the MSSM is an attractive model for the following reasons:

- The MSSM gives a solution to the hierarchy problem by introducing a new symmetry.
- In the R-parity conserving limit, it has a natural DM candidate.

However, the MSSM also suffers from other problems:

- The absence of signal from any superpartner at LHC pushes the limit of sparticle masses higher and higher. If the superpartners are too heavy, this reintroduces some fine-tuning in the Higgs mass. Taking only the top squark and the scalar stops, one has schematically $\delta m_H^2 \sim m_{\tilde{t}}^2$ from the loops of top quarks and stops and becomes problematic if $m_{\tilde{t}} \gg m_H$. This is sometimes refered to as the little hierarchy problem.
- The Z mass is given in the MSSM by some combination of μ and the soft masses m_{H_u}, m_{H_d}. But μ is a supersymmetry-preserving parameter and m_{H_u}, m_{H_d} come from the supersymmetry breaking, so we would expect the hierarchy $\mu \gg m_{H_u}, m_{H_d} \gg m_Z$ again resulting in fine-tuning. This "μ-problem" can be solved by adding a new chiral superfield S in a model called the next to minimal supersymmetric standard model (NMSSM).
- There are sources of flavour violation outside of the SM Yukawa terms for example in the soft squark masses. One has to impose more structure in order to keep flavour changing neutral currents as small as observed experimentally. Also individual lepton numbers are in general not conserved (they are broken by soft slepton masses). Here also, more structure has to be imposed to comply with experimental bounds.

1.2.1 The neutralino and chargino sector

The two Higgs doublets are composed of the fields: $H_u = (H_u^+, H_u^0)$ and $H_d = (H_d^0, H_d^-)$. In the scalar Higgs sector, the two charged Higgs field do not get a vacuum expectation value (VEV), only the two neutral scalars do: $\langle h_u^0 \rangle = v_u/\sqrt{2}$ and $\langle h_d^0 \rangle = v_d/\sqrt{2}$ with $v_u^2 + v_d^2 = v^2 = (246\,\text{GeV})^2$ the parameter measured from G_F. One usually introduces the parameter $\tan\beta = \frac{v_u}{v_d}$.

The scalar Higgs sector contains 8 real degrees of freedom, 3 are Goldstone bosons so there remains 5 physical real scalars, usually denoted h^0, H^0, A^0 and $H^\pm$.

In the fermionic sector of the MSSM, the neutral Higgsinos $\tilde{H}_u^0$ and $\tilde{H}_d^0$ mix with the neutral electroweak gauginos $\tilde{B}, \widetilde{W}^0$ to form four neutralinos, and the charged components of the Higgsinos and Wino also mix, yielding two charginos. In the gauge eigenstate basis $\psi_{\tilde{N}} = \left(\tilde{B}, \widetilde{W}^0, \tilde{H}_u^0, \tilde{H}_d^0\right)$, the neutralino mass matrix is [22]:

$$M_{\tilde{N}} = \begin{pmatrix} M_1 & 0 & -c_\beta s_W m_Z & s_\beta s_W m_Z \\ 0 & M_2 & c_\beta c_W m_Z & -s_\beta c_W m_Z \\ -c_\beta s_W m_Z & c_\beta c_W m_Z & 0 & -\mu \\ s_\beta s_W m_Z & -s_\beta c_W m_Z & -\mu & 0 \end{pmatrix} \tag{1.24}$$

where M_1, M_2 are the soft gaugino masses for $\tilde{B}, \widetilde{W}$; μ comes from the superpotential and the remaining terms are fixed by the gauge interactions. In order to avoid large CP-violating effects in the Higgs sector, we restrict ourselves to real mass parameters μ, M_1, M_2 but we allow for one non-trivial relative sign between them.

The chargino mass matrix in the gauge-eigenstate basis $\psi_{\tilde{C}} = \left(\widetilde{W}^+, \tilde{H}_u^+, \widetilde{W}^-, \tilde{H}_d^-\right)$ is, in block form:

$$M_{\tilde{C}} = \begin{pmatrix} 0 & X^T \\ X & 0 \end{pmatrix} \quad \text{where} \quad X = \begin{pmatrix} M_2 & \sqrt{2} s_\beta m_W \\ \sqrt{2} c_\beta m_W & \mu \end{pmatrix} \tag{1.25}$$

At tree level, the chargino masses can be computed explicitly:

$$m^2_{\tilde{C}_1, \tilde{C}_2} = \frac{1}{2}\left[|M_2|^2 + |\mu|^2 + 2m_W^2 \mp \sqrt{\left(|M_2|^2 + |\mu|^2 + 2m_W^2\right)^2 - 4|\mu M_2 - m_W^2 \sin 2\beta|^2} \right] \tag{1.26}$$

In order to have a viable neutalino DM candidate, one needs the lightest neutralino $\tilde{N}_1$ to be the LSP and in particular $m_{\tilde{N}_1} < m_{\tilde{C}_1}$. In what follows, we will detail two commonly studied limits of the MSSM gaugino sector, the Higgsino limit and the Wino limit, and study the phenomenology of the DM candidate.

1.2.2 The Higgsino limit

The Higgsino limit correspond to taking the limit $M_1, M_2 \to \infty$ such that the Wino and Bino decouple leaving two neutralinos and one chargino state remaining. This corresponds to keeping only the mass term $-\mu \tilde{H}_u \cdot \tilde{H}_d$ in the fermionic sector and giving infinite soft masses

to the Wino and Bino. In this limit, the theory gains an additional $U(1)_{\tilde{H}}$ symmetry leading to Higgsino number conservation. The two weak doublets $\tilde{H}_u$ and $\tilde{H}_d$ have opposite Higgsino number and can be combined into a single Dirac doublet χ with mass μ and Higgsino number +1. We choose χ to have positive hypercharge +1/2 such that it contains a positive and a neutral state: $\chi = \left(\chi^+, \chi^0\right)^T$. In four components notation, the Lagrangian simply reads:

$$\mathscr{L}_{\text{doublet}} = i\bar{\chi}\not{D}\chi - \mu\bar{\chi}\chi \tag{1.27}$$

which corresponds to a vector-like doublet added to the SM with only one additional parameter, the mass μ. This mass will be fixed by the DM relic density (see section 1.3) and is around 1 TeV.

The mass of the charged state M_{χ^+} and the mass of the neutral state M_{χ^0} are not exactly equal beacuse $SU(2)_L$ is broken: loop corrections to the wave-function renormalization from γ and Z boson are different for the charged and neutral state. At one loop, the resulting mass splitting is [23]:

$$\delta m_{\text{EW}} = M_{\chi^+} - M_{\chi^0} = \frac{\alpha M}{2\pi}\int_0^1 dx\,(1+x)\log\left(1+\frac{1-x}{x^2}\frac{m_Z^2}{M^2}\right) \underset{M\gg m_Z}{\rightarrow} \frac{\alpha m_Z}{2\pi} \tag{1.28}$$

where $M = \mu$ is the doublet mass. In the limit we are interested in, namely $\mu \gg m_Z$ this integral reduces to $\delta m_{\text{EW}} = \alpha m_Z/2\pi = 344$ MeV (we use the value of $\alpha(m_Z)$ for the numerics). We will refer to this value of the mass splitting $\delta m = 344$ MeV coming only from electroweak effects as the *nominal splitting*.

There is another source of mass splitting in the MSSM coming from the large but finite value of the soft masses M_1, M_2. After integrating out the heavy Wino and Bino at tree-level, we obtain the dimension-5 operators:

$$\mathscr{L}_{\text{eff}} = \frac{g_Y^2}{4M_1}(h_u^*\tilde{H}_u - h_d^*\tilde{H}_d)^2 + \frac{g_L^2}{4M_2}(h_u^*\sigma^a\tilde{H}_u + h_d^*\sigma^a\tilde{H}_d)^2 + c.c. \tag{1.29}$$

from which, after setting the scalar Higgses to their VEVs, we get the following masses:

$$m_{\tilde{N}_{1,2}} = |\mu| - \frac{\sin 2\beta}{2}\frac{\mu}{|\mu|}\left(\frac{m_Z^2 s_W^2}{M_1} + \frac{m_W^2}{M_2}\right) \pm \frac{1}{2}\left|\frac{m_Z^2 s_W^2}{M_1} + \frac{m_W^2}{M_2}\right| + O\left(\frac{m_W^2}{|M_1|^2}, \frac{m_W^2}{|M_2|^2}\right) \tag{1.30}$$

$$m_{\tilde{C}_1} = |\mu| - \sin 2\beta\frac{\mu}{|\mu|}\frac{m_W^2}{M_2} + O\left(\frac{m_W}{|M_2|^2}\right) \tag{1.31}$$

The tree-level mass splitting between the lightest chargino and lightest neutralino is given by

$$\delta m_{\text{tree}} = m_{\tilde{C}_1} - m_{\tilde{N}_1} = \frac{\sin 2\beta}{2}\frac{\mu}{|\mu|}\left(\frac{m_Z^2 s_W^2}{M_1} - \frac{m_W^2}{M_2}\right) + \frac{1}{2}\left|\frac{m_Z^2 s_W^2}{M_1} + \frac{m_W^2}{M_2}\right| + O\left(\frac{m_W^2}{|M_1|^2}, \frac{m_W^2}{|M_2|^2}\right) \tag{1.32}$$

at leading order in m_W/M_1, m_W/M_2. From the equation, one can see that this contribution

can be positive or negative. When M_1 and M_2 have opposite sign, they partially cancel in the absolute value and the contribution can be negative for parameters in the region:

$$-M_2 \tan^2\theta_W \frac{1+\sin 2\beta}{1-\sin 2\beta} < M_1 < -M_2 \tan^2\theta_W \frac{1-\sin 2\beta}{1+\sin 2\beta} \tag{1.33}$$

This region is the entire quadrant $M_1 < 0$, $M_2 > 0$ when $\tan\beta = 1$ and narrows to the line of equation $M_1 = -M_2 \tan^2\theta_W$ as $\tan\beta$ goes to infinity. We plot in figure 1.4 the value of δm as function of M_1, M_2 for different values of $\tan\beta$, adding both the loop contribution (1.28) and the MSSM contribution (1.32). For a fixed value of M_2, the extreme values of equation (1.32) are $\delta m_{\text{tree}} = \pm \frac{m_W^2}{M_2}$ corresponding to ± 1.6 GeV for $M_2 \sim 4$ TeV.

For the doublet χ to be a suitable DM candidate, the mass splitting δm must be positive so that the charged component χ^+ is unstable and decays to the stable χ^0 component (protected by R-symmetry). In what follows, we will consider δm as a free parameter. In the MSSM case one can have the mass splitting varying in the range [0, 2 GeV] and the DM candidate behaving as a pure Higgsino doublet.

Note that finite M_1, M_2 break the $U(1)_{\tilde{H}}$ symmetry, generating a mass splitting between the two neutral Majorana states:

$$\delta m_0 = M_{\tilde{N}_2} - M_{\tilde{N}_1} = m_Z^2 \left| \frac{s_W^2}{M_1} + \frac{c_W^2}{M_2} \right| + O\left(\frac{m_W^2}{|M_1|^2}, \frac{m_W^2}{|M_2|^2} \right) \tag{1.34}$$

which is of the same order than the charged neutral splitting δm. This makes the neutral component a pseudo-Dirac fermion and will have important consequenses for direct detection (we will develop this point in section 1.3). For all other processes, we will neglect this splitting and treat χ^0 as a Dirac fermion.

1.2.3 The Wino limit

The Wino limit on the other hand corresponds to taking the parameters μ, M_1 to infity, decoupling the Bino and Higgsino from the theory and leaving only the Wino $\widetilde{W}^a$, the superpartners of the $SU(2)_L$ gauge bosons. They form a triplet of $SU(2)_L$ with zero hypercharge, giving a neutral and two charged Majorana states. We will also use the chage eigenstates (χ^+, χ^0, χ^-) with $\chi^\pm = \frac{1}{\sqrt{2}}(\widetilde{W}^1 \mp \widetilde{W}^2)$. The Lagrangian is simply:

$$\mathscr{L}_{\text{triplet}} = i(\widetilde{W}^a)^\dagger \bar{\sigma}_\mu \partial^\mu \widetilde{W}^a - \frac{M_2}{2}\widetilde{W}^a \widetilde{W}^a + c.c. = i(\chi^a)^\dagger \bar{\sigma}_\mu \partial^\mu \chi^a - \frac{M_2}{2}\chi^0\chi^0 - M_2\chi^+\chi^- + c.c. \tag{1.35}$$

with identical tree-level mass for the charged state and the neutral state. This mass will be fixed by the relic density with the result $M_2 = 2.9$ TeV.

Similarly to the Higgsino case, this mass degeneracy is broken by loop corrections from γ and

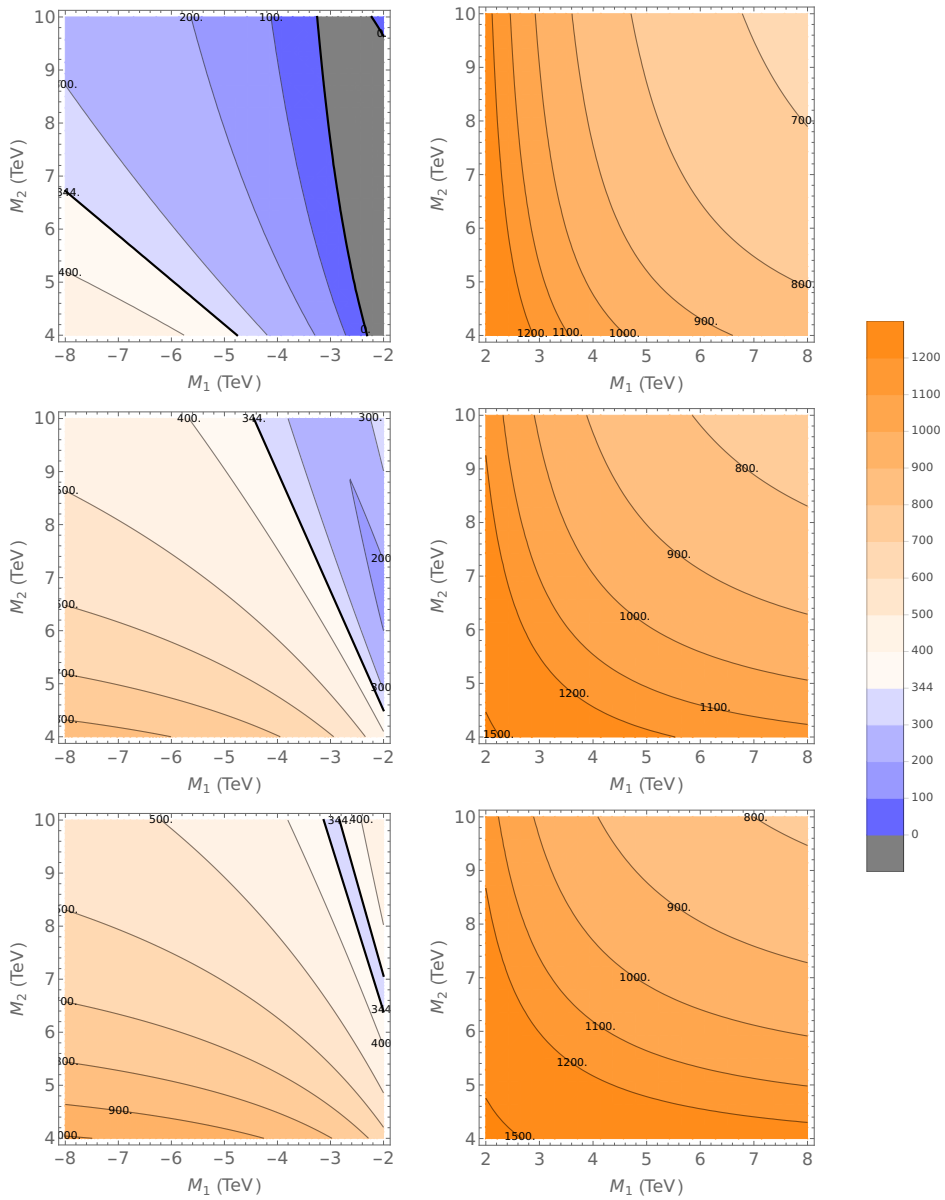

Figure 1.4 – Contours of the total charged-neutral mass splitting $\delta m = \delta m_{\text{EW}} + \delta m_{\text{tree}}$ (see equations (1.28) and (1.32)), in MeV, in the pure Higgsino limit of the MSSM as a function of M_1 and M_2, for $\tan\beta = 3$ (top), $\tan\beta = 10$ (middle) and $\tan\beta = 80$ (bottom).

Z. The resulting mass splitting is, in the $M_2 \gg m_Z$ limit [24]:

$$\delta m_{\rm EW} = \alpha_L m_W \sin^2 \frac{\theta_W}{2} = 165\,{\rm MeV} \tag{1.36}$$

We will also refer to this value as the nominal splitting for the triplet.

For finite values of μ, $M_1 \gg M_2$, we can integrate out the Higgsino and Bino at tree-level to obtain the effective Lagrangian

$$\mathscr{L}_{\rm eff} = -\frac{g_L^2}{2\mu} h_u^* \cdot h_d^* \widetilde{W}^a \widetilde{W}^a + \frac{g_L^2 g_Y^2}{2M_1\mu^2} \left(h_u^* \cdot (h_d^* \sigma^a) \widetilde{W}^a\right)^2 \tag{1.37}$$

Setting the scalars to their VEVs, we get the following masses:

$$m_{\tilde{N}_1} = M_2 - \frac{m_W^2}{\mu} \sin 2\beta - \frac{m_W^4}{\mu^2 M_1} \sin^2 2\beta \tan^2 \theta_W \qquad \text{and} \qquad m_{\tilde{C}_1} = M_2 - \frac{m_W^2}{\mu} \sin 2\beta \tag{1.38}$$

Unlike the doublet, here the mass splitting is only affected by the dimension seven operator making it much smaller. Explicitly:

$$\delta m_{\rm tree} = m_{\tilde{C}_1} - m_{\tilde{N}_1} = \frac{m_W^4}{\mu^2 M_1} \sin^2 2\beta \tan^2 \theta_W \tag{1.39}$$

which can be positive or negative, depending on the sign of M_1. However it is numerically negligible in front of the electroweak contribution, for $\mu, M_1 \sim 4$ TeV, one gets $\delta m_{\rm tree} \sim 0.1$ MeV.

For values of the mass parameters such that M_2 is smaller than M_1, μ but of the same order, the DM candidate remains very Wino-like because all mixing terms in the mass matrix 1.24 are proportional to $m_W \ll M_2, M_1, \mu$. The contribution of a heavier neutralino i to the relic density calculation will be suppressed by a factor $\exp\left(-\frac{M_i - M_2}{T_F}\right)$ with $T_F \sim 100$ GeV the freeze-out temperature and can be neglected for $M_i - M_2 \sim 500$ GeV. The mass splitting however goes like m_W^4 divided by differences of M_2, M_1, μ to the cube, resulting in larger values of δm compared to the previous paragraph. In the MSSM, the DM candidate can be very close to a pure Wino with the contribution to δm from heavy states comparable to the electroweak value for $M_2 = 2.9$ TeV (computed in the following section) and m_1, μ in the $3.3 - 3.5$ TeV range.

1.2.4 Minimal dark matter point of view

One can also consider the Higgsino and Wino models from the minimal dark matter (MDM) perspective [24, 25]. The minimum addition to the SM in order to have a DM candidate is a scalar or fermion multiplet of $SU(2)_L$ containing a neutral particle. A fermion doublet must have hypercharge $Y = \pm 1/2$ so only a Dirac doublet is possible, giving the Higgsino model. The Wino model is the Majorana triplet with zero hypercharge. Other models with higher multiplets or different charge assignments is also possible. These models have in common that after specifying the new multiplet, there is only one additional parameter, the DM mass,

and it is fixed by requiring that the model reproduces the correct relic abundance.

In these models, the stability of the DM candidate must be enforced by hand by a global symmetry (equivalent to R-parity in the MSSM). Also the mass splitting is fixed and equal to the electroweak contribution given above. In order to treat δm as an additionnal parameter, one must invoke new physics contributing to the DM mass. One can parametrize the effects of such new states by higher dimensional operators.

In the Higgsino case, there are two such operators at dimension-5:

$$\mathscr{L}_{D=5} = c_1 H^\dagger H \bar{\chi}\chi + c_2 H^\dagger \frac{\sigma^a}{2} H \bar{\chi} \frac{\sigma^a}{2} \chi \tag{1.40}$$

the first one being a shift of the doublet mass and the second one giving rise to the mass splitting:

$$\delta m = M_{\chi^+} - M_{\chi^0} = \frac{c_2 v^2}{2} = \frac{c_2 m_W^2}{2 g_L^2} \tag{1.41}$$

which could be as large as 2 GeV for a new physics mass $M_* \sim 4$ TeV with generic coupling $g_* \sim 1$.

For the Wino, the first operator affecting the mass splitting is of dimension-7:

$$c_3 \left(H^\dagger \frac{\sigma^a}{2} H \chi^a \right)^2 + \text{c.c.} \tag{1.42}$$

resulting in a mass splitting:

$$\delta m = M_{\chi^\pm} - M_{\chi^0} = 2 c_3 \frac{m_W^4}{g_L^4} \tag{1.43}$$

In order to have a contribution to the mass splitting comparable to the electroweak loop value, one has to allow for strongly coupled new physics close to the Wino scale.

1.3 Higgsino DM

In this section, we will review the phenomenology of the DM candidate in the Higgsino model, including Sommerfeld enhancement. The mass splitting here is fixed to the nominal value.

1.3.1 Sommerfeld enhancement

In the Higgsino model, the DM doublet χ carries a conserved DM number. The only process of DM annihilation to SM particles is the following: $\chi\bar{\chi} \to$ SM. Since the doublet has two states, there are four possible initial states $\chi^+\chi^-$, $\chi^+\bar{\chi}^0$, $\chi^0\chi^-$, $\chi^0\bar{\chi}^0$ and the Sommerfeld factor should be a 4×4 matrix. However, all these initial states do not mix through electroweak interactions and can be classified by the electric charge of the initial state.

The $Q=1$ sector include the initial states $\chi^+\bar{\chi}^0$ and $\chi^0\chi^-$ which do not mix with any other state and behave the same way being linked by charge conjugation. The $Q=0$ sector include the initial states $(\chi^+\chi^-, \chi^0\bar{\chi}^0)$ that can flip to one another via $W^\pm$ exchange. The nonrelativistic potential due to electroweak interactions is:

$$V_{Q=0} = \begin{pmatrix} 2\delta m - \alpha_{em}/r - \alpha_L(2c_W^2-1)^2 e^{-M_Z r}/4rc_W^2 & -\alpha_L e^{-m_W r}/2r \\ -\alpha_L e^{-m_W r}/2r & -\alpha_L e^{-m_Z r}/4rc_W^2 \end{pmatrix} \tag{1.44}$$

$$V_{Q=1} = \frac{\alpha_L}{r} e^{-m_Z r} \frac{2c_W^2-1}{4c_W^2} \tag{1.45}$$

and the corresponding 'annihilation matrices' Γ (the absorptive part of the two-to-two cross section, see (1.10)) for the s-wave ($l=0$) contribution are:

$$\Gamma_{Q=0} = \frac{\pi\alpha_L^2}{128M^2} \begin{pmatrix} 31+4t_W^2+43t_W^4 & -22-4t_W^2+43t_W^4 \\ -22-4t_W^2+43t_W^4 & 31+4t_W^2+43t_W^4 \end{pmatrix}$$
$$\Gamma_{Q=1} = \frac{\pi\alpha_L^2}{64M^2}(25+4t_W^2) \tag{1.46}$$

where we have used the shorthand notation $c_W = \cos\theta_W$ and $t_W = \tan\theta_W$.

Analytic approximation

We can try to get some understanding of the Sommerfeld factors in the Higgsino case by simplifying the potential (1.44)-(1.45) and using the analytical approximations detailed in section 1.1.

We know that in the relic density calculation, freeze-out happens around $x \sim 25$ corresponding to a peak in the velocity distribution around $\beta \sim 0.2$. For a TeV Higgsino with order GeV splitting, the threshold for $\chi^+\chi^-$ happens at around $\beta_{\text{th}} \sim 2\times10^{-2}$ so we can safely neglect δm in front of the electroweak potential. Also we expect the $SU(2)_L$ potential to dominate, since $g_L > g_Y$ and we are before the point where the Sommerfeld factor from a Yukawa potential begins to saturate. So we will take the limit $\delta m \to 0$ and $\sin\theta_W \to 0$ in the potential (1.44). In this simple limit, the potential matrix in the $Q=0$ sector can be diagonalized:

$$V_{Q=0}(r) = R \begin{pmatrix} \frac{1}{4} & 0 \\ 0 & -\frac{3}{4} \end{pmatrix} R^T \frac{\alpha_L}{r} e^{-M_W r} \quad \text{where} \quad R = \frac{1}{\sqrt{2}} \begin{pmatrix} 1 & 1 \\ -1 & 1 \end{pmatrix} \tag{1.47}$$

yielding one attractive channel and one repulsive channel. Then we can use the approximate analytical result (1.16) to estimate the Sommerfeld factors.

The largest Sommerfeld factors come from attractive potential so the important channel is the attractive one with effective coupling $\frac{3}{4}\alpha_L = 0.025$. We can estimate the Higgsino mass at which a divergent Sommerfeld factor is predicted using equation (1.17) and we get the first resonance at $M = \frac{4km_W}{3\alpha_L} = 5.25$ TeV. When switching on $\sin\theta_W$ and δm, the position of the

resonance has to be computed numerically, see figure 1.3.

For the one dimensional potential (1.45), one can directly use the approximation (1.16) with $M_V = m_Z$ and $\alpha_{\text{eff}} = \alpha_L \frac{2c_W^2 - 1}{4c_W^2} = 0.006$, a repulsive Yukawa potential.

1.3.2 Relic density calculation

Neglecting the mass splitting and all SM particle masses with respect to the large dark matter mass M, we get the following tree-level annihilation cross-section in the center of mass frame, in the non-relativistic limit:

$$\sigma(\chi\bar{\chi} \to \text{SM}) = \frac{\pi}{256M^2\beta}\left[\left(81\alpha_L^2 + 12\alpha_L\alpha_Y + 43\alpha_Y^2\right) - \left(90\alpha_L^2 - 12\alpha_L\alpha_Y + \frac{158}{3}\alpha_Y^2\right)\beta^2 + O(\beta^4)\right] \tag{1.48}$$

where β is the dark matter velocity in the centre-of-mass frame of the annihilating states.

Using this annihilation cross-section and the formula in appendix (A.2), one finds that for $M = 1.1$ TeV, the Higgsino model reproduces the correct DM relic density.

Now we can use our analytic approximation of the Sommerfeld factors to compute the Higgsino relic density for different masses. The result is plotted on figure 1.5; we see that Sommerfeld enhancement is completely negligible at all masses. This is confirmed by the numerical calculation with the full potential but is not plotted on the figure because the three lines would be almost superimposed. In conclusion, Sommerfeld enhancement has a negligible effect on the relic mass of the nominal Higgsino DM with $\delta m = 344$ MeV, which remains unchanged at $M = 1.1$ TeV.

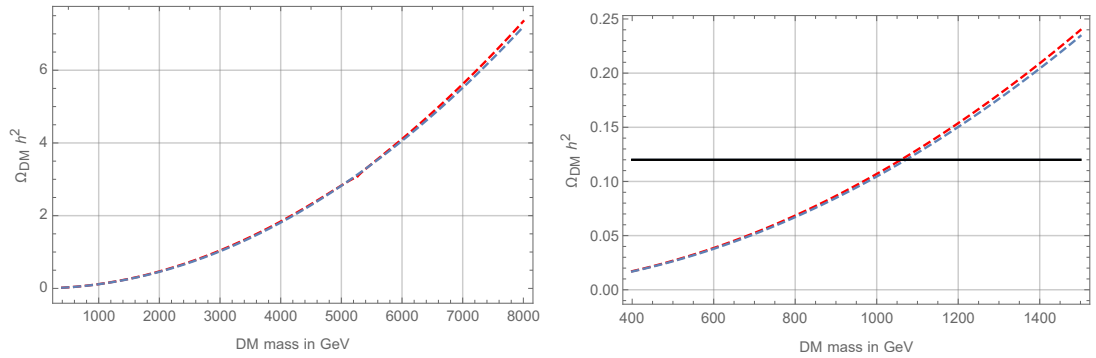

Figure 1.5 – Relic density for a thermal Higgsino as a function of Higgsino mass. We show the standard tree-level perturbative result for the $l = 0$ channel (blue dashed line), and the corresponding result including the non-perturbative effect computed using the analytical Sommerfeld factor in the $\sin\theta_W, \delta m \to 0$ limit (red dashed line), as described in the text.

In the previous paragraph, we predicted a resonance in the Sommerfeld factors at 5.25 TeV but it has no visible effect on figure 1.5. In the full potential, this resonance is located at 6.4 TeV but also has no effect on the relic density: the Sommerfeld factor becomes very large only at

low velocities where the thermal distribution is very suppressed.

1.3.3 Direct detection constraints

Because it has a non-zero hypercharge, the Higgsino doublet has a direct coupling to the Z boson and a scattering cross-section on nuclei around 10^{-39} cm^2, several orders of magnitude larger than the limits imposed by direct detection experiments [26]. This means that the MDM doublet model is completely excluded as a DM candidate.

A way around this is to assume that the neutral state χ^0 has a mass mixing with a neutral Majorana state that splits the Dirac fermion into two Majorana fermions χ_1 and χ_2. The lightest state χ_1 is the DM candidate and has no diagonal $Z\chi_1\chi_1$ coupling. This scenario occurs naturally in the MSSM where the neutral Higgsino components mix with the Bino and neutral Wino, resulting in the mass splitting (1.34). Then the direct detection process goes through the off-diagonal Z-coupling and is the inelastic reaction: $\chi_1 N \to \chi_2 N$. If $M_{\chi_2} - M_{\chi_1} \geq 350$ keV or so (depending on the nucleus), this process is kinematically forbidden and cannot be seen in direct detection experiments [27]. In the remainder of this work we will be assuming that such a neutral splitting is present, and is large enough to avoid direct detection constraints, but has a negligible effect on our Sommerfeld calculations. The effect of the neutral splitting on Sommerfeld enhancement is studied in [28].

1.3.4 Indirect detection constraints

At present day, only neutral Higgsino remain in the universe as DM so the process relevant for indirect detection is $\chi^0\bar{\chi}^0 \to$ SM. Today, the velocity of the DM halo in our galaxy is very low, around $\beta = 10^{-3}$ thus Sommerfeld effect is more important than in the relic case. However, we are in the very low velocity regime so we cannot trust the analytical approximation we used earlier.

In order to compute the cross-section to gauge boson, we separate the corresponding annihilation matrices:

$$\Gamma_{WW} = \frac{\pi\alpha_L^2}{16M^2}\begin{pmatrix}1 & 1\\ 1 & 1\end{pmatrix} \qquad \Gamma_{ZZ} = \frac{\pi\alpha_L^2}{32M^2\cos^4\theta_W}\begin{pmatrix}(1-2\sin^2\theta_W)^4 & (1-2\sin^2\theta_W)^2\\ (1-2\sin^2\theta_W)^2 & 1\end{pmatrix} \tag{1.49}$$

and the decay to photons happens only at loop level.

We find that Sommerfeld enhancement is important and give a large boost to the annihilation cross-section but it still remains a factor 20 or so below the HESS and Fermi limits.

1.4 Wino DM

1.4.1 Sommerfeld enhancement

In the Wino case, there is no notion of DM particle or antiparticle, the relevant annihilation cross-section is $\chi^a\chi^b \to$ SM. The triplet χ^a contains the states (χ^+,χ^0,χ^-) so there are 9 different possible initial states. Here also all initial pairs do not mix by exchange of electroweak gauge bosons and the potential can be split in five different sectors depending on the total charge Q and total spin S [25]:

- $S=0$, $Q=0$. (This is the only sector containing mixing between two different two-particle states $\chi^+\chi^-$ and $\chi^0\chi^0$):

$$\Gamma^{S=0}_{Q=0} = \frac{\pi\alpha_L^2}{9M^2}\begin{pmatrix} 3 & \sqrt{2} \\ \sqrt{2} & 2 \end{pmatrix} \qquad V^{S=0}_{Q=0} = \begin{pmatrix} 2\delta m - A & -\sqrt{2}B \\ -\sqrt{2}B & 0 \end{pmatrix} \tag{1.50}$$

- $S=1$, $Q=0$ ($\chi^+\chi^-$):

$$\Gamma^{S=1}_{Q=0} = \frac{25\pi\alpha_L^2}{36M^2} \qquad V^{S=1}_{Q=0} = 2\delta m - A \tag{1.51}$$

- $S=0$, $Q=1$ ($\chi^+\chi^0$ and $\chi^-\chi^0$):

$$\Gamma^{S=0}_{Q=1} = \frac{\pi\alpha_L^2}{9M^2} \qquad V^{S=0}_{Q=1} = \delta m + B \tag{1.52}$$

- $S=1$, $Q=1$ ($\chi^+\chi^0$ and $\chi^-\chi^0$):

$$\Gamma^{S=1}_{Q=1} = \frac{25\pi\alpha_L^2}{36M^2} \qquad V^{S=1}_{Q=0} = \delta m - B \tag{1.53}$$

- $S=0$, $Q=2$ ($\chi^+\chi^+$ and $\chi^-\chi^-$):

$$\Gamma^{S=0}_{Q=2} = \frac{\pi\alpha_L^2}{9M^2} \qquad V^{S=0}_{Q=2} = 2\delta m + A \tag{1.54}$$

where we have defined:

$$A = \frac{\alpha}{r} + \frac{\alpha_L c_W^2}{r}e^{-M_Z r} \qquad \text{and} \qquad B = \frac{\alpha_L}{r}e^{-M_W r} \tag{1.55}$$

The annihilation matrices Γ are the ones appearing in equation (1.10) and are computed in the limit of massless SM particles.

Analytical approximation

As in the Higgsino case, at velocities relevant for the relic density calculation we expect the Sommerfeld factors to be dominated by the $SU(2)_L$ part of the potential , and we can make an analytical estimate of the Sommerfeld factors in the limit $\sin\theta_W, \delta m \to 0$. In the $Q=0, S=0$ sector the potential matrix can be diagonalized:

$$V_{Q=0}^{S=0}(r) = R\begin{pmatrix}1 & 0\\ 0 & -2\end{pmatrix}R^T \frac{\alpha_L}{r}e^{-M_W r} \quad \text{where} \quad R = \frac{1}{\sqrt{3}}\begin{pmatrix}1 & \sqrt{2}\\ -\sqrt{2} & 1\end{pmatrix} \tag{1.56}$$

resulting again in one attractive channel and one repulsive channel. For all other sectors, we only take the $\delta m \to 0$ limit and approximate the Sommerfeld factor by the expression (1.16) optained for the Hulthén potential.

We can already estimate the position of the resonances in the different attractive sectors using equation (1.17). In the $S0Q0$ channel, the attractive Yukawa potential has an effective coupling $2\alpha_L$ so the first resonance is predicted to be at $M = \frac{km_W}{2\alpha_L} = 1.97$ TeV. In the $S1Q1$ channel, equation (1.17) gives: $M = 3.94$ TeV and in the $S1Q0$ channel $M = 5.81$ TeV. The first resonance in the $S0Q0$ sector is close to the value of the Wino DM mass predicted by the perturbative calculation and will be the most important one for Wino DM phenomenology.

When switching on the mass splitting δm, the position of the resonance shifts as shown in figure 1.2; in the nominal case $\delta m = 165$ MeV the resonance lies at a higher mass $M = 2.37$ TeV.

1.4.2 Relic density

For the triplet Wino DM, the total annihilation cross section to SM particles in the nonrelativistic limit (again neglecting SM masses and δm) is:

$$\sigma(\chi\chi \to \text{SM}) = \frac{\pi\alpha_L^2}{24M^2\beta}\left[37 - 20\beta^2 + O(\beta^4)\right] \tag{1.57}$$

Using only the perturbative result in the relic density calculation leads to a Wino relic mass $M = 2.2$ TeV.

We compute the Wino relic density as function of the DM mass and plot the result on figure 1.6, showing the perturbative calculation, the analytical approximation detailed above and the full numerical calculation (from [11]). We see that, unlike in the Higgsino case, Sommerfeld enhancement has an significant effect on the Wino relic density, of order 40 %. The difference with the Higgsino scenario comes from two features of the Wino model. First in the diagonalization of the potential matrices, we see that the attractive channel has a larger effective coupling in the Wino case than in the Higgsino case resulting in overall larger Sommerfeld factors. Second, the off-diagonal terms in the annihilation matrices are negative for the Higgsino and positive for the Wino; in other words interferences between the charged and neutral

channel are constructive for the Wino and destructive for the Higgsino. Including Sommerfeld effect moves the Wino relic mass to Wino DM mass to $M = (2925 \pm 15)$ GeV.

Moreover we see that the full numerical calculation and the analytical approximation are in excellent agreement except in the region around the resonance in the $S0Q0$ sector (located at $M = 2.37$ TeV for nominal $\delta m = 165$ MeV). The analytical formula underestimates the effect of the resonance on the annihilation cross-section but it has a visible effect only in a narrow window of one or two hundred GeV.

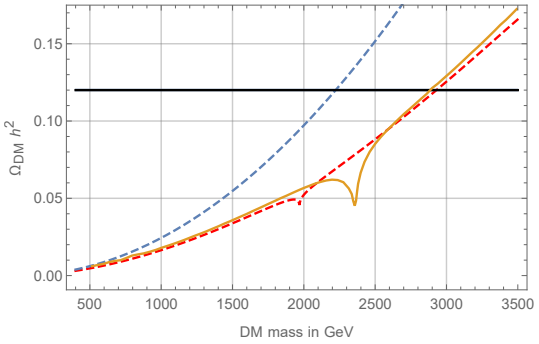

Figure 1.6 – Relic density for thermal Wino DM as a function of Wino mass. We show the standard tree-level perturbative result for the $l = 0$ channel (blue dashed line), and the corresponding result including the non-perturbative effect computed using the analytical Sommerfeld factor in the $\sin\theta_W, \delta m \to 0$ limit (red dashed line), as described in the text. The solid orange line shows the numerical result extracted from [11], corrected to include the one-loop running of the gauge couplings.

1.4.3 Direct detection

In the Wino model, the DM candidate χ^0 is a Majorana fermion and thus has no direct coupling to the Z-boson. It can upscatter to $\chi^\pm$ by exchange of a $W^\pm$ but the charged neutral mass splitting δm makes this process kinematically very suppressed. The lowest order scattering $\chi^0 N \to \chi^0 N$ where N is a nucleon is through a one-loop bow diagram with two W exchange. The resulting cross-section is still safely below experimental constraints.

1.4.4 Indirect detection

The current velocity of the DM halo in our galaxy is much smaller than the thermal velocity at freeze-out so Sommerfeld enhancement is even more important. In order to compute the present day annihilation to SM gauge bosons, we give the corresponding annihilation matrices [25]:

$$\Gamma_{WW} = \frac{\pi\alpha_L^2}{4M^2}\begin{pmatrix} 2 & \sqrt{2} \\ \sqrt{2} & 4 \end{pmatrix} \qquad \Gamma_{ZZ} = \frac{\pi\alpha_L^2}{M^2}\begin{pmatrix} \cos^4\theta_W & 0 \\ 0 & 0 \end{pmatrix} \tag{1.58}$$

The annihilation cross section for a pure Wino thermal relic with nominal splitting receives a

significant boost from Sommerfeld enhancement, due to its proximity to a zero-mass resonance, bringing it well above the bound from HESS, and comparable to that from Fermi-LAT. Note however that the HESS bound is computed using the Einasto profile for the halo density, which is cuspy towards the galactic centre, and using a cored profile would significantly relax this constraint [29].

1.5 Effect of the mass splitting

Instead of considering δm as fixed by the electroweak loop contribution, we treat it as a new parameter in the Higgsino and Wino model and investigate its effect on DM phenomenology. Its effect on the Sommerfeld factor can be important, especially at low velocities such as today's indirect detection process.

1.5.1 Changing the Higgsino mass splitting

Effect on the relic density

We have seen that the Sommerfeld effect in the relic density calculation is dominated by the $SU(2)_L$ part of the potential taking the $\delta m \to 0$ limit. Thus, as long as δm is negligible compared to the freeze-out temperature $T_F = M/x_F \sim 20$ GeV, its effect on the relic density calculation is negligible. This is true in the whole range of δm we are considering and we conclude that the Higgsino relic mass value $M = 1.1$ TeV is robust and changing the splitting from 0 to a few GeV does not change the relic calculation significantly. This is confirmed by explicit numerical calculation for different values of the mass splitting.

The main effect of changing the mass splitting is to shift the position of the resonance from the Yukawa attractive potential. In the nominal Higgsino case, it happens at $M = 6.4$ TeV. Decreasing the mass splitting brings the resonance lower in mass; however on resonance the boost in the Sommerfeld factor happens for velocities too low to significantly affect the thermal averaged cross-section at freeze-out.

Effect on indirect detection signal

In the absence of low-velocity resonances in the Sommerfeld factor, the enhancement saturates at a constant value and can be factorized out of the thermal average. The Sommerfeld-enhanced annihilation cross section can then be computed by simply multiplying the tree-level cross section by the value of the Sommerfeld factor at saturation. Provided saturation occurs above $\beta \sim 10^{-3}$, we will obtain equal annihilation cross section for both the galactic centre and dwarf galaxies [30]. In the presence of Coulomb resonances however, this is no longer the case, and we need to account for the spread in velocity of DM particles in calculating the thermally-averaged cross section. We do this by approximating the DM velocity as a thermal distribution, centred at $\beta = 10^{-3}$ ($x = 10^6$) for galactic signals, and $\beta = 5 \times 10^{-5}$

($x = 4 \times 10^8$) for dwarf spheroidals.

In contrast to the relic calculation, Sommerfeld enhancement gives a large boost to the present day annihilation cross-section of Higgsino DM to gauge bosons. From our previous discussion in section 1.1, the Sommerfeld factors will receive a large enhancement in one of two scenarios: first when the dark matter mass is close to the resonant mass where there is a zero-energy bound state due to the Yukawa potential (this is the case for the thermal Wino with nominal splitting); and second, for any dark matter mass, when a Coulomb resonance coincides with the central value for the corresponding dark matter velocity distribution.

The first scenario, bringing the Yukawa resonance down to the relic mass $M = 1.1$ TeV seems impossibile numerically (or requires very small splittings). The second scenario can only occur when the mass splitting is tuned to be of order the Coulomb binding energy. We can use the naive estimate in equation (1.20) to conclude that the indirect-detection signal due to pure Higgsinos in the galactic centre will receive a large boost at splittings $\delta m \sim 9.0, 2.7$ MeV, due to Coulomb resonances with $n = 1, 2$. Similarly, solving for $\beta \sim 5 \times 10^{-5}$ we can estimate a similar enhancement to the indirect-detection signal in dwarf galaxies at $\delta m \sim 8.4, 2.1$ MeV. For larger splittings, the annihilation cross-section to WW and ZZ will remain an order of magnitude below the indirect detection bounds of HESS and Fermi-LAT [30].

This back-of-the-envelope estimate is borne out by the numerical results, presented in figure 1.7 for pure Higgsino mass close to the thermal relic value. For dark matter in the galactic centre (left panel), the annihilation cross-section stays roughly constant as we decrease the splitting until we reach $\delta m \sim 20$ MeV. As we decrease the splitting still further we encounter a very narrow peak near $\delta m = 9$ MeV that boosts the thermally-averaged cross section by two orders of magnitude. As we decrease the splitting even further, the $n = 1$ Coulomb resonance crosses the $\chi^0\chi^0$ threshold and we lose the enhancement. The same phenomenon recurs around $\delta m = 2$ Mev, where we encounter the $n = 2$ resonance. For dwarf galaxies (right panel) the picture is even clearer. The figure shows two large but very narrow peaks slightly shifted in comparison to the ones for galactic centre measuremnts, but compatible with the values predicted by the naive formula. Although these enhancements are large, they are well within the limit due to perturbative unitarity constraints. From this we can conclude that for a pure Higgsino thermal relic, charged-neutral mass splittings in the range $\delta m \in [8.5, 10.5]$ MeV and $[2, 2.5]$ MeV are excluded by measurements of the indirect-detection cross-section by HESS. Similarly Fermi-LAT observations exclude a very narrow region around $\delta m = 8.5$ MeV and around $\delta m = 2.1$ MeV. These results are relatively stable under small variations in the Higgsino mass.

Note that only dark matter states are including in computing the Sommerfeld factors, and hence the resonance widths; we are therefore neglecting the broadening effect on the resonance of direct decays to SM final states.

Here we tuned the splittings to these specific, small values in order to probe regions where the effect due to Coulomb resonances is significant. One could instead envision a future

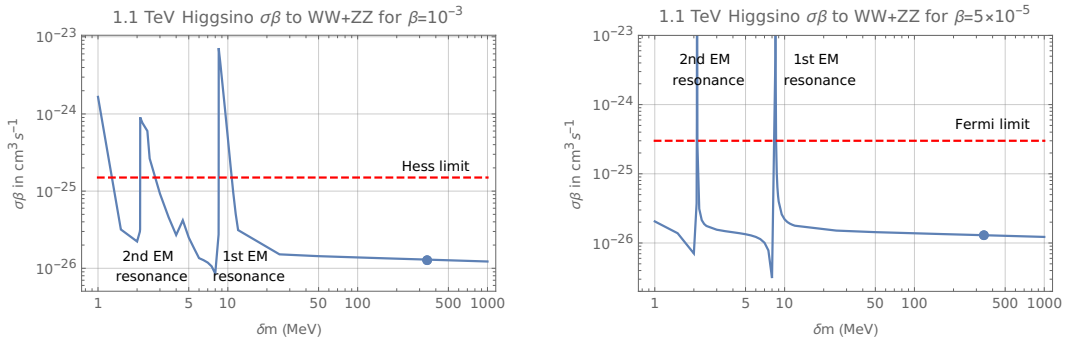

Figure 1.7 – Thermally-averaged annihilation cross-section to $WW + ZZ$ for a thermal relic Higgsino as a function of the charged-neutral splitting for: (left panel) galactic velocities $\beta = 10^{-3}$ and (right) dwarf-spheroidal velocities $\beta = 5 \times 10^{-5}$. The red dashed lines are the experimental limits due to HESS (left) and Fermi-LAT (right), respectively, as taken from [30]. The nominal value for the splitting is shown as a large dot.

where indirect-detection signals are measured in galaxies and clusters at many different scales, allowing us to 'scan' over a range of dark matter velocities in search of resonant effects.

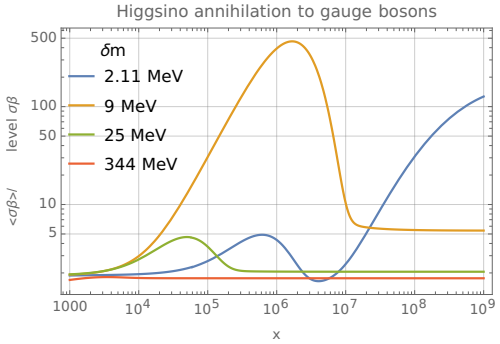

Figure 1.8 – Thermally-averaged annihilation cross section for 1.1 TeV pure Higgsino for some discrete values of the charged-neutral mass splitting δm. The thermal average is computed using a Maxwell-Boltzman distribution for the dark matter velocity, centred at varying x, in order to mimic potential future measurements taken in galaxies and clusters of different scales.

We can study this possibility by computing the annihilation cross-section while varying the effective x of the thermal velocity distribution used in the thermal averaging procedure, to mimic results due to dark matter in clusters of different scales. In figure 1.8 we show the variation of the sommerfeld-enhanced, thermally-averaged annihilation cross section for a 1.1-TeV pure Higgsino with x in the dark matter distribution (see equation (A.5)). The same large enhancements at $\delta m = 2.1$, 9 MeV are also visible here, at x corresponding to the average dark matter velocity in dwarf galaxies, and the galactic centre, respectively. As the splitting grows, we see the resonance moving to lower values in x, corresponding to larger cluster sizes. Measuring the continuum signal in galactic clusters with $x \sim 4 \times 10^4$, for example, would allow us to probe Higgsino mass splittings $\delta m \sim 25$ MeV. However increasing the splitting moves the resonances to larger velocities, resulting in smaller enhancements which can be

washed out in the thermal averae. The enhancement for 25 MeV splitting is just a factor of 5 at its maximum, whereas for nominal splitting there are many resonances that are rather close together, and the enhancement is washed out entirely in the thermal average. For nominal splitting Higgsino, the Coulomb resonances are just too narrow to give a significant enhancement of the annihilation cross-section for the velocity spread of a realistic celestial body.

In principle we should include thermal effects in the above computations, the main of which would be to cut off the Coulomb enhancement in the charged channel due to the thermal mass of the photon. We have verified that these have a negligible effect on the results quoted above, and we omit them.

1.5.2 Changing the Wino mass splitting

Effect on the relic density

The Sommerfeld enhancement in the Wino thermal relic calculation is, as for the Higgsino relic, dominated by the potential from the weak interaction and is well approximated by the $\delta m \to 0$ limit. We see on figure 1.6 that the analytical curve is a very good approximation for the relic density outside of the resonance dip (around $M = 2.37$ TeV) where the relic density is overestimated. Changing the mass splitting will not affect the analytical approximation but will move the resonance, around which our approximation is not valid anymore.

For a thermal Wino relic we are always in the regime $\delta m \ll T_F$ so we expect the analytic prediction (matched by the numerical calculation for the nominal splitting $\delta m = 165$ MeV) of $M = 2.9$ TeV to be valid for all values of the mass splitting as long as the resonance is not located right at 2.9 TeV. This happens for $\delta m = 450$ MeV; around this value we expect the relic mass to change by order a few hundred GeV. We consider that this mass splitting is too large for a realistic Wino model and we do not study this scenario further.

Effect on indirect detection signal

The present day annihilation cross-section for Wino DM with nominal splitting is very boosted by the presence of the zero-energy bound state at $M = 2.37$ TeV. The precise value of the cross-section is very sensitive to the position of the resonance and how close it is from the relic value $M = 2.9$ TeV.

Decreasing the charged-neutral splitting from the nominal value should shift the resonant mass to lower values, further away from the thermal relic mass, thus decreasing the annihilation cross section. As the mass splitting gets smaller still, below $\delta m \sim 20$ MeV, as estimated from equation (1.20), the first Coulomb resonance will come into play, again resulting in an enhanced cross section.

Numerical results for the thermally averaged annihilation cross-section for pure Wino mass around the thermal relic value are shown in figure 1.9. As before, dark matter today is taken to have a thermal velocity distribution centred on $\beta = 10^{-3}$ for galactic centre measurements (left panel) and $\beta = 5 \times 10^{-5}$ for Fermi-LAT measurements (right panel). As argued above, we see a range of intermediate splittings $\delta m \in [20, 55]$ MeV for HESS measurements and $\delta m \in [15, 200]$ MeV for Fermi-LAT, for which the annihilation cross section is smallest. Above this value, there is a large enhancement due to a zero-energy bound state held together by the Yukawa potential; below this value the enhancement is due to a Coulomb resonance. In this window the cross-section is around a factor of two below the HESS limit, well into the uncertainty band of the J-factor [31]. Varying the relic mass results in a small shift of this window.

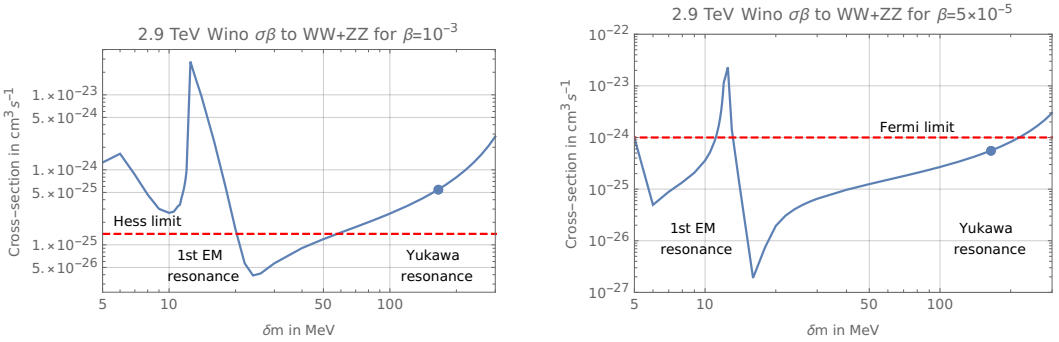

Figure 1.9 – Thermally-averaged annihilation cross-section to $WW + ZZ$ for a thermal relic Wino as a function of the charged-neutral mass splitting for: (left panel) galactic velocities $\beta = 10^{-3}$ and (right) dwarf-spheroidal velocities $\beta = 5 \times 10^{-5}$. The red dashed lines are the experimental limits due to HESS (left) and Fermi-LAT (right), respectively, as taken from [30]. The nominal value for the splitting is shown as a large dot.

1.6 Conclusion

In this chapter, we studied the Sommerfeld effect from the long-range potential due to the exchange of electroweak gauge bosons. We point out several features that are general to heavy WIMP interacting through the SM electroweak gauge group and not limited to the Higgsino or the Wino model. At high velocity $\beta \gg \frac{m_W}{M}$, β_{th} with β_{th} given by (1.18), the Sommerfeld effect is well approximated by taking only the $SU(2)_L$ limit of the potential for which we have an (approximate) analytical expression. On the other hand, at low velocity Sommerfeld factors have to be computed numerically. Two important effects arise at low velocity: first, for specific DM mass M, we approach a zero-energy bound state of the Yukawa potential and the Sommerfeld factor grows to very large values. The position of these resonances are dependent on the mass splitting and on the details of the full potential. Second, there are important enhancement of the Sommerfeld factor at specific velocities below threshold. These can be understood as $\chi^+\chi^-$ bound states from the electromagnetic interaction. In practise there are very narrow and they have physical effects only if the bound state energy $E_B \sim \alpha^2 M$ is

of the order of the mass splitting δm which requires some tuning between the electroweak contribution to the mass splitting and the UV contribution.

From this, we can study the effect of varying the mass splitting δm on the phenomenology of the DM candidate. At freeze-out, we are in the high velocity regime $\beta \gg \frac{m_W}{M}, \beta_{th}$ and the charged-neutral splitting can be neglected. Thus the relic mass is largely insensitive to the value of δm, as long as $\delta m \ll T_F \sim M/25$.

The story for indirect detection is much more interesting: for galactic velocities $\beta \sim 10^{-3}$ and lower for smaller bodies, the Sommerfeld factor is very sensitive to the presence of a resonance M^* close to the DM mass M as in the Wino case. In this case, changing the splitting δm displaces the value of M^* and can raise dramatically the annihilation cross-section if M^* goes close to M.

This is illustrated by the Wino triplet model where the present annihilation cross-section with Sommerfeld enhancement for nominal splitting is above the HESS limit and comparable to the Fermi-LAT limit (at least for the Einasto profile of the halo density) because of the large enhancement due to the resonance located at $M^* = 2.37$ TeV. Decreasing δm brings the resonance down, further from the relic value $M = 2.9$ TeV and lowers the annihilation cross-section below the HESS bound (see figure 1.9). We expect our conclusions to be valid for other models of electroweak DM where this feature $M^* \approx M$ happens such as for the scalar triplet with zero hypercharge or the fermion quintuplet with zero hypercharge [25].

In the Higgsino model, the resonance M^* lies very far above $M = 1.1$ TeV so the indirect detection phenomenology is very different. The annihilation cross-section receives a much smaller boost from Sommerfeld enhancement than in the Wino model because the resonance is far away. Changing δm does not impact the Sommerfeld factors dramatically except for specific masses where the DM velocity hits the Coulomb bound state (see figure 1.7) for which the cross-section can gain two orders of magnitude. This happens for very low charged-neutral splitting $\delta m \sim 9$ MeV and $\delta m \sim 2$ MeV.

Although interesting, these results suffer from theoretical and experimental problems. In order to have such a small charged-neutral splitting while keeping the neutralino lighter, one needs an unnatural tuning between the contribution of the UV physics and that due to electroweak loop corrections. In the pure Wino case there is the additional complication that the leading tree-level operator affecting the splitting has mass dimension seven; making this contribution of the same order as the loop correction will require some strongly-coupled new physics. On the experimental side, electroweak multiplets with very small charged-neutral splittings will already be strongly constrained, perhaps even excluded, both by collider searches such as [32], as well as by capture and decay/annihilation of the heavy state in dense objects like the sun [33].

Instead we highlight the mechanism brought to light in this work which is rather generic, and will apply in any scenario where the dark matter two-to-two scattering contains an inelastic

channel to a final state with constituents that are acted upon by a long-range force. In analogy with the electroweakino example detailed above, this will give rise to resonances that lie below the energy threshold for final-state production due to the formation of 'Coulombic' quasi-bound states, which are excited at specific incoming velocities of the annihilating dark matter, thus enhancing the annihilation cross section. However in the pure electroweakino case both the nominal charged-neutral splitting and the Coulomb binding energies are set by the same interaction and are rather disparate in size, requiring a tuning to make the resonance velocities relevant to existing measurements. This does not have to be the case more generally; the two relevant quantities could be unrelated, or could be naturally of the same order, which would automatically excite the Coulomb resonances at relevant velocities.

2 Dark sector models

Instead of considering DM candidates interacting with the SM through the weak $SU(2)_L$ gauge interaction, one can imagine that the DM candidate comes from a dark sector carrying no SM charge. Then the dark sector can only interact with the SM via a SM neutral operator (often called portal). In this case, the new particle need not to be heavy, it escaped experimental detection because it has a very small coupling ϵ to SM particles. This direction of research towards particles with very low coupling is called the *intensity frontier* and is typically probed by fixed-target experiments which have higher luminosity than colliders.

Interestingly, there are only three SM singlet operators with dimension less than 4 that can be built out of SM fields: $B^{\mu\nu}$ (the hypercharge field-strength), $H^\dagger H$ and $\ell \cdot H$ leading to a restricted dark sector phenomenology. Thus, in a renormalizable theory, the three possible interactions between the dark sector and the SM are:

- Coupling to $B^{\mu\nu}$: in this case the dark sector contains at least a spin-1 field A'^{μ} of field strength $F'^{\mu\nu}$ and coupled to the SM through the operator:

  $$\mathscr{L} = \epsilon B^{\mu\nu} F'_{\mu\nu}$$

  A' is called the dark photon.

- Coupling to $H^\dagger H$: the dark sector needs a scalar S and can couple to the SM via:

  $$\mathscr{L} = \epsilon H^\dagger H \left(mS + |S|^2\right)$$

  This is the dark Higgs, or Higgs portal.

- Coupling to $\ell_i \cdot H$: in this case, new fermions $N_{j'}$ can interact with the SM with the following Lagrangian:

  $$\mathscr{L} = F_{i\,j'}\, \ell_i \cdot H N_{j'} + c.c.$$

  The $N_{j'}$ are called Heavy Neutral Leptons (HNL) and behave like right-handed neutrinos.

Dark sectors can also couple to the SM through higher dimensional operators such as $a\epsilon^{\mu\nu\rho\sigma}F_{\mu\nu}F_{\rho\sigma}$ where a is an axion-like particle, or $\epsilon^{\mu\nu\rho\sigma}H^\dagger D_\mu H V_\nu B_{\rho\sigma}$ for a vector particle V (Chern-Simmons portal). However in this chapter, we will focus on the renormalizable interactions.

The interest in dark sector models has grown in recent years and significant efforts have been made to recast the results of past experiments in terms of exclusion limits of various dark sector models. These dark sectors could come from string theory or grand unified theories and can be relevant for DM and baryogenesis (in the HNL case). Several experiments have been suggested to probe dark sector models such as SHiP [34]. SHiP is a fixed-target experiment using the CERN SPS 400 GeV. Other proposed experiments include FASER [35], CODEX-b [36] and MATHUSLA [37]. These experiments take advantage of the LHC collisions and are designed to detect long lived particles that would escape the LHC detector.

The goal of this chapter is to study the reach of a fixed-target experiment parasitic to a future muon collider. A way to produce muons is to shoot a positron beam at a target with energy tuned just above the muon threshold. The primary positron beam has to be extremely intense to produce enough muons and can be used as a fixed target experiment simply by placing a detector in the beam direction and shielded from the SM particles produced at the target.

We will first describe the phenomenology of three dark sector scenarios, first the dark photon in section 2.1, then dark Higgs models in section 2.2 and HNLs in section 2.3. In section 2.4 we study the reach of such an experimental setup for the three benchmark models presented before.

2.1 Dark photon

2.1.1 Simplified model

We consider the SM augmented with a dark sector charged under a $U(1)_D$ gauge group. The associated force carrier is the vector field A'^0_μ with a mass term $m_{A'}$ coming for example from another Higgs mechanism. The only interaction between the SM and the dark sector is from the mixing of the dark field strength with the $U(1)_Y$ field strengh. The full Lagrangian of the theory is given by:

$$\mathscr{L} = \mathscr{L}_{SM} - \frac{1}{4}F'^0_{\mu\nu}F'^{0\mu\nu} + \frac{m^2_{A'}}{2}A'^0_\mu A'^{0\mu} + g_D A'^0_\mu J^\mu_D + \frac{\epsilon_Y}{2}B^{0\mu\nu}F'^0_{\mu\nu} \tag{2.1}$$

where ϵ_Y is constrained by experiment to be a small number. After electroweak symmetry breaking, the mixing term becomes, in terms of the SM fields A^0_μ and Z^0_μ:

$$\frac{\epsilon_Y}{2}\left(\cos\theta_W F^{0\mu\nu} - \sin\theta_W Z^{0\mu\nu}\right)F'^0_{\mu\nu} \tag{2.2}$$

In order to remove these mixing terms at first order in ϵ_Y, one can make the following field redefinitions:

$$\begin{cases} A_\mu = A^0_\mu - \epsilon_Y \cos\theta_W A'^0_\mu \\ A'_\mu = A'^0_\mu + \epsilon_Y \sin\theta_W Z^0_\mu \end{cases} \tag{2.3}$$

However, this reintroduces a mixing in the mass term $\frac{m^2_{A'}}{2} A'^0_\mu A'^{0\mu}$ between A'_μ and Z_μ. In order to avoid those terms, one has to simultaneously diagonalize the kinetic and mass matrix. This can be done by replacing the previous transformation by the following one:

$$\begin{cases} A_\mu = A^0_\mu - \epsilon_Y \cos\theta_W A'^0_\mu \\ Z_\mu = Z^0_\mu - \epsilon_Y \sin\theta_W \frac{m^2_{A'}}{m^2_Z - m^2_{A'}} A'^0_\mu \\ A'_\mu = A'^0_\mu + \epsilon_Y \sin\theta_W \frac{m^2_Z}{m^2_Z - m^2_{A'}} Z^0_\mu \end{cases} \tag{2.4}$$

Then writing the current terms $eA^0_\mu J^\mu_{em} + g_Z Z^0_\mu J^\mu_Z + g_D A'^0_\mu J^\mu_D$ with the physical fields give rise to new couplings compared to the SM ones:

$$\begin{aligned} \mathscr{L} = &\mathscr{L}_{SM} - e\epsilon_Y \cos\theta_W A'_\mu J^\mu_{em} - g_Z \epsilon_Y \sin\theta_W \frac{m^2_{A'}}{m^2_Z - m^2_{A'}} A'_\mu J^\mu_Z \\ &+ g_D \epsilon_Y \sin\theta_W \frac{m^2_Z}{m^2_Z - m^2_{A'}} Z_\mu J^\mu_D \end{aligned} \tag{2.5}$$

- The dark photon A'_μ is coupled to the electromagnetic current with strength $\epsilon_Y \cos\theta_W \times e \equiv \epsilon e$. This coupling is the one relevant for our study and permits us to produce dark photons from SM particles.

- The dark photon also couples to the Z-current but in the limit $m_{A'} \ll m_Z$, this is further suppressed by a factor $m^2_{A'}/m^2_Z$. In beam dump experiments, the available energy is much below the Z-mass and so we will neglect this coupling.

- The Z-boson gets a coupling to particles in the dark sector with strength $g_D \times \epsilon_Y \sin\theta_W$. This can open new decay channels for the $Z \to$ invisible channel depending on the particle content of the dark sector.

In what follows, in order to study the reach of different experiments, we will consider a simplified model where the dark photon is the only new particle. There is no particle in the dark sector, or they are too massive to be produced. We keep only the dark photon with mass $m_{A'}$ and interacting with charged particles with strength $\epsilon \times eQ$. We will focus on the mass range 1 MeV to 10 GeV relevant for fixed-target experiments so the couplings inherited from the mixing with the Z-boson can safely be neglected. Our benchmark model contains only two free parameters: the dark photon mass $m_{A'}$ and its coupling to the SM ϵ.

2.1.2 Dark photon lifetime

In a generic model, the main decay channel of the dark photon is to dark particles of mass m_D such that $2m_D < m_{A'}$. The width to dark sector particles goes like α_D whereas all SM decay is suppressed by a factor ϵ^2. The decay to a pair of Dirac fermions χ has a width:

$$\Gamma(A' \to \chi\bar{\chi}) = \frac{\alpha_D m_{A'}}{3}\left(1+\frac{2m_\chi^2}{m_{A'}^2}\right)\sqrt{1-\frac{4m_\chi^2}{m_{A'}^2}} \tag{2.6}$$

However in our benchmark model there are no dark particles and the only decay channels are to SM particles. The decay to leptons is straightforward to compute:

$$\Gamma(A' \to \ell^+\ell^-) = \epsilon^2 \times \frac{\alpha m_{A'}}{3}\left(1+\frac{2m_\ell^2}{m_{A'}^2}\right)\sqrt{1-\frac{4m_\ell^2}{m_{A'}^2}} \tag{2.7}$$

The decay width to quarks gets important non perturbative QCD contributions and cannot be computed in the same way but can be deduced from the spectral fuction extracted from the measurement of the ratio $R_{\text{had}} = \frac{\sigma(e^+e^-\to\text{hadrons})}{\sigma(e^+e^-\to\mu^+\mu^-)}$. Then the hadronic width is given by:

$$\Gamma(A' \to \text{hadrons}) = \epsilon^2 \times \frac{\alpha m_{A'}}{3}\left(1+\frac{2m_\ell^2}{m_{A'}^2}\right)\sqrt{1-\frac{4m_\ell^2}{m_{A'}^2}}R_{\text{had}}(s=m_{A'}^2) \tag{2.8}$$

Taking the measurement from the PDG, we get the lifetime of the dark photon as function of its mass plotted in figure 2.1. The large dips around 0.7 and 1 GeV are due to the QCD ρ, ω and ϕ resonances. In a concrete model, this picture can be significantly modified by the presence of light states in the dark sector; however this curve is an upper bound for the lifetime of the dark photons since the decay channels to the SM do not depend on the details of the dark sector.

For even lighter dark photon $m_{A'} \leq 2m_e$, the decay channel to electrons is not kinematically accessible. The main SM decay channel is $A' \to 3\gamma$ (as the decay to two photons is forbidden by the Lee-Yang theorem) and in the limit $m_{A'} \ll m_e$ can be computed from the Euler-Heisenberg Lagrangian, giving the result [38]:

$$\Gamma(A' \to 3\gamma) = \epsilon^2 \times \frac{17\alpha^4}{2^7 3^6 5^3 \pi^3}\frac{m_{A'}^9}{m_e^8} \tag{2.9}$$

The full 1-loop result around the electron threshold is given in [39].

The other decay channel to neutrinos $A' \to \nu\nu$ acquired by the mixing with the Z boson is suppressed by $\epsilon^2 \times m_{A'}^4/m_Z^4$ and is given by

$$\Gamma(A' \to \nu\bar{\nu}) = \epsilon^2 \times \frac{\alpha}{2\cos^4\theta_W}\frac{m_{A'}^5}{m_Z^4} \tag{2.10}$$

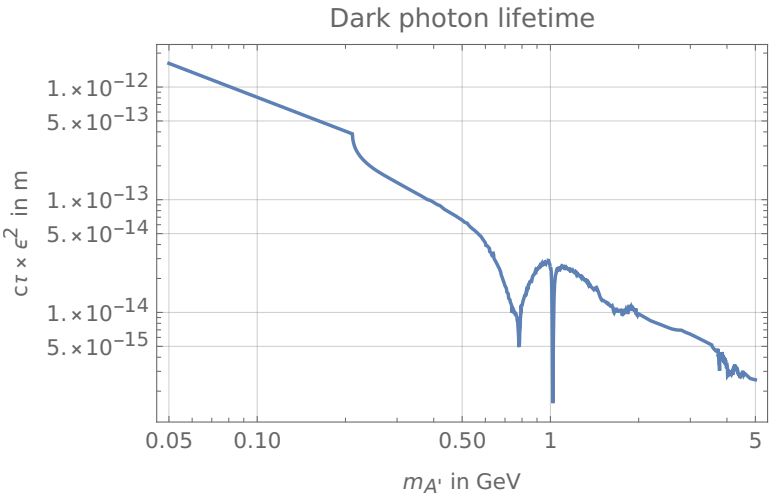

Figure 2.1 – Dark photon lifetime factoring out the ϵ^{-2} dependence in meters as function of $m_{A'}$ in GeV. The first kink is the muon threshold, the two dips at 0.7 and 1 GeV are due to hadronic resonances.

These two decay channels are negligible above the threshold $m_{A'} \geq 2m_e$ and will play no role in our analysis.

2.1.3 Experimental probes

Beam dump experiments

In the mass range 1 MeV $\leq m_{A'} \leq 1-10$ GeV, the most stringent constraints on dark photon models come from beam dump experiments. The main features of these experiments are as follows: a beam of electrons or protons is directed against a target, producing copious amounts of particles through QCD and EM interactions. A shield behind the interaction point blocks the charged and hadronic particles and a detector is placed after the shield. Dark photons (or other weakly interacting particles) produced in the collision or from secondary decay of SM particles will fly through the shielding and with some probability decay back to SM particles in the detector. The signal consists in a pair of charged particles appearing out of nothing in the detector with constant invariant mass. The main SM background comes from neutrinos which are not stopped by the shielding and can scatter through the process $\nu_\ell N \to \ell N'$ creating a charged lepton. Also residual muons can travel through thick shielding and be seen as lines in the detector tracker.

Assuming that the detector has a length L and is located at a distance D from the interaction point, the number of dark sector particles decaying in the dectector is given by the following formula:

$$N_{\text{obs}} = \mathscr{L}\sigma e^{-\frac{D}{l_d}}\left(1-e^{-\frac{L}{l_d}}\right)R_{\text{vis}} \tag{2.11}$$

where

- $\mathscr{L}$ is the luminosity and depends on the machine characteristics.
- σ is the dark photon production cross-section. Since the new state couples to SM particles with strength ϵ, we have $\sigma \propto \epsilon^2$.
- l_d is the decay length of the dark photon. For a dark photon of mass $m_{A'}$ and boost factors β and γ, the decay length is given by:

$$l_d = \frac{\beta\gamma l_0}{\epsilon^2} \tag{2.12}$$

  where l_0 is the decay legth in the rest frame for unit ϵ given in figure 2.1.
- The first exponential gives the probability of the dark photon surviving the distance D until the detector. The second factor is the probability of the dark particle to decay into the detector of length L.
- R_{vis} is the branching fraction to visible decay product, including detection efficiency.

The reach of the experiment at small ϵ is limited by the small number of dark particles produced ($\mathscr{L}\sigma \propto \epsilon^2$) and the long lifetime of the particle: most of them fly through the detector without decaying. The first exponential goes to 1 and after expanding the second exponential we get:

$$N_{\text{obs}} \sim \mathscr{L}\sigma\frac{L}{l_d}R_{\text{vis}} \propto \epsilon^4 \tag{2.13}$$

In order to improve the reach of the detector in ϵ, we need a big increase in luminosity $\mathscr{L}$ or in detector length L.

On the other hand, for large ϵ, the decay length becomes short and most of the dark photons decay before reaching the detector: we are mostly limited by the distance to the interaction point D. For large mixing, the number of observed events goes like:

$$N_{\text{obs}} \sim \epsilon^2 e^{-\epsilon^2} \tag{2.14}$$

A trade-off between a small distance D to increase the reach at large ϵ and a larger D for better shielding in order to reduce the background is necessary in the detector design.

The main production mechanism from an electron beam is the radiation of a dark photon particle from the electron, similarly to photon bremsstrahlung. The cross-section for this process can be computed in the Weizsäcker-Williams approximation [40]. More details about the approximation and the cross-section calculation will be given in section 2.4 and appendix. For an electron beam of energy E_0, the differential cross-section for producing a dark photon A' with energy $E_{A'}$ and with a polar angle $\theta_{A'}$ compared to the incoming beam is:

$$\frac{d\sigma}{dx\,d\cos\theta_{A'}} \approx 4\alpha^3\epsilon^2\chi\frac{E_0^2 x}{U^2}\left[2-2x+x^2+\frac{2(1-x)^2 m_{A'}^2}{U^2}\left(m_{A'}^2+\frac{xU}{1-x}\right)\right] \tag{2.15}$$

where x is the ratio $x = E_{A'}/E_0$, χ is a form factor depending on the target nucleus and the kinematics and U is the virtuality of the intermediate electron in initial state radiation and is given by:

$$U \approx E_0^2 \theta_{A'}^2 x + m_{A'}^2 \frac{1-x}{x} + m_e^2 x \tag{2.16}$$

The electron propagator gives the U^{-2} factor and makes the A' bremsstrahlung process strongly peaked at $x = 0$ and at $\theta_{A'} = 0$. Most of the produced dark photons are collinear to the incoming beam and a small detector opening is enough to capture most of the produced dark states.

For a proton beam, the dark photon production mechanism are more diverse. To the similar bremsstrahlung process, one must also add dark photons produced in secondary decays of mesons produced by the strong interaction and direct production of A' (such as $q\bar{q} \to A'$). However, the ϵ-scaling of the production rate and decay in the detector is the same as described above so we do not give more details about the proton beam case.

A list of beam dump experiments using proton and electron beam with their main characteristics is given in table 2.1 (for more details see for example [41]). The exclusion region in the $\epsilon - m_{A'}$ parameter plane is plotted in figure 2.2 top and middle panel for electron beam dump and proton beam dump respectively. As explained above, the upper reach in coupling ϵ is very dependent on the distance to the interaction point D since for too large ϵ, the produced dark photons decay before reaching the detector. On the other hand, the lower reach in coupling mostly depend on the luminosity and on the detector fiducial length (2.13). In order to improve the limits, one has to overcome the ϵ^4 suppression in the number of events at low coupling.

For the reach at high mass, the limit is a combination of kinematics and decay length of the dark photon, the absolute limit being the center-of-mass energy of the primary collision $\sqrt{s} = \sqrt{2E_0 m_p}$. At small mass, the reach is limited by $m_{A'} = 2m_e$ when the last visible decay $A' \to e^+e^-$ becomes kinematically forbidden. The only SM decay channel remaining is $A' \to 3\gamma$ but the dark photon is too long-lived to be seen in detectors.

Meson decay

The dark photon can also be searched in the decays of mesons involving a photon. In this case, the reach in the mass of the new state is limited by the mass of the mother meson and the reach in ϵ is limited the statistics and by the length of the detector. (Flavour factories are very suited for this kind of searches,)

At CERN, the NA48 experiment [52] and at COSY the WASA experiment [53] searched for the dark photon throught the process $\pi^0 \to \gamma A'$ and subsequent decay $A' \to e^+e^-$. The width is

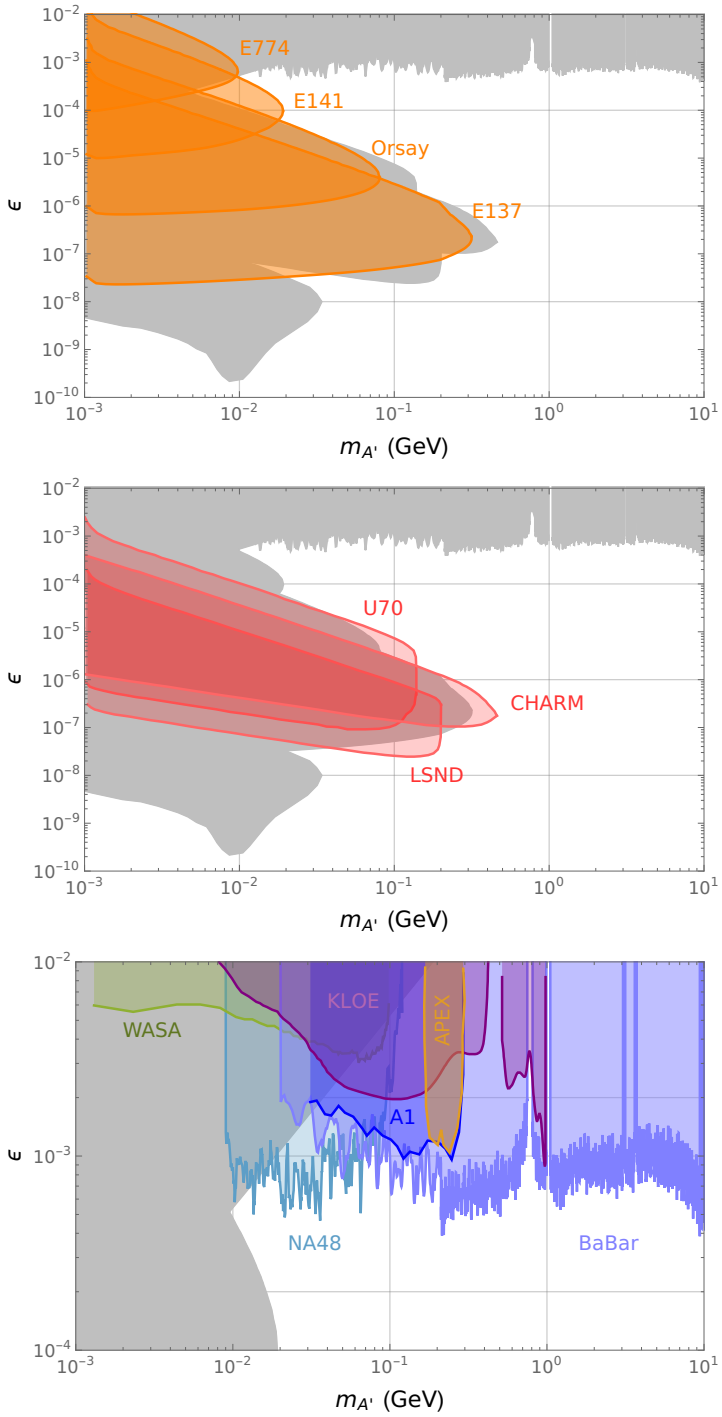

Figure 2.2 – Dark photon model exclusion limits in the $m_{A'} - \epsilon$ plane. The grey area is excluded by experimental data, with limits from electron beam dump experiments listed in table 2.1 highlighted in orange in the top panel (the limit from KEK is not shown because it is entirely contained in the region excluded by Orsay and E137). In the middle panel, the exclusion regions of proton beam dump are shown in red. In the bottom panel, exclusion limits from meson decay (WASA, KLOE, NA48), e^+e^- colliders (BaBar, KLOE) and fixed target experiments (APEX, A1) are shown.

Experiment	Beam	Target	Energy	POT	Dist to IP	Length
E774 [42]	e^-	W	275 GeV	5.2×10^9	0.3 m	2 m
E141 [43]	e^-	W	9 GeV	2×10^{15}	0.12 m	35 m
Orsay [44]	e^-	W	1.6 GeV	2×10^{16}	1 m	2 m
KEK [45]	e^-	W	2.5 GeV	1.69×10^{17}	2.4 m	2.2 m
E137 [46]	e^-	Al	20 GeV	1.87×10^{20}	179 m	204 m
CHARM [47]	p	Cu	400 GeV	2.4×10^{18}	480 m	35 m
LSND [48]	p	H_2O	0.8 GeV		30 m	
U70 [49,50]	p	Fe	70 GeV	1.71×10^{18}	64 m	23 m

Table 2.1 – Summary of main beam dump experiments and their characteristics. The interpretation of the results of electron beam dump experiments in terms of the dark photon model is performed in [40,51].

given by:

$$\Gamma(\pi^0 \to \gamma A') = 2\epsilon^2 \left(1 - \frac{m_{A'}^2}{m_{\pi^0}^2}\right)^3 \times \Gamma(\pi^0 \to \gamma\gamma) \tag{2.17}$$

The analysis is done assuming prompt dark photon decay, meaning at the interaction point, which is only true for sufficiently large mixing parameter ϵ. On the other hand, unlike in beam dump experiments, there is no upper limit to the reach in ϵ.

The KLOE detector [54] at the DAΦNE ϕ-factory searched for $\phi \to \eta A'$, and subsequent decay $A' \to e^+e^-$. The exclusion limit from these experimental searches are plotted in figure 2.2 (lower panel).

Collider searches

Dark photons can also be directly produced in colliders and detected by their decay products (usually lepton pairs). The process $e^+e^- \to \gamma A'$ was looked for by KLOE [55,56] and BaBar [57] by searching for a bump in $e^+e^- \to \gamma\ell^+\ell^-$. No such bump was found, leading to the limits plotted in figure 2.2 (bottom panel).

Anomalous magnetic moment

The dark photon contributes to the leptons anomalous magnetic moment by the same vertex diagram than the leading QED effect. The resulting $g-2$ contribution is:

$$a_\ell^{\mathrm{DP}} = \epsilon^2 \times \frac{\alpha}{2\pi} \times \int_0^1 \frac{2z(1-z^2)m_\ell^2}{(1-z)^2 m_\ell^2 + m_{A'}^2 z} dz \tag{2.18}$$

This expression has the limits:

$$a_\ell^{\mathrm{DP}} \underset{m_{A'} \ll m_\ell}{\rightarrow} \frac{\alpha\epsilon^2}{2\pi} \qquad \text{and} \qquad a_\ell^{\mathrm{DP}} \underset{m_{A'} \gg m_\ell}{\rightarrow} \frac{\alpha\epsilon^2}{3\pi}\frac{m_\ell^2}{m_{A'}^2} \tag{2.19}$$

If ϵ is too large, the contribution to the electron anomalous magnetic moment would be problematic. The region excluded by the measurement of a_e is coloured in red in figure 2.3 and is independent at leading order of the decay channels of the dark photon.

Note that the dark photon contribution to the muon anomalous magnetic moment has the correct sign to account for the longstanding $\sim 3\sigma$ discrepancy between the experimental measurement and the theoretical calculation [58]. On the other hand, the experimental value of the electron magnetic moment is about 2σ below the theory prediction, with the wrong sign to be explained by the dark photon. So in our simple model, from equation (2.19), we need to be in the regime $m_{A'} \ll m_\mu$ in order to have a large contribution to a_μ and a negligible one to a_e.

When putting together experimental limits from beam dump experiments, meson decays and collider searches, the entire region favored by the muon magnetic moment anomaly is ruled out in the simplest dark photon model. Even if these constraints depend strongly on the decay channels of A' the dark photon solution is also ruled out by invisible decay searches. Only a dark photon model with a larger coupling to the muon can solve the muon $g-2$ anomaly, such as the dark photon coming from gauging the $L_\mu - L_\tau$ symmetry.

Supernova cooling

An important astrophysical constraint on dark photon models comes from the observation of the core-collapse supernova SN1987A in the Large Magellanic Cloud galaxy. The exclusion curve obtained by the analysis [59] is plotted in figure 2.3.

In our current understanding of the supernova physics, most of the liberated energy (about 99%) is carried by emitted neutrinos. The expected neutrino burst obtained by SM simulations of the collapse is in good agreement with the observed events at the neutrino observatories Kamioka, IMB and Baksan. However, the presence of long-lived dark sector particles coupled to the SM with a sizeable production rate and able to free-stream out of the core provides an energy-depleting mechanism competing with the neutrino. Despite large astrophysical uncertainties, the energy loss through other means than neutrinos is severly constrained by SN1987A.

For a dark photon of mass smaller than the supernova temperature (about 10 MeV), its coupling to the SM ϵ must be either small enough so that its production during the supernova is negligible or large enough such that the scattering on SM particles traps them efficiently in the core, reprocessing their energy to SM neutrinos.

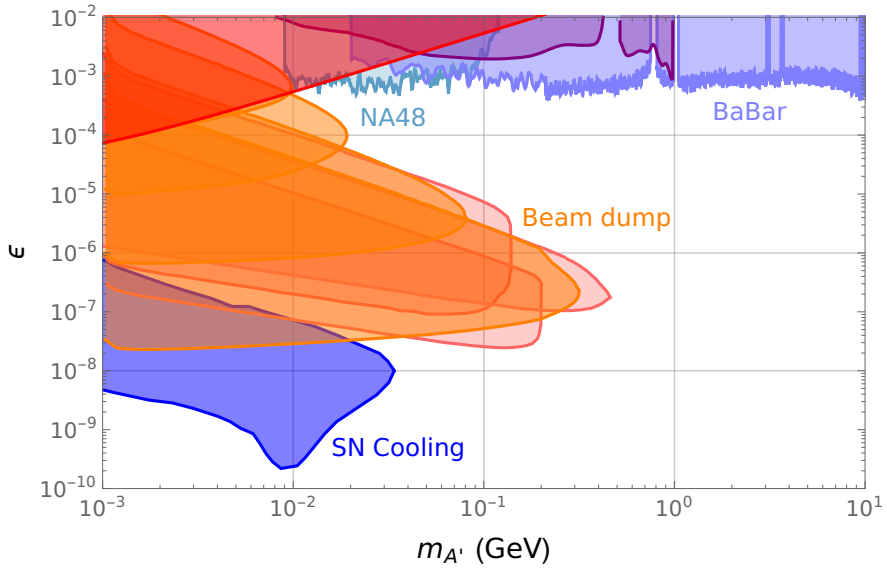

Figure 2.3 – Dark photon model excluded parameter space in the $m_{A'} - \epsilon$ plane. The exclusion region from beam dump experiments, NA48, BaBar and KLOE are shown. The blue region is the limit from SN1987A and the red region is excluded by the measurement of the electron magnetic moment.

Invisible dark photon decay

The experimental limits presented above can be significantly weakened if the dark photon decays mostly to invisible states, diluting the detectable SM decays. If the dark sector contains a state χ kinematically accessible, the decay $A' \to \chi\bar{\chi}$ (given in the fermion case by (2.6)) dominates. Only the limits from the anomalous magnetic moment are independent from A' lifetime. There are two main search strategies in this case that are briefly summarized below.

- Search for χ scattering: the setup is similar to the beam dump setup. Dark photons are created by a beam on a target and subsequently decay to $\chi\bar{\chi}$ pairs. The dark particles can then scatter on nuclei via A' exchange $\chi N \to \chi N$ similarly to DM direct detection experiments. This process being doubly suppressed by ϵ^2 (A' production and χN scattering), it requires an intense primary beam to maximize the luminosity. The interpretation of the E137 experiment in terms of invisible A' decay is performed in [60]. Note that the limits now depend on 4 parameters $\epsilon, m_{A'}, \alpha_D, m_\chi$.

- Meson decay to invisible: bumps can be searched in decays of mesons with missing energy. The analysis of BaBar searches for $\Upsilon \to \gamma A'$ with invisible A' decay was done first in [61] and refined in [62]. Also the measurement of the kaon rare decay $K^+ \to \pi^+ \nu\bar{\nu}$ can place limits on the decay $K^+ \to \pi^+ A'$ with on-shell dark photon [61]. These limits are independent of the content of the dark sector can be cast in the $m_{A'}, \epsilon$ plane.

2.1.4 Theory motivations for the dark photon

String and GUT theory

From the top-down perspective, additional $U(1)$ gauge groups can appear from string theory. Predictions from string theory are difficult to make because of the large number of string vacua, however in contrete models certain features such as axions [63], extended gauge sectors and additional $U(1)$s [64], additional scalars, arise commonly from string compactification. Also, the breaking of larger gauge groups in grand unified theories (GUT) often leads to additional gauged $U(1)$s, from example in $SO(10)$ [65]. Then integrating out heavy particles coupling both to the SM and to the additional $U(1)$ generates the ϵ mixing.

If additional gauged $U(1)$s appear easily in theoretical construction, there is no generic prediction of the mass $m_{A'}$ and coupling ϵ of the dark photon. From this perspective, there is no compelling reason for $m_{A'}$ to be in the GeV range.

Dark matter

An interesting scenario would be to have the DM candidate in a dark sector, carrying no SM charges and interacting with the SM only through by the dark photon. As we have seen in the previous section, electroweak WIMP dark matter have masses in the TeV range, fixed by the strength of the weak interaction. In order to have lighter DM, one need a new mediator with smaller coupling constant. Direct detection constraints are evaded because of the smallness of ϵ and because typical experiments like XENON loose sensitivity for light DM below a GeV.

We will consider here the very simple model with one Dirac fermion χ charged under $U(1)_D$ and a dark photon mixing with the SM photon. A' is unstable because of its coupling to the SM but χ is stable by conservation of the dark charge and can be a DM candidate.

A simple possibility is to have DM density produced by the freeze-out mechanism. If $m_\chi \leq m_{A'}$, then the main DM decay channel to SM particles is $\chi\bar{\chi} \to f\bar{f}$ mediated by an off-shell dark photon in the s-channel. The dark fermions start in thermal equilibrium with the SM and decouple from the thermal bath when $T \sim m_\chi$. The other possibility is that $m_\chi \geq m_{A'}$, then the decay $\chi\bar{\chi} \to A'A'$ is much more efficient than the one to SM particles. This reaction sets the relic abundance at decoupling and all the produced dark photons eventually decay to SM particles.

In the first case $m_\chi \leq m_{A'}$, the annihilation cross-section is given in the non-relativistic limit by:

$$\langle \sigma\beta \rangle = 4\pi\epsilon^2\alpha_D\alpha\sqrt{1-\frac{m_\ell^2}{m_\chi^2}}\frac{2m_\chi^2+m_\ell^2}{(4m_\chi^2-m_{A'}^2)^2} \approx 8\pi\epsilon^2\alpha_D\alpha\frac{m_\chi^2}{m_{A'}^4} \tag{2.20}$$

for $m_\ell \ll m_\chi \ll m_{A'}$ (here the annihilation is given for one lepton only, one has to sum over the available SM decay channels). In order to get the correct relic density, one needs

$\langle\sigma\beta\rangle \approx 3\times10^{-26}\,\mathrm{cm^3 s^{-1}}$ which is possible for light m_χ and $m_{A'}$.

In the second case $m_\chi \geq m_{A'}$, the annihilation cross-section does not depend on ϵ and reads:

$$\langle\sigma\beta\rangle = \frac{\pi\alpha_D^2}{2m_\chi^2} \tag{2.21}$$

in the limit $m_\chi \gg m_{A'}$. The only constraint on ϵ comes from A' being in thermal equilibrium with the SM for the formula to hold. To reproduce the correct relic abundance, the dark matter mass needs to be $m_\chi \sim \alpha_D \times 20$ TeV, in the TeV range for SM-like coupling.

Light mediators can help address some astrophysical anomalies. The PAMELA experiment [66] reported an excess in the positron flux from space at energies $E > 10$ GeV while the antiproton flux does not show any anomaly. This was latewr confirmed by the measurement of AMS [67]. A model with a light mediator $m_{A'} \leq m_p$ can explain the DM annihilation $\chi\bar{\chi} \to A'A'$ followed by $A' \to e^+e^-$ producing positrons but no antiprotons. Also a mediator in the 1-100 MeV range can explain the 511 keV line from the galactix center measured by INTEGRAL [68]. However, it is not clear if these anomalies can be explained by more conventional astrophysical sources.

2.2 Dark Higgs

2.2.1 Simplified model

We consider the SM with an additional singlet CP-even scalar S. This scalar could come from supersymmetry or be the field giving mass to the dark photon presented before via a Higgs mechanism. As a simplified model, we consider only the singlet S. In this case, the most general renormalisable Lagrangian is:

$$\mathscr{L} = \mathscr{L}_{SM} + \frac{1}{2}\partial_\mu S\partial^\mu S + (\lambda_1 S + \lambda_2 S^2)H^\dagger H + V(S) \tag{2.22}$$

In this case, the interaction of the new scalar with the SM goes only through the operator $H^\dagger H$. The phenomenology of this new singlet is very different if the linear mixing λ_1 is present or not. In the first case, the new scalar mixes with the SM Higgs boson and inherits its couplings to SM fermions and gauge bosons suppressed by the mixing angle. In the second case, if a Z_2-symmetry forbids the linear term, the scalar does not mix with the Higgs and can only be pair produced from SM states (note that however if S develops a vacuum expectation value the term $S^2H^\dagger H$ also induces a linear mixing). We will first describe in detail the first scenario with a linear mixing and say a few words about the second scenario at the end of this section.

After electroweak symmetry breaking, the Higgs-S quadratic terms are given in the unitary gauge by:

$$\mathscr{L}_m = \frac{1}{2}m_h^2 h_0^2 + \frac{1}{2}m_S^2 S^2 + \lambda_1 v S h_0 \tag{2.23}$$

where $v/\sqrt{2}$ is the H vacuum expectation value, $v = 246$ GeV in the small mixing limit. Diagonalizing the mass matrix, as:

$$\begin{pmatrix} h_0 \\ S \end{pmatrix} = \begin{pmatrix} \cos\theta & \sin\theta \\ -\sin\theta & \cos\theta \end{pmatrix} \begin{pmatrix} h \\ h_D \end{pmatrix} \tag{2.24}$$

with h the physical Higgs boson and h_D the new scalar (dark Higgs), we get the mixing angle:

$$\tan 2\theta = -\frac{2v\lambda_1}{m_h^2 - m_S^2} \tag{2.25}$$

which in the limit $m_S \ll m_h$ and $\lambda_1 \ll v$ is a small parameter and is approximatively given by: $\theta \approx -\lambda_1 v/m_h^2$. The couplings of the dark Higgs to SM fermions are the same as the standard Higgs suppressed by the angle $\sin\theta$ and in particular are proportional to the fermion mass: $g_{h_D f\bar{f}} = \sin\theta m_f/v$. In what follows we will call $\epsilon \equiv \sin\theta$ the parameter controlling the coupling strengh of the new scalar to the SM and study the phenomenology of the model in the parameter plane (m_S, ϵ). Only for experiments at energies above the weak scale does the precise form of the potential $V(h,S)$ matters and more parameters describing the $h-S$ couplings are needed.

2.2.2 Dark Higgs lifetime and decay

The dark Higgs S essentially behaves like the SM Higgs boson with couplings suppressed by a factor ϵ. Thus the studies on the Higgs lifetime before its mass was known are relevant for the dark Higgs lifetime. Just as for the dark photon, we are looking at a simplified model where the new scalar cannot decay to dark sector states but a neutral scalar mixing with the Higgs will have at least the following decay channels.

The decay to a lepton pair is straightforward to compute:

$$\Gamma(S \to \ell^+\ell^-) = \epsilon^2 \times \frac{m_\ell^2 m_S}{8\pi v^2}\left(1 - 4\frac{m_\ell^2}{m_S^2}\right)^{\frac{3}{2}} \tag{2.26}$$

but the decay to quarks is more difficult to estimate because of the complex hadronic resonances. If S is very massive, one can use the spectator quark approach and get:

$$\Gamma(S \to q\bar{q}) = \epsilon^2 \times \frac{3m_q^2 m_S}{8\pi v^2}\left(1 - 4\frac{m_q^2}{m_S^2}\right)^{\frac{3}{2}} \tag{2.27}$$

and

$$\Gamma(S \to gg) = \epsilon^2 \times \frac{\alpha_s(m_S)^2 m_S^3}{8\pi^3 v^2}\left|\sum_q I\left(\frac{m_q^2}{m_S^2}\right)\right| \tag{2.28}$$

where the function I is a loop function given below in equation (2.30). For m_S between the two pion threshold and approximatively 2 GeV, we refer to the prediction of [69].

In the case of a very light scalar, $m_S < 2m_e$, the only possible decay channel is to photons. We give the formula for completeness:

$$\Gamma(S \to \gamma\gamma) = \epsilon^2 \times \frac{\alpha^2 m_S^3}{16\pi^3 v^2} \left| N_C \sum_q Q_f^2 I\left(\frac{m_q^2}{m_S^2}\right) - I_W\left(\frac{m_W^2}{m_S^2}\right) \right| \tag{2.29}$$

where the loop functions are

$$\begin{aligned} I(z) =& 2z + 2z(1-4z)\arcsin^2 \frac{1}{2\sqrt{z}} \\ I_W(z) =& \frac{1}{2} + 3z + 6z(1-2z)\arcsin^2 \frac{1}{2\sqrt{z}} \end{aligned} \tag{2.30}$$

coming respectively from a triangle loop of fermions and of W bosons.

2.2.3 Experimental probes

Meson decay

The dark higgs can be produced in decays of heavy mesons. In particular, the presence of the scalar can lead to large enhancement of rare flavour-changing decays such as $K \to \pi S$ or $B \to KS$ coming from the penguin diagrams. Integrating out the W boson gives an effective $d_i d_j S$ operator [70]:

$$\mathscr{L}_{\text{eff}} = \epsilon \times \frac{3g_L^3}{128\pi^2} \frac{m_i m_t^2}{m_W^3} V_{tj}^* V_{ti}\, \bar{d}_{jL} d_{iR} S + h.c. \tag{2.31}$$

where i, j are family indexes and $i > j$. The factor m_i comes from the helicity flip (we have neglected the term proportional to m_j) and the factor m_t^2 comes from GIM mechanism: all terms independent from m_k the mass of the up-type quark running in the loop come with a factor $\sum_k V_{kj}^* V_{ki}$ which is zero from CKM unitarity. Thus the similar operator involving up-type quarks is further suppressed by a factor m_b^2/m_t^2 and is negligible in the dark Higgs phenomenology. The result (2.31) and the expressions for the K and B meson decay are detailed in appendix B.2.

Several experiments measuring meson branching ratio can constrain the dark Higgs parameter space. The kaon decay $K^\pm \to \pi^\pm \mu^+ \mu^-$ measured at NA48 and $K^\pm \to \pi^\pm X$ at E949 are sensitive to dark scalars in the kinematically accessible region. Similar B decays measured at Belle, BaBar and LHCb $B^\pm \to K^\pm \mu^+ \mu^-$ give stronger limits because the CKM factor is larger and can access higher mass. The excluded regions are lotted on figure 2.4.

Finally, the Υ decay $\Upsilon \to S\gamma$ with subsequent decay $S \to \ell^+\ell^-$ can be searched for at BaBar. Here the production of the dark Higgs goes through the direct coupling to b quarks.

Beam dump experiments

Beam dump experiments are also sensitive to the dark Higgs. The general principle has been discussed in section 2.1.3, however, unlike in the dark photon case, direct production of S are suppressed by first-generation Yukawa coupling and are negligible. The main scalar production mechanism is through secondary flavour-changing decay of mesons produced in the collision such as $K \to \pi S$ and $B \to K S$ detailed in appendix B.2.

In this model, proton beam dumps have a distinct advantage over electron beam dumps as they produce more mesons by QCD interactions. The most sensitive beam dump experiment is CHARM, mainly through the secondary decay $K \to \pi S$, its exclusion limit is plotted on figure 2.4.

Collider searches

At LEP, the Higgs was searched for in the Bjorken process $e^+e^- \to Z \to Z^* H$. The search results can be recast as bounds on the dark Higgs model and are the best bound available for high masses $m_S > m_B - m_K$ [71].

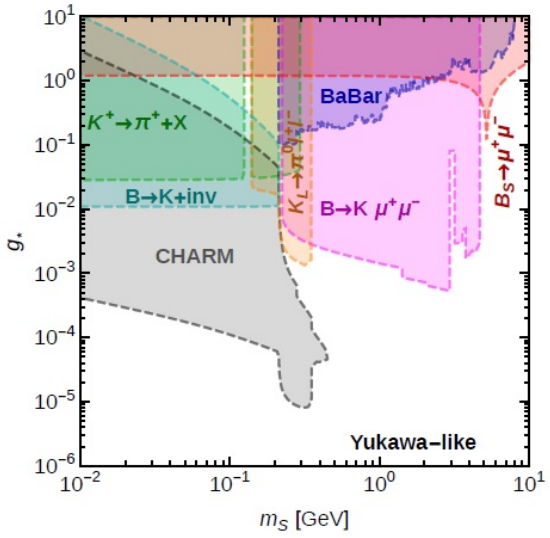

Figure 2.4 – Experimental limits on the Dark Higgs model in the $m_S - \epsilon$ plane from beam dump experiments (CHARM) and various meson decay measurements described in the text. This figure is taken from reference [34].

2.2.4 Theory motivations

There are many theories with additional scalars such as Supersymmetry or two Higgs doublet models. Scalars can also come from string remnants or from composite states of a strongly coupled sector. If another scalar S exists, the only relevant operator with SM fields is $SH^\dagger H$

so we expect this term to remain sizeable, even if it is generated at a very high scale. Again, there is no prediction for the mass of the new scalar; in Supersymmetry and two Higgs doublet models they are usually heavier than the Higgs boson and are out of reach of a fixed-target experiment.

Similarly to the dark photon, the dark Higgs could be a mediator between the SM and a dark sector containing a DM candidate. This can also give light DM or light mediators which can explain the astrophysical anomalies mentionned before.

2.3 Heavy Neutral Leptons

2.3.1 The model

The last renormalizable way to couple SM neutral particles to the SM is through the operator $\bar{L}H^c$ where L is the left-handed lepton doublet. To manipulate Majorana fermions, we will in this section switch to two-component spinor notation.

In the SM, the left-handed lepton doublet is described by the spinors $L = (\nu, e)$ carrying $SU(2)_L \times U(1)_Y$ charge $(2, -\frac{1}{2})$ and the right-handed charged lepton is described by the spinor $\bar{e}$ with charge $(1,1)$. The kinetic and Yukawa terms in the Lagrangian are given by:

$$\mathscr{L} = i\ell^\dagger \bar{\sigma}^\mu \partial_\mu \ell + i\bar{e}^\dagger \bar{\sigma}^\mu \partial_\mu \bar{e} - y_e \ell H^\dagger \bar{e} + c.c. \tag{2.32}$$

where family indices have been suppressed and y_e is a 3×3 matrix in family space. Setting H to its VEV gives the mass term for the charged leptons:

$$\mathscr{L}_M = -\frac{y_e v}{\sqrt{2}} \left(\bar{e}e + \bar{e}^\dagger e^\dagger \right) \tag{2.33}$$

and the neutrinos remain massless. Here we are in the basis where the charged leptons are in their mass eigenstate so the matrix y_e is real and diagonal with $m_{e_i} = (y_e)_{ii} v/\sqrt{2}$.

We now add SM-neutral two-components spinors $N_{i'}$ with $i' = 1, ..., n$. In what follows, primed indices run from 1 to n while unprimed indices are family indices. Since the Ns carry no SM charges, they can have a Majorana mass term (unlike the left-handed neutrino) and their only renormalizable interaction with the SM is through a Yukawa term with left handed leptons:

$$\mathscr{L} = \mathscr{L}_{SM} + N_{j'}^\dagger \bar{\sigma}^\mu \partial_\mu N_{j'} - F_{i j'} \ell_i \cdot H N_{j'} - \frac{1}{2} M_{i' j'} N_{i'} N_{j'} + c.c. \tag{2.34}$$

where ℓ and H are contracted with an epsilon tensor.

We will call the Ns heavy neutral leptons (HNLs) but they are sometimes called right-handed neutrinos or sterile neutrinos (because they carry no SM charges, in contrast with the left-handed neutrinos or active neutrinos). If $n = 3$, each SM left-handed neutrino gets its right-

handed counterpart and the 3 families structure is retained.

After electroweak symmetry breaking, the Yukawa term gives a Dirac mass term mixing ν and N on top of the Majorana mass term for the HNLs. The full active and sterile neutrino mass matrix is then given by:

$$M_\nu = \begin{pmatrix} 0 & F_{ij'}\frac{v}{\sqrt{2}} \\ (F_{ij'})^T\frac{v}{\sqrt{2}} & M_{i'j'} \end{pmatrix} \tag{2.35}$$

where the Lagrangian mass term is given by $\mathscr{L}_M = -\frac{1}{2}\Psi^T M_\nu \Psi + c.c.$ and Ψ is the $n+3$ vector $\Psi = \begin{pmatrix} \nu & N \end{pmatrix}^T$.

Below the HNL mass, one can integrate out the Ns and get the following effective Lagrangian:

$$\mathscr{L}_{\text{eff}} = \frac{1}{4} F_{ij'} (M^{-1})_{j'k'} F_{jk'} (\ell_i \cdot H)\left(\ell_j \cdot H\right) + c.c. \tag{2.36}$$

which is precisely the Weinberg operator. A generic HNL model gives mass and oscillation to the active neutrinos and gives rise to lepton number violation.

Toy model with one HNL

In order to better understand HNL phenomenology, we consider the toy model where $n = 1$. The Lagrangian is given by:

$$\mathscr{L} = \mathscr{L}_{SM} + N^\dagger \bar{\sigma}^\mu \partial_\mu N - F_i\, \ell_i \cdot H N - \frac{1}{2} M N N + c.c. \tag{2.37}$$

and the neutrino-HNL mass matrix is explicitly:

$$M_\nu = \begin{pmatrix} 0 & 0 & 0 & F_e v/\sqrt{2} \\ 0 & 0 & 0 & F_\mu v/\sqrt{2} \\ 0 & 0 & 0 & F_\tau v/\sqrt{2} \\ F_e v/\sqrt{2} & F_\mu v/\sqrt{2} & F_\tau v/\sqrt{2} & M \end{pmatrix} \tag{2.38}$$

with M_ν defined by $\mathscr{L}_M = -\frac{1}{2}\Psi^T M_\nu \Psi + c.c.$ and $\Psi = \begin{pmatrix} \nu_e & \nu_\mu & \nu_\tau & N \end{pmatrix}^T$.

We can diagonalize the matrix $M_\nu^\dagger M_\nu$ and get the square masses of the neutrinos and HNL. Before proceeding, it is easy to see that the mass matrix above has rank 2, giving mass to one neutrino and one HNL. In general, one needs n HNLs to give masses to n neutrinos (for $n \leq 3$, after that all active and sterile neutrino have mass). Since neutrino oscillation experiments measure two different mass splittings $\Delta m^2_\odot$ and Δm^2_{atm}, the one HNL only ($n = 1$) toy model is excluded by experiments. One needs at least two HNLs (in which case the lightest neutrino is massless) in order to reproduce neutrino oscillation data.

The advantage of the $n = 1$ case is that the masses and mixings can be solved explicitly. If $U^\dagger M_\nu^\dagger M_\nu U = D$ with U a unitary matrix and $D = \text{diag}(m_1^2, m_2^2, m_3^2, m_4^2)$ a diagonal matrix with

positive entries, the masses read:

$$\begin{aligned} m_1^2 = m_2^2 &= 0 \\ m_3^2, m_4^2 &= \frac{1}{2}\left[|M|^2 + \sum |F_i|^2 v^2 \mp |M|\sqrt{|M|^2 + 2v^2 \sum |F_i|^2}\right] \end{aligned} \tag{2.39}$$

and the mixing matrix is given by the diagonalization matrix U. The matrix between neutrino flavour eigenstates and mass eigenstates U_{PNMS} (defined in equation (2.46)) is given by the first three rows and columns of the full mixing matrix and is not in general a unitary matrix. Only the full 4×4 mixing matrix is unitary.

In the case $M \gg F_i v$, one can naturally identify $\nu_{1,2,3}$ with the active neutrinos and ν_4 with the HNL. In this limit, the masses are:

$$m_1^2 = m_2^2 = 0 \qquad m_3^2 \approx \frac{v^4}{4|M|^2}\left(\sum |F_i|^2\right)^2 \qquad m_4^2 \approx |M|^2 \tag{2.40}$$

and we see that the mass of the active neutrino is inversely proportional to the mass of the HNL M, hence the name *seesaw mechanism*. The mechanism presented here is called type I seesaw. The ν_4 state almost coincide with N but gets a small admixture of active neutrino ν_i given to first order by:

$$|U_{i4}|^2 = \frac{v^2}{2|M|^2}|F_i|^2 \ll 1 \tag{2.41}$$

and so the massive HNL gets a small SM weak charge. This mixing allows us to produce the heavy neutrino N from SM weak interactions and probe the parameter space.

With one Dirac HNL

Here we repeat the exercise with two fermions N and $\bar{N}$ that can be combined in a Dirac fermion. We have the following Lagrangian:

$$\mathscr{L} = \mathscr{L}_{SM} + N^\dagger \bar{\sigma}^\mu \partial_\mu N + \bar{N}^\dagger \bar{\sigma}^\mu \partial_\mu \bar{N} - F_i \ell_i \cdot H \bar{N} - \frac{1}{2} M N \bar{N} + c.c. \tag{2.42}$$

from which we can see that we can assign lepton number $+1$ to N and -1 to $\bar{N}$ and lepton number is conserved. Thus the Weinberg operator cannot be generated by this model and active neutrinos remain massless. One can check this explicitly by diagonalizing the mass matrix:

$$M_\nu = \begin{pmatrix} 0 & 0 & 0 & 0 & F_e v/\sqrt{2} \\ 0 & 0 & 0 & 0 & F_\mu v/\sqrt{2} \\ 0 & 0 & 0 & 0 & F_\tau v/\sqrt{2} \\ 0 & 0 & 0 & 0 & M \\ F_e v/\sqrt{2} & F_\mu v/\sqrt{2} & F_\tau v/\sqrt{2} & M & 0 \end{pmatrix} \tag{2.43}$$

where $\Psi = \begin{pmatrix} \nu_e & \nu_\mu & \nu_\tau & N & \bar{N} \end{pmatrix}^T$. The resulting masses are:

$$\begin{aligned} m_1^2 &= m_2^2 = m_3^2 = 0 \\ m_4^2 &= m_5^2 = \frac{1}{2}\left[|M|^2 + \sum |F_i|^2 v^2 + |M| \sqrt{|M|^2 + 2v^2 \sum |F_i|^2} \right] \end{aligned} \tag{2.44}$$

whith the three active neutrinos massless as advertised above and two same mass HNLs which can be combined in a single Dirac fermion.

Simplified model

In our analysis, we will consider a simplified model where only *one HNL is kinematically accessible* to the experiment. Other HNLs can be present but they are heavier than a few tens of GeV. This model has four parameters, chosen to be the HNL mass M_N and the three (small) mixing angle with the active neutrinos U_{i4}. We will in the analysis consider the three limiting cases $U_e = U_{14} \neq 0, U_{24} = U_{34} = 0$ (mixing with electron neutrino only), $U_\mu = U_{24} \neq 0, U_{14} = U_{34} = 0$ (mixing with muon neutrino only) and $U_\tau = U_{34} \neq 0, U_{14} = U_{24} = 0$ (mixing with tau neutrino only).

In the $n = 1$ case, the relation between the mixing angle U and the Lagrangian parameters F_i is given by equation 2.41, for $n \leq 2$ they are related by complicated roots resulting from the mass matrix diagonalization.

Note that in the one HNL case, assuming that the neutrino masses and mixing come from another mechanism, there is an upper limit on the mixing angle as function of the mass, else its contribution to the neutrino mass is too large. If the resulting neutrino mass is smaller than the atmospheric splitting $\Delta m^2_{\text{atm}} = 2.46 \times 10^{-3}\,\text{eV}^2$, then:

$$m_3^2 \leq \Delta m^2_{\text{atm}} \qquad \Rightarrow \qquad \sum |U_{i4}|^2 \leq \sqrt{\frac{\Delta m^2_{\text{atm}}}{M_N^2}} = 5.0 \times 10^{-11} \left(\frac{1\,\text{GeV}}{M_N} \right) \tag{2.45}$$

which is a very small mixing angle for HNL masses in the GeV range.

This relation does not hold anymore for $n \geq 2$ because contributions from different HNLs can cancel each other. In what follows, we will consider the simplified model above with one sterile neutrino N_1 of mass in the MeV - GeV range and with mixing angle larger than the bound 2.45. One can interpret this model in two ways: either more massive HNLs are present but kinematically inaccessible with correct masses and mixing angles to cancel the contribution of N_1 to active neutrino masses; or N_1 is a Dirac fermion, in which case its contribution to active neutrino masses is zero and another mechanism is responsible for neutrino oscillations.

2.3.2 Neutrino oscillations

In the SM neutrinos are massless and the three family states $(\nu_e, \nu_\mu, \nu_\tau)$ are defined by their charged lepton (e, μ, τ) counterpart in the weak interaction doublet. However, experimental results on neutrino oscillations show that these flavour states are not eigenstates of the full Hamiltonian describing neutrino propagation. The mass eigenstates are denoted (ν_1, ν_2, ν_3) and are related to the family states by the relation:

$$\begin{pmatrix} \nu_e \\ \nu_\mu \\ \nu_\tau \end{pmatrix} = U_{\text{PNMS}} \begin{pmatrix} \nu_1 \\ \nu_2 \\ \nu_3 \end{pmatrix} \tag{2.46}$$

where U_{PNMS} (Pontecorvo-Maki-Nakagawa-Sakata) is a 3×3 complex matrix experimentally consistent with a unitary matrix.

If U_{PNMS} is a unitary matrix, it contains four physical parameters (six if neutrinos are Majorana particles) usually taken to be three Euler angles $(\theta_{12}, \theta_{13}, \theta_{23})$ and a CP-violating phase δ (plus two Majorana phases α_1, α_2). The parametrization is:

$$U_{\text{PNMS}} = \begin{pmatrix} c_{12}c_{13} & s_{12}s_{13} & s_{13}e^{-i\delta} \\ -c_{23}s_{12} - s_{23}c_{12}s_{13}e^{i\delta} & c_{23}c_{12} - s_{23}s_{12}s_{13}e^{i\delta} & s_{23}c_{13} \\ s_{23}s_{12} - c_{23}c_{12}s_{13}e^{i\delta} & -s_{23}c_{12} - c_{23}s_{12}s_{13}e^{i\delta} & c_{23}c_{13} \end{pmatrix} \times \begin{pmatrix} 1 & 0 & 0 \\ 0 & e^{i\alpha_1} & 0 \\ 0 & 0 & e^{i\alpha_2} \end{pmatrix} \tag{2.47}$$

with $s_{ab} = \sin\theta_{ab}$ and $c_{ab} = \cos\theta_{ab}$.

Neutrino oscillations

This difference between the mass eigenstates and interaction eigenstates lead to neutrino oscillations. The neutrino produced in the source are in a flavour eigenstate $|\nu_\ell\rangle$ but the propagation states are the mass eigenstates $|\nu_i\rangle$. So after time t, the produced neutrino are in the state:

$$|\nu_\ell, t\rangle = U_{\ell j}|\nu_j, t\rangle = U_{\ell j}e^{-iE_j t}|\nu_j\rangle = U_{\ell j}e^{-iE_j t}|\nu_j\rangle = U_{\ell j}e^{-iE_j t}U^*_{\ell' j}|\nu_{\ell'}\rangle \tag{2.48}$$

where we have used that $U^{-1} = U^\dagger$. Then the transition amplitude from flavour ℓ to ℓ' is:

$$A_{\ell\ell'}(t) = \langle\nu_{\ell'}|\nu_\ell, t\rangle = U_{\ell j}e^{-iE_j t}U^*_{\ell' j} \tag{2.49}$$

and so the probability of going from flavour ℓ to ℓ' after time t is:

$$\begin{aligned} P_{\ell\ell'}(t) = |A_{\ell\ell'}(t)|^2 &= U_{\ell j}U^*_{\ell' j}U^*_{\ell k}U_{\ell' k}e^{-i(E_j - E_k)t} \\ &= \delta_{\ell\ell'} + 2\text{Re}\left[\sum_{j<k} U_{\ell j}U^*_{\ell' j}U^*_{\ell k}U_{\ell' k}e^{-i(E_j - E_k)t}\right] \end{aligned}$$

	Δm^2_{atm} (eV^2)	$\Delta m^2_{\odot}$ (eV^2)	θ_{12}	θ_{13}	θ_{23}	δ
NH	$(2.46 \pm 0.05) \times 10^{-3}$	$(7.5 \pm 0.2) \times 10^{-5}$	33.5 ± 0.8	8.5 ± 0.2	$42.3^{+3}_{-1.6}$	306^{+39}_{-70}
IH	$(-2.45 \pm 0.05) \times 10^{-3}$	$(7.5 \pm 0.2) \times 10^{-5}$	33.5 ± 0.8	8.5 ± 0.2	$49.5^{+1.5}_{-2.2}$	254^{+63}_{-62}

Table 2.2 – Summary of experimental values for the neutrino parameters (taken from [72]) in the normal and inverted mass ordering.

where we again used the unitarity of U. Then we can rearrange:

$$E_j - E_k = \frac{E_j^2 - E_k^2}{E_j + E_k} = \frac{m_j^2 - m_k^2}{E_j + E_k} \approx \frac{m_j^2 - m_k^2}{2E} \tag{2.50}$$

valid in the limit $m_i \ll E$ the neutrino beam energy. Then we get to the well-known formula:

$$\begin{aligned} P_{\ell\ell'}(t) = \delta_{\ell\ell'} - 4 \sum_{j<k} \text{Re}\left[U_{\ell j} U^*_{\ell' j} U^*_{\ell k} U_{\ell' k}\right] \sin^2 \frac{(m_j^2 - m_k^2)L}{4E} \\ - 2 \sum_{j<k} \text{Im}\left[U_{\ell j} U^*_{\ell' j} U^*_{\ell k} U_{\ell' k}\right] \sin \frac{(m_j^2 - m_k^2)L}{2E} \end{aligned} \tag{2.51}$$

which has two parts: one dependent on the different mixing angles and one oscillating term depending on the square mass differences and the baseline length. In practise, one performs experiments at $E/L \sim m_j^2 - m_k^2$ one of the mass splittings in order to be able to resolve the oscillations.

Neutrino parameters

The result of the global fit of all neutrino oscillation experiments [72] is presented in table 2.2. The absolute mass scale of the neutrino is not yet known (the lightest neutrino could be massless) and the mass ordering is also unknown. There are two possibilities: normal hierarchy (NH) where $m_3 > m_1, m_2$ in which case $\Delta m^2_{\text{atm}} = m_3^2 - m_1^2$ and inverted hierarchy (IH) where $m_3 < m_1, m_2$ and where $\Delta m^2_{\text{atm}} = m_3^2 - m_2^2$. The Majorana or Dirac nature of the neutrino is also not settled experimentally.

Neutrino anomalies

To conclude the quick review on neutrino oscillations, let us mention that although the standard PNMS scenario explains very well numerous neutrino data in terms of two mass splittings and three mixing angles, there remain some anomalies that cannot be explained by this scenario.

The LSND anomaly [73] is the observation of an excess of $\bar{\nu}_e$ in a $\bar{\nu}_\mu$ beam from pion decay ($\pi^+ \to \mu^+ \nu_\mu$ and followed by $\mu^+ \to e^+ \nu_e \bar{\nu}_\mu$) where $\bar{\nu}_e$ are identified by the well-studied reaction

$\bar{\nu}_e p \to e^+ n$. The excess of $\bar{\nu}_e$ compared to the prediction of the standard neutrino oscillation picture (almost no oscillation because of the short travelling path of the neutrino beam) can be interpreted as conversion of $\bar{\nu}_\mu$ to $\bar{\nu}_e$. The new mass splitting associated to this oscillation is of order $\Delta m^2 \sim \text{eV}^2$, much larger than solar or atmospheric splittings.

The MiniBooNE experiment was designed to investigate the LSND anomaly in terms of neutrino oscillations with a beam of muon neutrino and anti-neutrino. MiniBooNE saw an excess of ν_e at low energies [74], consistent with the oscillation interpretation of the LSND anomaly.

Moreover, recent reanalysis of older reactor neutrino data showed a deficit of observed $\bar{\nu}_e$ compared to the expected flux at similar L/E [75, 76]. To finish, ν_e observations from radioactive sources also hint at a deficit of electron neutrinos ("Gallium anomaly").

Put together, these observations known as short-baseline anomalies are consistent with a new mass difference in the eV range. Since the number of active neutrino is very well measured by the Z boson invisible decay width, the new mass scale must come from a sterile neutrino. On the other hand, the one HNL interpretation of the anomalies is in tension with ν_μ dissapearance experiments at similar L/E which see no muon neutrino deficit. This seem to favor models with two or three HNLs where CP-violation can explain the difference between neutrino and anti-neutrino experiments (for more details on the sterile neutrino interpretation of neutrino data see [77, 78]). In any case, more experiments are scheduled to investigate these anomalies.

2.3.3 HNL Lifetime

Due to the mixing with active neutrinos, HNLs are unstable and decay back to SM particles. The widths of different HNL decay channels are reproduced from [79] in appendix B.3. The lifetime of the HNL as function of the mass is slightly different depending on the mixing we are considering, because of the difference in kinematics of the associated charged lepton.

The HNL lifetime computed from these formulas and their charged conjugate is plotted on figure 2.5. The hadronic resonances are not taken into account so our estimate is probably underestimating the decay width around 700 MeV - 1 GeV.

2.3.4 Experimental probes

Sterile neutrinos couple to SM particles through the (small) mixing angle with active neutrinos due to the misalignment between flavour states and mass eigenstates. HNLs can thus be probed through any weak interactions involving active neutrinos. $N_{j'}$ behaves just like an active neutrino ν_i but with its couplings suppressed by the mixing angle $U_{ij'}$ and with different kinematics due to the different masses. The summary of current existing limits on the HNLs considering the simplified model described before is plotted on figure 2.6.

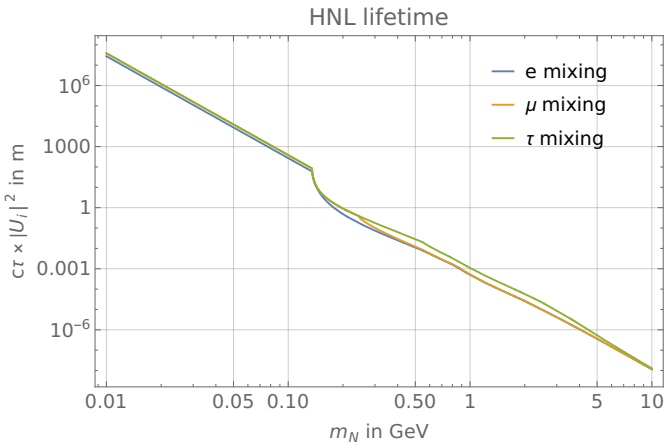

Figure 2.5 – HNL lifetime factoring out the $|U_i|^{-2}$ dependence in meters as function of M_N in GeV. Three curves are shown for each of the three mixing assuming the two other mixing angle are zero.

Peak and kink searches

Two-body leptonic decays of mesons $P \to \ell\nu$ produces a neutrino and a charged lepton. If there is a HNL N lighter than $m_P - m_\ell$, the process $P \to \ell N$ is also possible and suppressed by $|U_\ell|^2$. Then we expect two peaks (or more if there are several HNLs in this mass range) in the charged lepton spectrum measured in the meson rest frame, at:

$$E_\ell = \frac{m_P^2 + m_\ell^2}{2m_P} \qquad \text{and} \qquad E_\ell = \frac{m_P^2 - m_N^2 + m_\ell^2}{2m_P} \tag{2.52}$$

for respectively a (almost) massless neutrino and a massive HNL. Searches for a second peak in the lepton spectrum have been performed in the following decays: $\pi \to eN$ at TRIUMF [80], $\pi \to \mu N$, $K \to eN$, $K \to \mu N$ at E949 [81]. In order to probe the tau mixing, similar decays $\tau \to \pi N$, $\tau \to KN$ can be probed at B-factories.

In three body decays $X \to Y\ell(\nu \text{ or } N)$, the presence of an HNL results in a kink in the charged lepton spectrum at the point where the sterile neutrino becomes kinematically accessible. For very low HNL masses, one can use radioactive β decays of nuclei to probe the electron mixing angle.

Fixed target experiments

HNLs can also be produced in fixed target experiments, primarily through leptonic and semi-leptonic decays of hadrons since direct production is suppressed by the W mass. We refer to [79, 82] for the expressions of the decay rates for various mesons and decay channels. Then the HNLs produced at the interaction point can be detected by their SM decay channels listed in section 2.3.3 (for example $N \to \ell^+\ell^-\nu$). Fixed target experiments are very powerful probes

of HNL models for masses around a GeV but are limited by the meson masses produced at the interaction point.

If HNL production and decay happens in one detector, the HNL signature is a displaced vertex, with the HNL decay products coming out of nothing at some distance from the primary meson decay point. The number of events is suppressed for small mixing as $|U_i|^4$ ($|U_i|^2$ from the production rate and $|U_i|^2$ for the decay within the detector volume).

Experiments of this type include B-factories searching for HNLs in B-meson decays such as Belle [83] and LHCb [84].

The detector can also be placed far from the interaction point. The main advantage is the possibility of shielding the detector from SM particles produced at the interaction point (and thus use a more intense primary beam to get more events) at the cost of loosing information on the production mechanism. The HNL signature is as before charged tracks appearing out of nothing.

Beam dump experiments of this type include the Fermilab experiment NuTeV E813 [85], FMMF [86] and the CERN experiments PS191 [87], NA3, CHARM [88], CHARM II [89, 90], WA66 [91], NOMAD [92] as well as JINR [93].

Collider searches

HNLs heavier than a few GeV can be produced directly at colliders. The most stringent bounds for masses below the Z-boson mass come from LEP-I searches of $Z \to N\nu$ decays and subsequent N decay. Analyses were performed by L3 [94] and DELPHI [95] and the obtained limits are shown in figure 2.6.

For $M \geq m_Z$, LEP-II put bounds on HNLs by looking for direct production $e^+e^- \to N\nu$. The L3 collaboration searched for this process followed by the charged current decay $N \to \ell W$ and $W \to$ jets [96, 97]. Here the reach in HNL mass is limited by the LEP-II center-of-mass collision energy of $\sqrt{s} = 208$ GeV.

For even higher masses, limits are set by LHC searches for N production. The main analysis focuses on the process $pp \to W^* \to N\ell^+$ followed by $N \to \ell^+ jj$ (same sign dilepton searches) and its charged conjugate. This process clearly violates lepton number and has no SM background but it is possible only for Majorana HNLs. Such searches have been performed at CMS [98] and ATLAS. In case of Dirac HNL, the similar process (opposite sign dilepton) has too much SM background and the best search channel is the trilepton process [99] $pp \to W^* \to N\ell_1^+$ and $N \to \ell_2^-\ell_3^+\nu$ and charged conjugate. These bounds apply to the electron and muon mixing but not for the third family mixing because of the difficult tau reconstruction in hadron colliders.

At high mass, the present bounds from direct collider searches are less competitive than the

indirect bounds from electroweak precision tests [100–102] (see figure 2.6). Even if HNLs are not kinematically accessible, the presence of the mixing angle with active neutrinos reduces the coupling of the W-boson to the neutrino ν_i by a factor $(1-|U_i|^2)$. This affects precision observables such as the Z invisible decay width, the Z decay to leptons $\Gamma(Z \to \ell\ell)$ and the lepton universality tests such as $R^{\pi}_{e\mu} = \Gamma(\pi \to \mu\nu)/\Gamma(\pi \to e\nu)$. Also they affect the effective value of G_F measured from muon decay by cascade affect all other precision observables. These bounds are relatively independent of the HNL mass and constitute the most stringent bounds (and the only bound for the mixing to ν_τ) at high HNL mass above 100 GeV.

2.3.5 Theoretical motivations

The first motivation for the HNL model comes from neutrino masses. This model is renormalizable and can explain neutrino masses with the type-1 seesaw mechanism. As stated before, at least two HNLs are necessary to fit the two mass differences measured by neutrino oscillations. The short-baseline anomalies are further motivations for HNLs but it is difficult to give a unique explanation to all anomalies with a simple HNL model.

From the top-down perspective, right-handed neutrinos appear in Left-Right symmetric models to mirror the left-handed particle content. They also appear in some GUT theories like $SO(10)$ in order to fill the 16 dimensional representation.

The sterile neutrino can be a DM candidate [103] in the form of warm keV DM. In order for the HNL to be stable on cosmoogical time scales, one needs a very small mixing to active neutrinos. The neutrino mass differences are caused by two additional HNLs, much heavier than the DM candidate and almost degenerate in mass. Interestingly, the model with 3 HNLs can also explain the baryon asymmetry in the universe [104]. This extension of the SM is called the neutrino minimal Standard Model (νMSM) and can solve three observations: neutrino masses, dark matter and baryogenesis.

2.4 Our experimental setup

A muon collider would be very interesting for high energy physics [105, 106]. As electron colliders it has the advantage over hadron collider of having cleaner events, less pileup and QCD background. Also, for circular rings, the muon being heavier than the electron, it suffers less from energy loss by bremsstralung and can be accelerated to higher energies. On the physics point of view, the Higgs cross-section is much higher by a factor m_μ^2/m_e^2, allowing for better statistics on Higgs properties. It could also test lepton universality and search for models with new particles coupling only to the second and third family, motivated by the muon $g-2$ anomaly, the proton radius puzzle or the B anomalies. The main disadvantage is of course the muon finite lifetime which causes considerable technical difficulties.

The first step of a muon collider is the production of a muon beam whith a small energy spread.

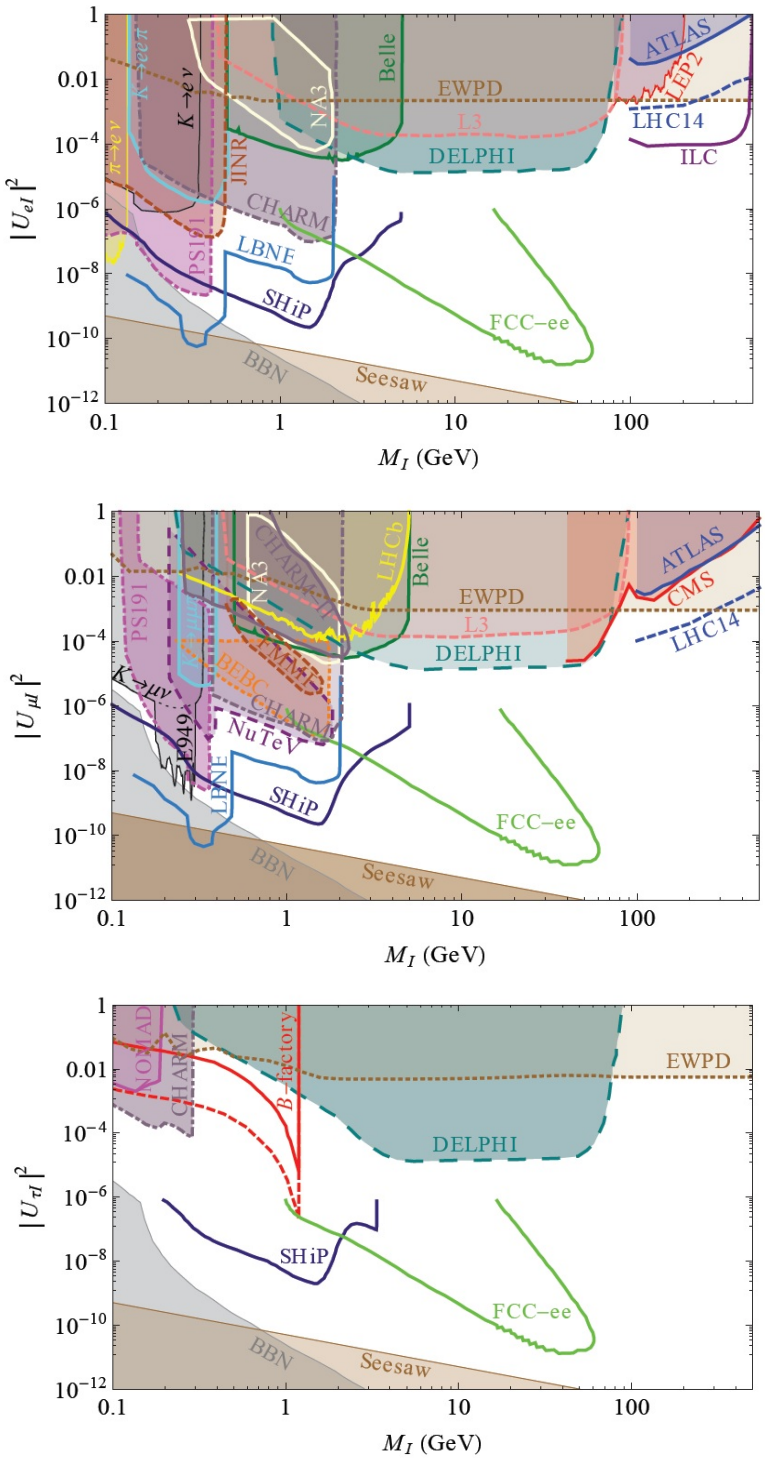

Figure 2.6 – Current experimental limits on the HNL simplified model assuming that one HNL only is kinematically accessible. The top figure represents the case where only the mixing angle U_e to ν_e is non zero. The middle figure is the case where only the mixing angle to the muon neutrino is non zero. The bottom figure is assuming only a mixing to the tau neutrino. The three figures are copied from the paper [34].

Muon beams are usually obtained from pion decay, with the meson produced by a proton beam on target. This requires a muon cooling system to focus and to reduce the emittance (the spread in energy) of the beam. Another possibity, suggested by [107, 108] is to use a positron beam on a fixed target, with energy tuned just above the muon pair threshold and produce the muon beam through the process $e^+e^- \to \mu^+\mu^-$. This creates a highly collimated muon beam with small emittance of energy $E_b \sim 20$ GeV. However, due to the small cross-section of the pair production process $\sigma \sim 1\,\mu b$, a very intense beam of positrons and a very dense target is required to produce sufficient muons. Ref. [107] suggests a setup with a 45 GeV positron beam in a circular ring with an intensity up to 1.5×10^{18} positrons per second on a beryllium target.

The goal of this section is to study the performance of this very intense positron beam on target as a beam dump experiment searching for very weakly coupled new physics. The main advantage of this setup is the extraordinarily intense primary beam compared to past experiments or future experiments such as SHiP, resulting in a larger luminosity. Also, with a leptonic beam, there are less QCD events at the interaction point compared to a proton beam. This on the one hand means a smaller meson production rate and thus less reach for Dark Higgs and HNL models; on the other hand it means less SM background and less shielding necessary after the interaction point. The experiment consists of a long detector with fiducial length L placed at a distance d from the interaction point in the beamline direction. It is totally independent from the muon acceleration or any other use of the muon beam and can be run as a parasitic experiment to the muon collider program. Depending on the size and the complexity of the detector, it can be a relatively cheap experiment.

In order to study the performances of such a detector, we consider the following experimental setup: the primary positron beam has energy $E_0 = 45$ GeV and intensity 1.5×10^{18} e^+ per second during 3 years of data taking resulting in the huge $N_e \approx 1.4 \times 10^{26}$ positrons on target. The target is a beryllium target of thickness $T = 3$ mm (about 0.01 radiation length). The total luminosity is given by the formula (valid for thin targets only):

$$\mathscr{L} = N_e \frac{N_A \rho T}{A} = 5.25 \times 10^{21}\,\text{mb}^{-1} \tag{2.53}$$

where $A = 9.01\,\text{g}\cdot\text{mol}^{-1}$ is the beryllium atomic mass, $\rho = 1.848\,\text{g}\cdot\text{cm}^{-3}$ is the target density and $N_A = 6.02 \times 10^{23}\,\text{mol}^{-1}$ is the Avogadro number. We consider a detector of fiducial length $L = 200$ m and located at a distance $d = 20$ m in the beamline direction.

In this thesis, we do not study precisely the background from SM muons and neutrinos produced at the target and that can interact in the detector. Compared to similar experiments such as SHiP, we expect less background because the incoming beam is leptonic and is less energetic. We also do not specify the details of the detector design, leaving this for a more complete study. Thus it is difficult to estimate a precise reach for our experiment. In what follows, we will consider that the threshold for discovering a dark sector particle is at 10 decay events in the detector volume, slightly higher than for similar experiments. We will also show the curves for 100 events, corresponding to a very conservative estimate, and for 1 event,

which would be the reach in an ideal background free experiment.

2.4.1 Dark photon reach

In our setup, dark photons are primarily produced by A' radiation from the positron in the positron-nucleus interaction. This can be estimated using the Weizsäcker-Williams approximation with more details presented in appendix B.1. This separates the total cross-section in two pieces, one where the intermediate photon is considered as a real photon in the 2 to 2 process $e^+\gamma \to e^+A'$, the second giving the effective photon flux from the nucleus electromagnetic field. The resulting differential cross-section is:

$$\frac{d\sigma}{dx\,d\cos\theta_{A'}} \approx 4\alpha^3\epsilon^2\chi\frac{E_0^2 x}{U^2}\left[2-2x+x^2+\frac{2(1-x)^2 m_{A'}^2}{U^2}\left(m_{A'}^2+\frac{xU}{1-x}\right)\right] \tag{2.54}$$

where $E_{A'}$ is the dark photon energy, x is the ratio $x = E_{A'}/E_0$, $\theta_{A'}$ is the A' polar angle in the laboratory frame and U is the virtuality of the intermediate electron given by:

$$U \approx E_0^2\theta_{A'}^2 x + m_{A'}^2\frac{1-x}{x} + m_e^2 x \tag{2.55}$$

The photon flux χ encodes the properties of the target nucleus. It is given by the following integral over the electric form factor [40]:

$$\chi = \int_{t_{\min}}^{t_{\max}} dt\,\frac{t-t_{\min}}{t^2}G_2(t) \tag{2.56}$$

where $t_{\min}$ and $t_{\max}$ are given in appendix B.16 and the explicit form of the electric form factor $G_2(t)$ can be found in appendix B.27,B.28. To a good approximation, one can neglect the dependence of χ on the kinematics $x,\theta_{A'}$ and set $t_{\min} = (m_{A'}^2/2E_0)^2$ and $t_{\max} = m_{A'}^2 + m_e^2$, simplifying the total rate calculation. We will call this improved Weizsäcker-Williams (IWW) approximation.

The U^{-2} dependence of the cross-section makes the A' angular distribution strongly peaked at $\theta_{A'} = 0$, justifying a detector in the beam axis. The number of dark photons decaying in our detector is given by:

$$N_{\text{obs}} = \mathscr{L}\int_0^{\theta^\star} d\theta_{A'}\int_{m_{A'}/E_0}^1 dx\epsilon^2\frac{d\sigma}{dx\,d\theta_{A'}}\exp\left(-\frac{Dm_{A'}\epsilon^2}{\beta x E_0 l_0}\right)\left[1-\exp\left(-\frac{Lm_{A'}\epsilon^2}{\beta x E_0 l_0}\right)\right] \tag{2.57}$$

where we have pulled out the explicit dependence on ϵ in the formula. The decay legth l_0 is given in figure 2.1 and the luminosity is given in equation 2.53. The formula we use for $\frac{d\sigma}{dx\,d\theta_{A'}}$ is the formula B.25 with only Weizsäcker-Williams approximation. The numerical calculation shows that the results of B.25 are very close to the ones with one more layer of approximations B.26 and the IWW approximation.

The signature of a dark photon decaying is the detector is very simple: it consists of two

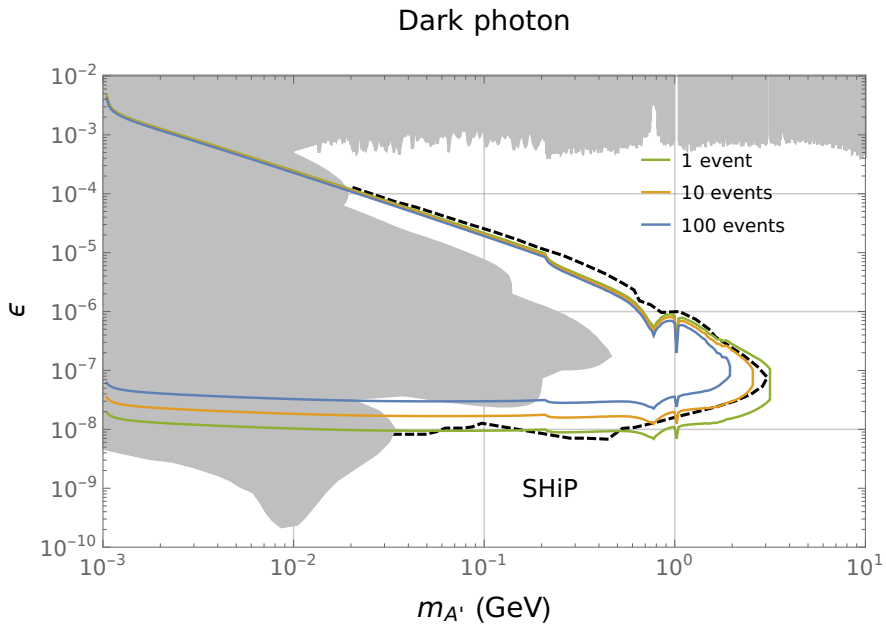

Figure 2.7 – Region in the parameter plane ($m_{A'} - \epsilon$) where out experimental setup is expected to see 1, 10 and 100 dark photon events. The estimated exclusion limit from the SHiP experiment [34] is plotted in black dashed line. The experimentally excluded region is shaded in grey. See text for more details on the current experimental status.

charged tracks appearing out of nothing, coming from the interaction point and with invariant mass equal to $m_{A'}$. The branching ratio of A' to a pair of charged SM particles is very close to 1 so we do not add any term accounting for detection efficiency. We consider an opening angle $\theta^\star = 0.01$ rad. The region of parameter space $m_{A'} - \epsilon$ where our apparatus is expected to see more than 100, 10 and 1 event is plotted in figure 2.7.

We consider that 10 events is a reasonable estimate of the reach of our experiment. 1 event corresponds to the ideal case with zero background, whereas 100 events is a very conservative threshold given that the dark photon signal is very clean. We see that our experiment could improve significantly the limits from beam dump experiments, especially for high dark photon mass around 1 GeV. The exclusion region in the ideal zero-background is very comparable to the SHiP expected reach [34] and is slightly smaller in the more realistic estimate.

2.4.2 Meson production

The number of mesons produced by the primary positron beam is very important to evaluate in order to estimate the dark Higgs and HNL production from secondary decay. In order to compute the number of mesons produced by our setup, we use the GiBUU (Giessen Boltzmann-Uehling-Uhlenbec) model and code [109], a transport model for elementary particle interaction with nuclei.

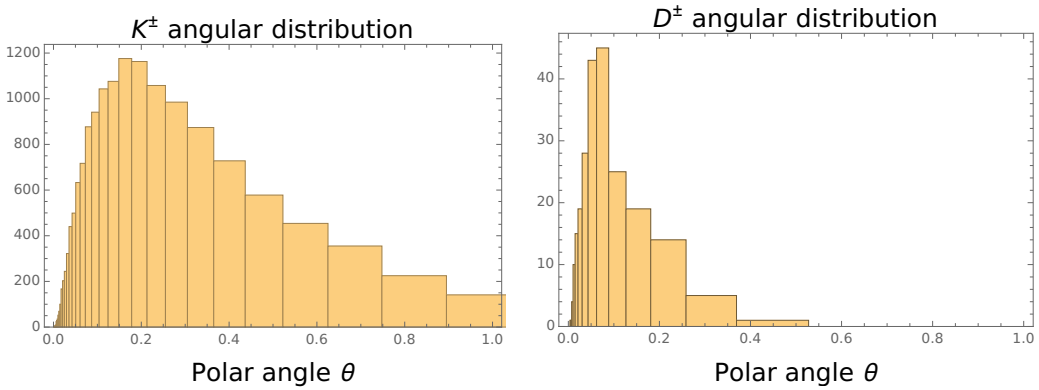

Figure 2.8 – Angular distribution of charged kaons (left panel) and charged D mesons (right panel) produced by a 45 GeV positron beam against a beryllium target obtained with the GiBUU code [109].

Kaon production

For our experimental setup, at 45 GeV positron beam striking a beryllium target, the GiBUU code predicts the following kaon production cross-sections:

$$\sigma(K^{\pm}) = 9.2 \times 10^{-5}\,\text{mb} \qquad \text{and} \qquad \sigma(K^0, \overline{K}^0) = 8.9 \times 10^{-5}\,\text{mb} \tag{2.58}$$

leading to a production of 5×10^{17} charged kaons and a similar number of neutral kaons.

The distribution of the charged kaon polar angle in the laboratory frame (with respect to the incoming positron beam) is plotted on figure 2.8, left panel. We can see that unlike for the dark photon, kaons are produced with relatively large polar angle: the median angle is $\theta_{\text{med}} = 0.15$ rad and only 0.8% of charged kaons are produced towards the detector (with polar angle smaller than 0.01). Compared to proton beam dump experiments such as CHARM or SHiP, the meson production cross-section is lower (from electromagnetic interaction instead of QCD interaction) but also the angular spread is larger because the primary beam is less energetic (45 GeV against 400 GeV for CHARM and SHiP).

D meson production

The production cross sections for various charmed mesons are also estimated using GiBUU:

$$\sigma(D^{\pm}) = 2.4 \times 10^{-7}\,\text{mb} \qquad \sigma(D^0, \overline{D}^0) = 5.3 \times 10^{-7}\,\text{mb} \qquad \text{and} \qquad \sigma(D_s^{\pm}) = 5.5 \times 10^{-8}\,\text{mb} \tag{2.59}$$

which translates with our experimental setup to 1.3×10^{15} charged D mesons, 3×10^{15} neutral D mesons and 3×10^{14} D_s mesons.

Figure 2.8, right panel, shows the angular distribution of the charged D mesons in the laboratory frame. The angular spread is narrower than for kaons, with a median angle of 0.06 rad

and about 3% of the charged charmed mesons produced in the direction of the detector.

D mesons are an important source of HNLs in the GeV range. Also, they produce tau leptons from $D_s \to \tau \bar{\nu}_\tau$ decay, themselves important for probing the HNL mixing with ν_τ. From the branching ratio $BR(D_s \to \tau \nu_\tau) = 5.5\%$, we expect 1.6×10^{13} tau leptons from D_s decay, more than from direct QED production.

B meson production

For a proton in the beryllium nucleus, the energy of the positron-proton collision is $\sqrt{s} = \sqrt{2E_0 m_p + m_p^2} = 9.2$ GeV, below the two B meson threshold. Thus the number of produced b-quark is negligible because of the kinematics. This has important consequences for the reach of our experimental setup: dark Higgs and HNLs heavier than the charm quark can only be produced in B-meson decays.

2.4.3 Dark Higgs

The dark Higgs is mostly produced in decays of down type quarks, in our case charged and neutral kaons. The production from charm quark decay is strongly suppressed as we have seen. From the kaon cross-section (2.58) and estimating that 0.5% of the produced dark Higgs enter the detector, one can estimate that the reach in the mass-coupling plane is similar to the one of the CHARM experiment. Since our apparatus does not improve the existing experimental bounds, we do not study the dark Higgs any further.

2.4.4 HNLs

HNLs are primarily produced by meson decays since direct production involve a W-boson and is strongly suppressed at low energies. The two-body leptonic decay width of a pseudoscalar meson h is given by:

$$\Gamma(h^\pm \to \ell_i^\pm N) = |U_i|^2 \times \frac{G_F^2 f_h^2 m_h}{8\pi} |V_h|^2 \left[1 - \frac{M_N^2}{m_h^2} + 2\frac{m_\ell^2}{m_h^2} + \frac{m_\ell^2}{M_N^2}\left(1 - \frac{m_\ell^2}{m_h^2}\right)\right] \lambda(m_h, M_N, m_\ell) \tag{2.60}$$

where f_h is the meson decay constant, V_h is the relevant CKM element and the function λ is the standard expression:

$$\lambda(m_h, M_N, m_\ell) = m_h^2 + M_N^2 + m_\ell^2 - 2m_h M_N - 2m_\ell M_N - 2m_h m_\ell \tag{2.61}$$

Three body semi-leptonic decays $h \to h' \ell N$ also produce HNLs but are subleading compared to the two body decay, except for low M_N. For the full expression of the three body decay width we refer to [79, 82].

We first do a preliminary estimate of the reach of our experimental setup by restricting ourselves to two-body leptonic decays $K \to \ell N$, $D \to \ell N$ and $D_s \to \ell N$. We use the meson cross-section production obtained with GiBUU and estimate that only 0.5% and 2% of the HNLs respectively from kaon and D, D_s decays are produced in the direction of the detector. In order to probe the HNL mixing with ν_τ, it is important to include the production from τ decay. The tau lepton mainly comes from D_s decay. We also estimate that 0.5% of HNLs from tau decay are produced towards the detector. The exclusion limit from this simple calculation asking 10 HNL decays to two charged particles in the detector are plotted in figure 2.9. In the case of HNL mixing with ν_e or ν_μ, we do not show the events from τ decay becay they are negligible compared to the ones from D, D_s decays. Also, we do not take into account pion decay because this channel only probes very light HNLs in a region already well probed by experiments.

We stress that these are only preliminary estimates where the kinematics and angular distribution are oversimplified. Using the meson kinematic and angular distribution obtained with GiBUU, we will simulate the leptonic and semi-leptonic decays to get the energy and angular distribution of the produced HNLs. These computations are still ongoing and the results will be shown in the final version of this thesis.

We see that our experiment could improve the existing experimental limits on HNLs, especially in the 1 GeV region with events coming from charmed meson decay for HNLs mixing with ν_e, ν_μ. Our reach at high mass is limited by the charmed meson masses since we need $m_N \leq m_{D_s} - m_\ell$. For the mixing with tau neutrinos, the improvement is even more important due to the large number of tau leptons produced in the experiment. In the tau mixing case, meson decay can only probe masses $m_N \leq m_{D_s} - m_\tau \sim 200$ MeV. This is why HNLs produced from tau decays $\tau \to NX$ are very important.

However, in all three cases, the exclusion limits are well within the SHiP expected bounds [34]. At high mass, this is because of the lack of B-mesons, and the lower number of D, D_s mesons. At low mass, the limits coming from kaon decay are better than SHiP, this is because in the latter experiment, most kaons are stopped right after the interaction point by the shielding before they have time to decay. In our case, a more careful study of the background is necessary to decide if our shield can be placed further from the target in order to have more kaon decays.

2.4.5 Conclusion

We presented an fixed target experiment searching for dark sector particles that could be run in parallel to a future muon collider program. The intense positron beam hitting a target in order to produce the muons can also be used as a fixed-target experiment by adding a shielding and a detector in the beam direction. The extreme intensity of the primary positron beam makes it possible to have more particles on target than any previous electron beam dump experiment.

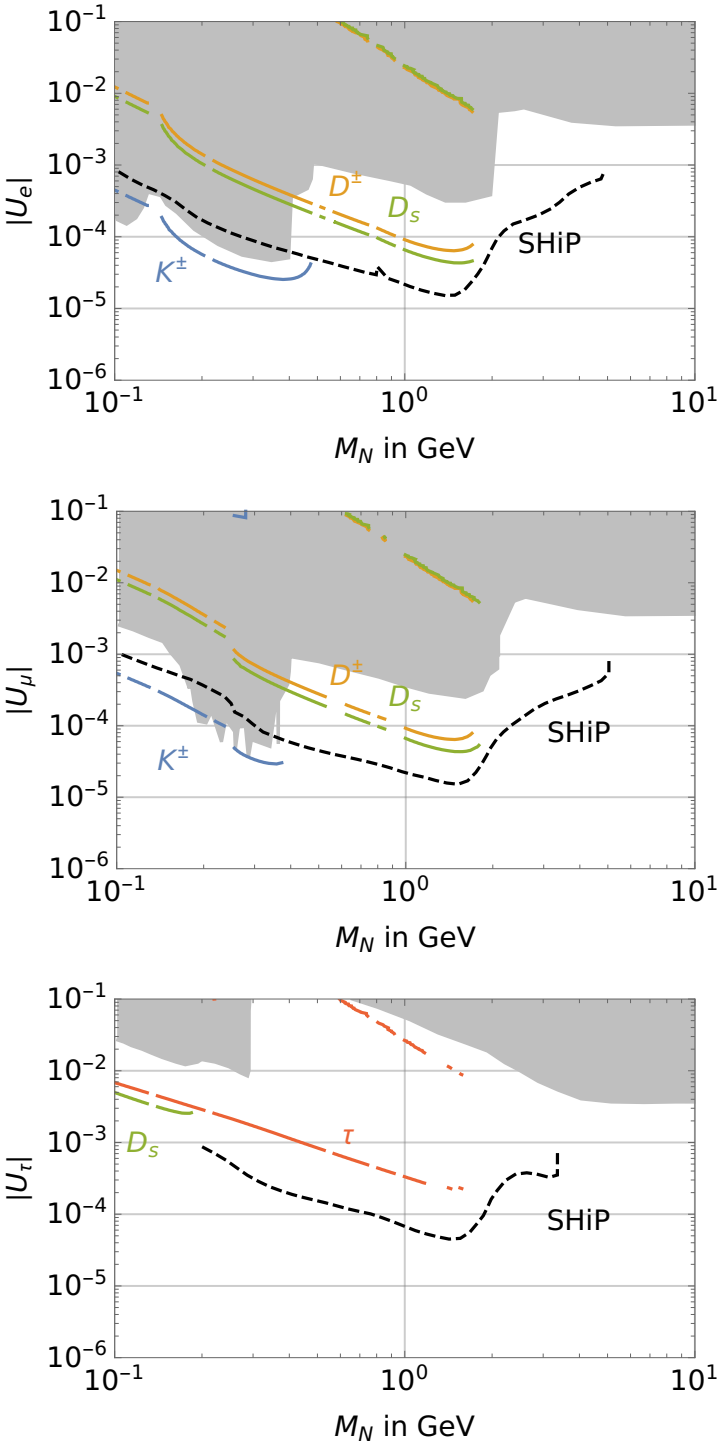

Figure 2.9 – Preliminary plots for the expected exclusion limit from our experimental setup. The lines correspond to 10 decays to charged particles in the detector, with different curves for HNLs coming from kaon decay (blue), $D^{\pm}$ decay (orange), D_S decay (green) and τ decay (red). The SHiP limits are shown in black dashed for comparison and the current experimental limits are shaded in grey. The top panel shows the scenario with only mixing to ν_e, the middle panel the one with mixing to ν_μ only and the bottom panel the scenario with mixing to ν_τ only.

Compared to the proton fixed target experiment SHiP, our setup has more luminosity but suffers from smaller meson production cross-section. On the one hand this reduces the SM background, simplifying the shield design but on the other hand makes our experiment less competitive in models where the dark particle mainly comes from secondary meson decay.

We studied the expected reach for the dark photon, the dark Higgs and the HNL models. In the dark photon, our experiment could bring a large improvement in the experimental limits in the region $m_{A'} \sim 1$ GeV and $\epsilon \sim 10^{-6} - 10^{-7}$. Our result is plotted in figure 2.7. For the dark Higgs model, our setup does not improve significantly current experimental bounds, mainly because the energy of the positron beam is too low to produce B-mesons. Finally for the HNL model, our experiment has the potential to improve bounds for e and μ mixing in the $M_N \sim 1$ GeV region from the large number of charmed quarks. In the τ mixing case, significant progress can be made for $M_N \leq m_\tau$ from the production of HNL from tau lepton decay. The expected limits in the three cases obtained from a preliminary simplified calculation are shown in figure 2.9.

In order to have a more precise idea of the reach of our proposed experimental setup, a more careful study of the SM background, the different shielding possibilities and of the detector design is necessary. On the physics side, it would be interesting to estimate its exclusion potential for other dark sector models such as axion-like particles. Such an experiment could also have applications in neutrino physics, being an important source of tau neutrino.

A muon collider would have tremendous discovery potential in the energy frontier. With little more instrumentation, it can also contribute a lot to the intensity frontier. Such an ambitious program would greatly improve our understanding of the Standard Model and shed light on the problems of modern particle physics and on their possible solutions.

3 Standard Model effective field theory

3.1 Introduction

The ongoing exploration of the high-energy frontier at the LHC strongly suggests that the only fundamental degrees of freedom at the weak scale are the Standard Model ones. Moreover, their perturbative interactions are well described by the most general renormalizable SM Lagrangian invariant under the $SU(3)_C \times SU(2)_L \times U(1)_Y$ local symmetry. However, theoretical problems of the SM suggest that new physics should be not much heavier than the weak scale. One can be agnostic about new physics and try to study its effect in a model-independent way. One framework designed to describe such new physics effects in a systematic fashion goes under the name of the SM Effective Field Theory (SMEFT).

In this approach, the effects of new particles with masses above the weak scale are encoded in higher-dimensional operators suppressed by inverse powers of the SM cutoff:

$$\mathscr{L} = \mathscr{L}_{\text{SM}} + \sum_i \frac{c_i}{\Lambda_{\text{SM}}} O_i^{D=5} + \sum_i \frac{c_i}{\Lambda_{\text{SM}}^2} O_i^{D=6} + \cdots \tag{3.1}$$

The goal of this program is to study directly the effects of the different operators O_i and put constraints on the value of the Wilson coefficients c_i (fixing Λ_{SM} to a reference value). One can then analyze experimental searches once and for all within this framework. The output of such analysis, namely numerical values for the Wilson coefficients of higher-dimensional operators, can then be applied to any new physics model covered by the SMEFT. Significant progress has been recently achieved concerning the automation of this EFT matching [110–113]. The efficient SMEFT program should be compared with model-dependent studies where non-trivial hadronic effects, PDFs, radiative corrections, experimental errors, cuts, etc., have to be taken into account for each model.

We have seen in the introduction that assuming that dimension-5 terms are present leads to neutrino masses, lepton number violation, and assuming c_i to be of order one leads to a very large estimate of $\Lambda_{\text{SM}} \sim 10^{14}$ GeV. Here we assume that new physics at the cutoff can have additional symmetry structure, maybe leading to a large hierarchy between different

Wilson coefficients. In particular, we assume lepton and baryon number conservation so that dimension-5 operators are absent and leading SMEFT contributions originate from dimension-6 operators [114, 115]. In this framework, there are 2499 independent operators in $\mathscr{L}^{D=6}$. Among them, a lot of operators mediate FCNC or violate individual lepton number and must be small.

There is a vigorous program to characterize the effects of the dimension-6 operators on precision observables and derive constraints on their Wilson coefficients in the SMEFT Lagrangian [116–154]. Most of these analyses assume that the dimension-6 operators respect some flavour symmetry in order to reduce the number of independent parameters. On the other hand, Refs. [139, 150] allowed for a completely general set of dimension-6 operators, demonstrating that the more general approach is feasible.

In this work, we further pursue the approach of Refs. [139, 150], providing new constraints on the SMEFT where all independent dimension-6 operators may be simultaneously present with an arbitrary flavour structure. We compile information from a plethora of low-energy flavour-conserving experiments sensitive to electroweak gauge boson interactions with fermions and to 4-fermion operators with 2 leptons and 2 quarks (LLQQ) and 4 leptons (LLLL). There are two main novelties compared to the existing literature. First, precision constraints on the LLQQ operators have not been attempted previously in the flavour-generic situation. Therefore our results are relevant to a larger class of UV completions where new physics couples with a different strength to the SM generations. Note that, in particular, all models addressing the recent B-meson anomalies (see e.g. [155–159]) must necessarily involve exotic particles with flavour non-universal couplings to quarks and leptons. Our analysis provides model-independent constraints that have to be satisfied by all such constructions. Second, we include in our analysis the low-energy flavour observables (nuclear, baryon and meson decays) recently summarized in Ref. [160]. At the parton level these processes are mediated by the quark transitions $d(s) \to u\ell\bar{\nu}_\ell$, hence they can probe the LLQQ operators. We will show that for certain operators the sensitivity of these observables is excellent, such that new stringent constraints can be obtained. Moreover, the low-energy flavour observables offer a sensitive probe of the W boson couplings to right-handed quarks.

Our analysis is performed at the leading order in the SMEFT. We ignore the effects of dimension-6 operators suppressed by a loop factor, except for the renormalization group running within a small subset of the LLQQ operators. Moreover all dimension-8 and higher operators are neglected, and only the linear contributions of the dimension-6 Wilson coefficients are taken into account. The corollary is that the likelihood we obtain for the SMEFT parameters is Gaussian. All in all, we provide simultaneous constraints on 61 linear combinations of the dimension-6 Wilson coefficients. We quote the central values, the 68% confidence level (CL) intervals and the full correlation matrix, which allows one to reconstruct the complete likelihood function. The final results are also provided in an electronic form as supplementary material in the publication [161], so that they can be more easily integrated into other analyses.

In this chapter, we first present the theoretical framework and the notation in section 3.2. We review the experimental input of our analysis in section 3.3 and show the results of our fit section 3.4, in the general case and in the flavour symmetric limit. Finally section 3.5 discusses the interplay with LHC searches, and section 3.6 contains our conclusions. This chapter is taken from the two publications [150, 161].

3.2 Formalism and notation

3.2.1 SMEFT with dimension-6 operators

Our framework is that of the baryon- and lepton-number conserving SMEFT [114, 115]. The Lagrangian is organized as an expansion in $1/\Lambda^2$, where Λ is interpreted as the mass scale of new particles in the UV completion of the effective theory. We truncate the expansion at $\mathcal{O}(\Lambda^{-2})$, which corresponds to retaining operators up to the canonical dimension D=6 and neglecting operators with $D \geq 8$. The Lagrangian takes the form

$$\mathscr{L} = \mathscr{L}_{\text{SM}} + \sum_i \frac{c_i}{v^2} O_i^{D=6}, \tag{3.2}$$

where $\mathscr{L}_{\text{SM}}$ is the SM Lagrangian, $v = (\sqrt{2}G_F)^{-1/2} \simeq 246$ GeV, each $O_i^{D=6}$ is a gauge-invariant operator of dimension D=6, and c_i are the corresponding Wilson coefficients that are $\mathcal{O}(\Lambda^{-2})$. $O_i^{D=6}$ span the complete space of dimension-6 operators, see Refs. [162, 163] for examples of such sets.

In order to connect the SMEFT to observables it is convenient to rewrite equation (3.2) using the mass eigenstates after electroweak symmetry breaking. Then the effects of dimension-6 operators show up as corrections to the SM couplings between fermion, gauge and Higgs fields, or as new interaction terms not present in the SM Lagrangian. The discussion and notation below follows closely that in Section II.2.1 of Ref. [164]. We define the mass eigenstates such that all kinetic and mass terms are diagonal and canonically normalized. We also redefine couplings such that, at tree level, the relation between the usual SM input observables G_F, α, m_Z and the Lagrangian parameters g_L, g_Y, v is the same as in the SM. See Ref. [164] for complete definition of conventions and the complete list of interaction terms with up to 4 fields. In the following we only highlight the parts of the mass eigenstate Lagrangian directly relevant for our analysis.

Without loss of generality, the Lagrangian can be brought to a form where the kinetic terms for the electroweak gauge boson are given by

$$\mathscr{L} \supset -\frac{1}{2} W^+_{\mu\nu} W^-_{\mu\nu} - \frac{1}{4} Z_{\mu\nu} Z_{\mu\nu} - \frac{1}{4} A_{\mu\nu} A_{\mu\nu} + \frac{g_L^2 v^2}{4} (1+\delta m)^2 W^+_\mu W^-_\mu + \frac{(g_L^2+g_Y^2)\, v^2}{8} Z_\mu Z_\mu \tag{3.3}$$

where δm parametrizes the relative correction to the W boson mass that may arise in the presence of D=6 operators. By construction, there is no correction to the Z boson mass: a

possible shift due to D=6 operators has been absorbed into the definition of the electroweak parameters g_L, g_Y and v.

One important effect of the dimension-6 operators from the point of view of precision measurements is the shift of the interaction strength of the weak bosons. We parametrize the interactions between the electroweak gauge bosons and fermions as

$$\begin{aligned}
\mathscr{L} \supset\ & eA^\mu \sum_{f=u,d,e} Q_f \left(f_I^\dagger \bar{\sigma}_\mu f_I + \bar{f}_I^\dagger \bar{\sigma}_\mu \bar{f}_I \right) \\
+\ & \frac{g_L}{\sqrt{2}} \left[W^{\mu+} \nu_I^\dagger \bar{\sigma}_\mu \left(\delta_{IJ} + [\delta g_L^{We}]_{IJ} \right) e_J + W^{\mu+} u_I^\dagger \bar{\sigma}_\mu \left(V_{IJ} + \left[\delta g_L^{Wq} \right]_{IJ} \right) d_J + \text{c.c.} \right] \\
+\ & \frac{g_L}{\sqrt{2}} \left[W^{\mu+} \bar{u}_I \sigma_\mu \left[\delta g_R^{Wq} \right]_{IJ} \bar{d}_J^\dagger + \text{h.c.} \right] \\
+\ & \sqrt{g_L^2 + g_Y^2} Z^\mu \sum_{f=u,d,e,\nu} f_I^\dagger \bar{\sigma}_\mu \left((T_3^f - s_\theta^2 Q_f) \delta_{IJ} + \left[\delta g_L^{Zf} \right]_{IJ} \right) f_J \\
+\ & \sqrt{g_L^2 + g_Y^2} Z^\mu \sum_{f=u,d,e} \bar{f}_I \sigma_\mu \left(-s_\theta^2 Q_f \delta_{IJ} + \left[\delta g_R^{Zf} \right]_{IJ} \right) \bar{f}_J^\dagger
\end{aligned} \tag{3.4}$$

Here, g_L, g_Y are the gauge couplings of the $SU(2)_L \times U(1)_Y$ local symmetry, the electric coupling is $e = g_L g_Y / \sqrt{g_L^2 + g_Y^2}$, the sine of the weak mixing angle is $s_\theta = g_Y / \sqrt{g_L^2 + g_Y^2}$, and $I, J = 1,2,3$ are the generation indices. For the fermions we use the 2-component spinor formalism.[1] The SM fermions f_J, $\bar{f}_J$ are in the basis where the mass terms are diagonal, and then the CKM matrix V appears in the quark doublets as $q_I = (u_I, V_{IJ} d_J)$. The effects of dimension-6 operators on the couplings to gauge bosons are parameterized by the vertex corrections δg that in general can be flavour-violating. For flavour-diagonal interactions we will employ the shorter notation $[\delta g_{L/R}^{Vf}]_{JJ} \equiv \delta g_{L/R}^{Vf_J}$.

The vertex corrections can be expressed as linear combinations of the Wilson coefficients c_i in equation (3.2), see C.1 for the map to the Warsaw basis. We find more transparent to recast the results of precision experiments as constraints on δg's. This is completely equivalent, provided one takes into account that not all δg's in equation (3.4) are independent.[2] Indeed, the mapping between the vertex corrections and the Wilson coefficients implies the relations $[\delta g_L^{Z\nu}]_{IJ} - [\delta g_L^{Ze}]_{IJ} = [\delta g_L^{We}]_{IJ}$, and $[\delta g_L^{Wq}]_{IJ} = [\delta g_L^{Zu}]_{IK} V_{KJ} - V_{IK} [\delta g_L^{Zd}]_{KJ}$.

Moreover, the W mass correction δm in (3.3) is not independent and is related to the leptonic vertex corrections and one 4-lepton operators [166]:

$$\delta m = \frac{\delta g_L^{We} + \delta g_L^{W\mu}}{2} - \frac{[c_{\ell\ell}]_{1221}}{4} \tag{3.5}$$

[1] Compared to [165], we use a different normalization of the antisymmetric product of the σ matrices: $\sigma_{\mu\nu} = \frac{i}{2}(\sigma_\mu \bar{\sigma}_\nu - \sigma_\nu \bar{\sigma}_\mu)$, $\bar{\sigma}_{\mu\nu} = \frac{i}{2}(\bar{\sigma}_\mu \sigma_\nu - \bar{\sigma}_\nu \sigma_\mu)$.

[2] More generally, it is often convenient to parametrize the space of dimension-6 operators using δg's and other independent parameters in the mass eigenstate Lagrangian that are in a 1-to-1 linear relation with the set of Wilson coefficients c_i [131]. One example of such parametrization goes under the name of the Higgs basis and is defined in Ref. [164].

Chirality conserving ($I,J=1,2,3$)	Chirality violating ($I,J=1,2,3$)
$[O_{\ell q}]_{IIJJ} = \left(\ell_I^\dagger \bar{\sigma}_\mu \ell_I\right)\left(q_J^\dagger \bar{\sigma}^\mu q_J\right)$	$[O_{\ell equ}]_{IIJJ} = \left(\ell_I^\dagger \bar{e}_I^\dagger\right)\cdot\left(q_J^\dagger \bar{u}_J^\dagger\right)$
$[O^{(3)}_{\ell q}]_{IIJJ} = \left(\ell_I^\dagger \bar{\sigma}_\mu \sigma^i \ell_I\right)\left(q_J^\dagger \bar{\sigma}^\mu \sigma^i q_J\right)$	$[O^{(3)}_{\ell equ}]_{IIJJ} = \left(\ell_I^\dagger \bar{\sigma}_{\mu\nu} \bar{e}_I^\dagger\right)\cdot\left(q_J^\dagger \bar{\sigma}_{\mu\nu} \bar{u}_J^\dagger\right)$
$[O_{\ell u}]_{IIJJ} = \left(\ell_I^\dagger \bar{\sigma}_\mu \ell_I\right)\left(\bar{u}_J \sigma^\mu \bar{u}_J^\dagger\right)$	$[O_{\ell edq}]_{IIJJ} = \left(\ell_I^\dagger \bar{e}_I^\dagger\right)\left(\bar{d}_J q_J\right)$
$[O_{\ell d}]_{IIJJ} = \left(\ell_I^\dagger \bar{\sigma}_\mu \ell_I\right)\left(\bar{d}_J \sigma^\mu \bar{d}_J^\dagger\right)$	
$[O_{eq}]_{IIJJ} = \left(\bar{e}_I \sigma_\mu \bar{e}_I^\dagger\right)\left(q_J^\dagger \bar{\sigma}^\mu q_J\right)$	
$[O_{eu}]_{IIJJ} = \left(\bar{e}_I \sigma_\mu \bar{e}_I^\dagger\right)\left(\bar{u}_J \sigma^\mu \bar{u}_J^\dagger\right)$	
$[O_{ed}]_{IIJJ} = \left(\bar{e}_I \sigma_\mu \bar{e}_I^\dagger\right)\left(\bar{d}_J \sigma^\mu \bar{d}_J^\dagger\right)$	

Table 3.1 – Flavor-conserving **2-lepton-2-quark** operators in the SMEFT Lagrangian of equation (3.2). The dot $\cdot$ denotes the contraction of $SU(2)_L$ indices with an epsilon tensor.

One flavour ($I=1,2,3$)	Two flavours ($I<J=1,2,3$)
$[O_{\ell\ell}]_{IIII} = \frac{1}{2}\left(\ell_I^\dagger \bar{\sigma}_\mu \ell_I\right)\left(\ell_I^\dagger \bar{\sigma}^\mu \ell_I\right)$	$[O_{\ell\ell}]_{IIJJ} = \left(\ell_I^\dagger \bar{\sigma}_\mu \ell_I\right)\left(\ell_J^\dagger \bar{\sigma}^\mu \ell_J\right)$
	$[O_{\ell\ell}]_{IJJI} = \left(\ell_I^\dagger \bar{\sigma}_\mu \ell_J\right)\left(\ell_J^\dagger \bar{\sigma}^\mu \ell_I\right)$
$[O_{\ell e}]_{IIII} = \left(\ell_I^\dagger \bar{\sigma}_\mu \ell_I\right)\left(\bar{e}_I \sigma^\mu \bar{e}_I^\dagger\right)$	$[O_{\ell e}]_{IIJJ} = \left(\ell_I^\dagger \bar{\sigma}_\mu \ell_I\right)\left(\bar{e}_J \sigma^\mu \bar{e}_J^\dagger\right)$
	$[O_{\ell e}]_{JJII} = \left(\ell_J^\dagger \bar{\sigma}_\mu \ell_J\right)\left(\bar{e}_I \sigma^\mu \bar{e}_I^\dagger\right)$
	$[O_{\ell e}]_{IJJI} = \left(\ell_I^\dagger \bar{\sigma}_\mu \ell_J\right)\left(\bar{e}_J \sigma^\mu \bar{e}_I^\dagger\right)$
$[O_{ee}]_{IIII} = \frac{1}{2}\left(\bar{e}_I \sigma_\mu \bar{e}_I^\dagger\right)\left(\bar{e}_I \sigma^\mu \bar{e}_I^\dagger\right)$	$[O_{ee}]_{IIJJ} = \left(\bar{e}_I \sigma_\mu \bar{e}_I^\dagger\right)\left(\bar{e}_J \sigma^\mu \bar{e}_J^\dagger\right)$

Table 3.2 – Flavor-conserving **4-lepton operators** in the SMEFT Lagrangian of equation (3.2).

Again, this relation is a consequence of the linearly realized SM gauge symmetry and the absence of operators with dimensions greater than 6. It also ensures that the Fermi constant G_F measured in muon decays is given at tree-level by $G_F = 1/\sqrt{2}v^2$ as in the SM.

In this work we focus on flavour-conserving observables that target flavour-diagonal Wilson coefficients. We will express the experimental constraints using the following set of independent flavour-diagonal vertex corrections:

$$\delta g_L^{Ze_I},\ \delta g_R^{Ze_I},\ \delta g_L^{We_I},\ \delta g_L^{Zu_I},\ \delta g_R^{Zu_I},\ \delta g_L^{Zd_I},\ \delta g_R^{Zd_I},\ \delta g_R^{Wq_I}. \tag{3.6}$$

The vertex corrections correspond to 24 linear combinations of dimension-6 Wilson coefficients, 3 of which are complex (those entering δg_R^{Wq}). We consider only CP-conserving observables, thus the imaginary part enters at the quadratic level and is neglected. To simplify the notation we will omit Re in front of complex Wilson coefficients.

We will also discuss constraints on flavour-diagonal 4-fermion operators in the SMEFT La-

grangian of equation (3.2). We work with the same set of 4-fermion operators as in Ref. [162] and employ a similar notation.[3] The main focus is on the flavour-conserving 2-lepton-2-quark (LLQQ) and 4-lepton (LLLL) dimension-6 operators. The LLQQ operators are summarized in table 3.1, and are defined in the flavour basis where the up-quark Yukawa matrices are diagonal. Overall, there are $10 \times 3 \times 3 = 90$ such operators, of which 27 (the chirality-violating ones) are complex. In the latter case the corresponding Wilson coefficient is complex, and the Hermitian conjugate operator is included in equation (3.2). We also list in table 3.2 the LLLL operators which include $3 \times 3 + 6 \times 3 = 27$ flavour-conserving 4-lepton operators , 3 of which are complex ($[O_{\ell e}]_{IJJI}$).

All in all, our analysis eyes 147 linear combinations of dimension-6 operators displayed in equation (3.6), table 3.1, and table 3.2. The observables discussed here will not depend on all of them, and thus we will be able to constrain only a limited number of the combinations. In particular the operators involving the third generation fermions are currently, with a few exceptions, poorly constrained by experiment. Nevertheless, the constraints we derive are robust, in the sense that they do not involve any strong assumptions about the unconstrained operators, other than the validity of the SMEFT description at the weak scale. We assume that our results are not invalidated by $\mathcal{O}\left(\frac{1}{16\pi^2\Lambda^2}\right)$ corrections, which arise at one loop in the SMEFT and inevitably introduce dependence of our observables on other D=6 Wilson coefficients. We will also treat V as the unit matrix when it multiplies dimension-6 Wilson coefficients. This ignores all contributions to observables where the Wilson coefficients are multiplied by an off-diagonal CKM element.[4]

In the last section, we will also particularize our results to more restrictive scenarios, such as the so-called flavour-universal SMEFT, where dimension-6 operators respect the $U(3)^5$ global flavour symmetry acting in the generation space on the SM fermion fields q, ℓ, $\bar{u}$, $\bar{d}$, $\bar{e}$.

3.2.2 Weak interactions below the weak scale

Precision experiments with a characteristic momentum transfer $Q \ll m_Z$ can be conveniently described using the low-energy effective theory where the SM W and Z bosons are integrated out. In this framework, weak interactions between quark and leptons are mediated by a set of 4-fermion operators. Within the SM, these operators effectively appear due to the exchange of W and Z bosons at tree level or in loops, and their coefficients can be calculated by the standard matching procedure. Once the SM is extended by dimension-6 operators, these

[3] One difference is that for operators with the $SU(2)_L$ singlet contraction of fermionic currents we omit the superscript $^{(1)}$. We also rename $\mathcal{Q}_{qe} \to O_{eq}$ so that the first (last) two flavour indices of all LLQQ operators correspond to the leptons (quarks).

[4] Such an approach is not completely satisfactory, since the Cabibbo angle is not small enough to always justify neglecting it. However, including the new physics contributions suppressed by the Cabibbo angle would require extending our analysis to include flavour-violating observables, which we leave for future publications. On the other hand, one naively expects the neglected operators to be severely constrained by other observables where the CKM suppression is not present, which would justify our approximation. Also, including CKM parameters in our analysis requires to take into account the effect of the dimension-6 operators in the measurements of the CKM parameters themselves [167].

coefficients may be modified, either due to modified propagators and couplings of W and Z, or due to the presence of contact 4-fermion operators in the SMEFT Lagrangian.

Below we define the low-energy operators that are relevant for the precision measurements we include in our analysis. We follow the PDG notation [168] (Section 10), and we present the matching between the coefficients of the low-energy operators and the parameters of the SMEFT.

Charged-current (CC) interactions: $qq'\ell\nu$

The low-energy CC interactions of leptons with the first generation quarks are described by the effective 4-fermion operators:

$$\begin{aligned}\mathscr{L}_{\text{eff}} \supset -\frac{2\tilde{V}_{ud}}{v^2}\Bigg[&\left(1+\epsilon_L^{de_J}\right)(e_J^\dagger\bar{\sigma}_\mu\nu_J)(u^\dagger\bar{\sigma}^\mu d)+\epsilon_R^{de}(e_J^\dagger\bar{\sigma}_\mu\nu_J)(\bar{u}\sigma^\mu\bar{d}^\dagger) \\ &+\frac{\epsilon_S^{de_J}+\epsilon_P^{de_J}}{2}(\bar{e}_J\nu_J)(\bar{u}d)+\frac{\epsilon_S^{de_J}-\epsilon_P^{de_J}}{2}(\bar{e}_J\nu_J)(u^\dagger\bar{d}^\dagger)+\epsilon_T^{de_J}(\bar{e}_J\sigma_{\mu\nu}\nu_J)(\bar{u}\sigma_{\mu\nu}d)+\text{h.c.}\Bigg].\end{aligned} \tag{3.7}$$

To make contact with low-energy flavour observables, we defined the rescaled CKM matrix element $\tilde{V}_{ud}$ [160]. It is distinct from the *actual* V_{ud}, i.e., the 11 element of the unitary matrix V that appears in the Lagrangian after rotating quarks to the mass eigenstate basis. The two are related by $V_{ud}=\tilde{V}_{ud}(1+\delta V_{ud})$ where δV_{ud} is chosen such as to impose the relation $\epsilon_L^{de}=-\epsilon_R^{de}$ in equation (3.7).[5]

Let us note that in general $\tilde{V}_{ud}$ is also different from the phenomenological value obtained within the SM, which we will denote by V_{ud}^{PDG}. Currently this value comes from superallowed nuclear beta decays [169] that depend on the vector couplings via the combination $\epsilon_L^{de}+\epsilon_R^{de}$. By setting $\epsilon_L^{de}=-\epsilon_R^{de}$, this nonstandard effect has been conveniently absorbed into the definition of $\tilde{V}_{ud}$. However, the relevant transitions also depend, each in a different way, on the scalar coefficient ϵ_S^{de}. Thus $\tilde{V}_{ud}$ and V_{ud}^{PDG} only coincide if ϵ_S^{de} vanishes, whereas in general it is not possible to redefine away all new physics contributions through $\tilde{V}_{ud}$. For this reason we treat $\tilde{V}_{ud}$ as a free parameter that is fit together with the EFT Wilson coefficients [160]. In principle the difference between $\tilde{V}_{ud}$ and V_{ud}^{PDG} must be taken into account every time the latter is used to calculate any given SM prediction. In practice, this effect will be negligible in most cases, given the strong constraints on ϵ_S^{de} from the same nuclear decay data, *cf.* equation (3.43).

[5] The bar in the $\epsilon_L^{de_J}$ coefficient reminds the reader that this coefficient is not the usual $\epsilon_L^{de_J}$ (see e.g. Ref. [160]) where the shift of NP effects into $\tilde{V}_{ud}$ is not carried out. These two are trivially related by $V_{ud}(1+\epsilon_L^{de_J})=\tilde{V}_{ud}(1+\epsilon_L^{de_J})$.

At tree level, the low-energy parameters are related to the SMEFT parameters as

$$\begin{aligned}
\delta V_{ud} &= -\delta g_L^{Wq_1} - \delta g_R^{Wq_1} + \delta g_L^{W\mu} - \frac{1}{2}[c_{\ell\ell}]_{1221} + [c_{lq}^{(3)}]_{1111}, \\
\epsilon_R^{de} = -\epsilon_L^{de} &= \delta g_R^{Wq_1}, \\
\epsilon_L^{d\mu} &= -\delta g_R^{Wq_1} + \delta g_L^{W\mu} - \delta g_L^{We} + [c_{lq}^{(3)}]_{1111} - [c_{lq}^{(3)}]_{2211}, \\
\epsilon_S^{de_J} &= -\frac{1}{2}\left([c_{lequ}]_{JJ11}^* + [c_{ledq}]_{JJ11}^*\right), \\
\epsilon_P^{de_J} &= -\frac{1}{2}\left([c_{lequ}]_{JJ11}^* - [c_{ledq}]_{JJ11}^*\right), \\
\epsilon_T^{de_J} &= -\frac{1}{2}[c_{lequ}^{(3)}]_{JJ11}^* ,
\end{aligned} \tag{3.8}$$

As indicated earlier, at $\mathcal{O}(\Lambda^{-2})$ we treat the CKM matrix as the unit matrix. In this limit, the effective parameters in equation (3.7) depend only on flavour-diagonal vertex corrections and 4-fermion operators. Note also that the rescaled CKM matrix is no longer unitary. In particular we have $|\tilde{V}_{ud}|^2 + |V_{us}|^2 \approx 1 + \Delta_{\rm CKM}$, where

$$\Delta_{\rm CKM} = -2\delta V_{ud} = 2\delta g_L^{Wq_1} + 2\delta g_R^{Wq_1} - 2\delta g_L^{W\mu} + [c_{\ell\ell}]_{1221} - 2[c_{lq}^{(3)}]_{1111} \tag{3.9}$$

Although the extraction of the V_{us} element is also affected by dimension-6 operators, their contribution to this unitarity test is suppressed by V_{us} and therefore it can be neglected in our approximation ($V \approx 1$ at order Λ^{-2}).

Neutral-current (NC) neutrino interactions: $\ell\ell\nu\nu$ and $qq\nu\nu$

At energies below the weak scale, the NC neutrino-electron interactions can be parametrized by the effective Lagrangian:

$$\mathscr{L} \supset -\frac{1}{v^2}\left(\nu_J^\dagger \bar{\sigma}_\mu \nu_J\right)\left[\left(g_{LV}^{\nu_J e} + g_{LA}^{\nu_J e}\right)(e^\dagger \bar{\sigma}_\mu e) + \left(g_{LV}^{\nu_J e} - g_{LA}^{\nu_J e}\right)(\bar{e}\sigma_\mu \bar{e}^\dagger)\right] \tag{3.10}$$

Matching to the SMEFT one finds the relations

$$\begin{aligned}
g_{LV}^{\nu_J e} &= -\frac{1}{2} + 2s_\theta^2 - \left(1 - 4s_\theta^2\right)\delta g_L^{Z\nu_J} + \delta g_L^{Ze} + \delta g_R^{Ze} - \frac{1}{2}\left([c_{\ell\ell}]_{11JJ} + [c_{\ell e}]_{JJ11}\right) \\
g_{LA}^{\nu_J e} &= -\frac{1}{2} - \delta g_L^{Z\nu_J} + \delta g_L^{Ze} - \delta g_R^{Ze} - \frac{1}{2}\left([c_{\ell\ell}]_{11JJ} - [c_{\ell e}]_{JJ11}\right)
\end{aligned} \tag{3.11}$$

Similarly, the low-energy NC neutrino interactions with light quarks are described by the effective 4-fermion operators:

$$\mathscr{L}_{\rm eff} \supset -\frac{2}{v^2}\left(\nu_J^\dagger \bar{\sigma}^\mu \nu_J\right)\left(g_{LL}^{\nu_J u} u^\dagger \bar{\sigma}_\mu u + g_{LR}^{\nu_J u} \bar{u}\sigma_\mu \bar{u}^\dagger + g_{LL}^{\nu_J d} d^\dagger \bar{\sigma}_\mu d + g_{LR}^{\nu_J d} \bar{d}\sigma_\mu \bar{d}^\dagger\right) \tag{3.12}$$

At tree level, the low-energy parameters are related to the SMEFT parameters as

$$\begin{aligned}
g_{LL}^{\nu_J u} &= \frac{1}{2} - \frac{2s_\theta^2}{3} + \delta g_L^{Zu} + \left(1 - \frac{4s_\theta^2}{3}\right)\delta g_L^{Z\nu_J} - \frac{1}{2}([c_{lq}]_{JJ11} + [c_{lq}^{(3)}]_{JJ11}) \\
g_{LR}^{\nu_J u} &= -\frac{2s_\theta^2}{3} + \delta g_R^{Zu} - \frac{4s_\theta^2}{3}\delta g_L^{Z\nu_J} - \frac{1}{2}[c_{lu}]_{JJ11} \\
g_{LL}^{\nu_J d} &= -\frac{1}{2} + \frac{s_\theta^2}{3} + \delta g_L^{Zd} - \left(1 - \frac{2s_\theta^2}{3}\right)\delta g_L^{Z\nu_J} - \frac{1}{2}([c_{lq}]_{JJ11} - [c_{lq}^{(3)}]_{JJ11}) \\
g_{LR}^{\nu_J d} &= \frac{s_\theta^2}{3} + \delta g_R^{Zd} + \frac{2s_\theta^2}{3}\delta g_L^{Z\nu_J} - \frac{1}{2}[c_{ld}]_{JJ11}
\end{aligned} \tag{3.13}$$

The experiments probing these couplings usually normalize the NC cross section using its CC counterpart. Thus, it is convenient to define the following combinations of effective couplings:

$$(g_{L/R}^{\nu_J})^2 \equiv \frac{(g_{LL/LR}^{\nu_J u})^2 + (g_{LL/LR}^{\nu_J d})^2}{\left(1 + \epsilon_L^{de_J}\right)^2}, \qquad \theta_{L/R}^{\nu_J} \equiv \arctan\left(\frac{g_{LL/LR}^{\nu_J u}}{g_{LL/LR}^{\nu_J d}}\right), \tag{3.14}$$

where we took into account that SMEFT dimension-6 operators modify in general both NC and CC processes. Let us notice that additional (linear) effects in the normalizing CC process due to ϵ_R^{de} and $\epsilon_{S,P,T}^{de_J}$ can be neglected because they are suppressed by the ratio $m_u m_d/E^2$ and m_{e_J}/E respectively. The effect due to the possible difference between $\tilde{V}_{ud}$ and $V_{ud}^{\rm PDG}$ can also be safely neglected here, given the limited precision of the neutrino scattering experiments included in our fit. Last, the same holds for the δV_{ud} contribution that appears if the unitarity of the CKM matrix is used in the SM determination.

Neutral-current charged-lepton interactions: $\ell\ell\ell\ell$ and $qq\ell\ell$

For low energy electron-electron scattering we use:

$$\mathscr{L} \supset \frac{1}{2v^2} g_{AV}^{ee}\left[-(e^\dagger\bar{\sigma}_\mu e)(e^\dagger\bar{\sigma}_\mu e) + (\bar{e}\sigma_\mu\bar{e}^\dagger)(\bar{e}\sigma_\mu\bar{e}^\dagger)\right] \tag{3.15}$$

Matching to the SMEFT, one finds

$$g_{AV}^{ee} = \frac{1}{2} - 2s_\theta^2 - 2\left(1 - 2s_\theta^2\right)\delta g_L^{Ze} - 4s_\theta^2\delta g_R^{Ze} - \frac{1}{2}[c_{\ell\ell}]_{1111} + \frac{1}{2}[c_{ee}]_{1111} \tag{3.16}$$

Finally, we parametrize[6] the 4-fermion operators with 2 charged leptons and 2 light quarks as

$$\begin{aligned}
\mathscr{L} \supset\ & \frac{1}{2v^2}\left[g_{AV}^{e_J q}(\bar{e}_J\gamma_\mu\gamma_5 e_J)(\bar{q}\gamma_\mu q) + g_{VA}^{e_J q}(\bar{e}_J\gamma_\mu e_J)(\bar{q}\gamma_\mu\gamma_5 q)\right] \\
& + \frac{1}{2v^2}\left[g_{VV}^{e_J q}(\bar{e}_J\gamma_\mu e_J)(\bar{q}\gamma_\mu q) + g_{AA}^{e_J q}(\bar{e}_J\gamma_\mu\gamma_5 e_J)(\bar{q}\gamma_\mu\gamma_5 q)\right]
\end{aligned} \tag{3.17}$$

[6] For the parity-violating electron couplings, another frequently used notation is $g_{AV}^{eq} \equiv C_{1q}$, $g_{VA}^{eq} \equiv C_{2q}$.

where we momentarily switch to the Dirac notation with $\gamma_5\psi_L = -\psi_L$, $\gamma_5\psi_R = +\psi_R$. Also, q stands for the u or d Dirac spinor and not for the left-handed quark doublet. At tree level, the parameters $g_{XY}^{e_i q}$ are related to the SMEFT parameters as

$$\begin{aligned}
g_{AV}^{e_J u} &= -\frac{1}{2} + \frac{4}{3}s_\theta^2 - \left(\delta g_L^{Zu} + \delta g_R^{Zu}\right) + \frac{3-8s_\theta^2}{3}\left(\delta g_L^{Ze_J} - \delta g_R^{Ze_J}\right) + \frac{1}{2}\left[c_{lq}^{(3)} - c_{lq} - c_{lu} + c_{eq} + c_{eu}\right]_{JJ11} \\
g_{AV}^{e_J d} &= \frac{1}{2} - \frac{2}{3}s_\theta^2 - \left(\delta g_L^{Zd} + \delta g_R^{Zd}\right) - \frac{3-4s_\theta^2}{3}\left(\delta g_L^{Ze_J} - \delta g_R^{Ze_J}\right) + \frac{1}{2}\left[-c_{lq}^{(3)} - c_{lq} - c_{ld} + c_{eq} + c_{ed}\right]_{JJ11} \\
g_{VA}^{e_J u} &= -\frac{1}{2} + 2s_\theta^2 - \left(1-4s_\theta^2\right)\left(\delta g_L^{Zu} - \delta g_R^{Zu}\right) + \left(\delta g_L^{Ze_J} + \delta g_R^{Ze_J}\right) + \frac{1}{2}\left[c_{lq}^{(3)} - c_{lq} + c_{lu} - c_{eq} + c_{eu}\right]_{JJ11} \\
g_{VA}^{e_J d} &= \frac{1}{2} - 2s_\theta^2 - \left(1-4s_\theta^2\right)\left(\delta g_L^{Zd} - \delta g_R^{Zd}\right) - \left(\delta g_L^{Ze_J} + \delta g_R^{Ze_J}\right) + \frac{1}{2}\left[-c_{lq}^{(3)} - c_{lq} + c_{ld} - c_{eq} + c_{ed}\right]_{JJ11} \\
g_{AA}^{e_J u} &= \frac{1}{2} + \delta g_L^{Zu} - \delta g_R^{Zu} - \delta g_L^{Ze_J} + \delta g_R^{Ze_J} + \frac{1}{2}\left[-c_{lq}^{(3)} + c_{lq} - c_{lu} - c_{eq} + c_{eu}\right]_{JJ11} \\
g_{AA}^{e_J d} &= -\frac{1}{2} + \delta g_L^{Zd} - \delta g_R^{Zd} + \delta g_L^{Ze_J} - \delta g_R^{Ze_J} + \frac{1}{2}\left[c_{lq}^{(3)} + c_{lq} - c_{ld} - c_{eq} + c_{ed}\right]_{JJ11}
\end{aligned} \tag{3.18}$$

We do not display the expressions for $g_{VV}^{e_i q}$ here because they will not be needed in the following.

3.2.3 Renormalization and scale running of the Wilson coefficients

In general the Wilson coefficients display renormalization-scale dependence that is to be canceled in the observables by the opposite dependence in the quantum corrections to the matrix elements. Let us first discuss the QCD running, which can have a numerically significant impact due to the magnitude of the strong coupling constant α_s. This effect is further enhanced by the large separation of scales of the experiments discussed in this work (from low-energy precision measurements to LHC collisions). Among the coefficients involved in our analysis, only the three chirality-violating ones, $c_{lequ}, c_{ledq}, c_{lequ}^{(3)}$ (i.e. $\epsilon_{S,P,T}^{d\ell}$ in the low-energy EFT), present a non-zero 1-loop QCD anomalous dimension, namely [170]

$$\frac{d\,\vec{x}(\mu)}{d\log\mu} = \frac{\alpha_s(\mu)}{2\pi}\begin{pmatrix} -4 & 0 & 0 \\ 0 & -4 & 0 \\ 0 & 0 & 4/3 \end{pmatrix}\vec{x}(\mu), \tag{3.19}$$

where $\vec{x}$ refers to the SMEFT coefficients $\vec{c} = (c_{ledq}, c_{lequ}, c_{lequ}^{(3)})$ if the scale μ is above the weak scale or to the low-energy EFT coefficients $\vec{\epsilon} = (\epsilon_S^{d\ell}, \epsilon_P^{d\ell}, \epsilon_T^{d\ell})$ below it. We find that higher-loop QCD corrections to the running are numerically significant, and we include them in our analysis.[7]

On the other hand we neglect in this work the electromagnetic/weak running of the SMEFT Wilson coefficients, which is expected to have a much smaller numerical importance simply

[7] We use the 3-loop QCD anomalous dimension [171], and we include the threshold corrections at m_b and m_t extracted from Refs. [172] and [173] for scalar and tensor operators respectively. See Ref. [174] for further details.

due to the smallness of the corresponding coupling constants. There is however one exception to this, namely the chirality-violating operators discussed above, for two reasons: (i) contrary to the QCD running, the QED/weak running involves mixing between these operators; (ii) pion decay makes possible to set bounds of order 10^{-7} on the pseudoscalar coupling $\epsilon_P^{d\ell}(\mu_{\text{low}})$, which can give important bounds on scalar and tensor via mixing despite the smallness of α_{em}. In order to take into account this effect, equation (3.19) has to be replaced by

$$\frac{d\,\vec{x}(\mu)}{d\log\mu} = \left(\frac{\alpha_{em}(\mu)}{2\pi}\gamma_x + \frac{\alpha_s(\mu)}{2\pi}\gamma_s\right)\vec{x}(\mu)\,, \tag{3.20}$$

where we will use the 1-loop QED (electroweak) anomalous dimension, $\gamma_x = \gamma_{em(w)}$, to evolve the coefficients $\vec{\epsilon}$ ($\vec{c}$) below (above) the weak scale [174–177]:

$$\gamma_{\text{em}} = \begin{pmatrix} \frac{2}{3} & 0 & 4 \\ 0 & \frac{2}{3} & 4 \\ \frac{1}{24} & \frac{1}{24} & -\frac{20}{9} \end{pmatrix}, \quad \gamma_{\text{w}} = \begin{pmatrix} -\frac{4}{3c_\theta^2} & 0 & 0 \\ 0 & -\frac{11}{6c_\theta^2} & \frac{15}{c_\theta^2}+\frac{9}{s_\theta^2} \\ 0 & \frac{5}{16c_\theta^2}+\frac{3}{16s_\theta^2} & \frac{1}{9c_\theta^2}-\frac{3}{2s_\theta^2} \end{pmatrix}, \tag{3.21}$$

where we neglect terms suppressed by Yukawa couplings [177, 178]. Integrating numerically the coupled differential renormalization group equations we find

$$\begin{pmatrix} \epsilon_S^{d\ell} \\ \epsilon_P^{d\ell} \\ \epsilon_T^{d\ell} \end{pmatrix}_{(\mu = m_Z)} = \begin{pmatrix} 0.58 & 1.42\times10^{-6} & 0.017 \\ 1.42\times10^{-6} & 0.58 & 0.017 \\ 1.53\times10^{-4} & 1.53\times10^{-4} & 1.21 \end{pmatrix} \begin{pmatrix} \epsilon_S^{d\ell} \\ \epsilon_P^{d\ell} \\ \epsilon_T^{d\ell} \end{pmatrix}_{(\mu = 2\text{ GeV})} \tag{3.22}$$

$$\begin{pmatrix} c_{ledq} \\ c_{lequ} \\ c_{lequ}^{(3)} \end{pmatrix}_{(\mu = 1\text{ TeV})} = \begin{pmatrix} 0.84 & 0 & 0 \\ 0 & 0.84 & 0.16 \\ 0 & 3.3\times10^{-3} & 1.04 \end{pmatrix} \begin{pmatrix} c_{ledq} \\ c_{lequ} \\ c_{lequ}^{(3)} \end{pmatrix}_{(\mu = m_Z)}. \tag{3.23}$$

These results use the QCD beta function and anomalous dimensions up to 3 loops, and we included the bottom and top quark thresholds effects, see Ref. [174] for details. The diagonal entries would change by ~ 12% if just 1-loop QCD running were included, while two-loop results differ by only ~ 1.5%. In our subsequent analysis we will use the numerical results in equation (3.22) and equation (3.23).

3.3 Low-energy experiments

3.3.1 Z- and W-pole observables

The vertex corrections in (3.4) can be probed by measurements of leptonic decays of on-shell Z and W bosons. Precise measurements of observables ultimately related to various Z and W partial decay widths were performed in LEP-1 (Z) [179] and LEP-2 (W) [180]. In these observables, the dependence on four-fermion operators is suppressed by Γ_V/m_V and can be neglected [116]. Simultaneous constraints on all flavour-preserving vertex corrections were

derived in reference [139], and we use directly these results.

Note that *all* leptonic vertex corrections are strongly constrained by the data in a model-independent way. In particular, the constraints on charged leptons couplings to Z (dominated by LEP-1) are at a per-mille level, while the constraints on lepton couplings to W (dominated by LEP-2) are at a percent level. The quark vertex corrections are also all constrained at percent level, except $[\delta g_R^{Zu}]$ because there is no $e^+e^- \to t\bar{t}$ data.

3.3.2 W mass

The W boson mass was measured very precisely at LEP-2 and the Tevatron. We use the result from Ref. [181], $m_W = (80.385 \pm 0.015)$ GeV, where the SM prediction is $m_W = 80.364$ GeV. This trivially translates into the constraint on the parameter δm in (3.3),

$$\delta m = (2.6 \pm 1.9) \times 10^{-4} \tag{3.24}$$

which by virtue of (3.5) translates to a constraint on a combination of leptonic vertex correction and one four-lepton operator.

3.3.3 Neutrino scattering

Neutrino scattering experiments measure the ratio of neutral- and charged-current neutrino or anti-neutrino scattering cross sections on nuclei:

$$R_{\nu_i} = \frac{\sigma(\nu_i N \to \nu X)}{\sigma(\nu_i N \to \ell_i^- X)} \qquad R_{\bar{\nu}_i} = \frac{\sigma(\bar{\nu}_i N \to \bar{\nu} X)}{\sigma(\bar{\nu}_i N \to \ell_i^+ X)} \tag{3.25}$$

At leading order and for isoscalar nucleus targets (equal number of protons and neutrons) one has the so-called Llewellyn-Smith relations [182]:

$$R_{\nu_i} = (g_L^{\nu_i})^2 + r(g_R^{\nu_i})^2 \qquad R_{\bar{\nu}_i} = (g_L^{\nu_i})^2 + r^{-1}(g_R^{\nu_i})^2 \tag{3.26}$$

where r is the ratio of ν to $\bar{\nu}$ charged-current cross sections on N that can be measured separately, and the effective couplings $g_{L/R}^{\nu_i}$ are defined in equation (3.14). In some experiments the beam is a mixture of neutrinos and anti-neutrinos, and the following ratio is measured

$$R_{\nu_i\bar{\nu}_i} = \frac{\sigma(\nu_i N \to \nu X) + \sigma(\bar{\nu}_i N \to \bar{\nu} X)}{\sigma(\nu_i N \to \ell_i^- X) + \sigma(\bar{\nu}_i N \to \ell_i^+ X)} = (g_L^{\nu_i})^2 + (g_R^{\nu_i})^2 \tag{3.27}$$

ν_e data.- The CHARM experiment [183] made a measurement of electron-neutrino scattering cross sections:

$$R_{\nu_e\bar{\nu}_e} = 0.406^{+0.145}_{-0.135} \tag{3.28}$$

where the uncertainties quoted here and everywhere else in this work are 1-sigma (68%C.L.)

Experiment	Observable	Experimental value	SM value	Ref.
CHARM ($r = 0.456$)	R_{ν_μ}	0.3093 ± 0.0031	0.3156	[184]
	$R_{\bar{\nu}_\mu}$	0.390 ± 0.014	0.370	[184]
CDHS ($r = 0.393$)	R_{ν_μ}	0.3072 ± 0.0033	0.3091	[185]
	$R_{\bar{\nu}_\mu}$	0.382 ± 0.016	0.380	[185]
CCFR	κ	0.5820 ± 0.0041	0.5830	[186]

Table 3.3 – The results of muon-neutrino scattering experiments most relevant for constraining dimension-6 operators in the SMEFT. The SM values of R_{ν_μ} and κ include subleading corrections [187], whereas those of $R_{\bar{\nu}_\mu}$ are the tree-level values, which should be sufficient taking into account the larger experimental errors.

errors. To avoid dealing with asymmetric errors we approximate it as $R_{\nu_e\bar{\nu}_e} = 0.41 \pm 0.14$, and we estimate the SM expectation as $R^{\rm SM}_{\nu_e\bar{\nu}_e} = 0.33$. To our knowledge, this weakly constraining measurement is currently the best probe of the electron-neutrino neutral-current interactions.

ν_μ data.- For the muon-neutrino scattering the experimental data are much more abundant and precise. We summarize the relevant results in table 3.3. The observable κ measured in CCFR probes the following combinations of couplings [186]:

$$\kappa = 1.7897 (g_L^{\nu_\mu})^2 + 1.1479 (g_R^{\nu_\mu})^2 - \frac{0.0916 \left[(g_{LL}^{\nu_\mu u})^2 - (g_{LL}^{\nu_\mu d})^2 \right] + 0.0782 \left[(g_{LR}^{\nu_\mu u})^2 - (g_{LR}^{\nu_\mu d})^2 \right]}{(1 + \bar{\epsilon}_L^{d\mu})^2} \tag{3.29}$$

The additional small dependence on the difference of the up and down effective couplings appears when one takes into account that the target (in this case iron) is not exactly isoscalar. For the reasons explained in Ref. [168], in our fits we do not take into account the results of the NuTeV experiment.

The observables in table 3.3 constrain 3 independent combinations of the SMEFT coefficients. Rather then combining these results ourselves, we use the PDG combination [168] that also uses additional experimental input [188] from neutrino induced coherent neutral pion production from nuclei [189, 190] and elastic neutrino-proton scattering [191, 192]. Although their precision is quite limited, their inclusion allows one to constrain the 4 muon-neutrino effective couplings to quarks [187]. The results of the latest PDG fit are [168]:

$$\begin{aligned} (g_L^{\nu_\mu})^2 &= 0.3005 \pm 0.0028 \qquad (g_R^{\nu_\mu})^2 = 0.0329 \pm 0.0030 \\ \theta_L^{\nu_\mu} &= 2.50 \pm 0.035 \qquad \theta_R^{\nu_\mu} = 4.56^{+0.42}_{-0.27} \end{aligned} \tag{3.30}$$

The correlations are quoted to be small in Ref. [168] and in the following we neglect them. We symmetrize the uncertainty on θ_R taking the larger of the errors, so as to avoid dealing with asymmetric errors. The corresponding SM predictions are given in table 3.4. To evaluate their dimension-6 EFT corrections in equation (3.13) we will use $s^2_\theta = 0.23865$, which is the central value in the $\overline{MS}$ scheme at low energies [168]. We neglect the error of the SM predictions

when it is much smaller than the experimental uncertainties; otherwise we combine it in quadrature.

We note that LLQQ (and 4-lepton) operators can also be probed via matter effects in neutrino oscillations, see e.g. [193, 194]. However, the resulting constraints are not available in the model-independent form where all 4-fermion operators can be present simultaneously. Moreover, neutrino oscillations probe linear combinations of lepton-flavour-diagonal operators and of the off-diagonal ones (which we marginalize over). For these reasons, we do not include the oscillation constraints. A SMEFT analysis of reactor neutrino data is performed in reference [195].

ν_μ scattering on electrons.- Similar scattering of muon neutrino and anti-neutrino on electrons were measured at the CHARM [196], CHARM-II [197], and BNL-734 [198] experiments. We use the result of the PDG fit [168] in our analysis:

$$g_{LV}^{\nu_\mu e} = -0.040 \pm 0.015 \qquad \text{and} \qquad g_{LA}^{\nu_\mu e} = -0.507 \pm 0.014 \tag{3.31}$$

with the correlation coefficient $\rho = -0.05$ where the SM prediction is $g_{LV}^{\nu_\mu e} = -0.0396$ and $g_{LA}^{\nu_\mu e} = -0.5064$. The effect of 4-leptons operators is given in equation (3.11).

3.3.4 Parity violation in atoms and in scattering

Parity violation in Møller scattering $e^-e^- \to e^-e^-$ was measured at the SLAC E158 experiment [199]. The parity-violating asymmetry is defined as $A_{PV} = (\sigma_R - \sigma_L)/(\sigma_R + \sigma_L)$ where $\sigma_{L(R)}$ is the cross-section for incident left- (right-) handed electrons. The E158 experiment used a polarized electron beam of energy $E \approx 50$ GeV against an electron target at rest which corresponds to a center-of-mass energy of $\sqrt{s} \approx \sqrt{2 m_e E} \approx 0.2$ GeV, far below the Z pole. Parity violating processes no not compete against the elctromagnetic interaction and are direct probes of the weak interaction even at low energies. The result quoted in the PDG is

$$g_{AV}^{ee} = 0.0190 \pm 0.0027 \tag{3.32}$$

where the SM prediction is $g_{AV}^{ee} = 0.0225$ and the contribution of dimension-6 operators is given in equation (3.16).

Atomic parity violation (APV) and parity-violating electron scattering experiments access the parity-violating effective couplings of electrons to quarks g_{AV}^{eq} and g_{VA}^{eq}. In particular, APV and elastic scattering on a target with Z protons and N neutrons probe its so-called weak charge Q_W that is given by

$$Q_W(Z,N) = -2\Big((2Z+N)g_{AV}^{eu} + (Z+2N)g_{AV}^{ed}\Big) \tag{3.33}$$

up to small radiative corrections [168, 187]. The most precise determination is performed in

^{133}Cs, where $Q_W(55,133-55) \approx -376 g_{AV}^{eu} - 422 g_{AV}^{ed}$. Taking into account recent re-analyses [200] of the measured parity-violating transitions in cesium atoms [201], the latest edition of the PDG Review [168] quotes

$$Q_W^{\rm Cs} = -72.62 \pm 0.43 \tag{3.34}$$

where the SM prediction is $Q_{W,\rm SM}^{\rm Cs} = -73.25 \pm 0.02$ [168]. Other APV measurements, e.g. with thallium atoms, probe slightly different combinations of the g_{AV}^{eq} couplings, although with larger errors.

Instead, a very different linear combination of g_{AV}^{eu} and g_{AV}^{ed} is precisely probed by measurements of the weak charge of the proton, $Q_W^{\rm p} = Q_W(1,0)$, in scattering experiments with low-energy polarized electrons. The QWEAK experiment [202] finds

$$Q_W^{\rm p} = 0.064 \pm 0.012 \tag{3.35}$$

where the SM prediction is $Q_{W,\rm SM}^{\rm p} = 0.0708 \pm 0.0003$ [168].

In order to access the effective couplings g_{VA}^{eq} one needs to resort to deep-inelastic scattering of polarized electrons. Currently, the most precise of these is the PVDIS experiment [203] that studies electron scattering on deuterium targets. The experiment is sensitive to the following two linear combinations of effective couplings [203]:

$$\begin{aligned} A_1^{\rm PVDIS} &= 1.156 \times 10^{-4} \left(2 g_{AV}^{eu} - g_{AV}^{ed} + 0.348 (2 g_{VA}^{eu} - g_{VA}^{ed}) \right) \\ A_2^{\rm PVDIS} &= 2.022 \times 10^{-4} \left(2 g_{AV}^{eu} - g_{AV}^{ed} + 0.594 (2 g_{VA}^{eu} - g_{VA}^{ed}) \right) \end{aligned} \tag{3.36}$$

The measured values are [203]

$$A_1^{\rm PVDIS} = (-91.1 \pm 4.3) \times 10^{-6}, \qquad A_2^{\rm PVDIS} = (-160.8 \pm 7.1) \times 10^{-6} \tag{3.37}$$

where the SM predictions are $A_{1,SM}^{\rm PVDIS} = -(87.7 \pm 0.7) \times 10^{-6}$, $A_{2,SM}^{\rm PVDIS} = -(158.9 \pm 1.0) \times 10^{-6}$ [203].

The PDG combines the results of APV, QWEAK, and PVDIS experiments into correlated constraints on 3 linear combinations of g_{VA}^{eq} and g_{AV}^{eq} [168]:

$$\begin{pmatrix} g_{AV}^{eu} + 2 g_{AV}^{ed} \\ 2 g_{AV}^{eu} - g_{AV}^{ed} \\ 2 g_{VA}^{eu} - g_{VA}^{ed} \end{pmatrix} = \begin{pmatrix} 0.489 \pm 0.005 \\ -0.708 \pm 0.016 \\ -0.144 \pm 0.068 \end{pmatrix} \qquad \rho = \begin{pmatrix} & -0.94 & 0.42 \\ & & -0.45 \\ & & \end{pmatrix} \tag{3.38}$$

To disentangle g_{VA}^{eu} and g_{VA}^{ed} one needs more input from earlier (less precise) measurements of parity-violating scattering. We include two results provided by the SAMPLE collaboration [204]:

$$g_{VA}^{eu} - g_{VA}^{ed} = -0.042 \pm 0.057 \qquad g_{VA}^{eu} - g_{VA}^{ed} = -0.12 \pm 0.074 \tag{3.39}$$

from the scattering of polarized electrons on deuterons in the quasi-elastic kinematic regime at two different values of the beam energy. Combining the likelihood obtained from equation

(3.38) with the SAMPLE results we find the following constraints:

$$\begin{pmatrix} \delta g_{AV}^{eu} \\ \delta g_{AV}^{ed} \\ \delta g_{VA}^{eu} \\ \delta g_{VA}^{ed} \end{pmatrix} = \begin{pmatrix} 0.0033 \pm 0.0054 \\ -0.0047 \pm 0.0051 \\ -0.041 \pm 0.081 \\ -0.032 \pm 0.11 \end{pmatrix} \qquad \rho = \begin{pmatrix} & -0.98 & -0.37 & -0.27 \\ & & 0.37 & 0.27 \\ & & & 0.94 \\ & & & \end{pmatrix} \tag{3.40}$$

Here δg_{XY}^{eq} are shifts of the effective couplings away from the SM values, whose dependence on the dimension-6 Wilson coefficients can be read off from equation (3.18).

There are also results concerning effective muon couplings to quarks. A CERN SPS experiment [205] measured a DIS asymmetry using polarized muon and anti-muon scattering on an isoscalar carbon target. The results can be recast as the measurement of the observable b_{SPS} defined as

$$b_{\text{SPS}} = \frac{3}{5e^2v^2}\left(g_{AA}^{\mu d} - 2g_{AA}^{\mu u} + \lambda(g_{VA}^{\mu d} - 2g_{VA}^{\mu u})\right) \tag{3.41}$$

where λ is the muon beam polarization fraction. Two measurements of b_{SPS} at different beam energies and polarization fractions were carried out [205]:

$$\begin{aligned} b_{\text{SPS}} &= -(1.47 \pm 0.42) \times 10^{-4}\,\text{GeV}^{-2} \text{ for } \lambda = 0.81 \;\Rightarrow\; b_{\text{SPS}}^{\text{SM}} = -1.56 \times 10^{-4}\,\text{GeV}^{-2} \\ b_{\text{SPS}} &= -(1.74 \pm 0.81) \times 10^{-4}\,\text{GeV}^{-2} \text{ for } \lambda = 0.66 \;\Rightarrow\; b_{\text{SPS}}^{\text{SM}} = -1.57 \times 10^{-4}\,\text{GeV}^{-2} \end{aligned} \tag{3.42}$$

3.3.5 Low-energy flavour

The partonic process $d_j \to u_i \ell \bar{\nu}_\ell$ underlies a plethora of (semi)leptonic hadron decays. Ref. [160] studied $d(s) \to u \ell \bar{\nu}_\ell$ transitions, such as nuclear, baryon and meson decays, within the SMEFT framework and obtained bounds for 14 combinations of effective low-energy couplings between light quarks and leptons ($\epsilon_i^{d_I e_J}$). Ignoring the CKM mixing at $\mathcal{O}(\Lambda^{-2})$, the effective couplings of strange quarks depend only on flavour-off-diagonal Wilson coefficients (see C.2). Marginalizing over them, we obtain the likelihood for 6 combinations of effective couplings together with the $\tilde{V}_{ud}$ CKM parameter:[8]

$$\begin{pmatrix} \tilde{V}_{ud} \\ \Delta_{\text{CKM}} \\ \epsilon_R^{de} \\ \epsilon_S^{de} \\ \epsilon_P^{de} \\ \epsilon_T^{de} \\ \Delta_{LP}^{d} \end{pmatrix} = \begin{pmatrix} 0.97451(38) \\ -(1.2 \pm 8.4) \cdot 10^{-4} \\ -(1.3 \pm 1.7) \cdot 10^{-2} \\ (1.4 \pm 1.3) \cdot 10^{-3} \\ (4.0 \pm 7.8) \cdot 10^{-6} \\ (1.0 \pm 8.0) \cdot 10^{-4} \\ (1.9 \pm 3.8) \cdot 10^{-2} \end{pmatrix}, \; \rho = \begin{pmatrix} 1. & 0.88 & 0. & 0.82 & 0.01 & 0. & 0.01 \\ 0.88 & 1. & 0. & 0.73 & 0.01 & 0. & 0.01 \\ 0. & 0. & 1. & 0. & -0.87 & 0. & -0.87 \\ 0.82 & 0.73 & 0. & 1. & 0.01 & 0. & 0.01 \\ 0.01 & 0.01 & -0.87 & 0.01 & 1. & 0. & 0.9995 \\ 0. & 0. & 0. & 0. & 0. & 1. & 0. \\ 0.01 & 0.01 & -0.87 & 0.01 & 1. & 0. & 1. \end{pmatrix}, \tag{3.43}$$

[8] There is a small (but nonzero) correlation with the effective couplings of strange quarks that we marginalized over. This must be taken into account when going to specific scenarios. The full likelihood is available in Ref. [160].

in the $\overline{MS}$ scheme at $\mu = 2$ GeV. The effective couplings ϵ were defined in section 3.2.2, and $\Delta^d_{LP} \approx \epsilon^{de}_L - \epsilon^{d\mu}_L + 24\epsilon^{d\mu}_P$. See C.2 for the complete likelihood [160] that also involves the effective couplings of the strange quarks and allows one to constrain some off-diagonal Wilson coefficients. Using equation (3.22) we can run these results up to the weak scale, where the matching with the SMEFT is carried out, *cf.* equation (3.8) and equation (3.9).

It is useful to recall the physics behind these bounds [160]. Roughly speaking, $\tilde{V}_{ud}$ and $\epsilon^{de}_{R,S,P,T}$ were obtained comparing the total rates of various superallowed nuclear decays and $\pi \to e\nu_e$, as well as using various differential distributions in $\pi \to e\nu\gamma$ and neutron decay. The comparison with $\Gamma(\pi \to \mu\nu_\mu)$ provides us with Δ^d_{LP}, and the combination of the obtained $\tilde{V}_{ud}$ with V_{us}, extracted from (semi)leptonic kaon decays, makes possible to extract Δ_{CKM}.

3.3.6 Fermion pair production in e^+e^- collisions

Electron-positron colliders operating at center-of-mass energies above or below the Z mass provide complementary information about 4-fermion operators containing electrons.

Muon and tau pair production

The LEP-2 experiment measured differential cross sections for the processes $e^+e^- \to \ell^+\ell^-$, $\ell = e, \mu, \tau$ at energies above the Z boson resonance. Away from the Z-pole, these processes probe not only Z couplings to leptons but also 4-lepton operators, and the effect of the latter increases with increasing center-of-mass energy.

Let us first focus on the processes $e^-e^+ \to \mu^-\mu^+$ ($e^-e^+ \to \tau^-\tau^+$ is analogous). For the experimental input, we will use the total cross-sections and forward-backward asymmetries measured at 12 different center-of-mass energies between $\sqrt{s} \approx 130$ GeV and $\sqrt{s} \approx 209$ GeV [180]. We are interested in $\mathcal{O}(\Lambda^{-2})$ corrections to these observables from D=6 operators, which translates to linear corrections in the vertex corrections and Wilson coefficients of 4-fermion operators (i.e. the interference term between SM and new physics). At that order, the observables are affected by 5 four-leptons operators $[O_{\ell\ell}]_{1122}$, $[O_{\ell\ell}]_{1221}$, $[O_{ee}]_{1122}$, $[O_{\ell e}]_{1122}$, and $[O_{\ell e}]_{2211}$. In the limit of vanishing fermion masses, their effect on the forward (σ_F) and backward (σ_B) $e^-e^+ \to \mu^-\mu^+$ cross sections is given by

$$\begin{aligned}
\delta(\sigma_F + \sigma_B) &= \frac{1}{24\pi v^2}\Big\{e^2\left([c_{\ell\ell}]_{1122} + [c_{\ell\ell}]_{1221} + [c_{ee}]_{1122} + [c_{\ell e}]_{1122} + [c_{\ell e}]_{2211}\right) \\
&+ \frac{s(g_L^2+g_Y^2)}{s-m_Z^2}\left[(g^{Ze}_{L,\mathrm{SM}})^2\left([c_{\ell\ell}]_{1122} + [c_{\ell\ell}]_{1221}\right) + (g^{Ze}_{R,\mathrm{SM}})^2[c_{ee}]_{1122} + g^{Ze}_{L,\mathrm{SM}}g^{Ze}_{R,\mathrm{SM}}\left([c_{\ell e}]_{1122} + [c_{\ell e}]_{2211}\right)\right]\Big\} \\
\delta(\sigma_F - \sigma_B) &= \frac{1}{32\pi v^2}\Big\{e^2\left([c_{\ell\ell}]_{1122} + [c_{\ell\ell}]_{1221} + [c_{ee}]_{1122} - [c_{\ell e}]_{1122} - [c_{\ell e}]_{2211}\right) \\
&+ \frac{s(g_L^2+g_Y^2)}{s-m_Z^2}\left[(g^{Ze}_{L,\mathrm{SM}})^2\left([c_{\ell\ell}]_{1122} + [c_{\ell\ell}]_{1221}\right) + (g^{Ze}_{R,\mathrm{SM}})^2[c_{ee}]_{1122} - g^{Ze}_{L,\mathrm{SM}}g^{Ze}_{R,\mathrm{SM}}\left([c_{\ell e}]_{1122} + [c_{\ell e}]_{2211}\right)\right]\Big\}
\end{aligned} \tag{3.44}$$

where $g^{Ze}_{L,\mathrm{SM}} = -\frac{1}{2} + s^2_\theta$, $g^{Ze}_{R,\mathrm{SM}} = s^2_\theta$ are the couplings of the Z to left- and right-handed electrons. The effect of the vertex corrections δg^{Ze}_L, δg^{Ze}_R, $\delta g^{Z\mu}_L$, and $\delta g^{Z\mu}_R$ is also taken into account in the fit, but is not displayed here. The operator $[O_{\ell e}]_{1221}$ does not interfere with the SM due to the different helicity structure; thus it enters only at the quadratic ($\mathcal{O}(\Lambda^{-4})$) level and is neglected in this analysis.

One observes that measurements of the total cross section and asymmetry in $e^-e^+ \to \mu^-\mu^+$ in principle can constrain 3 linear combinations of the 5 four-lepton operators that enter in (3.44). $[O_{\ell\ell}]_{1122}$ and $[O_{\ell\ell}]_{1221}$ are indistinguishable for this process because their parts involving charged leptons are related by a Fierz transformation. $[O_{\ell e}]_{1122}$ and $[O_{\ell e}]_{2211}$ are also indistinguishable in this process, which can be traced to lepton flavour universality of the SM couplings. Accidentally, the LEP-2 observables depend very weakly on the combination $[O_{\ell\ell}]_{1122} + [O_{\ell\ell}]_{1221} - [O_{ee}]_{1122}$ due to the fact that, numerically, $(g^{Ze}_{L,\mathrm{SM}})^2 \approx (g^{Ze}_{R,\mathrm{SM}})^2$.

In the muon sector, this degeneracy will be resolved by the addition of the muon-neutrino scattering data described before. In the tau sector, e add the measurement of τ polarization and its FB asymmetry in $e^+e^- \to \tau^+\tau^-$ production at $\sqrt{s} = 58$ GeV by the VENUS collaboration [206].

Bhabha scattering

We move to the process $e^-e^+ \to e^-e^+$ (Bhabha scattering). In Ref. [180], LEP-2 quotes the differential cross sections for the scattering angle $\cos\theta$ in the interval $[-0.9, 0.9]$, and the center-of-mass energies from 189 GeV to 207 GeV. Bhabha scattering is affected by the three four-leptons operators $[O_{\ell\ell}]_{1111}$, $[O_{ee}]_{1111}$ and $[O_{\ell e}]_{1111}$. In the limit of vanishing fermion masses their effect on the differential cross section is given by

$$\begin{aligned}
\delta\frac{d\sigma}{d\cos\theta} \quad = \tfrac{1}{8\pi s}\tfrac{1}{v^2} \quad & \left\{ u^2 \left[e^2([c_{\ell\ell}]_{1111} + [c_{ee}]_{1111})\left(\frac{1}{s} + \frac{1}{t}\right) \right.\right. \\
& + (g_L^2 + g_Y^2)\left(\left(g^{Ze}_{L,\mathrm{SM}}\right)^2 [c_{\ell\ell}]_{1111} + \left(g^{Ze}_{R,\mathrm{SM}}\right)^2 [c_{ee}]_{1111}\right)\left(\frac{1}{s - m_Z^2} + \frac{1}{t - m_Z^2}\right)\Bigg] \\
& + t^2 \left[[c_{\ell e}]_{1111}\frac{e^2}{s} + [c_{\ell e}]_{1111}\frac{(g_L^2 + g_Y^2) g^{Ze}_{L,\mathrm{SM}} g^{Ze}_{R,\mathrm{SM}}}{s - m_Z^2} \right] \\
& \left. + s^2 \left[[c_{\ell e}]_{1111}\frac{e^2}{t} + [c_{\ell e}]_{1111}\frac{(g_L^2 + g_Y^2) g^{Ze}_{L,\mathrm{SM}} g^{Ze}_{R,\mathrm{SM}}}{t - m_Z^2} \right] \right\}
\end{aligned} \tag{3.45}$$

where $t = -\frac{s}{2}(1 - \cos\theta)$ and $u = -\frac{s}{2}(1 + \cos\theta)$. Again, the dependence on the vertex corrections δg^{Ze}_L, δg^{Ze}_R is taken into account in our analysis but not displayed here. In principle, Bhabha scattering at LEP-2 constrains independently all 3 four-electron operators, but again an approximate flat direction along the direction $[O_{\ell\ell}]_{1111} - [O_{ee}]_{1111}$ arises due to the numerical accident $(g^{Ze}_{L,\mathrm{SM}})^2 \approx (g^{Ze}_{R,\mathrm{SM}})^2$.

Quark pair production

Unlike the low-energy experiments discussed above, $e^+e^- \to q\bar{q}$ processes also probe flavour-conserving operators with strange, charm and bottom quarks. Typically, the experiments quote the total measured cross section for $\sigma_q \equiv \sigma(e^+e^- \to q\bar{q})$ and the asymmetry $A_{FB}^q = \frac{\sigma_q^{\rm FB}}{\sigma_q}$, where σ_q^{FB} is the difference between the cross sections with the electron going forward and backward in the center-of-mass frame. In the presence of dimension-6 operators, at $\mathcal{O}(\Lambda^{-2})$ these cross sections are modified as follows

$$\begin{aligned}
\delta\sigma_q &= \frac{1}{8\pi s}\left[-e^2(g_L^2+g_Y^2)\frac{s}{s-m_Z^2}\left(\delta A_{Fq}+\delta A_{Bq}\right)+(g_L^2+g_Y^2)^2\frac{s^2}{(s-m_Z^2)^2}\left(\delta B_{Fq}+\delta B_{Bq}\right)\right] \\
&+ \frac{1}{8\pi v^2}(g_L^2+g_Y^2)\frac{s}{s-m_Z^2}\left(\hat{g}_L^{Ze}\hat{g}_L^{Zq}c_{LL}+\hat{g}_L^{Ze}\hat{g}_R^{Zq}c_{LR}+\hat{g}_R^{Ze}\hat{g}_L^{Zq}c_{RL}+\hat{g}_R^{Ze}\hat{g}_R^{Zq}c_{RR}\right) \\
&- \frac{1}{8\pi v^2}e^2Q_q\left(c_{LL}+c_{LR}+c_{RL}+c_{RR}\right) \qquad (3.46)
\end{aligned}$$

$$\begin{aligned}
\delta\sigma_q^{\rm FB} &= \frac{3}{32\pi s}\left[-e^2(g_L^2+g_Y^2)\frac{s}{s-m_Z^2}\left(\delta A_{Fq}-\delta A_{Bq}\right)+(g_L^2+g_Y^2)^2\frac{s^2}{(s-m_Z^2)^2}\left(\delta B_{Fq}-\delta B_{Bq}\right)\right] \\
&+ \frac{3}{32\pi v^2}(g_L^2+g_Y^2)\frac{s}{s-m_Z^2}\left(\hat{g}_L^{Ze}\hat{g}_L^{Zq}c_{LL}+\hat{g}_R^{Ze}\hat{g}_R^{Zq}c_{RR}-\hat{g}_L^{Ze}\hat{g}_R^{Zq}c_{LR}-\hat{g}_R^{Ze}\hat{g}_L^{Zq}c_{RL}\right) \\
&- \frac{3}{32\pi v^2}e^2Q_q\left(c_{LL}+c_{RR}-c_{LR}-c_{RL}\right), \qquad (3.47)
\end{aligned}$$

where $\sqrt{s}$ is the center-of-mass energy of the e^+e^- collision, $\hat{g}^{Zf} \equiv T_f^3 - s_\theta^2 Q_f$ (i.e., the SM values), and

$$\begin{aligned}
\delta A_{Fq} &= Q_q\left(\delta g_L^{Ze}\hat{g}_L^{Zq}+\delta g_R^{Ze}\hat{g}_R^{Zq}+\hat{g}_L^{Ze}\delta g_L^{Zq}+\hat{g}_R^{Ze}\delta g_R^{Zq}\right), \qquad (3.48)\\
\delta A_{Bq} &= Q_q\left(\delta g_L^{Ze}\hat{g}_R^{Zq}+\delta g_R^{Ze}\hat{g}_L^{Zq}+\hat{g}_L^{Ze}\delta g_R^{Zq}+\hat{g}_R^{Ze}\delta g_L^{Zq}\right)\\
\delta B_{Fq} &= \hat{g}_L^{Ze}\left(\hat{g}_L^{Zq}\right)^2\delta g_L^{Ze}+\hat{g}_R^{Ze}\left(\hat{g}_R^{Zq}\right)^2\delta g_R^{Ze}+\left(\hat{g}_L^{Ze}\right)^2\hat{g}_L^{Zq}\delta g_L^{Zq}+\left(\hat{g}_R^{Ze}\right)^2\hat{g}_R^{Zq}\delta g_R^{Zq}\\
\delta B_{Bq} &= \hat{g}_L^{Ze}\left(\hat{g}_R^{Zq}\right)^2\delta g_L^{Ze}+\hat{g}_R^{Ze}\left(\hat{g}_L^{Zq}\right)^2\delta g_R^{Ze}+\left(\hat{g}_R^{Ze}\right)^2\hat{g}_L^{Zq}\delta g_L^{Zq}+\left(\hat{g}_L^{Ze}\right)^2\hat{g}_R^{Zq}\delta g_R^{Zq}
\end{aligned}$$

For the up-type quark production, $q = u_J$, the four-fermion Wilson coefficients c_{XY} in equation (3.46) and equation (3.47) are given by

$$c_{LL} = [c_{\ell q}]_{11JJ} - [c_{\ell q}^{(3)}]_{11JJ}, \quad c_{LR} = [c_{\ell u}]_{11JJ}, \quad c_{RL} = [c_{eq}]_{11JJ}, \quad c_{RR} = [c_{eu}]_{11JJ}, \qquad (3.49)$$

while for the down-type quark production, $q = d_J$,

$$c_{LL} = [c_{\ell q}]_{11JJ} + [c_{\ell q}^{(3)}]_{11JJ}, \quad c_{LR} = [c_{\ell d}]_{11JJ}, \quad c_{RL} = [c_{eq}]_{11JJ}, \quad c_{RR} = [c_{ed}]_{11JJ}. \qquad (3.50)$$

The operators $O_{\ell equ}$, $O_{\ell equ}^{(3)}$ and $O_{\ell eqd}$ do not enter at $\mathcal{O}(\Lambda^{-2})$ because they do not interfere with the SM amplitudes due to the different chirality structure.

The LEP-2 experiment studied e^+e^- collisions at energies above the Z-pole, ranging from $\sqrt{s}=$ 130 Gev to $\sqrt{s}=209$ GeV. Available data includes the total cross section $\sigma(q\bar{q})\equiv\sum_{q=u,d,s,c,b}\sigma_q$ [180], as well as the total cross section and forward-backward asymmetry for the charm and for the bottom quark production [207]. This amounts to 5 distinct observables, each measured at different $\sqrt{s}$. From equation (3.46) and equation (3.47), given the energy dependence, each of these observables should resolve 4 different combinations of dimension-6 Wilson coefficients.[9] In practice, the energy range scanned by LEP-2 is not large enough to efficiently disentangle these different combinations. Therefore, in our fit we also include earlier, less precise measurements of heavy quark production below the Z-pole. Specifically, we include the measurements from the VENUS [208] and TOPAZ [209] collaborations of the $c\bar{c}$ and $b\bar{b}$ pair production at $\sqrt{s}=58$ GeV (total cross sections and FB asymmetries).

3.3.7 Muon and tau decay

The leptonic tau decays $\tau^-\to e^-\nu_\tau\bar{\nu}_e$, $\tau^-\to\mu^-\nu_\tau\bar{\nu}_\mu$, and the conjugates provide additional information on 4-lepton operators involving τ. In particular, the provide the only constraint we are aware of on lepton-flavour conserving 4-lepton operators with muons and taus. The decays can be described by the following effective Lagrangian:

$$\mathscr{L}=\frac{4G_{\tau f}}{\sqrt{2}}(\nu_\tau^\dagger\bar{\sigma}_\rho\tau)(f^\dagger\bar{\sigma}_\rho\nu_f) \tag{3.51}$$

where $f=e,\mu$. At the linear level, the relative strength of the Fermi constant measured in the tau decays normalized to that measured in the muon decay is affected by the vertex corrections and four-lepton operators as

$$\begin{aligned} A_e &\equiv \frac{G_{\tau e}^2}{G_F^2}=1+2\delta g_L^{W\tau}+2\delta g_L^{We}-4\delta m-[c_{\ell\ell}]_{1331} \\ A_\mu &\equiv \frac{G_{\tau\mu}^2}{G_F^2}=1+2\delta g_L^{W\tau}+2\delta g_L^{W\mu}-4\delta m-[c_{\ell\ell}]_{2332} \end{aligned} \tag{3.52}$$

where the W mass corrections δm can be expressed by other EFT parameters, c.f. (3.24). The experimental values quoted by the PDG are [210]

$$\begin{aligned} A_e &= 1.0029\pm0.0046 \\ A_\mu &= 0.981\pm0.018 \end{aligned} \tag{3.53}$$

and the SM prediction is $A_f=1$.

For the muon decay, $\mu^-\to e^-\nu_\mu\bar{\nu}_e$ and the conjugate, the total rate defines the SM input parameter v and by itself it does not probe new physics. However, additional information can be extracted from differential distributions in (polarized) muon decay. Customarily, these

[9] Note that two of these combinations involve only vertex corrections though.

measurements are presented in the language of *Michel parameters* [211]. From the EFT perspective the most interesting are the so-called η and β'/A parameters, because they are the only ones that may receive contributions at $\mathcal{O}(1/\Lambda^2)$ [212,213]:

$$\eta = \frac{\text{Re}[c_{\ell e}]_{1221}}{2}, \qquad \beta'/A = -\frac{\text{Im}[c_{\ell e}]_{1221}}{4}. \tag{3.54}$$

These parameters have been measured in an experiment in the PSI [214]:

$$\eta = -0.0021 \pm 0.0071, \qquad \beta'/A = -0.0013 \pm 0.0036. \tag{3.55}$$

Analogous limits from tau decays are much weaker.

3.3.8 Neutrino trident production

Finally, we include the constraints from the trident production $\nu_\mu X \to \mu_\mu \mu^+ \mu^- Y$ [215,216].Dimension-6 operators modify the trident cross section as

$$\begin{aligned}
\frac{\sigma_{\text{trident}}}{\sigma_{\text{trident,SM}}} &\approx 1 + 2\frac{g^{\nu_\mu\mu}_{LL,\text{SM}}\delta g^{\nu_\mu\mu}_{LL} + g^{\nu_\mu\mu}_{LR,\text{SM}}\delta g^{\nu_\mu\mu}_{LR}}{(g^{\nu_\mu\mu}_{LL,\text{SM}})^2 + (g^{\nu_\mu\mu}_{LR,\text{SM}})^2}, \quad g^{\nu_\mu\mu}_{LL,\text{SM}} = \frac{1}{2} + s^2_\theta, \quad g^{\nu_\mu\mu}_{LR,\text{SM}} = s^2_\theta \\
\delta g^{\nu_\mu\mu}_{LL} &= -\delta g^{We}_L + 2s^2_\theta(\delta g^{W\mu}_L + \delta g^{Z\mu}_L) + \frac{[c_{\ell\ell}]_{1221} - [c_{\ell\ell}]_{2222}}{2} \\
\delta g^{\nu_\mu\mu}_{LL} &= \delta g^{Z\mu}_R + 2s^2_\theta(\delta g^{W\mu}_L + \delta g^{Z\mu}_L) - \frac{[c_{\ell e}]_{2222}}{2}
\end{aligned} \tag{3.56}$$

This observable is, to our knowledge, the only one constraining 4-muon operators.

3.4 Global Fit

3.4.1 Scope

The main goal of this work is to provide model-independent constraints on flavour-diagonal 2-lepton-2-quark operators summarized in table 3.1. Among the chirality-conserving ones, most of the observables considered here probe the operators involving the 1st generation leptons. There are 21 such operators and for an easy reference we list here their Wilson coefficients:

$$[c_{\ell q}]_{11JJ},\ [c^{(3)}_{\ell q}]_{11JJ},\ [c_{\ell u}]_{11JJ},\ [c_{\ell d}]_{11JJ},\ [c_{eq}]_{11JJ},\ [c_{eu}]_{11JJ},\ [c_{ed}]_{11JJ}\,, \qquad J = 1,2,3. \tag{3.1}$$

Scattering of muons and muon neutrinos on nucleons gives us access to chirality-conserving operators involving 2nd generation leptons and 1st generation quarks. There are 7 such operators:

$$[c_{\ell q}]_{2211},\ [c^{(3)}_{\ell q}]_{2211},\ [c_{\ell u}]_{2211},\ [c_{\ell d}]_{2211},\ [c_{eq}]_{2211},\ [c_{eu}]_{2211},\ [c_{ed}]_{2211}. \tag{3.2}$$

Class	Observable	Exp. value	Ref. & Comments	SM value
$\nu_e\nu_e qq$	$R_{\nu_e\bar{\nu}_e}$	0.41(14)	CHARM [183]	0.33
$\nu_\mu\nu_\mu qq$	$(g_L^{\nu_\mu})^2$	0.3005(28)	PDG [168], $\rho\approx 1$	0.3034
	$(g_R^{\nu_\mu})^2$	0.0329(30)		0.0302
	$\theta_L^{\nu_\mu}$	2.500(35)		2.4631
	$\theta_R^{\nu_\mu}$	$4.56^{+0.42}_{-0.27}$		5.1765
PV low-E $eeqq$	$g_{AV}^{eu}+2g_{AV}^{ed}$	0.489(5)	PDG [168], $\rho\neq 1$	0.4951
	$2g_{AV}^{eu}-g_{AV}^{ed}$	−0.708(16)		−0.7192
	$2g_{VA}^{eu}-g_{VA}^{ed}$	−0.144(68)		−0.0949
	$g_{VA}^{eu}-g_{VA}^{ed}$	−0.042(57) −0.120(74)	SAMPLE [204]	−0.0627
PV low-E $\mu\mu qq$	$b_{\rm SPS}(\lambda=0.81)$	$-1.47(42)\cdot 10^{-4}$	SPS [205]	$-1.56\cdot 10^{-4}$
	$b_{\rm SPS}(\lambda=0.66)$	$-1.74(81)\cdot 10^{-4}$		$-1.57\cdot 10^{-4}$
$d(s)\to u\ell\nu$	$\epsilon_i^{d_j\ell}$	equation (3.43)	Ref. [160]	0
$e^+e^-\to q\bar{q}$	$\sigma(q\bar{q})$	$f(\sqrt{s})$	LEPEWWG [180], $\rho\neq 1$	$f(\sqrt{s})$
	σ_c,σ_b		LEPEWWG [217], VENUS [208], TOPAZ [209]	
	A_{FB}^{cc},A_{FB}^{bb}			
$\nu_\mu\nu_\mu ee$	$g_{LV}^{\nu_\mu e}$	−0.040(15)	PDG [168], $\rho\neq 1$	−0.0396
	$g_{LA}^{\nu_\mu e}$	−0.507(14)		−0.5064
$e^-e^-\to e^-e^-$	g_{AV}^{ee}	0.0190(27)	PDG [168]	0.0225
$\nu_\mu\gamma^*\to\mu^+\mu^-\nu_\mu\gamma^*$	$\frac{\sigma}{\sigma_{\rm SM}}$	1.58(57) 0.82(28)	CHARM [215] CCFR [216]	1
$\tau\to\ell\nu\nu$	$G_{\tau e}^2/G_F^2$	1.0029(46)	PDG [168], $\rho\approx 1$	1
	$G_{\tau\mu}^2/G_F^2$	0.981(18)		1
$e^+e^-\to\ell^+\ell^-$	$\frac{d\sigma(ee)}{d\cos\theta}$	$f(\sqrt{s})$	LEPEWWG [180], $\rho\approx 1$	$f(\sqrt{s})$
	$\sigma_\mu,\sigma_\tau,\mathscr{P}_\tau$		LEPEWWG [217], VENUS [206]	
	$A_{FB}^{\mu},A_{FB}^{\tau}$			

Table 3.4 – Summary of experimental input (sensitive to LLQQ and LLLL contact interactions) used in our fit. The correlations that are taken into account in our fit are specified. Each observable in $e^+e^-\to f\bar{f}$ is measured at various c.o.m. energies, which we denote in the table by $f(\sqrt{s})$. The specific numerical values can be found in the corresponding original references. We also use the set of pole observables described in Ref. [139] in order to independently constrain the vertex corrections δg.

Finally, the likelihood in equation (3.43) summarizing the constraints from low-energy flavour observables gives us also access to chirality-violating operators involving 1st and 2nd generation leptons and and 1st generation quarks. There are 6 such operators:

$$[c_{lequ}]_{JJ11}\,,\ [c_{ledq}]_{JJ11}\,,\ [c^{(3)}_{lequ}]_{JJ11}\,, \qquad J=1,2\,, \tag{3.3}$$

which should be understood as evaluated at the renormalization scale $\mu = m_Z$ unless otherwise stated.

We will use the observables summarized in section 3.3 to constrain as many as possible of the 34 Wilson coefficients in Eqs. (3.1)-(3.3). We will also present simultaneous constraints on these parameter, together with the vertex corrections and 4-lepton Wilson coefficients.

3.4.2 Flat directions

Not all linear combinations of the parameters Eqs. (3.1)-(3.3) can be constrained by the observables we consider. Before venturing into a global fit, we need to count the independent constraints and determine the flat directions in the parameter space. In table 3.4 we have the following probes of LLQQ operators:

- 1 combination of the parameters in equation (3.1) is constrained (poorly) via the only $\nu_e\nu_e qq$ measurement ($R_{\nu_e\bar{\nu}_e}$);
- 4 combinations in equation (3.2) are constrained via $\nu_\mu\nu_\mu qq$ measurements;
- 4 new combinations in equation (3.1) are constrained via PV low-energy $eeqq$ measurements ($g^{eq}_{VA/AV}$);
- 1 different combination in equation (3.2) is constrained (poorly) via PV low-energy $\mu\mu qq$ measurements ($b_{\rm SPS}$), which also probe a second combination already constrained by $\nu_\mu\nu_\mu qq$ data;
- 5 additional combinations in Eqs. (3.1)-(3.3) are constrained by low-energy flavour observables ($d(s) \to u\ell\nu_\ell$ transitions);[10]
- 10 additional combinations in equation (3.1) are probed by $e^+e^- \to q\bar{q}$ data, through the measurement of the the total hadronic cross section and heavy flavour (b and c) fractions and asymmetries.

[10] The likelihood in equation (3.43) also independently constrains $\delta g_R^{Wq_1}$.

All together we have 25 constraints on 34 parameters, which leaves 9 flat directions. These can be characterized quite concisely:

$$
\begin{aligned}
&(\mathbf{F1}): \quad [c_{\ell u}]_{1133}, \quad (\mathbf{F2}): \quad [c_{eu}]_{1133}, \quad (\mathbf{F3}): \quad [c^{(3)}_{\ell q}]_{1133} = -[c_{\ell q}]_{1133},\\
&(\mathbf{F4}): \quad [c^{(3)}_{\ell q}]_{1122} = [c_{\ell q}]_{1122}, \quad [c_{\ell d}]_{1122} = \left(-5 + \frac{3g_L^2}{g_Y^2}\right)[c_{\ell q}]_{1122}, \quad [c_{ed}]_{1122} = \left(3 - \frac{3g_L^2}{g_Y^2}\right)[c_{\ell q}]_{1122},\\
&(\mathbf{F5}): \quad [c_{\ell q}]_{1111} = -[c_{\ell u}]_{1111} = -[c_{\ell d}]_{1111} = -[c_{eq}]_{1111} = [c_{eu}]_{1111} = [c_{ed}]_{1111},\\
&(\mathbf{F6}): \quad [c_{eq}]_{2211} = -[c_{ed}]_{2211}, \quad (\mathbf{F7}): \quad [c_{eq}]_{2211} = 2[c_{eu}]_{2211},\\
&(\mathbf{F8},\mathbf{F9}): \quad 0.86[c_{ledq}]_{2211} - 0.86[c_{lequ}]_{2211} + 0.012[c^{(3)}_{ledq}]_{2211} = 0.
\end{aligned}
\tag{3.4}
$$

The flat directions F1, F2, F3 arise because low-energy precision measurements do not probe the top quark couplings, which may be amended one day by e^+e^- collider operating above the $t\bar{t}$ threshold. F4 is due to the insufficient information about the strange quark couplings, and it could be lifted by off Z-pole measurements of the strange asymmetry. F5 is the consequence of the fact that the parity conserving operator $(\bar{e}\gamma_\mu\gamma_5 e)\sum_q(\bar{q}\gamma_\mu\gamma_5 q)$ and the axial neutrino-quark interaction $(\bar{\nu}_L\gamma_\mu\nu_L)\sum_q(\bar{q}\gamma_\mu\gamma_5 q)$ are unconstrained by low-energy measurements and by e^+e^- colliders. F6 and F7 are due to little data on muon scattering on nucleons. Finally, F8 and F9 appear because, with our approximations, the low-energy flavour observables probe only one combination of light quark couplings to muons (through $\pi \to \mu\nu$). The low-energy constraint on $\epsilon_P^{d\mu} = ([c_{ledq}]_{2211} - [c_{lequ}]_{2211})/2$ at $\mu = 2$ GeV (via Δ^d_{LP} in equation (3.43)), after taking into account the running up to m_Z, becomes a constraint on the linear combination in the last line of equation (3.4).

In order to isolate the flat directions we define

$$
\begin{aligned}
[\hat{c}_{eq}]_{1111} &= [c_{eq}]_{1111} + [c_{\ell q}]_{1111}\\
[\hat{c}_{\ell u}]_{1111} &= [c_{\ell u}]_{1111} + [c_{\ell q}]_{1111} - [\hat{c}_{eq}]_{1111}\\
[\hat{c}_{\ell d}]_{1111} &= [c_{\ell d}]_{1111} + [c_{\ell q}]_{1111} - [\hat{c}_{eq}]_{1111}\\
[\hat{c}_{eu}]_{1111} &= [c_{eu}]_{1111} - [c_{\ell q}]_{1111}\\
[\hat{c}_{ed}]_{1111} &= [c_{ed}]_{1111} - [c_{\ell q}]_{1111}\\
[\hat{c}^{(3)}_{\ell q}]_{1122} &= [c^{(3)}_{\ell q}]_{1122} - [c_{\ell q}]_{1122}\\
[\hat{c}_{\ell d}]_{1122} &= [c_{\ell d}]_{1122} + \left(5 - \frac{3g_L^2}{g_Y^2}\right)[c_{\ell q}]_{1122} - [\hat{c}_{eq}]_{1111}\\
[\hat{c}_{ed}]_{1122} &= [c_{ed}]_{1122} - \left(3 - \frac{3g_L^2}{g_Y^2}\right)[c_{\ell q}]_{1122} - [\hat{c}_{eq}]_{1111}
\end{aligned}
$$

$$
\begin{aligned}
[\hat{c}^{(3)}_{\ell q}]_{1133} &= [c^{(3)}_{\ell q}]_{1133} + [c_{\ell q}]_{1133} \\
[\hat{c}_{eq}]_{2211} &= [c_{eq}]_{2211} + [c_{ed}]_{2211} - 2[c_{eu}]_{2211} \\
\epsilon_P^{d\mu}(2\text{ GeV}) &= 0.86[c_{ledq}]_{2211} - 0.86[c_{lequ}]_{2211} + 0.012[c^{(3)}_{ledq}]_{2211} \\
[\hat{c}_{\ell\ell}]_{2222} &= [c_{\ell\ell}]_{2222} + \frac{2g_Y^2}{g_L^2+3g_Y^2}[c_{\ell e}]_{2222}
\end{aligned}
\tag{3.5}
$$

The last variable projects out the flat direction among 4-muon operators in the trident observable. Using these variables, the global likelihood depends on the Wilson coefficients on the right-hand sides of Eqs. (3.5) only via the $\hat{c}$ and $\epsilon_P^{d\mu}(2\text{ GeV})$ combinations.[11] Moreover, the dependence on $[\hat{c}_{eq}]_{1111}$ appears only thanks to the loose $R_{\nu_e\bar{\nu}_e}$ constraint, and thus we know beforehand that there is no sensitivity to $[\hat{c}_{eq}]_{1111} \lesssim 1$.

3.4.3 Reconnaissance

We start by presenting the constraints in the case when only one of the LLQQ operators is present at a time, and all vertex corrections and 4-lepton operators vanish. We stress that this is just a warm-up exercise and not our main result. Indeed, one-by-one constraints are basis dependent and could be different if another basis of dimension-6 operators was used. Only the global likelihood encoding the correlated constraints on all Wilson coefficients in a given basis has a model-independent meaning. The main purpose of this exercise is to compare the sensitivity of various experiments to a few particular directions in the space of Wilson coefficients.

The one-by-one constraints on chirality-conserving LLQQ operators involving 1st generation quarks are shown in table 3.5. One can see that atomic parity violation is the most sensitive probe for most of the operators with electrons and the first generation quarks. The exception is $[O^{(3)}_{\ell q}]_{1111}$, which contributes to charged-current transitions and can be probed in $d \to ue\bar{\nu}_e$ decays.[12] We stress however that the less sensitive experiments will be absolutely crucial to probe more independent directions in the space of dimension-6 operators. For the operators involving the 2nd generation lepton doublet the muon-neutrino scattering is a fairly sensitive probe. Again, $[O^{(3)}_{\ell q}]_{2211}$ is very precisely probed by the low-energy flavour observables because it affects the charged current. The sensitivity of low-energy experiments to the operators involving the right-handed muons is very poor. However, this is not a pressing problem, given these directions are very well probed by the LHC [129], as will be discussed in section 3.5. The $(ee)(qq)$ bounds shown in Table 5 are in excellent agreement with the 1-by-1 results of Ref. [129], whereas our $(\mu\mu)(qq)$ bounds are more stringent due to the inclusion of additional experimental input.

[11] Let us stress that the LLQQ coefficients in the r.h.s. of $\epsilon_P^{d\mu}(2\text{ GeV})$ in equation (3.5) are defined at $\mu = m_Z$.

[12] The single-operator bounds from $d(s) \to u\ell\bar{\nu}_\ell$ data shown in this section are obtained using the likelihood of equation (3.43), which was marginalized over strange-quark couplings. Using instead the full likelihood [160] given in C.2 slightly stronger constraints (and central values closer to zero) are obtained.

$(ee)(qq)$

	$[c^{(3)}_{\ell q}]_{1111}$	$[c_{\ell q}]_{1111}$	$[c_{\ell u}]_{1111}$	$[c_{\ell d}]_{1111}$	$[c_{eq}]_{1111}$	$[c_{eu}]_{1111}$	$[c_{ed}]_{1111}$
CHARM	-80 ± 180	700 ± 1800	370 ± 880	-700 ± 1800	x	x	x
APV	27 ± 19	$\mathbf{1.6 \pm 1.1}$	$\mathbf{3.4 \pm 2.3}$	$\mathbf{3.0 \pm 2.0}$	$\mathbf{-1.6 \pm 1.1}$	$\mathbf{-3.4 \pm 2.3}$	$\mathbf{-3.0 \pm 2.0}$
QWEAK	7.0 ± 12	-2.3 ± 4.0	-3.5 ± 6.0	-7 ± 12	2.3 ± 4.0	3.5 ± 6.0	7 ± 12
PVDIS	-8 ± 12	24 ± 35	38 ± 48	-77 ± 96	-77 ± 96	-12 ± 17	24 ± 35
SAMPLE	-8 ± 45	x	-17 ± 90	17 ± 90	x	-17 ± 90	17 ± 90
$d_j \to u\ell\nu$	$\mathbf{0.38 \pm 0.28}$	x	x	x	x	x	x
LEP-2	3.5 ± 2.2	-42 ± 28	-21 ± 14	42 ± 28	-18 ± 11	-9.0 ± 5.7	18 ± 11

$(\mu\mu)(qq)$

	$[c^{(3)}_{\ell q}]_{2211}$	$[c_{\ell q}]_{2211}$	$[c_{\ell u}]_{2211}$	$[c_{\ell d}]_{2211}$	$[c_{eq}]_{2211}$	$[c_{eu}]_{2211}$	$[c_{ed}]_{2211}$
PDG ν_μ	20 ± 15	$\mathbf{4 \pm 21}$	$\mathbf{18 \pm 19}$	$\mathbf{-20 \pm 37}$	x	x	x
SPS	0 ± 1000	0 ± 3000	0 ± 1500	0 ± 3000	$\mathbf{40 \pm 390}$	$\mathbf{-20 \pm 190}$	$\mathbf{40 \pm 390}$
$d_j \to u\ell\nu$	$\mathbf{-0.4 \pm 1.2}$	x	x	x	x	x	x

Table 3.5 – 68% C.L. constraints (in units of 10^{-3}) on chirality-conserving $(ee)(qq)$ and $(\mu\mu)(qq)$ operators from different precision experiments. The bounds are derived assuming that only one operator is present at a time. See table 3.4 and main text for further details about the different experiments. The best constraint in each case is highlighted in blue, while 'x' signals that the operator is not probed at tree level by that experiment or combination.

The LEP-2 constraints on operators involving 2nd generation or bottom quarks are similar as those shown in table 3.5. We also give 1-by-1 constraints on the chirality-violating LLQQ operators from the low-energy flavour observables:

$$\begin{pmatrix} [c_{\ell equ}]_{1111} \\ [c_{\ell edq}]_{1111} \\ [c^{(3)}_{\ell equ}]_{1111} \end{pmatrix} = \begin{pmatrix} -(0.8 \pm 2.9) \cdot 10^{-7} \\ (0.8 \pm 2.9) \cdot 10^{-7} \\ (0.5 \pm 2.0) \cdot 10^{-5} \end{pmatrix}, \quad \begin{pmatrix} [c_{\ell equ}]_{2211} \\ [c_{\ell edq}]_{2211} \\ [c^{(3)}_{\ell equ}]_{2211} \end{pmatrix} = \begin{pmatrix} (1.7 \pm 5.8) \cdot 10^{-5} \\ -(1.7 \pm 5.8) \cdot 10^{-5} \\ -(1.2 \pm 4.1) \cdot 10^{-3} \end{pmatrix}. \tag{3.6}$$

This exceptional sensitivity arises because these operators violate the approximate symmetries of the SM, leading potentially to a large enhancement of several decays of low-mass hadrons.[13] In particular, new physics generating the pseudo-scalar $(ee)(qq)$ operator is probed up to $\Lambda/g_* \sim$100 TeV. Let us note that they dominate the $c^{(3)}_{\ell equ}$ bounds shown above, despite the fact that they probe them only via 1-loop QED mixing [174, 218]. For consistency with the rest of this work, these individual limits are obtained using $V = 1$ at order Λ^{-2}. Working instead with the full non-diagonal CKM matrix the limits are slightly modified, but more importantly one can set strong 1-by-1 limits in a long list of other (offdiagonal) operators.

Finally, for the sake of completeness we show the 1-by-1 bound on the W coupling to right-

[13] More specifically they violate the approximate flavour symmetry of the SM $U(1)_\ell \times U(1)_e$ that suppresses the decay $\pi \to \ell\nu_\ell$ by a factor m_ℓ^2/Λ^2_{QCD}. Thus, their bounds benefit from this large Λ_{QCD}/m_ℓ chiral enhancement. This does not apply however to the tensor operator $c^{(3)}_{\ell equ}$, whose tree-level contribution to this specific decay is zero by simple Lorentz invariance considerations.

handed 1st-generation quarks

$$\delta g_R^{Wq_1} = -(3.9 \pm 2.9) \cdot 10^{-4}, \tag{3.7}$$

which is completely dominated by its contribution to the CKM-unitarity test of equation (3.9).

3.4.4 All out

We now combine all the experimental observables summarized in table 3.4 along with the pole observables discussed in Ref. [139], which represent a total of 264 experimental input. These provide simultaneous constraints on 61 combinations of Wilson coefficients of dimension-6 operators in the SMEFT Lagrangian (21 vertex corrections δg, 25 LLQQ and 15 LLLL operators)

and on the $\tilde{V}_{ud}$ SM parameter. Marginalizing over $\tilde{V}_{ud}$ we find the following constraints:

$$\begin{pmatrix} \delta g_L^{We} \\ \delta g_L^{W\mu} \\ \delta g_L^{W\tau} \\ \delta g_L^{Ze} \\ \delta g_L^{Z\mu} \\ \delta g_L^{Z\tau} \\ \delta g_R^{Ze} \\ \delta g_R^{Z\mu} \\ \delta g_R^{Z\tau} \\ \delta g_L^{Zu} \\ \delta g_L^{Zc} \\ \delta g_L^{Zt} \\ \delta g_R^{Zu} \\ \delta g_R^{Zc} \\ \delta g_L^{Zd} \\ \delta g_L^{Zs} \\ \delta g_L^{Zb} \\ \delta g_R^{Zd} \\ \delta g_R^{Zs} \\ \delta g_R^{Zb} \\ \delta g_R^{Wq_1} \\ [c_{\ell\ell}]_{1111} \\ [c_{\ell e}]_{1111} \\ [c_{ee}]_{1111} \\ [c_{\ell\ell}]_{1221} \\ [c_{\ell\ell}]_{1122} \\ [c_{\ell e}]_{1122} \\ [c_{\ell e}]_{2211} \\ [c_{ee}]_{1122} \\ [c_{\ell\ell}]_{1331} \\ [c_{\ell\ell}]_{1133} \\ [c_{\ell e}]_{1133} \\ [c_{\ell e}]_{3311} \\ [c_{ee}]_{1133} \\ [\hat{c}_{\ell\ell}]_{2222} \\ [c_{\ell\ell}]_{2332} \end{pmatrix} = \begin{pmatrix} -1.00 \pm 0.64 \\ -1.36 \pm 0.59 \\ 1.95 \pm 0.79 \\ -0.023 \pm 0.028 \\ 0.01 \pm 0.12 \\ 0.018 \pm 0.059 \\ -0.033 \pm 0.027 \\ 0.00 \pm 0.14 \\ 0.042 \pm 0.062 \\ -0.8 \pm 3.1 \\ -0.15 \pm 0.36 \\ -0.3 \pm 3.8 \\ 1.4 \pm 5.1 \\ -0.35 \pm 0.53 \\ -0.9 \pm 4.4 \\ 0.9 \pm 2.8 \\ 0.33 \pm 0.17 \\ 3 \pm 16 \\ 3.4 \pm 4.9 \\ 2.30 \pm 0.88 \\ -1.3 \pm 1.7 \\ 1.01 \pm 0.38 \\ -0.22 \pm 0.22 \\ 0.20 \pm 0.38 \\ -4.8 \pm 1.6 \\ 1.5 \pm 2.1 \\ 1.5 \pm 2.2 \\ -1.4 \pm 2.2 \\ 3.4 \pm 2.6 \\ 1.5 \pm 1.3 \\ 0 \pm 11 \\ -2.3 \pm 7.2 \\ 1.7 \pm 7.2 \\ -1 \pm 12 \\ -2 \pm 21 \\ 3.0 \pm 2.3 \end{pmatrix} \times 10^{-2}, \quad \begin{pmatrix} [c_{\ell q}^{(3)}]_{1111} \\ [\hat{c}_{eq}]_{1111} \\ [\hat{c}_{\ell u}]_{1111} \\ [\hat{c}_{\ell d}]_{1111} \\ [\hat{c}_{eu}]_{1111} \\ [\hat{c}_{ed}]_{1111} \\ [\hat{c}_{\ell q}^{(3)}]_{1122} \\ [c_{\ell u}]_{1122} \\ [\hat{c}_{\ell d}]_{1122} \\ [c_{eq}]_{1122} \\ [c_{eu}]_{1122} \\ [\hat{c}_{ed}]_{1122} \\ [\hat{c}_{\ell q}^{(3)}]_{1133} \\ [c_{\ell d}]_{1133} \\ [c_{eq}]_{1133} \\ [c_{ed}]_{1133} \\ [c_{\ell q}^{(3)}]_{2211} \\ [c_{\ell q}]_{2211} \\ [c_{\ell u}]_{2211} \\ [c_{\ell d}]_{2211} \\ [\hat{c}_{eq}]_{2211} \\ [c_{\ell equ}]_{1111} \\ [c_{\ell edq}]_{1111} \\ [c_{\ell equ}^{(3)}]_{1111} \\ \epsilon_P^{d\mu}(2\text{ GeV}) \end{pmatrix} = \begin{pmatrix} -2.2 \pm 3.2 \\ 100 \pm 180 \\ -5 \pm 11 \\ -5 \pm 23 \\ -1 \pm 12 \\ -4 \pm 21 \\ -61 \pm 32 \\ 2.4 \pm 8.0 \\ -310 \pm 130 \\ -21 \pm 28 \\ -87 \pm 46 \\ 270 \pm 140 \\ -8.6 \pm 8.0 \\ -1.4 \pm 10 \\ -3.2 \pm 5.1 \\ 18 \pm 20 \\ -1.2 \pm 3.9 \\ 1.3 \pm 7.6 \\ 15 \pm 12 \\ 25 \pm 34 \\ 4 \pm 41 \\ -0.080 \pm 0.075 \\ -0.079 \pm 0.074 \\ -0.02 \pm 0.19 \\ -0.02 \pm 0.15 \end{pmatrix} \times 10^{-2}. \tag{3.8}$$

The correlation matrix is available in the Mathematica notebook attached as a supplemental material to the publication [161].

The model-independent bounds on the vertex corrections are practically the same as the ones

obtained from the pole observables only in Ref. [139]. This is due to the fact that there are more 4-fermion operators than independent off-pole observables. Hence the latter serve to bound 4-fermion Wilson coefficients but cannot further constrain δg. Nevertheless, there are non-zero correlations between the constraints on vertex corrections and 4-fermion operators that are captured by our analysis. It is worth stressing the CKM-unitarity test Δ_{CKM} of equation (3.9), which actually provides stronger one-by-one limits on the vertex corrections $\delta g_L^{Wq_1}$ and $\delta g_L^{W\mu}$ than all pole observables combined.

Furthermore, the low-energy flavour observables provide a percent level bound on the W boson coupling to right-handed light quarks $\delta g_R^{Wq_1}$ [160]. Recall that δg_R^{Wq} are not probed by the pole observables at tree level and $\mathcal{O}(\Lambda^{-2})$ in the SMEFT expansion, therefore the model-independent limit in equation (3.8) (from Ref. [160]) is a new result. It is weaker than the one in equation (3.7) because in the global fit the strong constraints from the CKM-unitarity test of equation (3.9) are diluted by marginalizing over less precisely probed dimension-6 parameters. Nevertheless, the constraint on $\delta g_R^{Wq_1}$ will typically be stronger in specific new physics scenarios, unless they predict that the particular linear combination on the r.h.s of equation (3.9) approximately vanishes at the sub-per-mille level.

The bounds on LLLL operators involving only electrons and/or muons are also similar to the ones previously obtained in Ref. [150], with the exception of $[c_{\ell\ell}]_{2222}$ which is now bound due to the inclusion of neutrino trident production data. For the $ee\tau\tau$ operators the bounds are much stronger thanks to including the VENUS $\tau\tau$ polarization data, which resolves the degeneracies present in the fit of Ref. [150].

Previous global SMEFT analyses targeting LLQQ operators [116, 117, 146] were carried out assuming some simplifying flavour structure, such as the $U(3)^5$ symmetry [116], which greatly reduces the number of independent Wilson coefficients. On the other hand, previous analyses working in a flavour general setup provided 1-by-1 bounds (see e.g. Ref. [122, 129]). Thus, the global bounds applicable for a completely arbitrary flavour structure are obtained for the first time in these two papers, and they represent our main result. They are relevant for a large class of new physics scenarios with or without approximate flavour symmetries. In particular, models addressing various flavour anomalies necessarily do not respect the $U(3)^5$ symmetry, and therefore the global likelihood we obtained may provide new constraints on their parameters.

We find several poorly constrained directions in the space of LLQQ operators. As discussed earlier, $[\hat{c}_{eq}]_{1111}$ is currently constrained only by very imprecise measurements of electron neutrino scattering on nucleons, such that the experiments are insensitive to $[\hat{c}_{eq}]_{1111} \lesssim 1$. More surprisingly, another practically unconstrained direction emerges in our fit, which roughly corresponds to the linear combination $[\hat{c}_{ed} + 0.6\,\hat{c}_{\ell d}]_{1122}$. This can be traced to the fact that the LEP-2 collider was scanning a fairly narrow range of $\sqrt{s}$ in e^+e^- collisions. For this reason, not all theoretically available combinations discussed in section 3.4.2 are resolved in practice. Again, it is should be noted that constraints in typical scenarios generating these

LLQQ operators will be stronger unless the operators accidentally align with the flat directions in our fit. We stress that the global likelihood retains the full information about the correlations.

3.4.5 Flavor-universal limit

The general likelihood presented in section 3.4.4 can be easily restricted to a smaller subspace relevant for any particular scenario. We present here the results for the flavour-universal limit, where dimension-6 operators are invariant under the global flavour symmetry $U(3)^5$. The symmetry implies that 1) all off-diagonal and chirality-violating operators as well as δg_R^{Wq} are absent, 2) the remaining operators do not carry the flavour index. The only subtlety concerns the $[c_{\ell\ell}]_{IJKL}$ coefficients, since two independent contractions of flavour indices are allowed by the $U(3)^5$ symmetry. We follow the common practice of parametrizing them in terms of the two $U(3)^5$-symmetric operators $O_{\ell\ell} \equiv \frac{1}{2}\sum_{I,J}(\bar\ell_I\bar\sigma_\mu\ell_I)(\bar\ell_J\bar\sigma_\mu\ell_J)$ and $O^{(3)}_{\ell\ell} \equiv \frac{1}{2}\sum_{I,J}(\bar\ell_I\sigma^i\bar\sigma_\mu\ell_I)(\bar\ell_J\sigma^i\bar\sigma_\mu\ell_J)$. All in all, with the parameterization of the dimension-6 space used in this paper, the $U(3)^5$ symmetry corresponds to the following pattern:

$$\begin{pmatrix}\delta g_L^{We_J}\\ \delta g_L^{Ze_J}\\ \delta g_R^{Ze_J}\\ \delta g_L^{Zu_J}\\ \delta g_R^{Zu_J}\\ \delta g_L^{Zd_J}\\ \delta g_R^{Zd_J}\end{pmatrix} = \begin{pmatrix}\delta g_L^{We}\\ \delta g_L^{Ze}\\ \delta g_R^{Ze}\\ \delta g_L^{Zu}\\ \delta g_R^{Zu}\\ \delta g_L^{Zd}\\ \delta g_R^{Zd}\end{pmatrix}, \quad \begin{pmatrix}[c_{\ell\ell}]_{JJJJ}\\ [c_{\ell\ell}]_{IJJI}\\ [c_{\ell\ell}]_{IIJJ}\\ [c_{\ell e}]_{IIJJ}\\ [c_{ee}]_{IIJJ}\end{pmatrix} = \begin{pmatrix}c_{\ell\ell}+c^{(3)}_{\ell\ell}\\ 2c^{(3)}_{\ell\ell}\\ c_{\ell\ell}-c^{(3)}_{\ell\ell}\\ c_{\ell e}\\ c_{ee}\end{pmatrix}, \quad \begin{pmatrix}[c^{(3)}_{\ell q}]_{IIJJ}\\ [c_{\ell q}]_{IIJJ}\\ [c_{eq}]_{IIJJ}\\ [c_{\ell u}]_{IIJJ}\\ [c_{\ell d}]_{IIJJ}\\ [c_{eu}]_{IIJJ}\\ [c_{ed}]_{IIJJ}\end{pmatrix} = \begin{pmatrix}c^{(3)}_{\ell q}\\ c_{\ell q}\\ c_{eq}\\ c_{\ell u}\\ c_{\ell d}\\ c_{eu}\\ c_{ed}\end{pmatrix} \tag{3.9}$$

and all the remaining vertex corrections and 4-fermion Wilson coefficients vanish. This setup corresponds to the SMEFT limit studied in the pioneering work of Ref. [116].[14]

It turns out that the global likelihood constrains the entire restricted parameter set introduced in equation (3.9). Thus, unlike in the flavour-generic case, there is no need to define new variables $\hat c$ in order to factor out the flat directions. Marginalizing over $\tilde V_{ud}$, we find the following constraints:

$$\begin{pmatrix}\delta g_L^{We}\\ \delta g_L^{Ze}\\ \delta g_R^{Ze}\\ \delta g_L^{Zu}\\ \delta g_R^{Zu}\\ \delta g_L^{Zd}\\ \delta g_R^{Zd}\end{pmatrix} = \begin{pmatrix}-1.22 \pm 0.81\\ -0.10 \pm 0.21\\ -0.15 \pm 0.23\\ -1.6 \pm 2.0\\ -2.1 \pm 4.1\\ 1.9 \pm 1.4\\ 15 \pm 7\end{pmatrix} \times 10^{-3} \tag{3.10}$$

[14] Let us note that the more recent analysis of Ref. [146] corresponds to a more restricted scenario, since the two independent coefficients $c_{\ell\ell}$ and $c^{(3)}_{\ell\ell}$ are controlled by one single coefficient $C_{\ell\ell}$ in that work.

$$\begin{pmatrix} c_{\ell\ell}^{(3)} \\ c_{\ell\ell} \\ c_{\ell e} \\ c_{ee} \end{pmatrix} = \begin{pmatrix} -3.0 & \pm & 1.7 \\ 7.2 & \pm & 3.3 \\ 0.2 & \pm & 1.3 \\ -2.5 & \pm & 3.0 \end{pmatrix} \times 10^{-3} \quad \begin{pmatrix} c_{\ell q}^{(3)} \\ c_{\ell q} \\ c_{eq} \\ c_{\ell u} \\ c_{\ell d} \\ c_{eu} \\ c_{ed} \end{pmatrix} = \begin{pmatrix} -4.8 & \pm & 2.3 \\ -15.4 & \pm & 9.1 \\ -14 & \pm & 23 \\ 4 & \pm & 24 \\ 6 & \pm & 42 \\ 4 & \pm & 11 \\ 26 & \pm & 18 \end{pmatrix} \times 10^{-3} \tag{3.11}$$

The correlation matrix reads ρ =

$$\begin{pmatrix}
1. & -0.5 & 0.2 & 0.1 & 0.1 & 0. & 0. & 1. & -0.5 & 0. & -0.1 & 0.4 & -0.1 & 0. & 0.1 & 0. & 0.1 & 0. \\
-0.5 & 1. & 0.3 & -0.1 & 0. & -0.2 & -0.2 & -0.5 & 0.2 & 0. & 0.1 & -0.1 & 0.1 & 0. & 0. & 0. & -0.1 & -0.1 \\
0.2 & 0.3 & 1. & 0. & 0. & -0.3 & -0.3 & 0.2 & -0.2 & 0. & 0.1 & 0.3 & 0. & 0.1 & 0.1 & 0.1 & 0. & -0.1 \\
0.1 & -0.1 & 0. & 1. & 0.8 & 0.2 & 0.1 & 0.1 & 0. & 0. & 0. & 0.7 & -0.3 & 0. & 0.1 & 0. & 0.5 & 0.1 \\
0.1 & 0. & 0. & 0.8 & 1. & 0.1 & 0.2 & 0.1 & 0. & 0. & 0. & 0.7 & -0.3 & 0. & 0.1 & 0. & 0.5 & 0.2 \\
0. & -0.2 & -0.3 & 0.2 & 0.1 & 1. & 0.9 & 0. & 0. & 0. & 0. & -0.4 & -0.2 & -0.1 & -0.1 & -0.2 & 0.2 & 0.4 \\
0. & -0.2 & -0.3 & 0.1 & 0.2 & 0.9 & 1. & 0. & 0. & 0. & 0. & -0.5 & -0.2 & -0.1 & -0.1 & -0.2 & 0.2 & 0.4 \\
1. & -0.5 & 0.2 & 0.1 & 0.1 & 0. & 0. & 1. & -0.5 & 0. & -0.1 & 0.4 & -0.1 & 0. & 0.1 & 0. & 0.1 & 0. \\
-0.5 & 0.2 & -0.2 & 0. & 0. & 0. & 0. & -0.5 & 1. & -0.2 & -0.6 & -0.2 & 0. & 0. & 0. & 0. & 0. & 0. \\
0. & 0. & 0. & 0. & 0. & 0. & 0. & 0. & -0.2 & 1. & -0.2 & 0. & 0. & 0. & 0. & 0. & 0. & 0. \\
-0.1 & 0.1 & 0.1 & 0. & 0. & 0. & 0. & -0.1 & -0.6 & -0.2 & 1. & 0. & 0. & 0. & 0. & 0. & 0. & 0. \\
0.4 & -0.1 & 0.3 & 0.7 & 0.7 & -0.4 & -0.5 & 0.4 & -0.2 & 0. & 0. & 1. & -0.1 & 0.1 & 0.2 & 0.1 & 0.3 & -0.1 \\
-0.1 & 0.1 & 0. & -0.3 & -0.3 & -0.2 & -0.2 & -0.1 & 0. & 0. & 0. & -0.1 & 1. & -0.2 & -0.7 & -0.6 & -0.5 & -0.9 \\
0. & 0. & 0.1 & 0. & 0. & -0.1 & -0.1 & 0. & 0. & 0. & 0. & 0.1 & -0.2 & 1. & 0.7 & 0.9 & -0.5 & 0.5 \\
0.1 & 0. & 0.1 & 0.1 & 0.1 & -0.1 & -0.1 & 0.1 & 0. & 0. & 0. & 0.2 & -0.7 & 0.7 & 1. & 0.9 & -0.1 & 0.8 \\
0. & 0. & 0.1 & 0. & 0. & -0.2 & -0.2 & 0. & 0. & 0. & 0. & 0.1 & -0.6 & 0.9 & 0.9 & 1. & -0.2 & 0.7 \\
0.1 & -0.1 & 0. & 0.5 & 0.5 & 0.2 & 0.2 & 0.1 & 0. & 0. & 0. & 0.3 & -0.5 & -0.5 & -0.1 & -0.2 & 1. & 0.3 \\
0. & -0.1 & -0.1 & 0.1 & 0.2 & 0.4 & 0.4 & 0. & 0. & 0. & 0. & -0.1 & -0.9 & 0.5 & 0.8 & 0.7 & 0.3 & 1.
\end{pmatrix} \tag{3.12}$$

where the rows and columns correspond to the ordering of the parameters in equation (3.10) and equation (3.11). The correlation matrix with more significant digits (necessary for practical applications) is given in the Mathematica notebook attached as supplemental material.

Thanks to lifting the exact and approximate flat directions, in the $U(3)^5$ symmetric limit typical constraints on the dimension-6 parameters are at the per-mille level. We note that the vertex corrections are constrained slightly better than when only the pole observables are used [139], thanks to the precise input from low-energy flavour measurements. Most of the LLQQ operators are constrained at the percent level.

Also working in the flavour-universal limit, Ref. [147] obtained bounds on 10 *additional* SMEFT coefficients using Higgs data and WW production at LEP2. The only flavour-universal SMEFT coefficients unconstrained by these two fits are those that are either CP-violating, or contain only quarks, only gluons or only higgses.

3.4.6 Oblique parameters

In the literature, precision constraints on new physics are often quoted in the language of *oblique parameters* S, T, W, Y [118, 219]. These correspond to a further restriction of the

pattern of the dimension-6 parameters in the $U(3)^5$ symmetric case [150, 220]:

$$\begin{aligned}
\delta g_{L/R}^{Zf} &= \alpha \left\{ T^3_{f_{L/R}} \frac{T - W - \frac{g_Y^2}{g_L^2} Y}{2} + Q_f \frac{2g_Y^2 T - (g_L^2+g_Y^2)S + 2g_Y^2 W + \frac{2g_Y^2(2g_L^2-g_Y^2)}{g_L^2} Y}{4(g_L^2-g_Y^2)} \right\} \\
\delta g_L^{We} &= \frac{\alpha}{2(g_L^2-g_Y^2)} \left(-\frac{g_L^2+g_Y^2}{2} S + g_L^2 T - (g_L^2 - 2g_Y^2) W + g_Y^2 Y \right) \\
c_{\ell\ell}^{(3)} &= c_{\ell q}^{(3)} = c_{qq}^{(3)} = -\alpha W \qquad c_{f_1 f_2} = -4 Y_{f_1} Y_{f_2} \frac{g_Y^2}{g_L^2} \alpha Y
\end{aligned} \tag{3.13}$$

where Y_{f_i} is the fermionic hypercharge. With this pattern, all vertex corrections and 4-fermion operators can be redefined away, such that new physics affects only the electroweak gauge boson propagators. Restricting the $U(3)^5$ symmetric likelihood using equation (3.13) we find the following constraints on the oblique parameters:

$$\begin{pmatrix} S \\ T \\ Y \\ W \end{pmatrix} = \begin{pmatrix} -0.10 \pm 0.13 \\ 0.02 \pm 0.08 \\ -0.15 \pm 0.11 \\ -0.01 \pm 0.08 \end{pmatrix}, \qquad \rho = \begin{pmatrix} 1. & 0.86 & 0.70 & -0.12 \\ . & 1. & 0.39 & -0.06 \\ . & . & 1. & -0.49 \\ . & . & . & 1. \end{pmatrix} \tag{3.14}$$

The constraints on the oblique corrections are dominated by the pole-observables and lepton-pair production in LEP-2. The new observables probing LLQQ operators do not affect these constraints significantly. In particular, the low-energy flavour observables do not probe the oblique corrections at all. Compared to the fit in Ref. [150], we only observe a small shift of the central values.[15]

3.5 Comments on LHC reach

Four-fermion LLQQ operators can be probed via the $q\bar{q} \to \ell^+\ell^-$ processes in hadron colliders. Previously several groups set bounds on their Wilson coefficients through the reanalysis within the SMEFT of various ATLAS and CMS exotic searches (see e.g. [129, 221]). In this section we update those bounds using the recently published measurements of the differential Drell-Yan cross sections in the dielectron and dimuon channels [222]. Our main goal here is to present a brief comparison between the sensitivity of the LHC run-1 and of the low-energy observables discussed in this paper.

Precision measurements in hadron collider environments are challenging. Individual observables are typically measured with much worse accuracy than in lepton colliders or very low-energy experiments. However, the effect of 4-fermion operators on scattering amplitudes grows with the collision energy E as $\sim c_{4f} E^2/v^2$. As a consequence, the superior energy reach

[15] The $\mathcal{O}(10\%)$ increase of some errors compared to [150] is due to using different values of the electroweak couplings to evaluate the dimension-6 shifts of the LEP-2 observables.

$(ee)(qq)$

	$[c^{(3)}_{\ell q}]_{1111}$	$[c_{\ell q}]_{1111}$	$[c_{\ell u}]_{1111}$	$[c_{\ell d}]_{1111}$	$[c_{eq}]_{1111}$	$[c_{eu}]_{1111}$	$[c_{ed}]_{1111}$
Low-energy	0.45 ± 0.28	1.6 ± 1.0	2.8 ± 2.1	3.6 ± 2.0	-1.8 ± 1.1	-4.0 ± 2.0	-2.7 ± 2.0
$\text{LHC}_{1.5}$	$-0.70^{+0.66}_{-0.74}$	$2.5^{+1.9}_{-2.5}$	$2.9^{+2.4}_{-2.9}$	$-1.6^{+3.4}_{-3.0}$	$1.6^{+1.8}_{-2.2}$	$1.6^{+2.5}_{-1.5}$	$-3.1^{+3.6}_{-3.0}$
$\text{LHC}_{1.0}$	$-0.84^{+0.85}_{-0.92}$	$3.6^{+3.6}_{-3.7}$	$4.4^{+4.4}_{-4.7}$	$-2.4^{+4.8}_{-4.7}$	$2.4^{+3.0}_{-3.2}$	$1.9^{+2.5}_{-1.9}$	$-4.6^{+5.4}_{-4.1}$
$\text{LHC}_{0.7}$	$-1.0^{+1.4}_{-1.5}$	5.9 ± 7.2	7.4 ± 9.0	-3.6 ± 8.7	3.8 ± 5.9	$2.1^{+3.8}_{-2.9}$	-8 ± 10

$(\mu\mu)(qq)$

	$[c^{(3)}_{\ell q}]_{2211}$	$[c_{\ell q}]_{2211}$	$[c_{\ell u}]_{2211}$	$[c_{\ell d}]_{2211}$	$[c_{eq}]_{2211}$	$[c_{eu}]_{2211}$	$[c_{ed}]_{2211}$
Low-energy	-0.2 ± 1.2	4 ± 21	18 ± 19	-20 ± 37	40 ± 390	-20 ± 190	40 ± 390
$\text{LHC}_{1.5}$	$-1.22^{+0.62}_{-0.70}$	1.8 ± 1.3	2.0 ± 1.6	-1.1 ± 2.0	1.1 ± 1.2	$2.5^{+1.8}_{-1.4}$	-2.2 ± 2.0
$\text{LHC}_{1.0}$	$-0.72^{+0.81}_{-0.87}$	$3.2^{+4.0}_{-3.5}$	$3.9^{+4.8}_{-4.4}$	$-2.3^{+4.9}_{-4.7}$	$2.3^{+3.1}_{-3.2}$	$1.6^{+2.3}_{-1.8}$	-4.4 ± 5.3
$\text{LHC}_{0.7}$	$-0.7^{+1.3}_{-1.4}$	$3.2^{+10.3}_{-4.8}$	$4.3^{+12.5}_{-6.4}$	-3.6 ± 9.0	3.8 ± 6.2	$1.6^{+3.4}_{-2.7}$	-8 ± 11

Chirality-violating operators ($\mu = 1$ TeV)

	$[c_{\ell equ}]_{1111}$	$[c_{\ell edq}]_{1111}$	$[c^{(3)}_{\ell equ}]_{1111}$	$[c_{\ell equ}]_{2211}$	$[c_{\ell edq}]_{2211}$	$[c^{(3)}_{\ell equ}]_{2211}$
Low-energy	$(-0.6 \pm 2.4)10^{-4}$	$(0.6 \pm 2.4)10^{-4}$	$(0.4 \pm 1.4)10^{-3}$	0.014(49)	−0.014(49)	−0.09(29)
$\text{LHC}_{1.5}$	0 ± 2.0	0 ± 2.6	0 ± 0.91	0 ± 1.2	0 ± 1.6	0 ± 0.56
$\text{LHC}_{1.0}$	0 ± 2.9	0 ± 3.7	0 ± 1.4	0 ± 2.9	0 ± 3.7	0 ± 1.4
$\text{LHC}_{0.7}$	0 ± 5.3	0 ± 6.6	0 ± 2.6	0 ± 5.5	0 ± 6.9	0 ± 2.6

Table 3.6 – Comparison of low-energy and LHC constraints (in units of 10^{-3}) on the Wilson coefficients of the chirality-conserving $(ee)(qq)$ and $(\mu\mu)(qq)$ and chirality-violating operators defined at the scale $\mu = 1$ TeV. The 68% CL bounds are derived assuming only one 4-fermion operator is present at a time, and that the vertex corrections and $[c_{\ell\ell}]_{1221}$ are absent. The low-energy constraints combine all experimental input summarized in table 3.4. The $\text{LHC}_{1.5}$ constraints use the $m_{\ell\ell} \in$ [0.5-1.5] TeV bins of the measured differential e^+e^- and $\mu^+\mu^-$ cross sections at the 8 TeV LHC [222]. We also separately show the constraints obtained when the $m_{\ell\ell} \in$ [0.5-1.0] TeV ($\text{LHC}_{1.0}$) and $m_{\ell\ell} \in$ [0.5-0.7] TeV ($\text{LHC}_{0.7}$) data range is used.

of the LHC compensates the inferior precision in this case [129, 221]. This message was recently stressed in Ref. [223] in the context of the determination of the oblique parameters, which encode new physics corrections to propagators of the electroweak gauge bosons. It turns out that the effect of the oblique parameters W and Y [118] on the high invariant-mass tail of $\frac{d\sigma(pp\to\ell^+\ell^-)}{dm_{\ell\ell}}$ also grows with E (as opposed to that of the more familiar S and T parameters [219]). The current LHC constraint on W and Y are already competitive with those obtained from low-energy precision experiments, and will become more accurate with the full run-2 dataset at $\sqrt{s} \approx$ 13-14 TeV [223]. In the SMEFT framework, W and Y correspond to a particular pattern of vertex corrections and 4-fermion operators [150, 220], *cf.* equation (3.13). Therefore we expect that similar arguments apply, and that competitive bounds on the LLQQ operators can be extracted from ATLAS and CMS measurements of $\frac{d\sigma(pp\to\ell^+\ell^-)}{dm_{\ell\ell}}$. Below we present some quantitative illustrations of this message.

In the situation when only one LLQQ operator is present at a time and all other dimension-6 operators are absent, the sensitivity of the LHC run-1 and of the low-energy observables is contrasted in table 3.6. To estimate the LHC reach we use 3 bins in the range $m_{\ell\ell} \in$ [0.5-1.5] TeV of the ATLAS measurement of the differential e^+e^- and $\mu^+\mu^-$ cross sections at the 8 TeV LHC

(20.3 fb^{-1}) [222]. This is shown under the label of LHC$_{1.5}$ constraints in table 3.4, and it is compared to the combined constraints using the low-energy input. For the chirality conserving $(ee)(qq)$ operators the two are indeed similarly sensitive. For the chirality conserving $(\mu\mu)(qq)$ operators the low-energy bounds are relatively weaker, especially for the operators that do not affect the muon neutrino couplings. With the exception of $[O^{(3)}_{\ell q}]_{2211}$ probed by the flavour observables, the LHC sensitivity is superior by at least an order of magnitude. Therefore in these directions in the parameter space of dimension-6 SMEFT the LHC is in a completely uncharted territory. The situation is quite opposite for the chirality-violating $(ee)(qq)$ and $(\mu\mu)(qq)$ operators. There the light quark transitions offer a superior sensitivity with which the LHC cannot compete in most cases. The exception is the $[O^{(3)}_{\ell equ}]_{2211}$ operator where the LHC reach is comparable.

An important difference between the LHC and low-energy constraints should be emphasized. The latter are obtained in the energy regime where it is very plausible to assume the validity of the EFT. Here, by validity we mean that the SMEFT with dimension-6 operators adequately describes the physics of the underlying UV completion. First of all, if such completion contains new states at ~ 1 TeV then clearly the LHC bounds in table 3.6 cannot be applied and a model-dependent approach becomes necessary. This is however not the case for the SMEFT bounds derived from low-energy data in the previous section, which are still valid. On the other hand, even in the absence of such "light" states one should analyze the sensitivity to $\mathcal{O}(\Lambda^{-4})$ terms. The precisely measured low-energy observables are dominated by $\mathcal{O}(\Lambda^{-2})$ contributions of dimension-6 operators, whereas the quadratic terms in the Wilson coefficients, formally $\mathcal{O}(\Lambda^{-4})$, are negligible. In contrast, the one-by-one LHC constraints on 4-fermion operators in table 3.6 have in general a similar sensitivity to linear and quadratic terms.[16] Notice that this problem becomes much more severe in a global fit and that in the particular case of the chirality-violating operators there is no interference at all. This may undermine the SMEFT $1/\Lambda^2$ expansion for generic UV completions, and it is not clear whether the dimension-8 and higher operators can be neglected in the analysis. As discussed in Ref. [224], in such a case the EFT is still valid for strongly coupled UV completions, where the dimension-6 squared terms are parametrically enhanced with respect to the dimension-8 contributions by a large NP coupling. On the other hand, for weakly coupled UV completion one should use weaker LHC bounds obtained by truncating the $\sqrt{s}$ range of the analyzed data at some $M_{\rm cut}$ above which
constraints with $M_{\rm cut} = 1$ TeV (LHC$_{1.0}$) and $M_{\rm cut} = 0.7$ TeV (LHC$_{0.7}$).

Another practical consequence of the quadratic terms domination at the LHC is that the likelihood for the Wilson coefficients is not approximately Gaussian. That means it is not fully characterized by the central values, 1 σ errors, and the correlation matrix, as is the case for the low-energy observables. This makes the presentation of the global fit results more cumbersome.

[16] In fact, in a few LHC$_{0.7}$ entries in table 3.6 there is an additional (not shown) second solution far from the origin.

Last, let us notice that the dilepton-production cross section is also sensitive to SMEFT coefficients that are flavour non-diagonal in the quark bilinear if we go beyond the $V = 1$ approximation at order Λ^{-2}. This was exploited in Ref. [160] to set bounds on the Wilson coefficients of chirality-violating $\ell\ell 21$ operators.

3.6 Conclusion

In this work, we compiled information from a number of experiments sensitive to flavour-conserving LLQQ operators. The main focus is on experiments probing physics well below the weak scale, such as neutrino scattering on nucleon targets, atomic parity violation, parity-violating electron scattering on nuclei, and so on. Information from e^+e^- collisions at the center-of-mass energies around the weak scale is also included. This is combined with previous analyses studying 4-lepton operators and the strength of the Z and W boson couplings to matter. The ensemble of data is interpreted as constraints on heavy new physics encoded in tree-level effects of dimension-6 operators in the SMEFT. The main strength of this analysis is that we allow all independent operators to be simultaneously present with an arbitrary flavour structure. Another novelty is the inclusion of low-energy flavour constraints from pion, neutron, and nuclear decays, recently summarized in Ref. [160]. The leading renormalization group running effects from low energies to the weak scale are taken into account.

We obtain simultaneous constraints on 61 linear combinations of Wilson coefficients in the SMEFT. The results are presented as a multi-dimensional likelihood function, which is provided in a Mathematica notebook attached as supplemental material. The likelihood can easily be projected onto more restricted new physics scenarios. As an illustration, we provide constraints on the SMEFT operators in the $U(3)^5$-symmetric scenario, and on the oblique parameters S, T, W, Y. The likelihood can be used to place limits on masses and couplings in a large class of theories beyond the SM when the mapping between these theories and the SMEFT is known.

Finally, a brief comparison of the sensitivity of low-energy experiments to LLQQ operators with that of the LHC is provided. For many directions in the SMEFT parameters space, dilepton production at the LHC is exploring virgin territories not constrained by previous experiments. This is especially true for the chirality-conserving $2\mu 2q$ operators, where q are light quarks, while for the chirality-conserving $2e2q$ operators the LHC and low-energy probes are similarly sensitive. It would be beneficial to recast the LHC dilepton results in a model-independent form of a global likelihood on the SMEFT Wilson coefficients. We leave this task for future publications.

The SMEFT constraints summarized in these two papers should be improved by current LHC data and future experiments. Measurements of the differential Drell-Yan production cross sections at the LHC run-2 provides a more powerful probe of operators involving the first generation quarks, thanks to the increased center-of-mass energy of the collisions. Progress is imminent on the low-energy front as well, e.g. thanks to more precise measurements of

the weak mixing angle via low-energy scattering of electrons in the Q-weak and MOLLER experiments. We have stressed the importance of probing the SMEFT operators with multiple low- and high-energy observables, which helps to lift flat directions in the global likelihood for the Wilson coefficients. Finally, the existence of poorly constrained directions in the SMEFT parameters space (especially for the operators involving the third generation quarks and leptons) could be an inspiration to design new experiments and observables.

Conclusion

In chapter 1, we studied two WIMP DM models coming from the MSSM. If the current experimental bounds on supersymmetric particles put the MSSM naturalness under pressure, the WIMP scenario is still an attractive DM model. We explored the Sommerfeld enhancement from electroweak interactions, showing that at low velocity, the Sommerfeld factor can grow very large in two cases. The first is when the DM mass M comes close to a resonance value M_*, due to the presence of a zero-energy bound state of the Yukawa potential. The second happens for every mass M but at specific velocity where the DM system has precisely the energy of a Coulombic $\chi^+\chi^-$ bound state.

We showed that for electroweak WIMP, the relic density calculation including Sommerfeld enhancement is independent of the precise value of the mass splitting δm, since at freeze-out $T_F \gg \delta m$. The situation is different however for indirect detection. The DM particles in the DM halo have very low velocity $\beta \sim 10^{-3}$ depending on the celestial body under consideration and the annihilation cross-section receives a large boost from Sommerfeld effect. In the Wino case, the DM mass is close to a resonance, leading to a large cross-section above experimental bounds from HESS. Changing the mass splitting can shift the position of the resonance and bring the cross-section below experimental bounds. In the Higgsino case, there is no such resonance near the relic mass. Coulomb resonances can boost the annihilation cross-section for very specific mass splittings. The effect of changing the Higgsino and Wino mass splittings on the indirect detection signal are shown in figure 1.7 and 1.9.

In chapter 2, we suggested a fixed-target experiment using the positron beam on target that produces muons for a future muon collider. If such a collider is built, then by making minimal changes in the design, adding a shield and a detector further in the beam direction, one can enlarge the physics potential of the machine. The very intense primary beam gives a large luminosity, allowing us to probe very weakly coupled new physics. If a dark particle if produced at the interaction point, it will fly through the shielding and with some probability decay back to SM particles in the detector.

Such weakly interacting long lived particles could be part of a dark sector carrying no SM charges. Then at the renormalizable level, interactions between the dark sector and our sector can only go through the dark photon, the dark Higgs or the HNL. We reviewed the phenomenology and search strategy for the three classes of models.

We studied the expected reach of our experimental proposal in a simplified model of each class. Of course, the limits depend on the details of the concrete model but these simplified models allow us to compare the reach of different experiments. Our results are shown in figure 2.7 for the dark photon case and in figure 2.9 for the HNLs. Except for the dark Higgs, our setup would greatly improve current experimental bounds and is competitive with similar projects such as SHiP. In order to have a better idea of the performances, one needs a more complete study of the detector design, the expected SM background and the shielding needed to reduce it.

In chapter 3, we compiled data from a number of experiments sensitive to flavour-conserving LLQQ and LLLL operators. We focused on low-energy experiments, such as neutrino scattering on nucleon targets, atomic parity violation, parity-violating electron scattering on nuclei, and so on. Measurements from LEP at and above the Z-pole are also included. These measurements are recasted as constraints on heavy new physics encoded in tree-level effects of dimension-6 operators in the SMEFT allowing all independent operators to be simultaneously present with an arbitrary flavour structure. This analysis is valid for a large class of models where new physics is heavy compared to the weak scale and conserves baryon and lepton number. However, one has to assume that dimension-6 operators are not suppressed for some reason and are always dominant compared to dimension-8 operators.

Our result consists in simultaneous constraints on 61 linear combinations of Wilson coefficients in the SMEFT. We see that most four-fermion operators involving the first generation are well constrained by experimental data but the bounds become very poor or non-existent for operators involving only second and third generations. In order to continue in this direction, one could include data from tau hadronic decays [225] and heavy quark decays. This would require a systematic treatment of the CKM matrix in the SMEFT framework, with one posibility suggested in [167]. In any case, the very large number of parameters in the SMEFT with arbitrary flavour structure makes it necessary to include as much experimental data as possible.

In the general case, the number of free parameters in the SMEFT is still much larger than the number of experimental measurements we can include. Our result can be used to test specific ideas or models giving some structure to the Wilson coefficients. One limit we presented is the flavour-symmetric limit with a $U(3)^5$ symmetry. We see that in this case, all vertex corrections, LLLL and LLQQ operators are constrained at the per-mille or percent level. It would be interesting to study the structure of the Wilson coefficients in scenarios relevant for the flavour puzzle and for the B-anomalies and test them with our result.

In this thesis, we have explored different models and directions in the search for BSM physics motivated by DM, naturalness and other problems of the SM. Future experimental progress at the energy frontier, at the intensity frontier and at the cosmology frontier will bring us closer to understanding the long-standing puzzles of the Standard Model.

A DM relic density calculation

The freeze-out mechanism is one of the most popular ways to explain why the DM density in our universe has its measured value. Here we will sketch the DM density evolution and give some order of magnitude estimations relevant for the WIMP case.

In the standard thermal DM scenario, the DM particles are in thermal equilibrium with the SM particles in the early universe. As the universe expands, their number density is given by the Boltzmann equation:

$$\frac{dn}{dt} + 3Hn = -\langle\sigma\beta\rangle_{12}(n^2 - n_{eq}^2) \tag{A.1}$$

where H is the expansion rate of the universe and $\langle\sigma\beta\rangle_{12}$ the thermal average of the annihilation cross-section of DM particles to SM states multiplied by their relative velocity. When the temperature of the universe decreases below the DM mass M, its equilibrium density drops exponentially and the annihilation rate $\Gamma = n\langle\sigma\beta\rangle_{12}$ becomes negligible compared to H. The DM particles are too rare to annihilate and their density is only diluting with the expansion of the universe. The temperature at which the DM particles decouple from the thermal bath is called the freeze-out temperature T_F.

Following the procedure described in [226], the thermal relic abundance of DM is given by:

$$\Omega_{\mathrm{DM}}h^2 = \sqrt{\frac{45}{\pi}}\frac{s_0}{\rho_c}\frac{1}{\sqrt{g_*}M_P}\left[\int_{x_F}^{\infty}\frac{\langle\sigma\beta\rangle_{12}}{x^2}dx\right]^{-1} \tag{A.2}$$

where $s_0 = 2891\,\mathrm{cm}^{-3}$ is the entropy density today, $\rho_c = 1.054\times10^{-5}h^2\,\mathrm{GeV\,cm}^3$ is the critical density of the universe (values taken from [210]), $x_F = \frac{M}{T_F}$ and g_* is the number of degrees of freedom at freeze-out. Since we expect T_F to be around 50 GeV we will take $g_* = 92$ in all the following calculations. The freeze-out temperature is computed recursively with the formula:

$$x_F = \log\left[\frac{5}{4}\sqrt{\frac{45}{8}}\frac{g}{2\pi^3}\frac{MM_P}{\sqrt{g_* x_F}}\langle\sigma\beta\rangle_{T=T_F}\right] \tag{A.3}$$

where g is the number of degrees of freedom of the DM species.

One can often take the non-relativistic limit in the thermal average computation using the Maxwell-Boltzmann distribution:

$$f(\beta_{12}, x) = 4\pi \left(\frac{x}{4\pi}\right)^{\frac{3}{2}} \beta_{12}^2 \exp\left(-\frac{x\beta_{12}^2}{4}\right) \tag{A.4}$$

The annihilation cross section is then expanded in the non-relativistic limit: $\sigma\beta_{12} = a + b\beta_{12}^2 + O(\beta_{12}^4)$. In this case, the thermal average can be computed explicitly and we get:

$$\int_{x_F}^{\infty} \frac{\langle\sigma\beta_{12}\rangle}{x^2} dx = \frac{1}{x_F}\left[a + \frac{3b}{x_F} + O\left(\frac{1}{x_F^2}\right)\right] \tag{A.5}$$

With co-annihilation In the case of co-annihilation where the DM is composed of N species $i = 1, ..., N$ almost degenerate in mass and in thermal equilibrium, one has to replace in the previous paragraph the cross-section σ by the temperature dependent effective annihilation cross-section given by:

$$\sigma_{\text{eff}} = \sum_{i,j}^{N} \sigma_{ij} \frac{g_i g_j}{g_{\text{eff}}} (1+\Delta_i)^{\frac{3}{2}} \left(1+\Delta_j\right)^{\frac{3}{2}} e^{-x(\Delta_i+\Delta_j)} \tag{A.6}$$

where $\sigma_{ij} = \sigma(\text{DM}_i\,\text{DM}_j \to \text{SM})$, $\Delta_i = (M_i - M)/M$ where M is the lightest DM particle mass and

$$g_{\text{eff}} = \sum_{i}^{N} g_i\,(1+\Delta_i)^{\frac{3}{2}}\, e^{-x\Delta_i}$$

In the Wino and Higgsino case, we are always in a regime where $T_F \gg \delta m$ so taking into account the Boltzmann factor gives only a small correction to the case where all DM species are degenerate in mass.

B Details in dark sector calculations

B.1 Weizsäcker-Williams approxinmation

The dark photon is produced in the positron-nucleon interaction by the following process: $e^+(p^\mu) + N(P_i^\mu) \to e^+(p'^\mu) + N(P_f^\mu) + A'(k^\mu)$. The nucleus is a Beryllium nucleus with $Z = 4$ and $A = 9$ of mass denoted M. We follow the derivation in [227]. The cross-section, if one can compute the amplitude, is given by:

$$\begin{aligned} d\sigma_{23} &= \frac{1}{2p}\frac{1}{2M}|\mathscr{M}_{23}|^2 \frac{d^3\mathbf{p}'}{(2\pi^3)2E'}\frac{d^3\mathbf{P}_f}{(2\pi)^3 2E_f}\frac{d^3\mathbf{k}}{(2\pi)^3 2E_k}(2\pi)^4\delta^{(4)}(p+P_i-P_f-p'-k) \\ &= \frac{1}{1024\pi^5}\frac{1}{pME_fE'E_k}|\mathscr{M}_{23}|^2\, d^3\mathbf{p}'\, d^3\mathbf{P}_f\, d^3\mathbf{k}\,\delta^{(4)}(p+P_i-P_f-p'-k) \end{aligned} \tag{B.1}$$

where the sum and average over polarizations is included in the two to three amplitude $\mathscr{M}_{23}$. We first integrate over $d^3\mathbf{p}'$ and trade P_f^μ for the intermediate photon four-vector $q^\mu = P_i^\mu - P_f^\mu$. We then choose spherical coordinates (Q, θ_q, ϕ_q) for $\mathbf{q}$ where the azimuthal direction is taken to be along the vector $\mathbf{v} = \mathbf{k} - \mathbf{p}$:

$$\begin{aligned} d\sigma_{23} &= \frac{1}{1024\pi^5}\frac{1}{pME_fE'E_k}|\mathscr{M}_{23}|^2\, d^3\mathbf{q}\, d^3\mathbf{k}\,\delta(E_0+q^0-E'-E_k) \\ &= \frac{1}{1024\pi^5}\frac{Q^2}{pME_fE'E_k}|\mathscr{M}_{23}|^2\, dQ\, d\cos\theta_q\, d\phi_q\, d^3\mathbf{k}\,\delta(E_0+q^0-E'-E_k) \end{aligned} \tag{B.2}$$

and the δ-function is explicitly given by:

$$\delta\left(E_0 + M - \sqrt{M^2+Q^2} - E_k - \sqrt{v^2+Q^2+2vQ\cos\theta_q + m_e^2}\right) \tag{B.3}$$

(where $v = |\mathbf{v}|$). We can then solve the δ-function for $\cos\theta_q$ and integrate over $d\cos\theta_q$. This gives a factor $\frac{E'}{Qv}$ and sets a range on Q, v and E_k for the solution to exist. We then change

variable to $t = -q^2$ the virtuality of the intermediate photon:

$$t = Q^2 - (q^0)^2 = 2M\left(\sqrt{M^2+Q^2} - M\right) \Rightarrow QdQ = \frac{E_f}{2M}dt \tag{B.4}$$

We are now left with:

$$d\sigma_{23} = \frac{1}{2048\pi^5}\frac{1}{pvM^2E_k}|\mathcal{M}_{23}|^2\, d^3\mathbf{k} \tag{B.5}$$

Finally, we decompose $\mathbf{k}$ in spherical coordinates $(K, \theta_{A'}, \phi_{A'})$ where the azimuthal angle is aligned with the incoming beam direction. Here $\phi_{A'}$ plays no role by cylindrical symmetry so we can integrate over it. Then we cange variable to $x = \frac{E_k}{E_0}$ such that $KdK = E_k E_0 dx$ which gives us our formula:

$$\frac{d\sigma_{23}}{dx\, d\cos\theta_{A'}} = \frac{1}{1024\pi^4}\frac{xE_0^2}{pvM^2}\sqrt{1-\frac{m_{A'}^2}{x^2E_0^2}}\int_{t_{\min}}^{t_{\max}} dt \int_0^{2\pi} d\phi_q\, |\mathcal{M}_{23}|^2 \tag{B.6}$$

In order to finalize our formula, we only need to compute $t_{\min}(x,\theta)$ and $t_{\max}(x,\theta)$ from equation (B.3) and plug in the expression of the amplitude.

We now turn our attention to the two to three amplitude. It can be separated in two pieces, the two to two amplitude $e^+\gamma \to e^+A'$ and the nucleus electromagnetic form factor F^μ linked by the virtual photon propagator:

$$\mathcal{M}_{23} = \mathcal{M}_{22}^\mu \frac{\eta_{\mu\nu}}{t} eF^\nu \tag{B.7}$$

We make a first assumption on the tensor structure of the nucleon form-factor:

$$\sum_{\text{pol}} F^\mu F^\nu = \eta^{\mu\nu} F(t)^2 \tag{B.8}$$

so that our formula becomes:

$$\frac{d\sigma_{23}}{dx\, d\cos\theta_{A'}} = \frac{\alpha}{256\pi^3}\frac{xE_0^2}{pvM^2}\sqrt{1-\frac{m_{A'}^2}{x^2E_0^2}}\int_{t_{\min}}^{t_{\max}} F(t)^2\frac{dt}{t^2}\int_0^{2\pi} d\phi_q\, |\mathcal{M}_{22}|^2 \tag{B.9}$$

Weizsäcker-Williams approximation

The Weizsäcker-Williams approximation relies on the following approximation dtailed in [228]:

$$\frac{1}{8M^2}\int_0^{2\pi}\frac{d\phi_q}{2\pi}|\mathcal{M}_{22}|^2 \approx \frac{t-t_{\min}}{2t_{\min}}|\mathcal{M}_{22}|^2_{t=t\min} \tag{B.10}$$

which simplifies our double-integral to one integral only, interpreted as the photon flux:

$$\frac{d\sigma_{23}}{dx\, d\cos\theta_{A'}} \approx \frac{\alpha\chi}{16\pi^2}\frac{xE_0^2}{pv}\beta_{A'}\frac{|\mathcal{M}_{22}|^2_{t=t\min}}{2t_{\min}} \quad \text{where} \quad \chi(x,\theta_{A'}) = \int_{t_{\min}}^{t_{\max}} F(t)^2\frac{t-t_{\min}}{t^2}dt \tag{B.11}$$

and where we have written $\beta_{A'} = \sqrt{1 - m_{A'}^2/E_k^2}$.

In order to recover the usual Weizsäcker-Williams formula, we introduce the two to two process $e^+(p^\mu) + \gamma(q^\mu) \to e^+(p'^\mu) + A'(k^\mu)$ where the photon is off-shell ($q^2 = -t_{\min}$). The corresponding Mandelstam variables will be denoted s_2, t_2 and u_2. From the PDG, we have the formula:

$$\frac{d\sigma_{22}}{dt_2} = \frac{1}{64\pi s_2}\frac{1}{|\mathbf{p}_{1\text{cm}}|^2}|\mathcal{M}_{22}|^2 = \frac{1}{16\pi}\frac{1}{(s_2 - m_e^2 - m_\gamma^2)^2 - 4m_e^2 m_\gamma^2}|\mathcal{M}_{22}|^2 \tag{B.12}$$

Here, we have considered that the photon had a negative mass given by $m_\gamma^2 = -t_{\min}$. Plugging this into our formula gives:

$$\frac{d\sigma_{23}}{dx\, d\cos\theta_{A'}} \approx \frac{\alpha}{\pi}\chi(x,\theta_{A'})\frac{xE_0^2}{pv}\beta_{A'}\frac{(s_2 - m_e^2 + t_{\min})^2 + 4m_e^2 t_{\min}}{2t_{\min}}\left.\frac{d\sigma_{22}}{dt_2}\right|_{t=t\min} \tag{B.13}$$

The rest is mostly kinematics and phase space. In order to simplify the phase space calculation (B.3), we take the large nucleon mass limit: the intermediate photon energy q^0 is of order $1/M^2$ and can be neglected. Thus the delta-function reduces to:

$$\delta\left(E_0(1-x) - \sqrt{v^2 + Q^2 + 2vQ\cos\theta_q + m_e^2}\right) \tag{B.14}$$

This has a solution in $\cos\theta_q$ only if:

$$-2vQ \leq (1-x)^2E_0^2 - v^2 - Q^2 - m_e^2 \leq 2vQ \tag{B.15}$$

which in turn has a solution in Q only for $1 - x \geq m_e/E_0$. Equation (B.14) fixes the minimum and maximum value of Q:

$$\begin{cases} Q_{\min} = \left|-v + \sqrt{(1-x)^2E_0^2 - m_e^2}\right| \\ Q_{\max} = v + \sqrt{(1-x)^2E_0^2 - m_e^2} \end{cases} \tag{B.16}$$

and we get the bounds of the t integral with $t = Q^2$. The minimum value $Q = Q_{\min}$ is reached when $\cos\theta_q = \pm 1$ so $\theta_q = 0$ or π, which means that the 3-vector $\mathbf{q}$ is collinear with $\mathbf{p} - \mathbf{k}$.

Following [40], we can make further simplifying assumptions: $m_e, m_{A'} \ll E_0$ and $\theta_{A'} \ll 1$ so we keep the leading order in m_e/E_0, $m_{A'}/E_0$ and $\theta_{A'}$. Then the Mandelstam variables for $t = t_{\min}$

simplify to:

$$\begin{aligned} u_2 = (p-k)^2 &\approx -x\theta_{A'}E_0^2 - \frac{1-x}{x}m_{A'}^2 + (1-x)m_e^2 \\ v = |\mathbf{p}-\mathbf{k}|^2 &\approx (1-x)E_0 \\ t_{\min} = Q_{\min}^2 &\approx \frac{\tilde{u}_2^2}{4E_0^2(1-x)^2} \\ s_2 = (p'+k)^2 &\approx \frac{-\tilde{u}_2}{1-x} + m_e^2 \\ t_2 = (p-p')^2 &\approx \frac{\tilde{u}_2 x}{1-x} + m_{A'}^2 \end{aligned} \tag{B.17}$$

where $\tilde{u}_2 = u_2 - m_e^2$. Using these, the prefactor of the total cross-section becomes:

$$\frac{xE_0^2}{pv}\frac{(s_2 - m_e^2 + t_{\min})^2 + 4m_e^2 t_{\min}}{2t_{\min}} = \frac{2x}{1-x}E_0^2 \tag{B.18}$$

so that we reproduce the well-known Weizsäcker-Williams formula:

$$\frac{d\sigma_{23}}{dx\,d\cos\theta_{A'}} \approx \frac{\alpha\chi(x,\theta_{A'})}{\pi}\frac{xE_0^2}{1-x}\beta_{A'}\,2\frac{d\sigma_{22}}{dt_2}\bigg|_{t=t\min} \tag{B.19}$$

In order to be consistent in our approximations, we can simplify $d\sigma_{22}$ using the Mandelstam variables given in equation (B.17). The result is [40]:

$$\frac{d\sigma_{22}}{dt_2} = 2\pi\alpha^2\epsilon^2\frac{1-x}{\tilde{u}_2^2}\left[1 + (1-x)^2 + \frac{2(1-x)^2 m_{A'}^2}{\tilde{u}_2^2}\left(m_{A'}^2 + \frac{\tilde{u}_2 x}{1-x}\right)\right] \tag{B.20}$$

Improved Weizsäcker-Williams approximation

Since most of the events take place at $\theta_{A'}$ close to 0 and x close to 1 where $t_{\min}$ is minimal, we can neglect the x and $\theta_{A'}$ dependence in the photon flux χ. We set $t_{\min}$ to its minimum value (dropping m_e^2 terms) and we set $t_{\max}$ to a constant value [40]:

$$t_{\min} = \left(\frac{m_{A'}^2}{2E_0}\right)^2 \qquad \text{and} \qquad t_{\max} = m_{A'}^2 + m_e^2 \tag{B.21}$$

Therefore, the photon flux χ can be pulled out of the x and $\theta_{A'}$ integral in the full cross-section calculation.

Let us derive an approximate result for the total cross-section. We start with the angular integral and change variable using $d\tilde{u}_2 = 2pk\,d\cos\theta A' \approx 2xE_0^2\,d\cos\theta_{A'}$, integrating $\tilde{u}_2$ from $\tilde{u}_2(\theta_{A'}) = 0 \equiv -u_0$ to the maximum (absolute) value of $\tilde{u}_2$ that we take to be $-\infty$. Then the

cross-section is:

$$\begin{aligned}\frac{d\sigma_{23}}{dx} =& 2\alpha^3\epsilon^2\chi\beta_{A'}\int_{-\infty}^{-u_0} d\tilde{u}_2 \frac{1}{\tilde{u}_2^2}\left[1+(1-x)^2+\frac{2(1-x)^2 m_{A'}^2}{\tilde{u}_2^2}\left(m_{A'}^2+\frac{\tilde{u}_2 x}{1-x}\right)\right] \\ =& 2\alpha^3\epsilon^2\chi\beta_{A'}\left[\frac{1+(1+x)^2}{u_0}-\frac{x(1-x)m_{A'}^2}{u_0^2}+\frac{2(1-x)^2 m_{A'}^4}{3u_0^2}\right]\end{aligned} \tag{B.22}$$

In the limit $m_{A'} \gg m_e$, this reduces to:

$$\frac{d\sigma_{23}}{dx} = \frac{4\alpha^3\epsilon^2\chi\beta_{A'}}{m_{A'}^2}\frac{x}{1-x}\left(1-x+\frac{x^2}{3}\right) \tag{B.23}$$

We see that the differential cross-section diverges as $x \to 1$, divergence cut-off by the electron mass $m_e^2/m_{A'}^2$. According to [40], the appromations break down for $(1-x)E_0 \leq Q$, giving another cut-off $m_{A'}^2/E_0^2$. Integrating over x, and keeping only the diverging part, we get:

$$\sigma_{23} \approx \frac{4\alpha^3\epsilon^2\chi\beta_{A'}}{3m_{A'}^2}\log\left(\frac{1}{1-x_c}\right) \quad \text{with} \quad 1-x_c = \max\left(\frac{m_e^2}{m_{A'}^2}, \frac{m_{A'}^2}{E_0^2}\right) \tag{B.24}$$

In conclusion

There are three layers of approximations we can use. The first one uses the approximations (B.8), (B.10) and (B.14), this is the WW approximation:

$$\boxed{\frac{d\sigma_{23}}{dx\,d\cos\theta_{A'}} \approx \frac{\alpha\chi(x,\theta_{A'})}{16\pi^2}\frac{xE_0^2}{pv}\beta_{A'}\frac{|\mathcal{M}_{22}|^2_{t=t\text{min}}}{2t_{\text{min}}}} \tag{B.25}$$

where we use the full amplitude and t_{min} is given by equation (B.16).

If we take $\theta_{A'}$ and all masses small in front of the beam energy, we use equations (B.17) and we have the usual WW formula:

$$\boxed{\frac{d\sigma_{23}}{dx\,d\cos\theta_{A'}} \approx \frac{\alpha\chi(x,\theta_{A'})}{\pi}\frac{xE_0^2}{1-x}\beta_{A'}\,2\frac{d\sigma_{22}}{dt_2}\bigg|_{t=t\text{min}}} \tag{B.26}$$

where the cross-section is given by the expression (B.20).

Finally, the improved Weizsäcker-Williams approximation consists of neglecting the $\theta_{A'}$ and x dependence of the photon flux χ.

The photon flux

To finish our calculation, we need to evaluate the photon flux $\chi(x,\theta_{A'}) = \int_{t_{\text{min}}}^{t_{\text{max}}} G_2(t)\frac{t-t_{\text{min}}}{t^2}dt$ with $G_2(t) \equiv F(t)^2$ the electric form factor. It is given by a sum of two terms [228], the elastic

form factor

$$G_{2,el}(t) = \left(\frac{a^2 t}{1+a^2 t}\right)^2 \left(\frac{1}{1+t/d}\right)^2 Z^2 \tag{B.27}$$

and the inelastic form factor

$$G_{2,in}(t) = \left(\frac{a'^2 t}{1+a'^2 t}\right)^2 \left(\frac{1+\frac{t}{m_p}(\mu_p^2-1)}{(1+t/d')^4}\right)^2 Z^2 \tag{B.28}$$

where we have $a = 111 Z^{-1/3}/m_e$ (parametrizing electron screening), $d = 0.164\,\text{GeV}^2 A^{-2/3}$, $a' = 773 Z^{-2/3}/m_e$, m_p is the proton mass, $\mu_p = 2.79$ and $d' = 0.71\,\text{GeV}^2$.

B.2 Dark Higgs production from meson decay

B.2.1 Meson decay widths

We compute the width of the decays $B^+ \to K^+ h$ and $K^+ \to \pi^+ h$. We use the following form factors [229]:

$$\langle K^+|\bar{s}_L b_R|B^+\rangle = \frac{1}{2}\frac{m_B^2 - m_K^2}{m_b - m_s} f_0(q^2) \quad \text{where} \quad f_0(q^2) = \frac{0.33}{1-\frac{q^2}{38\,\text{GeV}^2}} \tag{B.29}$$

$$\langle \pi^+|\bar{d}_L s_R|K^+\rangle = \frac{1}{2}\frac{m_K^2 - m_\pi^2}{m_s - m_d} \tag{B.30}$$

and we get

$$\Gamma(B^+ \to K^+ h) = \epsilon^2 \frac{9\alpha_L^3}{8192\pi^2}\frac{m_t^4 m_b^2}{m_W^6}\frac{\left(m_B^2 - m_K^2\right)^2}{(m_b - m_s)^2}\frac{|\vec{p}_h|}{m_B^2}|V_{tb}|^2|V_{ts}|^2 f_0(q^2)^2 \tag{B.31}$$

$$\Gamma(K^+ \to \pi^+ h) = \epsilon^2 \frac{9\alpha_L^3}{8192\pi^2}\frac{m_t^4 m_s^2}{m_W^6}\frac{\left(m_K^2 - m_\pi^2\right)^2}{(m_s - m_d)^2}\frac{|\vec{p}_h|}{m_K^2}|V_{ts}|^2|V_{td}|^2 \tag{B.32}$$

where $|\vec{p}_h|$ is found using two-body kinematics, for example for $B^+ \to K^+ h$ we have:

$$|\vec{p}_h| = \frac{\sqrt{m_B^4 + m_K^4 + m_h^4 - 2m_B^2 m_K^2 - 2m_B^2 m_h^2 - 2m_K^2 m_h^2}}{2m_B}. \tag{B.33}$$

Putting in numbers (especially $m_t = 176.7$ GeV) and using the B^+ and K^+ total width $\Gamma_B = 4.02 \times 10^{-13}$ and $\Gamma_K = 5.32 \times 10^{-17}$ GeV we reproduce the results of [71, 230]:

$$BR(B^+ \to K^+ h) = 0.50\,\epsilon^2 \frac{2|\vec{p}_h|}{m_B}\left(1 - \frac{m_h^2}{38\,\text{GeV}^2}\right)^{-2} \tag{B.34}$$

$$BR(K^+ \to \pi^+ h) = 0.0018\,\epsilon^2 \frac{2|\vec{p}_h|}{m_K} \tag{B.35}$$

(The numerical factor is very sensitive to the top mass, using the top $\overline{\text{MS}}$ mass of 160 GeV, the numerical factors become 0.33 and 0.0012 respectively).

B.2.2 Dark Higgs from two body meson decay

From this, we get the energy and angular distribution of Dark Higgs (neglecting the displacement of kaons before decaying) by the schematical formula:

$$dN_h = \int dE_K\, d\cos\theta_K\, d\phi_K \frac{dN_K}{dE_K d\cos\theta_K d\phi_K} \frac{d\Gamma(K \to h\pi)}{\Gamma_{tot}} \tag{B.36}$$

However, here the width of the Kaon is computed in the lab frame where the Kaon has momentum given by spherical coordinates (p_K, θ_K, ϕ_K). We have:

$$\begin{aligned} d\Gamma =& \frac{|\mathscr{M}|^2}{32\pi^2} \frac{1}{E_K E_h E_\pi} d^3p_h d^3p_\pi \delta^{(4)}(p_K - p_h - p_\pi) \\ =& \frac{|\mathscr{M}|^2}{32\pi^2} \frac{1}{E_K E_h E_\pi} p_h^2\, dp_h\, d\cos\theta\, d\phi\, \delta(E_K - E_h - E_\pi) \\ =& \frac{|\mathscr{M}|^2}{32\pi^2} \frac{p_h}{E_K E_\pi} dE_h\, d\cos\theta\, d\phi\, \delta(E_K - E_h - E_\pi) \end{aligned} \tag{B.37}$$

where the dark higgs has momentum given in spherical coordinates by (p_h, θ, ϕ) and the pion energy is given by:

$$E_\pi = \sqrt{p_K^2 + p_h^2 - 2p_K p_h(\sin\theta_K \sin\theta\cos(\phi_K - \phi) + \cos\theta_K\cos\theta) + m_\pi^2} \tag{B.38}$$

Now we trade the delta function on energies for a delta function on ϕ_K (this is possible only if $\cos(\theta + \theta_K) \leq \frac{2E_K E_h - m_K^2 - m_h^2 + m_\pi^2}{2p_h p_K} \leq \cos(\theta - \theta_K)$ else there is no solution):

$$\delta(E_K - E_h - E_\pi) = \delta(\phi_K - \phi_{K,0}) \frac{E_\pi}{p_h p_K \sin\theta_K \sin\theta \sin(\phi_K - \phi)} \tag{B.39}$$

Now we can plug back in our original formula, do the ϕ_K integral and trade ϕ_K for its expression from solving the equation in the delta function. In fact, we only need $\sin(\phi_K - \phi)$ and $\cos(\phi_K - \phi)$ as function of the parameters of the problem:

$$\begin{aligned} dN_h =& \int dE_K\, d\theta_K\, d\phi_K \frac{dN_K}{dE_K d\theta_K d\phi_K} \frac{d\Gamma(K \to h\pi)}{\Gamma_{tot}} \\ =& \int dE_K\, d\theta_K \frac{dN_K}{dE_K d\theta_K d\phi_K} \frac{|\mathscr{M}|^2}{\Gamma_{tot}} \frac{1}{32\pi^2} \frac{1}{E_K p_K \sin\theta_K \sin\theta \sin(\phi_K - \phi)} dE_h\, d\cos\theta\, d\phi \\ =& \int dE_K\, d\theta_K \frac{dN_K}{dE_K d\theta_K d\phi_K} \frac{|\mathscr{M}|^2}{\Gamma_{tot}} \frac{1}{32\pi^2} \frac{1}{E_K p_K u(E_K, E_h, \theta_K, \theta_h)} dE_h\, d\cos\theta\, d\phi \end{aligned}$$

where u is the following expression (comes from the delta function):

$$u(E_K,E_h,\theta_K,\theta_h) = \sqrt{\sin^2\theta_K\sin^2\theta - \left(\frac{2E_KE_h - m_K^2 - m_h^2 + m_\pi^2}{2p_hp_K} - \cos\theta_K\cos\theta\right)^2} \tag{B.40}$$

The precise value of $\phi_{K,0}$ is irrelevant because dN_K does not depend on ϕ_K. Thus all dependence on ϕ dissapears (as expected from the symmetries of the problem) and we can integrate over $d\phi$:

$$\frac{dN_h}{dE_h\,d\cos\theta} = \int dE_K\,d\theta_K \frac{dN_K}{dE_K d\theta_K}\frac{|\mathscr{M}|^2}{\Gamma_{tot}}\frac{1}{32\pi^2}\frac{1}{E_Kp_Ku(E_K,E_h,\theta_K,\theta_h)} \tag{B.41}$$

The last step is to work out the translation of the condition $\cos(\theta+\theta_K) \leq \frac{2E_KE_h-m_K^2-m_h^2+m_\pi^2}{2p_hp_K} \leq \cos(\theta-\theta_K)$ to bounds on the E_K,θ_K integral. First, we work out the condition on θ_K then the condition on E_K. We define:

$$E_{\min}(E_h) = \frac{E_h(m_K^2+m_h^2-m_\pi^2) - p_h\sqrt{m_K^4+m_h^4+m_\pi^4-2m_K^2m_h^2-2m_K^2m_\pi^2-2m_h^2m_\pi^2}}{2m_h^2}$$

$$E_{\max}(E_h) = \frac{E_h(m_K^2+m_h^2-m_\pi^2) + p_h\sqrt{m_K^4+m_h^4+m_\pi^4-2m_K^2m_h^2-2m_K^2m_\pi^2-2m_h^2m_\pi^2}}{2m_h^2}$$

$$v(E_K,E_h) = \frac{2E_KE_h - m_K^2 - m_h^2 + m_\pi^2}{2\sqrt{E_h^2-m_h^2}\sqrt{E_K^2-m_K^2}}$$

$$\theta_{\min}(E_K,E_h,\theta) = \max(\arccos v - \theta, \theta - \arccos v)$$

$$\theta_{\max}(E_K,E_h,\theta) = \min(\theta + \arccos v, 2\pi - \arccos v - \theta)$$

Finally, we have by Lorentz dilatation that $\Gamma_{tot} = \frac{1}{\gamma}\Gamma_0$ with Γ_0 the total width in the rest frame. So our final formula is:

$$\frac{dN_h}{dE_h\,d\cos\theta} = \int_{E_{\min}}^{E_{\max}} dE_K \int_{\theta_{\min}}^{\theta_{\max}} d\theta_K \frac{dN_K}{dE_K d\theta_K}\frac{|\mathscr{M}|^2}{32\pi^2 m_K\Gamma_0}\frac{1}{p_Ku(E_K,E_h,\theta_K,\theta_h)} \tag{B.42}$$

Number of events

Putting all together, the number of events in the detector is given by the four-fold integral:

$$N_h = \int_0^{\theta_A} d\theta \int dE \int_{E_{\min}}^{E_{\max}} dE_K \int_{\theta_{\min}}^{\theta_{\max}} d\theta_K\, A\cdot B\cdot C\cdot D \tag{B.43}$$

where

- A is the distribution of Kaons given by GiBUU

$$A = \frac{dN_K}{dE_K d\theta_K} \tag{B.44}$$

- B is the decay rate computed before

$$B = \frac{|\mathscr{M}|^2}{16\pi m_K \Gamma_0} = 0.0018\epsilon^2 \tag{B.45}$$

- C is a factor coming from boosting the angular distribution from the Kaon rest frame

$$C = \frac{1}{2\pi} \frac{\sin\theta}{p_K\, u(E_K, E_h, \theta_K, \theta)} \tag{B.46}$$

- D describes the propagation and decay of the dark higgs in the detector

$$D = \left(1 - e^{-\frac{m_h L}{Ec\tau}}\right) e^{-\frac{m_h d}{Ec\tau}} \tag{B.47}$$

  and can be refined by having d, L depend on θ.

Note that this formula, if correct, neglects the fight of the Kaons before decaying and considers that all dark higgses are produced at the interaction point. This should not be too problematic because we consider only kaons decaying before the shielding, not too far from the interaction point.

B.3 HNL decay

We collect here the expressions for various HNL decay channels [79, 82].

The fully leptonic decays include the decay to 3 neutrinos:

$$\Gamma\left(N \to \sum_{i,j} \nu_i \bar{\nu}_j \nu_j\right) = \frac{G_F^2 M_N^5}{192\pi^3} \times \sum_i |U_i|^2 \tag{B.48}$$

and to one neutrino and two different leptons ($i \neq j$):

$$\Gamma\left(N \to \ell_i^- \ell_j^+ \nu_j\right) = |U_i|^2 \times \frac{G_F^2 M_N^5}{192\pi^3} \left(1 - 8x^2 + 8x^6 - x^8 - 12x^4 \log x^2\right) \tag{B.49}$$

with $x = m_\ell^2 / M_N^2$ where m_ℓ is the heaviest lepton. The decay to one neutrino and a lepton pair is more complicated:

$$\begin{aligned}\Gamma\left(N \to \nu_i \ell_j^- \ell_j^+\right) = |U_i|^2 \times \frac{G_F^2 M_N^5}{192\pi^3} \Big[&\left(C_1(1-\delta_{ij}) + C_3\delta_{ij}\right)\left((1 - 14x^2 - 2x^4 - 12x^6)\sqrt{1-4x^2} + 12x^4(x^4-1)L\right) \\ &+ 4\left(C_2(1-\delta_{ij}) + C_4\delta_{ij}\right)\left((2 + 10x^2 - 12x^4)x^2\sqrt{1-4x^2} + 6x^4(1 - 2x^2 + 2x^4)L\right)\Big]\end{aligned}$$

where

$$L = \log\left[\frac{1-3x^2-(1-x^2)\sqrt{1-4x^2}}{x^2(1+\sqrt{1-4x^2})}\right] \qquad \text{and} \qquad x = \frac{m_\ell^2}{M_N^2} \tag{B.50}$$

and

$$C_1 = \frac{1}{4}(1-4s_W^2+8s_W^4) \quad C_2 = \frac{1}{2}(2s_W^2-1) \quad C_3 = \frac{1}{4}(1+4s_W^2+8s_W^4) \quad C_4 = \frac{1}{2}(2s_W^2+1) \tag{B.51}$$

Two-body decay modes involving mesons are:

$$\Gamma\left(N \to \pi^0 \nu_i\right) = |U_i|^2 \times \frac{G_F^2 f_\pi^2 M_N^3}{32\pi}\left(1-\frac{m_\pi^2}{M_N^2}\right) \tag{B.52}$$

and the same formula holds for η and η' with the corresponding decay constant. The decay to a charged pseudoscalar meson h is:

$$\begin{aligned}\Gamma\left(N \to h^+ \ell_i^-\right) =& |U_i|^2 \times \frac{G_F^2 f_h^2 M_N^3}{16\pi}|V_h|^2 \left[\left(1-\frac{m_\ell^2}{M_N^2}\right)^2 - \frac{m_h^2}{M_N^2}\left(1+\frac{m_\ell^2}{M_N^2}\right)\right] \\ &\times \sqrt{\left(1-\frac{(m_h-m_\ell)^2}{M_N^2}\right)\left(1-\frac{(m_h+m_\ell)^2}{M_N^2}\right)}\end{aligned} \tag{B.53}$$

The decay to a charged ρ meson:

$$\begin{aligned}\Gamma\left(N \to \rho^+ \ell_i^-\right) =& |U_i|^2 \times \frac{G_F^2 g_\rho^2 M_N^3}{16\pi m_\rho^2}|V_{ud}|^2 \left[\left(1-\frac{m_\ell^2}{M_N^2}\right)^2 + \frac{m_\rho^2}{M_N^2}\left(1+\frac{m_\ell^2-2m_\rho^2}{M_N^2}\right)\right] \\ &\times \sqrt{\left(1-\frac{(m_\rho-m_\ell)^2}{M_N^2}\right)\left(1-\frac{(m_\rho+m_\ell)^2}{M_N^2}\right)}\end{aligned} \tag{B.54}$$

and the decay to a neutral ρ meson reads:

$$\Gamma\left(N \to \rho^0 \nu_i\right) = |U_i|^2 \times \frac{G_F^2 M_N^3}{16\pi}\frac{g_\rho^2}{m_\rho^2}\left(1+2\frac{m_\rho^2}{M_N^2}\right)\left(1-\frac{m_\rho^2}{M_N^2}\right)^2 \tag{B.55}$$

C Warsaw basis and more general approach to flavour observables

C.1 Translation to Warsaw Basis

In this work, we parametrize the relevant part of the space of dimension-6 operators using an independent set of vertex corrections δg and Wilson coefficients of 4-fermion operators. The latter are directly inherited from the Warsaw basis, such that the translation is trivial. The former are related to the Wilson coefficients of dimension-6 operators in the Warsaw basis by the following linear transformation:

$$\begin{aligned}
\delta g_L^{We} &= c_{H\ell}^{(3)} + f(1/2,0) - f(-1/2,-1) \\
\delta g_L^{Ze} &= -\frac{1}{2}c_{H\ell}^{(3)} - \frac{1}{2}c_{H\ell} + f(-1/2,-1) \\
\delta g_R^{Ze} &= -\frac{1}{2}c_{He} + f(0,-1) \\
\delta g_R^{Wq} &= -\frac{1}{2}c_{Hud} \\
\delta g_L^{Zu} &= \frac{1}{2}c_{Hq}^{(3)} - \frac{1}{2}c_{Hq} + f(1/2,2/3) \\
\delta g_L^{Zd} &= -\frac{1}{2}V^\dagger c_{Hq}^{(3)} V - \frac{1}{2}V^\dagger c_{Hq} V + f(-1/2,-1/3) \\
\delta g_R^{Zu} &= -\frac{1}{2}c_{Hu} + f(0,2/3) \\
\delta g_R^{Zd} &= -\frac{1}{2}c_{Hd} + f(0,-1/3)
\end{aligned} \tag{C.1}$$

where

$$\begin{aligned}
f(T^3,Q) &= -I_3 Q \frac{g_L g_Y}{g_L^2 - g_Y^2} c_{HWB} \\
&+ I_3 \left(\frac{1}{4}[c_{\ell\ell}]_{1221} - \frac{1}{2}[c_{H\ell}^{(3)}]_{11} - \frac{1}{2}[c_{H\ell}^{(3)}]_{22} - \frac{1}{4}c_{HD}\right)\left(T^3 + Q\frac{g_Y^2}{g_L^2 - g_Y^2}\right)
\end{aligned} \tag{C.2}$$

and I_3 is the 3×3 identity matrix in the generation space. Using (C.1) one can easily recast the results of this paper as a likelihood for the Wilson coefficients in the Warsaw basis. See Ref. [164] for the dictionary between δg and the Wilson coefficients in the SILH basis.

C.2 More general approach to low-energy flavour observables

The low-energy flavour observables discussed in Ref. [160] also probe precisely 4-fermion operators with a strange quark. In the framework of the SMEFT the corresponding observables receive contributions from flavour off-diagonal dimension-6 operators, and in this paper we marginalized our likelihood over them. We also approximated the CKM matrix as $V=1$ when acting on $\mathcal{O}(\Lambda^{-2})$ terms in the Lagrangian. For completeness, in this appendix we provide the formalism that allows one to take into account the constraints from strange observables and retrieve the terms suppressed by off-diagonal elements of the CKM matrix. First, the effective low-energy Lagrangian in (3.7) is generalized to

$$\begin{aligned}\mathscr{L}_{\rm eff} \supset & -\sum_{I,J=1,2}\frac{2\tilde{V}_{uI}}{v^2}\Big[\Big(1+\epsilon_L^{d_Ie_J}\Big)(e_J^\dagger\bar{\sigma}_\mu\nu_J)(u^\dagger\bar{\sigma}^\mu d_I)+\epsilon_R^{d_Ie}(e_J^\dagger\bar{\sigma}_\mu\nu_J)(\bar{u}\sigma^\mu\bar{d}_I^\dagger)\\ & +\frac{\epsilon_S^{d_Ie_J}+\epsilon_P^{d_Ie_J}}{2}(\bar{e}_J\nu_J)(\bar{u}d_I)+\frac{\epsilon_S^{d_Ie_J}-\epsilon_P^{d_Ie_J}}{2}(\bar{e}_J\nu_J)(u^\dagger\bar{d}_I^\dagger)\\ & +\epsilon_T^{d_Ie_J}(\bar{e}_J\sigma_{\mu\nu}\nu_J)(\bar{u}\sigma_{\mu\nu}d_I)+c.c.\Big]\end{aligned} \tag{C.3}$$

such that it also includes charged currents with the strange quark ($s\to u\ell\nu_\ell$). At tree level, the low-energy parameters are related to the SMEFT parameters as

$$\begin{aligned}\epsilon_R^{de}=-\epsilon_L^{de} &= \frac{1}{V_{ud}}\delta g_R^{Wq_1}\\ \epsilon_R^{se}=-\epsilon_L^{se} &= \frac{1}{V_{us}}[\delta g_R^{Wq}]_{12}\\ \epsilon_L^{d\mu} &= -\frac{1}{V_{ud}}\delta g_R^{Wq_1}+\delta g_L^{W\mu}-\delta g_L^{We}+\Big([c_{lq}^{(3)}]_{111J}-[c_{lq}^{(3)}]_{221J}\Big)\frac{V_{Jd}}{V_{ud}}\\ \epsilon_L^{s\mu} &= -\frac{1}{V_{us}}[\delta g_R^{Wq}]_{12}+\delta g_L^{W\mu}-\delta g_L^{We}+\Big([c_{lq}^{(3)}]_{111J}-[c_{lq}^{(3)}]_{221J}\Big)\frac{V_{Js}}{V_{us}}\end{aligned} \tag{C.4}$$

$$
\begin{aligned}
\epsilon_S^{de_J} &= -\frac{1}{2V_{ud}}\left(V_{Kd}[c_{lequ}]^*_{JJK1} + [c_{ledq}]^*_{JJ11}\right) \\
\epsilon_P^{de_J} &= -\frac{1}{2V_{ud}}\left(V_{Kd}[c_{lequ}]^*_{JJK1} - [c_{ledq}]^*_{JJ11}\right) \\
\epsilon_S^{se_J} &= -\frac{1}{2V_{us}}\left(V_{Ks}[c_{lequ}]^*_{JJK1} + [c_{ledq}]^*_{JJ12}\right) \\
\epsilon_P^{se_J} &= -\frac{1}{2V_{us}}\left(V_{Ks}[c_{lequ}]^*_{JJK1} - [c_{ledq}]^*_{JJ12}\right) \\
\epsilon_T^{de_J} &= -\frac{V_{Kd}}{2V_{ud}}[c^{(3)}_{lequ}]^*_{JJK1} \\
\epsilon_T^{se_J} &= -\frac{V_{Ks}}{2V_{us}}[c^{(3)}_{lequ}]^*_{JJK1}
\end{aligned}
\tag{C.5}
$$

In addition to $\tilde{V}_{ud}$ we also introduce the the rescaled CKM matrix element parameter $\tilde{V}_{us}$. Both are distinct from the elements of the unitary matrix V, to which they are related by $V_{ud} = \tilde{V}_{ud}(1+\delta V_{ud})$, $V_{us} = \tilde{V}_{us}(1+\delta V_{us})$, where

$$
\begin{aligned}
\delta V_{ud} &= -\frac{1}{V_{ud}}\delta g_L^{Wq_1} - \frac{1}{V_{ud}}\delta g_R^{Wq_1} + \delta g_L^{W\mu} - \frac{1}{2}[c_{\ell\ell}]_{1221} + [c^{(3)}_{lq}]_{111J}\frac{V_{Jd}}{V_{ud}} \\
\delta V_{us} &= -\frac{1}{V_{us}}[\delta g_L^{Wq}]_{12} - \frac{1}{V_{us}}[\delta g_R^{Wq}]_{12} + \delta g_L^{W\mu} - \frac{1}{2}[c_{\ell\ell}]_{1221} + [c^{(3)}_{lq}]_{111J}\frac{V_{Js}}{V_{us}}
\end{aligned}
\tag{C.6}
$$

The purpose of this rescaling is to impose the relation $\epsilon_L^{d_I e} = -\epsilon_R^{d_I e}$ in (C.3). After the rescaling, $\tilde{V}_{ud}$ and $\tilde{V}_{us}$ are no longer related by the standard unitarity equation. In the limit where the mixing with the 3rd generation is neglected we have $|\tilde{V}_{ud}|^2 + |\tilde{V}_{us}|^2 = 1 + \Delta_{\rm CKM}$, where

$$
\begin{aligned}
\Delta_{\rm CKM} &= -2V_{ud}\delta V_{ud} - 2V_{us}\delta V_{us} \\
&= 2V_{ud}\left(\delta g_L^{Wq_1} + \delta g_R^{Wq_1} - [c^{(3)}_{lq}]_{111J}V_{Jd}\right) + 2V_{us}\left([\delta g_L^{Wq}]_{12} + [\delta g_R^{Wq}]_{12} - [c^{(3)}_{lq}]_{111J}V_{Js}\right) \\
&\quad -2\delta g_L^{W\mu} + [c_{\ell\ell}]_{1221}
\end{aligned}
\tag{C.7}
$$

As before, $\tilde{V}_{ud}$ may be affected by new physics contributing to ϵ_S^{de} and should be treated as a free parameter in the fit. Ref. [160] obtained the following constraints on the low-energy

parameters

$$\begin{pmatrix} \tilde{V}^e_{ud} \\ \Delta_{\rm CKM} \\ \Delta^s_L \\ \Delta^d_{LP} \\ \epsilon^{de}_P \\ \epsilon^{de}_R \\ \epsilon^{se}_P \\ \epsilon^{s\mu}_P \\ \epsilon^{s}_R \\ \epsilon^{s\mu}_S \\ \epsilon^{s\mu}_T \\ \epsilon^{de}_S \\ \epsilon^{de}_T \\ \epsilon^{se}_S \\ \epsilon^{se}_T \end{pmatrix} = \begin{pmatrix} 0.97451 \pm 0.00038 \\ -1.2 \pm 8.4 \\ 1.0 \pm 2.5 \\ 1.9 \pm 3.8 \\ 4.0 \pm 7.8 \\ -1.3 \pm 1.7 \\ -0.4 \pm 2.1 \\ -0.7 \pm 4.3 \\ 0.1 \pm 5.0 \\ -3.9 \pm 4.9 \\ 0.5 \pm 5.2 \\ 1.4 \pm 1.3 \\ 1.0 \pm 8.0 \\ -1.6 \pm 3.3 \\ 0.9 \pm 1.8 \end{pmatrix} \times 10^{\wedge} \begin{pmatrix} 0 \\ -4 \\ -3 \\ -2 \\ -6 \\ -2 \\ -5 \\ -3 \\ -2 \\ -4 \\ -3 \\ -3 \\ -4 \\ -3 \\ -2 \end{pmatrix} \tag{C.8}$$

in the $\overline{MS}$ scheme at $\mu = 2$ GeV. Here $\Delta^s_L = \epsilon^{s\mu}_L - \epsilon^{se}_L$ and $\Delta^d_{LP} \approx \epsilon^{de}_L - \epsilon^{d\mu}_L + 24\epsilon^{d\mu}_P$. The associated correlation matrix is given in Ref. [160]. We note that some entries in this matrix are very close to one, so it is crucial to take it into account.

Bibliography

[1] S. Weinberg, *Varieties of Baryon and Lepton Nonconservation*, *Phys. Rev.* **D22** (1980) 1694.

[2] **Super-Kamiokande** Collaboration, K. Abe et al., *Search for proton decay via $p \to e^+\pi^0$ and $p \to \mu^+\pi^0$ in 0.31 megaton-years exposure of the Super-Kamiokande water Cherenkov detector*, *Phys. Rev.* **D95** (2017), no. 1 012004, [arXiv:1610.03597].

[3] G. Isidori, Y. Nir, and G. Perez, *Flavor Physics Constraints for Physics Beyond the Standard Model*, *Ann. Rev. Nucl. Part. Sci.* **60** (2010) 355, [arXiv:1002.0900].

[4] P. W. Graham, D. E. Kaplan, and S. Rajendran, *Cosmological Relaxation of the Electroweak Scale*, *Phys. Rev. Lett.* **115** (2015), no. 22 221801, [arXiv:1504.07551].

[5] N. Arkani-Hamed, T. Cohen, R. T. D'Agnolo, A. Hook, H. D. Kim, and D. Pinner, *Solving the Hierarchy Problem at Reheating with a Large Number of Degrees of Freedom*, *Phys. Rev. Lett.* **117** (2016), no. 25 251801, [arXiv:1607.06821].

[6] **ATLAS, CMS, LHCb** Collaboration, E. Graverini, *Flavour anomalies: a review*, *J. Phys. Conf. Ser.* **1137** (2019), no. 1 012025, [arXiv:1807.11373].

[7] **Planck** Collaboration, N. Aghanim et al., *Planck 2018 results. VI. Cosmological parameters*, arXiv:1807.06209.

[8] R. Mahbubani and K. Mimouni, *Boosting the dark matter signal with Coulomb resonances*, arXiv:1903.00013.

[9] A. Sommerfeld, *Uber die beugung und bremsung der elektronen*, *Ann. Phys.* **11** (1931) 257.

[10] N. Arkani-Hamed, D. P. Finkbeiner, T. R. Slatyer, and N. Weiner, *A Theory of Dark Matter*, *Phys. Rev.* **D79** (2009) 015014, [arXiv:0810.0713].

[11] J. Hisano, S. Matsumoto, M. Nagai, O. Saito, and M. Senami, *Non-perturbative effect on thermal relic abundance of dark matter*, *Phys. Lett.* **B646** (2007) 34–38, [hep-ph/0610249].

[12] R. Iengo, *Sommerfeld enhancement: General results from field theory diagrams*, *JHEP* **05** (2009) 024, [arXiv:0902.0688].

[13] M. Beneke, C. Hellmann, and P. Ruiz-Femenia, *Non-relativistic pair annihilation of nearly mass degenerate neutralinos and charginos III. Computation of the Sommerfeld enhancements*, *JHEP* **05** (2015) 115, [arXiv:1411.6924].

[14] T. R. Slatyer, *The Sommerfeld enhancement for dark matter with an excited state*, *JCAP* **1002** (2010) 028, [arXiv:0910.5713].

[15] A. Mitridate, M. Redi, J. Smirnov, and A. Strumia, *Cosmological Implications of Dark Matter Bound States*, *JCAP* **1705** (2017), no. 05 006, [arXiv:1702.01141].

[16] S. Cassel, *Sommerfeld factor for arbitrary partial wave processes*, *J. Phys.* **G37** (2010) 105009, [arXiv:0903.5307].

[17] M. Cirelli, P. Panci, K. Petraki, F. Sala, and M. Taoso, *Dark Matter's secret liaisons: phenomenology of a dark U(1) sector with bound states*, *JCAP* **1705** (2017), no. 05 036, [arXiv:1612.07295].

[18] P. Asadi, M. Baumgart, P. J. Fitzpatrick, E. Krupczak, and T. R. Slatyer, *Capture and Decay of Electroweak WIMPonium*, *JCAP* **1702** (2017), no. 02 005, [arXiv:1610.07617].

[19] E. Braaten, E. Johnson, and H. Zhang, *Zero-range effective field theory for resonant wino dark matter. Part III. Annihilation effects*, *JHEP* **05** (2018) 062, [arXiv:1712.07142].

[20] A. Bhattacharya and T. R. Slatyer, *Bound States of Pseudo-Dirac Dark Matter*, arXiv:1812.03169.

[21] M. F. Sohnius, *Introducing Supersymmetry*, *Phys. Rept.* **128** (1985) 39–204.

[22] S. P. Martin, *A Supersymmetry primer*, hep-ph/9709356. [Adv. Ser. Direct. High Energy Phys.18,1(1998)].

[23] S. D. Thomas and J. D. Wells, *Phenomenology of Massive Vectorlike Doublet Leptons*, *Phys. Rev. Lett.* **81** (1998) 34–37, [hep-ph/9804359].

[24] M. Cirelli, N. Fornengo, and A. Strumia, *Minimal dark matter*, *Nucl. Phys.* **B753** (2006) 178–194, [hep-ph/0512090].

[25] M. Cirelli, A. Strumia, and M. Tamburini, *Cosmology and Astrophysics of Minimal Dark Matter*, *Nucl. Phys.* **B787** (2007) 152–175, [arXiv:0706.4071].

[26] **XENON** Collaboration, E. Aprile et al., *Dark Matter Search Results from a One Ton-Year Exposure of XENON1T*, *Phys. Rev. Lett.* **121** (2018), no. 11 111302, [arXiv:1805.12562].

[27] J. Bramante, P. J. Fox, G. D. Kribs, and A. Martin, *Inelastic frontier: Discovering dark matter at high recoil energy*, *Phys. Rev.* **D94** (2016), no. 11 115026, [arXiv:1608.02662].

[28] E. J. Chun, J.-C. Park, and S. Scopel, *Non-perturbative Effect and PAMELA Limit on Electro-Weak Dark Matter*, *JCAP* **1212** (2012) 022, [arXiv:1210.6104].

[29] M. Cirelli, T. Hambye, P. Panci, F. Sala, and M. Taoso, *Gamma ray tests of Minimal Dark Matter*, *JCAP* **1510** (2015), no. 10 026, [arXiv:1507.05519].

[30] R. Krall and M. Reece, *Last Electroweak WIMP Standing: Pseudo-Dirac Higgsino Status and Compact Stars as Future Probes*, *Chin. Phys.* **C42** (2018), no. 4 043105, [arXiv:1705.04843].

[31] **H.E.S.S.** Collaboration, H. Abdallah et al., *Search for dark matter annihilations towards the inner Galactic halo from 10 years of observations with H.E.S.S*, *Phys. Rev. Lett.* **117** (2016), no. 11 111301, [arXiv:1607.08142].

[32] **ATLAS** Collaboration, G. Aad et al., *Search for charginos nearly mass degenerate with the lightest neutralino based on a disappearing-track signature in pp collisions at* $\sqrt{(}s) = 8$ *TeV with the ATLAS detector*, *Phys. Rev.* **D88** (2013), no. 11 112006, [arXiv:1310.3675].

[33] S. Nussinov, L.-T. Wang, and I. Yavin, *Capture of Inelastic Dark Matter in the Sun*, *JCAP* **0908** (2009) 037, [arXiv:0905.1333].

[34] S. Alekhin et al., *A facility to Search for Hidden Particles at the CERN SPS: the SHiP physics case*, *Rept. Prog. Phys.* **79** (2016), no. 12 124201, [arXiv:1504.04855].

[35] J. L. Feng, I. Galon, F. Kling, and S. Trojanowski, *ForwArd Search ExpeRiment at the LHC*, *Phys. Rev.* **D97** (2018), no. 3 035001, [arXiv:1708.09389].

[36] V. V. Gligorov, S. Knapen, M. Papucci, and D. J. Robinson, *Searching for Long-lived Particles: A Compact Detector for Exotics at LHCb*, *Phys. Rev.* **D97** (2018), no. 1 015023, [arXiv:1708.09395].

[37] J. A. Evans, *Detecting Hidden Particles with MATHUSLA*, *Phys. Rev.* **D97** (2018), no. 5 055046, [arXiv:1708.08503].

[38] M. Pospelov, A. Ritz, and M. B. Voloshin, *Bosonic super-WIMPs as keV-scale dark matter*, *Phys. Rev.* **D78** (2008) 115012, [arXiv:0807.3279].

[39] S. D. McDermott, H. H. Patel, and H. Ramani, *Dark Photon Decay Beyond The Euler-Heisenberg Limit*, *Phys. Rev.* **D97** (2018), no. 7 073005, [arXiv:1705.00619].

[40] J. D. Bjorken, R. Essig, P. Schuster, and N. Toro, *New Fixed-Target Experiments to Search for Dark Gauge Forces*, *Phys. Rev.* **D80** (2009) 075018, [arXiv:0906.0580].

[41] M. Raggi and V. Kozhuharov, *Results and perspectives in dark photon physics*, *Riv. Nuovo Cim.* **38** (2015), no. 10 449–505.

[42] A. Bross, M. Crisler, S. H. Pordes, J. Volk, S. Errede, and J. Wrbanek, *A Search for Shortlived Particles Produced in an Electron Beam Dump*, *Phys. Rev. Lett.* **67** (1991) 2942–2945.

[43] E. M. Riordan et al., *A Search for Short Lived Axions in an Electron Beam Dump Experiment*, *Phys. Rev. Lett.* **59** (1987) 755.

[44] M. Davier and H. Nguyen Ngoc, *An Unambiguous Search for a Light Higgs Boson*, *Phys. Lett.* **B229** (1989) 150–155.

[45] A. Konaka, K. Imai, H. Kobayashi, A. Masaike, K. Miyake, T. Nakamura, N. Nagamine, N. Sasao, A. Enomoto, Y. Fukushima, E. Kikutani, H. Koiso, H. Matsumoto, K. Nakahara, S. Ohsawa, T. Taniguchi, I. Sato, and J. Urakawa, *Search for neutral particles in electron-beam-dump experiment*, *Phys. Rev. Lett.* **57** (Aug, 1986) 659–662.

[46] J. D. Bjorken, S. Ecklund, W. R. Nelson, A. Abashian, C. Church, B. Lu, L. W. Mo, T. A. Nunamaker, and P. Rassmann, *Search for Neutral Metastable Penetrating Particles Produced in the SLAC Beam Dump*, *Phys. Rev.* **D38** (1988) 3375.

[47] **CHARM** Collaboration, F. Bergsma et al., *Search for Axion Like Particle Production in 400-GeV Proton - Copper Interactions*, *Phys. Lett.* **157B** (1985) 458–462.

[48] **LSND** Collaboration, C. Athanassopoulos et al., *The Liquid scintillator neutrino detector and LAMPF neutrino source*, *Nucl. Instrum. Meth.* **A388** (1997) 149–172, [nucl-ex/9605002].

[49] J. BlÃ¼mlein et al., *Limits on neutral light scalar and pseudoscalar particles in a proton beam dump experiment*, *Z. Phys.* **C51** (1991) 341–350.

[50] J. BlÃ¼mlein and J. Brunner, *New Exclusion Limits on Dark Gauge Forces from Proton Bremsstrahlung in Beam-Dump Data*, *Phys. Lett.* **B731** (2014) 320–326, [arXiv:1311.3870].

[51] S. Andreas, C. Niebuhr, and A. Ringwald, *New Limits on Hidden Photons from Past Electron Beam Dumps*, *Phys. Rev.* **D86** (2012) 095019, [arXiv:1209.6083].

[52] **NA48/2** Collaboration, J. R. Batley et al., *Search for the dark photon in π^0 decays*, *Phys. Lett.* **B746** (2015) 178–185, [arXiv:1504.00607].

[53] **WASA-at-COSY** Collaboration, P. Adlarson et al., *Search for a dark photon in the $\pi^0 \to e^+e^-\gamma$ decay*, *Phys. Lett.* **B726** (2013) 187–193, [arXiv:1304.0671].

[54] **KLOE-2** Collaboration, D. Babusci et al., *Limit on the production of a light vector gauge boson in phi meson decays with the KLOE detector*, *Phys. Lett.* **B720** (2013) 111–115, [arXiv:1210.3927].

[55] **KLOE-2** Collaboration, D. Babusci et al., *Search for light vector boson production in $e^+e^- \to \mu^+\mu^-\gamma$ interactions with the KLOE experiment*, *Phys. Lett.* **B736** (2014) 459–464, [arXiv:1404.7772].

[56] **KLOE-2** Collaboration, A. Anastasi et al., *Limit on the production of a new vector boson in $e^+e^- \to U\gamma$, $U \to \pi^+\pi^-$ with the KLOE experiment*, *Phys. Lett.* **B757** (2016) 356–361, [arXiv:1603.06086].

[57] **BaBar** Collaboration, J. P. Lees et al., *Search for a Dark Photon in e^+e^- Collisions at BaBar*, *Phys. Rev. Lett.* **113** (2014), no. 20 201801, [arXiv:1406.2980].

[58] **Muon g-2** Collaboration, G. W. Bennett et al., *Final Report of the Muon E821 Anomalous Magnetic Moment Measurement at BNL*, *Phys. Rev.* **D73** (2006) 072003, [hep-ex/0602035].

[59] J. H. Chang, R. Essig, and S. D. McDermott, *Revisiting Supernova 1987A Constraints on Dark Photons*, *JHEP* **01** (2017) 107, [arXiv:1611.03864].

[60] B. Batell, R. Essig, and Z. Surujon, *Strong Constraints on Sub-GeV Dark Sectors from SLAC Beam Dump E137*, *Phys. Rev. Lett.* **113** (2014), no. 17 171802, [arXiv:1406.2698].

[61] R. Essig, J. Mardon, M. Papucci, T. Volansky, and Y.-M. Zhong, *Constraining Light Dark Matter with Low-Energy e^+e^- Colliders*, *JHEP* **11** (2013) 167, [arXiv:1309.5084].

[62] **BaBar** Collaboration, J. P. Lees et al., *Search for Invisible Decays of a Dark Photon Produced in e^+e^- Collisions at BaBar*, *Phys. Rev. Lett.* **119** (2017), no. 13 131804, [arXiv:1702.03327].

[63] A. Arvanitaki, S. Dimopoulos, S. Dubovsky, N. Kaloper, and J. March-Russell, *String Axiverse*, *Phys. Rev.* **D81** (2010) 123530, [arXiv:0905.4720].

[64] J. Halverson and P. Langacker, *TASI Lectures on Remnants from the String Landscape*, *PoS* **TASI2017** (2018) 019, [arXiv:1801.03503].

[65] R. W. Robinett and J. L. Rosner, *Prospects for a Second Neutral Vector Boson at Low Mass in SO(10)*, *Phys. Rev.* **D25** (1982) 3036. [Erratum: Phys. Rev.D27,679(1983)].

[66] **PAMELA** Collaboration, O. Adriani et al., *An anomalous positron abundance in cosmic rays with energies 1.5-100 GeV*, *Nature* **458** (2009) 607–609, [arXiv:0810.4995].

[67] **AMS** Collaboration, M. Aguilar et al., *First Result from the Alpha Magnetic Spectrometer on the International Space Station: Precision Measurement of the Positron Fraction in Primary Cosmic Rays of 0.5–350 GeV*, *Phys. Rev. Lett.* **110** (2013) 141102.

[68] J. Knodlseder et al., *The All-sky distribution of 511 keV electron-positron annihilation emission*, *Astron. Astrophys.* **441** (2005) 513–532, [astro-ph/0506026].

[69] J. F. Donoghue, J. Gasser, and H. Leutwyler, *The Decay of a Light Higgs Boson*, *Nucl. Phys.* **B343** (1990) 341–368.

[70] B. Grzadkowski and P. Krawczyk, *Higgs particle effects in flavour changing transitions*, *Zeitschrift für Physik C Particles and Fields* **18** (Mar, 1983) 43–45.

[71] J. D. Clarke, R. Foot, and R. R. Volkas, *Phenomenology of a very light scalar (100 MeV < m_h < 10 GeV) mixing with the SM Higgs*, *JHEP* **02** (2014) 123, [arXiv:1310.8042].

[72] M. C. Gonzalez-Garcia, M. Maltoni, and T. Schwetz, *Updated fit to three neutrino mixing: status of leptonic CP violation*, *JHEP* **11** (2014) 052, [arXiv:1409.5439].

[73] **LSND** Collaboration, A. Aguilar-Arevalo et al., *Evidence for neutrino oscillations from the observation of anti-neutrino(electron) appearance in a anti-neutrino(muon) beam*, *Phys. Rev.* **D64** (2001) 112007, [hep-ex/0104049].

[74] **MiniBooNE** Collaboration, A. A. Aguilar-Arevalo et al., *A Combined $\nu_\mu \to \nu_e$ and $\bar{\nu}_\mu \to \bar{\nu}_e$ Oscillation Analysis of the MiniBooNE Excesses*, 2012. arXiv:1207.4809.

[75] G. Mention, M. Fechner, T. Lasserre, T. A. Mueller, D. Lhuillier, M. Cribier, and A. Letourneau, *The Reactor Antineutrino Anomaly*, *Phys. Rev.* **D83** (2011) 073006, [arXiv:1101.2755].

[76] C. Giunti, M. Laveder, Y. F. Li, Q. Y. Liu, and H. W. Long, *Update of Short-Baseline Electron Neutrino and Antineutrino Disappearance*, *Phys. Rev.* **D86** (2012) 113014, [arXiv:1210.5715].

[77] J. M. Conrad, C. M. Ignarra, G. Karagiorgi, M. H. Shaevitz, and J. Spitz, *Sterile Neutrino Fits to Short Baseline Neutrino Oscillation Measurements*, *Adv. High Energy Phys.* **2013** (2013) 163897, [arXiv:1207.4765].

[78] J. Kopp, P. A. N. Machado, M. Maltoni, and T. Schwetz, *Sterile Neutrino Oscillations: The Global Picture*, *JHEP* **05** (2013) 050, [arXiv:1303.3011].

[79] D. Gorbunov and M. Shaposhnikov, *How to find neutral leptons of the νMSM?*, *JHEP* **10** (2007) 015, [arXiv:0705.1729]. [Erratum: JHEP11,101(2013)].

[80] **PIENU** Collaboration, M. Aoki et al., *Search for Massive Neutrinos in the Decay $\pi \to e\nu$*, *Phys. Rev.* **D84** (2011) 052002, [arXiv:1106.4055].

[81] **E949** Collaboration, A. V. Artamonov et al., *Search for heavy neutrinos in $K^+ \to \mu^+ \nu_H$ decays*, *Phys. Rev.* **D91** (2015), no. 5 052001, [arXiv:1411.3963]. [Erratum: Phys. Rev.D91,no.5,059903(2015)].

[82] K. Bondarenko, A. Boyarsky, D. Gorbunov, and O. Ruchayskiy, *Phenomenology of GeV-scale Heavy Neutral Leptons*, *JHEP* **11** (2018) 032, [arXiv:1805.08567].

[83] **Belle** Collaboration, D. Liventsev et al., *Search for heavy neutrinos at Belle*, *Phys. Rev.* **D87** (2013), no. 7 071102, [arXiv:1301.1105]. [Erratum: Phys. Rev.D95,no.9,099903(2017)].

[84] **LHCb** Collaboration, R. Aaij et al., *Search for Majorana neutrinos in $B^- \to \pi^+ \mu^- \mu^-$ decays*, *Phys. Rev. Lett.* **112** (2014), no. 13 131802, [arXiv:1401.5361].

[85] **NuTeV, E815** Collaboration, A. Vaitaitis et al., *Search for neutral heavy leptons in a high-energy neutrino beam*, *Phys. Rev. Lett.* **83** (1999) 4943–4946, [hep-ex/9908011].

[86] **FMMF** Collaboration, E. Gallas et al., *Search for neutral weakly interacting massive particles in the Fermilab Tevatron wide band neutrino beam*, *Phys. Rev.* **D52** (1995) 6–14.

[87] G. Bernardi et al., *FURTHER LIMITS ON HEAVY NEUTRINO COUPLINGS*, *Phys. Lett.* **B203** (1988) 332–334.

[88] **CHARM** Collaboration, F. Bergsma et al., *A Search for Decays of Heavy Neutrinos in the Mass Range 0.5-GeV to 2.8-GeV*, *Phys. Lett.* **166B** (1986) 473–478.

[89] **CHARM II** Collaboration, P. Vilain et al., *Search for heavy isosinglet neutrinos*, *Phys. Lett.* **B343** (1995) 453–458. [Phys. Lett.B351,387(1995)].

[90] J. Orloff, A. N. Rozanov, and C. Santoni, *Limits on the mixing of tau neutrino to heavy neutrinos*, *Phys. Lett.* **B550** (2002) 8–15, [hep-ph/0208075].

[91] **WA66** Collaboration, A. M. Cooper-Sarkar et al., *Search for Heavy Neutrino Decays in the BEBC Beam Dump Experiment*, *Phys. Lett.* **160B** (1985) 207–211.

[92] **NOMAD** Collaboration, P. Astier et al., *Search for heavy neutrinos mixing with tau neutrinos*, *Phys. Lett.* **B506** (2001) 27–38, [hep-ex/0101041].

[93] S. A. Baranov et al., *Search for heavy neutrinos at the IHEP-JINR neutrino detector*, *Phys. Lett.* **B302** (1993) 336–340.

[94] **L3** Collaboration, O. Adriani et al., *Search for isosinglet neutral heavy leptons in Z0 decays*, *Phys. Lett.* **B295** (1992) 371–382.

[95] **DELPHI** Collaboration, P. Abreu et al., *Search for neutral heavy leptons produced in Z decays*, *Z. Phys.* **C74** (1997) 57–71. [Erratum: Z. Phys.C75,580(1997)].

[96] **L3** Collaboration, M. Acciarri et al., *Search for heavy isosinglet neutrinos in $e^+ e^-$ annihilation at 130-GeV less than $S^{(1/2)}$ less than 189-GeV*, *Phys. Lett.* **B461** (1999) 397–404, [hep-ex/9909006].

[97] **L3** Collaboration, P. Achard et al., *Search for heavy isosinglet neutrino in $e^+ e^-$ annihilation at LEP*, *Phys. Lett.* **B517** (2001) 67–74, [hep-ex/0107014].

[98] **CMS** Collaboration, S. Chatrchyan et al., *Search for heavy Majorana Neutrinos in $\mu^{\pm}\mu^{\pm}$+ Jets and $e^{\pm}e^{\pm}$+ Jets Events in pp Collisions at $\sqrt{s}$ = 7 TeV*, *Phys. Lett.* **B717** (2012) 109–128, [arXiv:1207.6079].

[99] A. Das, P. S. Bhupal Dev, and N. Okada, *Direct bounds on electroweak scale pseudo-Dirac neutrinos from $\sqrt{s}$ = 8 TeV LHC data*, *Phys. Lett.* **B735** (2014) 364–370, [arXiv:1405.0177].

[100] L. Basso, O. Fischer, and J. J. van der Bij, *Precision tests of unitarity in leptonic mixing*, *EPL* **105** (2014), no. 1 11001, [arXiv:1310.2057].

[101] S. Antusch and O. Fischer, *Non-unitarity of the leptonic mixing matrix: Present bounds and future sensitivities*, *JHEP* **10** (2014) 094, [arXiv:1407.6607].

[102] S. Antusch and O. Fischer, *Testing sterile neutrino extensions of the Standard Model at future lepton colliders*, *JHEP* **05** (2015) 053, [arXiv:1502.05915].

[103] T. Asaka, S. Blanchet, and M. Shaposhnikov, *The nuMSM, dark matter and neutrino masses*, *Phys. Lett.* **B631** (2005) 151–156, [hep-ph/0503065].

[104] T. Asaka and M. Shaposhnikov, *The nuMSM, dark matter and baryon asymmetry of the universe*, *Phys. Lett.* **B620** (2005) 17–26, [hep-ph/0505013].

[105] J.-P. Delahaye et al., *Enabling Intensity and Energy Frontier Science with a Muon Accelerator Facility in the U.S.: A White Paper Submitted to the 2013 U.S. Community Summer Study of the Division of Particles and Fields of the American Physical Society*, in *Proceedings, 2013 Community Summer Study on the Future of U.S. Particle Physics: Snowmass on the Mississippi (CSS2013): Minneapolis, MN, USA, July 29-August 6, 2013*, 2013. arXiv:1308.0494.

[106] M. Palmer, *The US muon accelerator program*, in *Proceedings, 5th International Particle Accelerator Conference (IPAC 2014): Dresden, Germany, June 15-20, 2014*, p. TUPME012, 2014. arXiv:1502.03454.

[107] M. Antonelli, M. Boscolo, R. Di Nardo, and P. Raimondi, *Novel proposal for a low emittance muon beam using positron beam on target*, *Nucl. Instrum. Meth.* **A807** (2016) 101–107, [arXiv:1509.04454].

[108] M. Antonelli, E. Bagli, M. Biagini, M. Boscolo, G. Cavoto, P. Raimondi, and A. Variola, *Very Low Emittance Muon Beam using Positron Beam on Target*, in *Proceedings, 7th International Particle Accelerator Conference (IPAC 2016): Busan, Korea, May 8-13, 2016*, p. TUPMY001, 2016.

[109] O. Buss, T. Gaitanos, K. Gallmeister, H. van Hees, M. Kaskulov, O. Lalakulich, A. B. Larionov, T. Leitner, J. Weil, and U. Mosel, *Transport-theoretical Description of Nuclear Reactions*, *Phys. Rept.* **512** (2012) 1–124, [arXiv:1106.1344].

[110] B. Henning, X. Lu, and H. Murayama, *How to use the Standard Model effective field theory*, *JHEP* **01** (2016) 023, [arXiv:1412.1837].

[111] F. del Aguila, Z. Kunszt, and J. Santiago, *One-loop effective lagrangians after matching*, *Eur. Phys. J.* **C76** (2016), no. 5 244, [arXiv:1602.00126].

[112] S. A. R. Ellis, J. Quevillon, T. You, and Z. Zhang, *Mixed heavy?light matching in the Universal One-Loop Effective Action*, *Phys. Lett.* **B762** (2016) 166–176, [arXiv:1604.02445].

[113] B. Henning, X. Lu, and H. Murayama, *One-loop Matching and Running with Covariant Derivative Expansion*, arXiv:1604.01019.

[114] C. N. Leung, S. T. Love, and S. Rao, *Low-Energy Manifestations of a New Interaction Scale: Operator Analysis*, *Z. Phys.* **C31** (1986) 433.

[115] W. Buchmuller and D. Wyler, *Effective Lagrangian Analysis of New Interactions and Flavor Conservation*, *Nucl.Phys.* **B268** (1986) 621–653.

[116] Z. Han and W. Skiba, *Effective theory analysis of precision electroweak data*, *Phys.Rev.* **D71** (2005) 075009, [hep-ph/0412166].

[117] Z. Han, *Electroweak constraints on effective theories with U(2) x (1) flavor symmetry*, *Phys. Rev.* **D73** (2006) 015005, [hep-ph/0510125].

[118] R. Barbieri, A. Pomarol, R. Rattazzi, and A. Strumia, *Electroweak symmetry breaking after LEP-1 and LEP-2*, *Nucl.Phys.* **B703** (2004) 127–146, [hep-ph/0405040].

[119] C. Grojean, W. Skiba, and J. Terning, *Disguising the oblique parameters*, *Phys.Rev.* **D73** (2006) 075008, [hep-ph/0602154].

[120] G. Cacciapaglia, C. Csaki, G. Marandella, and A. Strumia, *The Minimal Set of Electroweak Precision Parameters*, *Phys.Rev.* **D74** (2006) 033011, [hep-ph/0604111].

[121] V. Cirigliano, J. Jenkins, and M. Gonzalez-Alonso, *Semileptonic decays of light quarks beyond the Standard Model*, *Nucl. Phys.* **B830** (2010) 95–115, [arXiv:0908.1754].

[122] M. Carpentier and S. Davidson, *Constraints on two-lepton, two quark operators*, *Eur. Phys. J.* **C70** (2010) 1071–1090, [arXiv:1008.0280].

[123] A. Filipuzzi, J. Portoles, and M. Gonzalez-Alonso, *$U(2)^5$ flavor symmetry and lepton universality violation in $W \to \tau\nu_\tau$*, *Phys. Rev.* **D85** (2012) 116010, [arXiv:1203.2092].

[124] J. de Blas, *Electroweak limits on physics beyond the Standard Model*, *EPJ Web Conf.* **60** (2013) 19008, [arXiv:1307.6173].

[125] A. Pomarol and F. Riva, *Towards the Ultimate SM Fit to Close in on Higgs Physics*, *JHEP* **1401** (2014) 151, [arXiv:1308.2803].

[126] J. Elias-Miro, J. Espinosa, E. Masso, and A. Pomarol, *Higgs windows to new physics through d=6 operators: constraints and one-loop anomalous dimensions*, *JHEP* **1311** (2013) 066, [arXiv:1308.1879].

[127] B. Dumont, S. Fichet, and G. von Gersdorff, *A Bayesian view of the Higgs sector with higher dimensional operators*, *JHEP* **1307** (2013) 065, [arXiv:1304.3369].

[128] C.-Y. Chen, S. Dawson, and C. Zhang, *Electroweak Effective Operators and Higgs Physics*, *Phys. Rev.* **D89** (2014), no. 1 015016, [arXiv:1311.3107].

[129] J. de Blas, M. Chala, and J. Santiago, *Global Constraints on Lepton-Quark Contact Interactions*, *Phys. Rev.* **D88** (2013) 095011, [arXiv:1307.5068].

[130] S. Willenbrock and C. Zhang, *Effective Field Theory Beyond the Standard Model*, arXiv:1401.0470.

[131] R. S. Gupta, A. Pomarol, and F. Riva, *BSM Primary Effects*, *Phys. Rev.* **D91** (2015), no. 3 035001, [arXiv:1405.0181].

[132] E. Masso, *An Effective Guide to Beyond the Standard Model Physics*, *JHEP* **1410** (2014) 128, [arXiv:1406.6376].

[133] J. de Blas, M. Ciuchini, E. Franco, D. Ghosh, S. Mishima, et al., *Global Bayesian Analysis of the Higgs-boson Couplings*, arXiv:1410.4204.

[134] M. Ciuchini, E. Franco, S. Mishima, M. Pierini, L. Reina, et al., *Update of the electroweak precision fit, interplay with Higgs-boson signal strengths and model-independent constraints on new physics*, arXiv:1410.6940.

[135] J. Ellis, V. Sanz, and T. You, *The Effective Standard Model after LHC Run I*, arXiv:1410.7703.

[136] A. Falkowski and F. Riva, *Model-independent precision constraints on dimension-6 operators*, *JHEP* **1502** (2015) 039, [arXiv:1411.0669].

[137] F. del Aguila, M. Chala, J. Santiago, and Y. Yamamoto, *Collider limits on leptophilic interactions*, *JHEP* **03** (2015) 059, [arXiv:1411.7394].

[138] T. Corbett, O. J. P. Eboli, D. Goncalves, J. Gonzalez-Fraile, T. Plehn, and M. Rauch, *The Higgs Legacy of the LHC Run I*, *JHEP* **08** (2015) 156, [arXiv:1505.05516].

[139] A. Efrati, A. Falkowski, and Y. Soreq, *Electroweak constraints on flavorful effective theories*, *JHEP* **07** (2015) 018, [arXiv:1503.07872].

[140] M. Gonzalez-Alonso, A. Greljo, G. Isidori, and D. Marzocca, *Electroweak bounds on Higgs pseudo-observables and $h \to 4\ell$ decays*, *Eur. Phys. J.* **C75** (2015) 341, [arXiv:1504.04018].

[141] A. Buckley, C. Englert, J. Ferrando, D. J. Miller, L. Moore, M. Russell, and C. D. White, *A global fit of top quark effective theory to data*, arXiv:1506.08845.

[142] J. de Blas, M. Chala, and J. Santiago, *Renormalization Group Constraints on New Top Interactions from Electroweak Precision Data*, *JHEP* **09** (2015) 189, [arXiv:1507.00757].

[143] A. Falkowski, *Effective field theory approach to LHC Higgs data*, *Pramana* **87** (2016), no. 3 39, [arXiv:1505.00046].

[144] F. del Aguila, M. Chala, J. Santiago, and Y. Yamamoto, *Four and two-lepton signals of leptophilic gauge interactions at large colliders*, *PoS* **CORFU2014** (2015) 109, [arXiv:1505.00799].

[145] J. D. Wells and Z. Zhang, *Status and prospects of precision analyses with $e^+e^- \to W^+W^-$*, arXiv:1507.01594.

[146] L. Berthier and M. Trott, *Consistent constraints on the Standard Model Effective Field Theory*, arXiv:1508.05060.

[147] A. Falkowski, M. Gonzalez-Alonso, A. Greljo, and D. Marzocca, *Global constraints on anomalous triple gauge couplings in effective field theory approach*, *Phys. Rev. Lett.* **116** (2016), no. 1 011801, [arXiv:1508.00581].

[148] J. Ellis and T. You, *Sensitivities of Prospective Future e+e- Colliders to Decoupled New Physics*, arXiv:1510.04561.

[149] C. Englert, R. Kogler, H. Schulz, and M. Spannowsky, *Higgs coupling measurements at the LHC*, arXiv:1511.05170.

[150] A. Falkowski and K. Mimouni, *Model independent constraints on four-lepton operators*, *JHEP* **02** (2016) 086, [arXiv:1511.07434].

[151] J. de Blas, M. Ciuchini, E. Franco, S. Mishima, M. Pierini, L. Reina, and L. Silvestrini, *Electroweak precision observables and Higgs-boson signal strengths in the Standard Model and beyond: present and future*, *JHEP* **12** (2016) 135, [arXiv:1608.01509].

[152] M. Ciuchini, J. de Blas, E. Franco, D. Ghosh, S. Mishima, M. Pierini, L. Reina, and L. Silvestrini, *Updates on fits to electroweak parameters*, *PoS* **LeptonPhoton2015** (2016) 013.

[153] M. BjÂ¿rn and M. Trott, *Interpreting W mass measurements in the SMEFT*, *Phys. Lett.* **B762** (2016) 426–431, [arXiv:1606.06502].

[154] C. Hartmann, W. Shepherd, and M. Trott, *The Z decay width in the SMEFT: y_t and λ corrections at one loop*, *JHEP* **03** (2017) 060, [arXiv:1611.09879].

[155] S. Descotes-Genon, J. Matias, and J. Virto, *Understanding the $B \to K^* \mu^+ \mu^-$ Anomaly*, *Phys. Rev.* **D88** (2013) 074002, [arXiv:1307.5683].

[156] W. Altmannshofer and D. M. Straub, *New Physics in $B \to K^* \mu\mu$?*, *Eur. Phys. J.* **C73** (2013) 2646, [arXiv:1308.1501].

[157] S. Jäger and J. Martin Camalich, *Reassessing the discovery potential of the $B \to K^* \ell^+ \ell^-$ decays in the large-recoil region: SM challenges and BSM opportunities*, *Phys. Rev.* **D93** (2016), no. 1 014028, [arXiv:1412.3183].

[158] M. Freytsis, Z. Ligeti, and J. T. Ruderman, *Flavor models for $\bar{B} \to D^{(*)} \tau \bar{\nu}$*, *Phys. Rev.* **D92** (2015), no. 5 054018, [arXiv:1506.08896].

[159] W. Altmannshofer, C. Niehoff, P. Stangl, and D. M. Straub, *Status of the $B \to K^* \mu^+ \mu^-$ anomaly after Moriond 2017*, arXiv:1703.09189.

[160] M. González-Alonso and J. Martin Camalich, *Global Effective-Field-Theory analysis of New-Physics effects in (semi)leptonic kaon decays*, *JHEP* **12** (2016) 052, [arXiv:1605.07114].

[161] A. Falkowski, M. González-Alonso, and K. Mimouni, *Compilation of low-energy constraints on 4-fermion operators in the SMEFT*, *JHEP* **08** (2017) 123, [arXiv:1706.03783].

[162] B. Grzadkowski, M. Iskrzynski, M. Misiak, and J. Rosiek, *Dimension-Six Terms in the Standard Model Lagrangian*, *JHEP* **1010** (2010) 085, [arXiv:1008.4884].

[163] R. Contino, M. Ghezzi, C. Grojean, M. Muhlleitner, and M. Spira, *Effective Lagrangian for a light Higgs-like scalar*, *JHEP* **1307** (2013) 035, [arXiv:1303.3876].

[164] **The LHC Higgs Cross Section Working Group** Collaboration, D. de Florian et al., *Handbook of LHC Higgs Cross Sections: 4. Deciphering the Nature of the Higgs Sector*, arXiv:1610.07922.

[165] H. K. Dreiner, H. E. Haber, and S. P. Martin, *Two-component spinor techniques and Feynman rules for quantum field theory and supersymmetry*, *Phys.Rept.* **494** (2010) 1–196, [arXiv:0812.1594].

[166] **LHC Higgs Cross Section Working Group 2** Collaboration, *Higgs Basis: Proposal for an EFT basis choice for LHC HXSWG*, LHCHXSWG-INT-2015-001 cds.cern.ch/record/2001958.

[167] S. Descotes-Genon, A. Falkowski, M. Fedele, M. González-Alonso, and J. Virto, *The CKM parameters in the SMEFT*, *JHEP* **05** (2019) 172, [arXiv:1812.08163].

[168] **Particle Data Group** Collaboration, C. Patrignani et al., *Review of Particle Physics*, *Chin. Phys.* **C40** (2016), no. 10 100001.

[169] J. C. Hardy and I. S. Towner, *Superallowed $0^+ \to 0^+$ nuclear ? decays: 2014 critical survey, with precise results for V_{ud} and CKM unitarity*, *Phys. Rev.* **C91** (2015), no. 2 025501, [arXiv:1411.5987].

[170] E. Eichten and B. R. Hill, *An Effective Field Theory for the Calculation of Matrix Elements Involving Heavy Quarks*, *Phys. Lett.* **B234** (1990) 511–516.

[171] J. A. Gracey, *Three loop MS-bar tensor current anomalous dimension in QCD*, *Phys. Lett.* **B488** (2000) 175–181, [hep-ph/0007171].

[172] K. G. Chetyrkin, B. A. Kniehl, and M. Steinhauser, *Decoupling relations to O (alpha-s**3) and their connection to low-energy theorems*, *Nucl. Phys.* **B510** (1998) 61–87, [hep-ph/9708255].

[173] M. Misiak and M. Steinhauser, *Large-m_c Asymptotic Behaviour of $O(\alpha_s^2)$ Corrections to $B \to X_s\gamma$*, *Nucl. Phys.* **B840** (2010) 271–283, [arXiv:1005.1173].

[174] M. González-Alonso, J. Martin Camalich, and K. Mimouni, *Renormalization-group evolution of new physics contributions to (semi)leptonic meson decays*, *Phys. Lett.* **B772** (2017) 777–785, [arXiv:1706.00410].

[175] A. Celis, J. Fuentes-Martin, A. Vicente, and J. Virto, *DsixTools: The Standard Model Effective Field Theory Toolkit*, arXiv:1704.04504.

[176] J. Aebischer, M. Fael, C. Greub, and J. Virto, *B physics Beyond the Standard Model at One Loop: Complete Renormalization Group Evolution below the Electroweak Scale*, arXiv:1704.06639.

[177] R. Alonso, E. E. Jenkins, A. V. Manohar, and M. Trott, *Renormalization Group Evolution of the Standard Model Dimension Six Operators III: Gauge Coupling Dependence and Phenomenology*, *JHEP* **1404** (2014) 159, [arXiv:1312.2014].

[178] E. E. Jenkins, A. V. Manohar, and M. Trott, *Renormalization Group Evolution of the Standard Model Dimension Six Operators II: Yukawa Dependence*, *JHEP* **01** (2014) 035, [arXiv:1310.4838].

[179] **ALEPH, DELPHI, L3, OPAL, SLD, LEP Electroweak Working Group, SLD Electroweak Group, SLD Heavy Flavour Group** Collaboration, S. Schael et al., *Precision electroweak measurements on the Z resonance*, *Phys.Rept.* **427** (2006) 257–454, [hep-ex/0509008].

[180] **DELPHI, OPAL, LEP Electroweak, ALEPH, L3** Collaboration, S. Schael et al., *Electroweak Measurements in Electron-Positron Collisions at W-Boson-Pair Energies at LEP*, *Phys. Rept.* **532** (2013) 119–244, [arXiv:1302.3415].

[181] **CDF and D0** Collaboration, T. E. W. Group, *2012 Update of the Combination of CDF and D0 Results for the Mass of the W Boson*, arXiv:1204.0042.

[182] C. H. Llewellyn Smith, *On the Determination of sin**2-Theta-w in Semileptonic Neutrino Interactions*, *Nucl. Phys.* **B228** (1983) 205–215.

[183] **CHARM** Collaboration, J. Dorenbosch et al., *Experimental Verification of the Universality of ν_e and ν_μ Coupling to the Neutral Weak Current*, *Phys. Lett.* **B180** (1986) 303–307.

[184] **CHARM** Collaboration, J. V. Allaby et al., *A Precise Determination of the Electroweak Mixing Angle from Semileptonic Neutrino Scattering*, *Z. Phys.* **C36** (1987) 611.

[185] A. Blondel et al., *Electroweak Parameters From a High Statistics Neutrino Nucleon Scattering Experiment*, *Z. Phys.* **C45** (1990) 361–379.

[186] **E770, E744, CCFR** Collaboration, K. S. McFarland et al., *A Precision measurement of electroweak parameters in neutrino - nucleon scattering*, *Eur. Phys. J.* **C1** (1998) 509–513, [hep-ex/9701010].

[187] J. Erler and S. Su, *The Weak Neutral Current*, *Prog. Part. Nucl. Phys.* **71** (2013) 119–149, [arXiv:1303.5522].

[188] J. Erler. Private communication.

[189] **NOMAD** Collaboration, C. T. Kullenberg et al., *A Measurement of Coherent Neutral Pion Production in Neutrino Neutral Current Interactions in NOMAD*, *Phys. Lett.* **B682** (2009) 177–184, [arXiv:0910.0062].

[190] **SKAT** Collaboration, H. J. Grabosch et al., *Coherent Pion Production In Neutrino And Anti-Neutrino Interactions On Nuclei Of Heavy Freon Molecules*, *Z. Phys.* **C31** (1986) 203.

[191] J. Horstkotte, A. Entenberg, R. S. Galik, A. K. Mann, H. H. Williams, W. Kozanecki, C. Rubbia, J. Strait, L. Sulak, and P. J. Wanderer, *Measurement of Neutrino - Proton and Anti-neutrinos - Proton Elastic Scattering*, *Phys. Rev.* **D25** (1982) 2743.

[192] L. A. Ahrens et al., *Measurement of Neutrino - Proton and anti-neutrino - Proton Elastic Scattering*, *Phys. Rev.* **D35** (1987) 785.

[193] M. C. Gonzalez-Garcia and M. Maltoni, *Determination of matter potential from global analysis of neutrino oscillation data*, *JHEP* **09** (2013) 152, [arXiv:1307.3092].

[194] P. Coloma, P. B. Denton, M. C. Gonzalez-Garcia, M. Maltoni, and T. Schwetz, *Curtailing the Dark Side in Non-Standard Neutrino Interactions*, *JHEP* **04** (2017) 116, [arXiv:1701.04828].

[195] A. Falkowski, M. González-Alonso, and Z. Tabrizi, *Reactor neutrino oscillations as constraints on Effective Field Theory*, *JHEP* **05** (2019) 173, [arXiv:1901.04553].

[196] **CHARM** Collaboration, J. Dorenbosch et al., *EXPERIMENTAL RESULTS ON NEUTRINO - ELECTRON SCATTERING*, *Z. Phys.* **C41** (1989) 567. [Erratum: Z. Phys.C51,142(1991)].

[197] **CHARM-II** Collaboration, P. Vilain et al., *Precision measurement of electroweak parameters from the scattering of muon-neutrinos on electrons*, *Phys. Lett.* **B335** (1994) 246–252.

[198] L. A. Ahrens et al., *Determination of electroweak parameters from the elastic scattering of muon-neutrinos and anti-neutrinos on electrons*, *Phys. Rev.* **D41** (1990) 3297–3316.

[199] **SLAC E158** Collaboration, P. L. Anthony et al., *Precision measurement of the weak mixing angle in Moller scattering*, *Phys. Rev. Lett.* **95** (2005) 081601, [hep-ex/0504049].

[200] V. A. Dzuba, J. C. Berengut, V. V. Flambaum, and B. Roberts, *Revisiting parity non-conservation in cesium*, *Phys. Rev. Lett.* **109** (2012) 203003, [arXiv:1207.5864].

[201] C. S. Wood, S. C. Bennett, D. Cho, B. P. Masterson, J. L. Roberts, C. E. Tanner, and C. E. Wieman, *Measurement of parity nonconservation and an anapole moment in cesium*, *Science* **275** (1997) 1759–1763.

[202] **Qweak** Collaboration, D. Androic et al., *First Determination of the Weak Charge of the Proton*, *Phys. Rev. Lett.* **111** (2013), no. 14 141803, [arXiv:1307.5275].

[203] **PVDIS** Collaboration, D. Wang et al., *Measurement of parity violation in electron-quark scattering*, *Nature* **506** (2014), no. 7486 67–70.

[204] E. J. Beise, M. L. Pitt, and D. T. Spayde, *The SAMPLE experiment and weak nucleon structure*, *Prog. Part. Nucl. Phys.* **54** (2005) 289–350, [nucl-ex/0412054].

[205] A. Argento et al., *Electroweak Asymmetry in Deep Inelastic Muon - Nucleon Scattering*, *Phys. Lett.* **B120** (1983) 245.

[206] **VENUS** Collaboration, H. Hanai et al., *Measurement of tau polarization in e+ e- annihilation at s**(1/2) = 58-GeV*, *Phys. Lett.* **B403** (1997) 155–162, [hep-ex/9703003].

[207] **DELPHI, OPAL, ALEPH, LEP Electroweak Working Group, L3** Collaboration, J. Alcaraz et al., *A Combination of preliminary electroweak measurements and constraints on the standard model*, hep-ex/0612034.

[208] **VENUS** Collaboration, K. Abe et al., *A Study of the charm and bottom quark production in e^+e^- annihilation at $\sqrt{s}$ = 58 GeV using prompt electrons*, *Phys. Lett.* **B313** (1993) 288–298.

[209] **TOPAZ** Collaboration, Y. Inoue et al., *Measurement of the cross-section and forward - backward charge asymmetry for the b and c quark in e^+e^- annihilation with inclusive muons at $\sqrt{s}$ = 58 GeV*, *Eur. Phys. J.* **C18** (2000) 273–282, [hep-ex/0012033].

[210] **Particle Data Group** Collaboration, K. A. Olive et al., *Review of Particle Physics*, *Chin. Phys.* **C38** (2014) 090001.

[211] C. Bouchiat and L. Michel, *Theory of μ-Meson Decay with the Hypothesis of Nonconservation of Parity*, *Phys. Rev.* **106** (1957) 170–172. [,89(1957)].

[212] M. Gonzalez-Alonso, *TAU2014 Opening Talk*, *Nucl. Part. Phys. Proc.* **260** (2015) 3–11, [arXiv:1411.4529].

[213] M. Gonzalez-Alonso, *Test del modelo estandar a energias bajas*, *Phd Thesis* (2010).

[214] N. Danneberg et al., *Muon decay: Measurement of the transverse polarization of the decay positrons and its implications for the Fermi coupling constant and time reversal invariance*, *Phys. Rev. Lett.* **94** (2005) 021802.

[215] **CHARM-II** Collaboration, D. Geiregat et al., *First observation of neutrino trident production*, *Phys. Lett.* **B245** (1990) 271–275.

[216] **CCFR** Collaboration, S. R. Mishra et al., *Neutrino tridents and W Z interference*, *Phys. Rev. Lett.* **66** (1991) 3117–3120.

[217] **SLD Electroweak Group, SLD Heavy Flavor Group, DELPHI, LEP, ALEPH, OPAL, LEP Electroweak Working Group, L3** Collaboration, t. S. Electroweak, *A Combination of preliminary electroweak measurements and constraints on the standard model*, hep-ex/0312023.

[218] M. B. Voloshin, *Upper bound on tensor interaction in the decay pi- —> e- anti-neutrino gamma*, *Phys. Lett.* **B283** (1992) 120–122.

[219] M. E. Peskin and T. Takeuchi, *Estimation of oblique electroweak corrections*, *Phys.Rev.* **D46** (1992) 381–409.

[220] J. D. Wells and Z. Zhang, *Effective theories of universal theories*, arXiv:1510.08462.

[221] V. Cirigliano, M. González-Alonso, and M. L. Graesser, *Non-standard Charged Current Interactions: beta decays versus the LHC*, *JHEP* **02** (2013) 046, [arXiv:1210.4553].

[222] **ATLAS** Collaboration, G. Aad et al., *Measurement of the double-differential high-mass Drell-Yan cross section in pp collisions at $\sqrt{s} = 8$ TeV with the ATLAS detector*, *JHEP* **08** (2016) 009, [arXiv:1606.01736].

[223] M. Farina, G. Panico, D. Pappadopulo, J. T. Ruderman, R. Torre, and A. Wulzer, *Energy helps accuracy: electroweak precision tests at hadron colliders*, arXiv:1609.08157.

[224] R. Contino, A. Falkowski, F. Goertz, C. Grojean, and F. Riva, *On the Validity of the Effective Field Theory Approach to SM Precision Tests*, *JHEP* **07** (2016) 144, [arXiv:1604.06444].

[225] V. Cirigliano, A. Falkowski, M. González-Alonso, and A. Rodríguez-Sánchez, *Hadronic τ Decays as New Physics Probes in the LHC Era*, *Phys. Rev. Lett.* **122** (2019), no. 22 221801, [arXiv:1809.01161].

[226] G. Servant and T. M. P. Tait, *Is the lightest Kaluza-Klein particle a viable dark matter candidate?*, *Nucl. Phys.* **B650** (2003) 391–419, [hep-ph/0206071].

[227] Y.-S. Liu, D. McKeen, and G. A. Miller, *Validity of the Weizsäcker-Williams approximation and the analysis of beam dump experiments: Production of a new scalar boson*, *Phys. Rev.* **D95** (2017), no. 3 036010, [arXiv:1609.06781].

[228] K. J. Kim and Y.-S. Tsai, *IMPROVED WEIZSACKER-WILLIAMS METHOD AND ITS APPLICATION TO LEPTON AND W BOSON PAIR PRODUCTION*, *Phys. Rev.* **D8** (1973) 3109.

[229] K. Schmidt-Hoberg, F. Staub, and M. W. Winkler, *Constraints on light mediators: confronting dark matter searches with B physics*, *Phys. Lett.* **B727** (2013) 506–510, [arXiv:1310.6752].

[230] G. Krnjaic, *Probing Light Thermal Dark-Matter With a Higgs Portal Mediator*, *Phys. Rev.* **D94** (2016), no. 7 073009, [arXiv:1512.04119].

**Ce document a été imprimé au Centre d'impression EPFL,
imprimerie climatiquement neutre, certifiée myClimate.**